NATIONAL INSTITUTE FOR FUSION SCIENCE

JSPS-NRF-NSFC A3 Foresight Program Seminar
Proceedings of Japan-China-Korea Joint Seminar on
Atomic and Molecular Processes in Plasma
Jul. 26 - 28, 2016, Chengdu, China

Edited by Daiji Kato, Zhengying Cui and Chenzhong Dong

(Received - Feb. 15, 2017)

NIFS-PROC-103

Mar. 17, 2017

JSPS-NRF-NSFC A3 Foresight Program Seminar

Proceedings of Japan-China-Korea Joint Seminar on Atomic and Molecular Processes in Plasma

Jul. 26 – 28, 2016, Chengdu, China

Edited by
Daiji Kato, Zhengying Cui and Chenzhong Dong

Abstract

As one of the activities of JSPS-NRF-NSFC A3 Foresight Program in the field of Plasma Physics "Study on Critical Physics Issues Specific to Steady State Sustainment of High-Performance Plasmas", Japan-China-Korea Joint Seminar on Atomic and Molecular Processes in Plasma (AMPP2016) was held on July 26 – 28, 2016, in Chengdu, China. The total number of the officially registered participants was 63. This seminar is the extension of the last five seminars that were held in 2004 in Lanzhou, in 2007 in Dunhuang, in 2009 in Xi'an, and in 2012 and 2014 in Lanzhou.

In the nuclear fusion plasma, there are quite a variety of atomic processes such as ionization, excitation, di-electronic recombination, collisional electron transfer, cascade radiation, and cascade Auger decay over the wide range of plasma temperature. The knowledge of those processes is indispensable for the evaluation and improvement of the plasma properties. Because of the diversity of the subjects, it is desirable to investigate them by international collaboration groups. This seminar is held to discuss achievement during the past two years from the last seminar in 2014 and issues for the future prospect.

Keywords:
EUV spectroscopy, tungsten, dielectronic recombination, visible forbidden line, LHD, tokamak, electron scattering, optical oscillator strength, EBIT, plasma spectroscopy, MCDF, UTA, charge exchange, electron momentum spectroscopy, solar wind, polarization, laser plasma source

Preface

As one of the activities of Post Japan-China Core University Program and JSPS-NSFC-NRF A3 Foresight Program in the field of Plasma Physics "Study on Critical Physics Issues Specific to Steady State Sustainment of High-Performance Plasmas", Japan-China-Korea Joint Seminar on Atomic and Molecular Processes in Plasma was held on July 26 – 28, 2016 in Chengdu, China. This seminar is the extension of the last five seminars that were held on March 6 – 11, 2004 in Lanzhou, China, on October 6 -12, 2007 in Dunhuang, China, on October 26 – 31, 2009 in Xi'an, China, on July 30 – August 4, 2012 in Lanzhou, China, and on July 28 – August 1, 2014 in Lanzhou, China.

Since the last seminar in 2014, researchers from Japan, China and Korea carried out a number of significant studies in atomic and molecular processes in relation to the fusion plasma. The proposal of the present joint seminar has placed its intention not only on the presentations of the collaborative studies, but also on offering an opportunity for the wide range of researchers from the countries to be acquainted with each other, who would have made an extensive exchange of information about the recent progress of the research activities, and also would have made an extensive discussion about the plan of the future collaborations.

In the present seminar, the total number of 35 oral talks was presented by experts from Japan, China and Korea. The total number of the officially registered participants was 63, in which 13 from Japan, 48 from China, and 2 from Korea.

The seminar was in always a friendly and active atmosphere. During the seminar, the participants exchanged their new research results, discussed about the outlook for new research fields. They tried to promote further developments in mutual collaborations between the countries and the experts. Among them, the topics highlighted in the seminar was spectroscopic studies on highly charged ions of heavy elements including tungsten which will be primary heavy impurities in ITER plasmas. The next seminar will be held in Hefei, China and hosted by Institute of Plasma Physics (ASIPP).

The present issue of the proceedings has collected 17 papers from the delegates of the seminar. It covers the fundamental properties of atoms and ions, the collisions of electrons, photons and ions with atoms, molecules and ions, the analysis and diagnostics of the confinement fusion plasma especially for the properties of tungsten atoms and ions, atomic processes in high-density laser induced plasmas and, further, topics from wide area of atomic physics. The present issue includes abstracts of all presentations in the seminar, the scientific program, the group photo as well as the list of participants.

On behalf of the organizing committee, we would like to express our sincerest thanks to all the participants who made active contributions not only in the formal presentations but also in the fruitful discussions. We would like to acknowledge everybody who devoted very hard work for preparing the seminar. Finally, we would like to acknowledge the administrative as well as the financial supports from Southwestern Institute of Physics and the National Institute for Fusion Science.

Organizing Committee:

Zhengying Cui

Local Chairperson,

Southwestern Institute of Physics, Chengdu, China

Daiji Kato

National Institute for Fusion Science, Toki, Japan

Chenzhong Dong

Northwest Normal University, Lanzhou, China

Contents


The 6th China -Japan-Korea Joint Seminar
on Atomic and Molecular Processes in Plasma (AMPP2016)

Evaluation of poloidal distribution of edge electron temperature in stochastic magnetic field layer of LHD using intensity ratio among impurity line emissions

S.Morita[1,2], E.H.Wang[3], M.Goto[1,2], X.L.Huang[1], Y.Liu[2], I.Murakami[1,2], T.Oishi[1,2] and H.M.Zhang[2]

[1] National Institute for Fusion Science, Toki 509-5292, Gifu, Japan

[2] SOKENDAI (Graduate University for Advanced Studies), Toki 509-5292, Gifu, Japan

[3] Institute of Plasma Physics Chinese Academy of Sciences, Hefei 230026, Anhui, China

Abstract

Two-dimensional distribution of impurity lines emitted from ergodic layer with stochastic magnetic field lines in Large Helical Device (LHD) has been observed using a space-resolved extreme ultraviolet (EUV) spectrometer. The two-dimensional electron temperature distribution in the ergodic layer is successfully measured from a line intensity ratio of Li-like NeVIII 2s-3p ($^2S_{1/2}$-$^2P_{3/2}$: 88.09 Å, $^2S_{1/2}$-$^2P_{1/2}$: 88.13 Å) to 2p-3s ($^2P_{1/2}$-$^2S_{1/2}$: 102.91 Å, $^2P_{3/2}$-$^2S_{1/2}$: 103.09 Å) transitions. The intensity ratio analyzed with ADAS code shows no dependence on the electron density below 10^{14} cm^{-3}. The result indicates the poloidal location at high-field side near helical coils has a slightly higher temperature, i.e., 220 eV, compared to the temperature near separatrix X-point, i.e., 170 eV.

Keywords: EUV spectroscopy, 2-D intensity distribution, intensity ratio, LHD, stochastic magnetic field layer

1. Introduction

The helical device is typically characterized by the presence of stochastic magnetic field layer in the plasma edge, in which the magnetic field structure is fully three-dimensional. LHD has the stochastic magnetic field layer outside the last-closed-flux surface (LCFS) which defines the core plasma. In the stochastic magnetic layer all the plasma parameters such as temperature and density have three-dimensional distribution. Therefore, it is very important for the transport study to evaluate a three-dimensional structure of the temperature and density in the stochastic magnetic field layer.

Line intensity ratio between two different transitions in the same ionization stage is an essential tool to measure the electron temperature and density in astrophysical plasmas [1]. In order to measure the electron temperature the ratio of 2s $^2S_{1/2}$-3p $^2P_{3/2}$ to 2s $^2S_{1/2}$-2p $^2P_{3/2}$ transitions for Li-like ions is generally used because both lines are very strong and the ratio is sufficiently sensitive to the electron temperature, e.g. CIV (312.4 Å/1548 Å) and NeVIII (88.1 Å/770.4 Å) [2]. However, it is generally difficult to measure the line pair simultaneously using a single spectrometer. It may introduce a large uncertainty if the intensity ratio is measured with two different types of spectrometers having a different observation volume and a different accuracy in the absolute sensitivity calibration. Therefore, the intensity ratio using two lines closely existing at adjacent wavelengths is desired to analyze the data accurately because those lines can be simultaneously

measured with a single spectrometer and the spectrometer sensitivity is practically the same between the two lines.

For the purpose the line ratio of Li-like CIV 2p-3d ($^2P_{1/2}$-$^2D_{3/2}$: 384.03 Å, $^2P_{3/2}$-$^2D_{5/2}$: 384.18 Å) to 2p-3s ($^2P_{1/2}$-$^2S_{1/2}$: 419.53 Å, $^2P_{3/2}$-$^2S_{1/2}$: 419.71 Å) transitions and NeVIII 2s-3p ($^2S_{1/2}$-$^2P_{3/2}$: 88.09 Å, $^2S_{1/2}$-$^2P_{1/2}$: 88.13 Å) to 2p-3s ($^2P_{1/2}$-$^2S_{1/2}$: 102.91 Å, $^2P_{3/2}$-$^2S_{1/2}$: 103.09 Å) transitions have been used for the temperature measurement in LHD [3,4]. These lines can be simultaneously measured using a space-resolved EUV spectrometer installed in LHD [5] and the line ratios are only sensitive to the electron temperature at $n_e \leq 10^{14}$ cm^{-3} which is an electron density range of the ergodic layer in LHD. The two-dimensional measurement of electron temperature in the ergodic layer is attempted based on the NeVIII line ratio. The intensity ratio used in this report is indicated by a ratio in photon numbers between relevant two spectral lines.

2. Possible combinations of intensity ratio for Be-like NeVII and Li-like NeVIII

Line emissions of NeI-VI are usually located in outer side of the ergodic layer due to the relatively low ionization energies, E_i, e.g., E_i=158eV for NeVI, while He-like NeIX (E_i=1196eV) and H-like NeX (E_i=1362eV) are located inside the LCFS due to the high ionization energy. Taking into account the temperature range of the ergodic layer, the use of Be-like NeVII (E_i=207eV) and Li-like NeVIII (E_i=239eV) seems to be the best choice for the present purpose.

Table I. Line pairs of neon for edge electron temperature measurement.

Ionization stages	Line pairs	
	Line 1	Line 2
Ne VII (Be-like)	465.220Å: $2s^2\ ^1S_0$ - $2s2p\ ^1P_1$	*97.496Å: $2s^2\ ^1S_0$ - $2s3p\ ^1P_1$
Ne VIII (Li-like)	770.410Å: $1s^22s\ ^2S_{1/2}$ - $1s^22p\ ^2P_{3/2}$ 780.325Å: $1s^22s\ ^2S_{1/2}$ - $1s^22p\ ^2P_{1/2}$	88.082Å: $1s^22s\ ^2S_{1/2}$ - $1s^23p\ ^2P_{3/2}$ 88.120Å: $1s^22s\ ^2S_{1/2}$ - $1s^23p\ ^2P_{1/2}$
	*98.116Å: $1s^22p\ ^2P_{1/2}$ - $1s^23d\ ^2D_{3/2}$ *98.260Å: $1s^22p\ ^2P_{3/2}$ - $1s^23d\ ^2D_{5/2}$ *98.275Å: $1s^22p\ ^2P_{3/2}$ - $1s^23d\ ^2D_{3/2}$	88.082Å: $1s^22s\ ^2S_{1/2}$ - $1s^23p\ ^2P_{3/2}$ 88.120Å: $1s^22s\ ^2S_{1/2}$ - $1s^23p\ ^2P_{1/2}$
	102.911Å: $1s^22p\ ^2P_{1/2}$ - $1s^23s\ ^2S_{1/2}$ 103.086Å: $1s^22p\ ^2P_{3/2}$ - $1s^23s\ ^2S_{1/2}$	88.082Å: $1s^22s\ ^2S_{1/2}$ - $1s^23p\ ^2P_{3/2}$ 88.120Å: $1s^22s\ ^2S_{1/2}$ - $1s^23p\ ^2P_{1/2}$
	102.911Å: $1s^22p\ ^2P_{1/2}$ - $1s^23s\ ^2S_{1/2}$ 103.086Å: $1s^22p\ ^2P_{3/2}$ - $1s^23s\ ^2S_{1/2}$	*98.116Å: $1s^22p\ ^2P_{1/2}$ - $1s^23d\ ^2D_{3/2}$ *98.260Å: $1s^22p\ ^2P_{3/2}$ - $1s^23d\ ^2D_{5/2}$ *98.275Å: $1s^22p\ ^2P_{3/2}$ - $1s^23d\ ^2D_{3/2}$

*NeVII 97.496Å is blended with NeVIII 98.116-98.275Å.

Possible candidates of the line pair for NeVII and NeVIII are listed in table I. The best line pair for the electron temperature measurement is to use the ratio of 2s-3p to 2s-2p transitions because the energy difference between the two transitions is large. That is, the ratios of I(97.496Å)/I(465.220Å) for NeVII and I(88.082Å+88.120Å)/I(770.410Å+780.325Å) for NeVIII can give the best solution. However, the wavelengths of these line pairs are too much separated each other. In particular, the NeVIII 2s-2p resonance transition is completely out of the wavelength range in the present EUV spectrometer. Although the NeVII 2s-2p resonance transition can be measured, two different discharges are necessary to measure the line ratio due to a limited wavelength interval of the EUV spectrometer. In practice, the

electron temperature from the NeVII 2s-2p transition measured using two discharges shows a large uncertainty. A small change in the edge plasma condition between the two discharges with neon puff brings a big uncertainty. On the other hand, the NeVII 2s-3p transition at 97.496Å is blended with NeVIII 2p-3d transitions at 98.116-98.275Å. It is also difficult to measure the line ratio using such transitions. At present, therefore, only the choice for the edge temperature measurement using neon is to use the line intensity ratio of NeVIII 2s-3p (88.082Å+88.120Å) to 2p-3s (102.911Å +103.086Å) transitions. Fortunately, no other lines are blended with these lines and the wavelengths of both lines closely exist. It enables us to measure the line ratio in a single discharge. Furthermore, the sensitivity of the EUV spectrometer can be expected to be the same if the two wavelengths are close each other.

3. Vertical profiles of electron temperature from Li-like NeVIII intensity ratio

The vertical profile of the NeVIII line emissions is plotted in Fig. 1(a). The vertical position of each observation chord is carefully calibrated using a toroidal slit with rectangular-corrugated edge installed between EUV spectrometer and LHD. The position of LCFS calculated by variation moments equilibrium code (VMEC) is indicated with dashed line as Z_{LCFS}=437mm. It is then clear that the NeVIII emissions are located inside the ergodic layer. The vertical profile in the intensity ratio of NeVIII 2s-3p to 2p-3s transitions, obtained from Fig. 1(a), is shown in Fig. 1(b). The ratio starts to decrease with increase in the vertical range near the helical coils (400≤Z≤485mm), while it roughly keeps

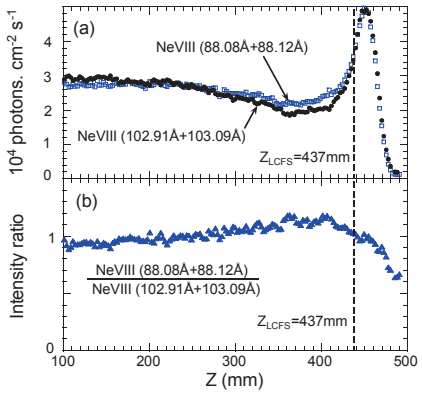

Fig.1 (a) Vertical profiles of NeVIII lines observed from horizontally elongated plasma cross section in R_{ax}=3.75m configuration and (b) intensity ratio calculated from (a). Position of LCFS is denoted with Z_{LCFS} (dashed line).

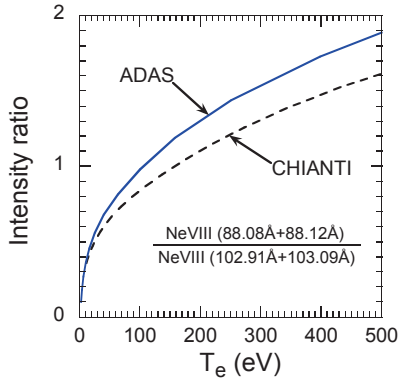

Fig.2 Line intensity ratio of NeVIII (3p-2s)/(3s-2p) calculated from ADAS (solid line) and CHIANTI (dashed line) as a function of electron temperature.

Atomic computer codes of ADAS [6] and CHIANTI v6.02 [7] with collisional-radiative (CR) model are used for edge electron temperature determination. ADAS originates in Joint European Tokamak (JET) experiments. At present it is commonly used for the fusion study, in particular, for the edge plasma study. CHIANTI is a database of assessed atomic parameters and transition rates necessary for the calculation of the emissivity. It is available for optically thin emissions in the 1–2000 Å range. The intensity ratios calculated at electron density $n_e=10^{13}$cm^{-3} are shown in Fig. 2 as a function of electron temperature. The line intensity ratio from ADAS is larger in the whole temperature range than that from CHIANTI. The

difference may be originated in different atomic database used in the codes. Discrepancy in the ratio between the two different results is 15% at T_e=50eV and 17% at T_e=239eV which corresponds to the ionization energy of Ne^{7+} ion. The ratio is entirely insensitive to the electron density, at least, below $n_e=10^{14}cm^{-3}$.

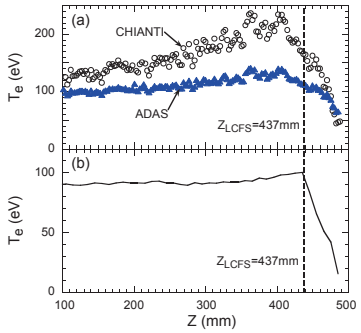

Fig.3 Vertical profiles of edge electron temperature obtained from (a) measurement and (b) simulation. Position of LCFS is denoted with Z_{LCFS}.

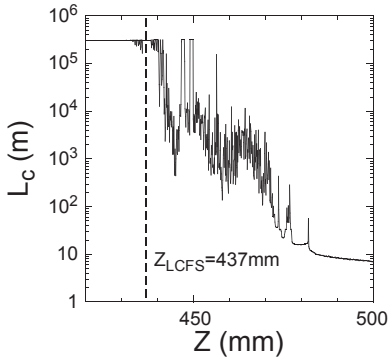

Fig.4 Vertical profile of magnetic field connection length, L_c, in ergodic layer.

The vertical profiles of electron temperature determined from NeVIII intensity ratio are shown in Fig. 3(a). Since the peak position of NeVIII is located near Z=450mm (see Fig. 1(a)), the electron temperature from Z=100 to Z=450mm in Fig. 3(a) indicates the chord-integrated edge temperature in a narrow radial region where the Ne^{7+} ion exists in the ergodic layer. Therefore, the radial profile in the ergodic layer can be expressed in the range of 450≤Z≤490mm. As seen in the figure the CHIANTI gives higher temperature than the ADAS. The spatial resolution in the measurement is 10cm and 2.5cm in the toroidal and vertical directions, respectively.

The edge temperature profile is simulated with three-dimensional edge transport code, EMC3-EIRENE. The result is shown in Fig. 3(b). In the simulation the effect of chord-integration is considered. The edge temperature simulated here indicates roughly 90eV at X-point region of 100≤Z≤300mm. This value shows a reasonably good agreement with the temperature from ADAS. The electron temperature at LCFS obtained from the present method is compared with Thomson scattering diagnostics, i.e., 110eV for ADAS, 170eV for CHIANTI and 120eV for Thomson. The comparison is also in a good agreement with the temperature from ADAS. Therefore, it seems that the ADAS can give accurate emission rate at least in the present transition.

Magnetic field connection length in the ergodic layer is calculated as shown in Fig. 4. It forms a complicate structure due to the appearance of many small and large island chains in the ergodic layer. At Z≥485mm the magnetic field changes the direction and the connection length is shorter. Therefore, the plasma cannot be sufficiently sustained in such a region. A temperature shoulder is appeared near Z=470mm in Fig. 3(b). It reflects a sudden change in the connection length (see Fig. 4). A similar shoulder can be also observed in the temperature profile from the present measurement (see Fig. 3(a)). However, the peak position in the temperature profile is clearly different between the measurement and simulation, whereas the same spatial resolution is adopted in the simulation. The reason is not clear at present. The measured edge boundary temperature at Z=485mm is larger than the simulated one. It

suggests that a smaller cross-field transport coefficient is required to explain the transport in the ergodic layer.

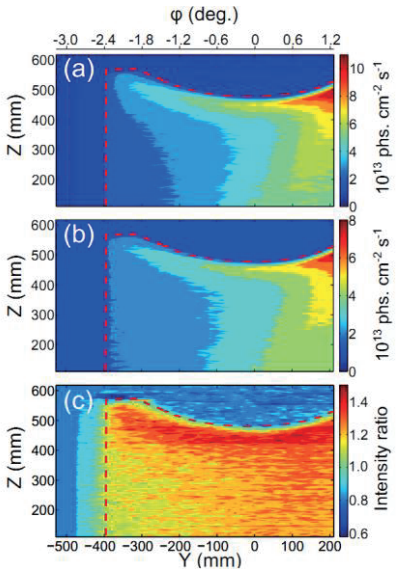

Fig.5 2-dimensional distributions of NeVIII (a) 2s-3p: 88 Å, (b) 2p-3s: 103 Å and (c) line intensity ratio of 2s-3p/2p-3s.

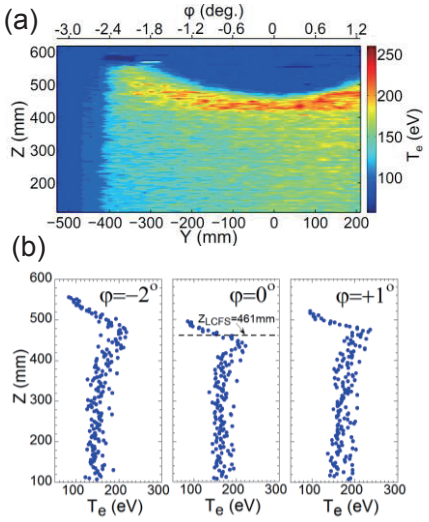

Fig.6 (a) 2-D distribution of edge T_e from NeVIII intensity ratio and (b) vertical profiles of edge T_e at different toroidal positions of φ=-2°, 0° and +1°. Position of LCFS is denoted with dashed line at φ=0°.

4. Two-dimensional distribution of electron temperature from Li-like NeVIII intensity ratio

2-D distribution of NeVIII line intensities are shown in Figs. 5 (a) and (b). The intensities decrease during the scan from Y=200 mm to -400 mm as a function of time, since the electron density gradually decreases. The area where the plasma exists is indicated in the 2-D distribution with dash line. The observation chord from Y=-400 mm to -520 mm is hidden by the spectrometer port and the plasma is absent at upper region above roughly Z=500 mm. The strong intensity of NeVIII near Y=200 mm and Z=500 mm is due to the Ne gas puffing at the beginning of ECH discharges. The NeVIII is located near the LCFS at all poloidal positions. The 2-D distribution of line intensity ratio, NeVIII 2s-3p/2p-3s, calculated from Figs. 5(a) and (b) is shown in Fig. 5(c). Although a considerably large non-uniformity is seen in the two-dimensional intensity distribution (see Figs. 5 (a) and (b)) based on the parameter change during the discharge, it can be deleted when the intensity ratio is taken.

The 2-D T_e distribution is analyzed from Fig. 5(c) and ADAS code in Fig. 2. The result is shown in Fig. 6(a). Although the electron temperature evaluated from NeVIII intensity ratio distributes in range of 130 - 170 eV in most of the region, it tends to increase when the radial position moves to the region near helical coils. The vertical profiles at three different toroidal positions of $\varphi=-2^o$, 0^o and $+1^o$ are reconstructed from Fig. 6(a), as shown in Fig. 6(b). The temperature profile in the ergodic layer can be clearly seen at the region near helical coils, i.e., 480≤Z≤560 mm at -=φ2 ,°440≤Z≤500 mm at φ=0° and 480≤Z≤520 mm at +=φ1°. It is clear that the temperature gradient in the ergodic layer is steeper depending on the thickness of the ergodic layer, when the observation chord moves from Z=100 to 500mm. It also indicates that the temperature in the ergodic layer has a similar value even if the poloidal position is different, at least in the vicinity of Z~450mm. The temperature profile at the place near helical coils gives the maximum value at the radial location where the observation chord positions a little inside the LCFS.

On the contrary, the temperature in the vicinity of separatrix X-point, i.e., 100≤Z≤400 mm at φ=-2°, 0° and +1°, is constant against the vertical position whereas the structure of stochastic magnetic field entirely different along the vertical observation chord. Therefore, a clear toroidal structure of the electron temperature is not seen in the vicinity of separatrix X-point at present. The result suggests that the Ne^{7+} ion distributions are the same among different poloidal positions in ergodic layer, although the magnetic field structure in ergodic layer entirely changes at different poloidal positions.

Acknowledgements

This work was partly supported by the JSPS-NRF-NSFC A3 Foresight Program in the field of Plasma Physics (NSFC: No.11261140328, NRF: No.2012K2A2A6000443). This work was also partially carried out under the LHD project financial support (NIFS16ULPP010) and the JSPS KAKENHI Grant Number 16H04088.

References

[1] H.E. Mason and B.C. Monsignori Fossi, Astron. Astrophys. Rev. **6** (1994) 123.

[2] L. Heroux, Proc. Phys. Soc. **83** (1964) 121.

[3] E.H.Wang, S.Morita, M.Kobayashi, I. Murakami, M.Goto and C.F.Dong, Rev. Sci. Instrum. **83** (2012) 10E509.

[4] E.H.Wang, S.Morita, C.F.Dong, M.Goto, I. Murakami and T.Oishi, Plasma Fusion Res. **8** (2013) 2402176.

[5] H.M. Zhang, S. Morita, T. Oishi, M. Goto and X.L. Huang, Jpn.J.Appl.Phys. **54** (2015) 086101.

[6] H. P. Summers, Atomic Data and Analysis Structure, JET Joint Undertaking Report JET-IR (94) 06 (1994).

[7] K.P. Dere, E. Landi, P.R. Young, G. Del Zanna, M. Landini and H.E. Mason, Astron. Astrophys. **498** (2009) 915.

Effective Recombination Rates for Tungsten Ions Derived with a Collisional-Radiative Model

I.Murakami[1,2] and A. Sasaki[3]

[1]National Institute for Fusion Science, National Institutes of Natural Sciences,Toki, Gifu, 5009-5292, Japan
[2]SOKENDAI (Graduate University for Advanced Studies), Toki, Gifu, 509-5292, Japan
[3]Kansai Photon Science Institute, National Institutes for Quantum and Radiological Science and Technology, Kizugawa, Kyoto 619-0215, Japan

Abstract

Although recombination rates of tungsten ions are highly required for the transport study and the spectroscopic diagnostics of tungsten in fusion plasmas, the rates are not fully studied yet. We applied our algorithm-based collisional-radiative model to tungsten ions in order to derive the effective ionization and recombination rate coefficients. The algorithm can construct a set of electron configurations which are important for population kinetics. We compared the derived effective recombination rates of W^{29+} and W^{28+} ions with other works and found that our rates were nearly one-order of magnitude larger than the others at the electron temperature of ~100 eV. The inclusion of autoionizing levels of inner-shell excited states such as $4s4d^{10}nl$ and $4s4d^{9}4fnl$ for W^{28+} ions enhances the effective recombination rate coefficients as the contribution of the dielectronic recombination channels increase. We assumed the outer-shell electron nl with n up to 8 as the excited levels in the model and this is not enough to include sufficient channels for dielectronic recombination process. We need to extend our model to include higher n shell levels for future study.

Keywords: tungsten, recombination rates, collisional-radiative model, computer algorithm, atomic structure

1. Introduction

Tungsten as one of the plasma-facing materials in fusion devices becomes a harmful impurity in plasmas, since tungsten is not fully ionized even in the core plasma of ITER with the electron temperature of 15-30 keV and a large amount of radiation power from the partially ionized tungsten would reduce the temperature of the core plasma. We need to know the tungsten behavior in plasmas by using spectroscopic method and the reliable atomic data and the spectroscopic model is required to analyze tungsten spectra. During last decades many spectroscopic studies on tungsten ions have been carried out and various spectra with different plasma temperature are obtained for wide wavelength regions. Tungsten spectra of extreme ultraviolet region for plasma with electron temperature 1-2 keV have characteristic feature so-called Unresolved Transition Array (UTA) at 4.5-7 nm (e.g. [1]). This structure is produced by overlapped numerous lines of 4d-4f and 4p-4d transitions of W^{25+} - W^{34+} ions [2]. For higher temperature (>3keV) plasmas the UTA disappears and discrete lines appears instead [3]. At 1.5-3.5 nm wavelength region, there

are many peaks like sawteeth are found and each peak is identified as 4f-5g, 4f-6g, and other n = 5-4 transitions from different charge states of W^{24+} - W^{33+} [2-4]. The peak wavelength shifts toward shorter wavelength as the charge state of the ion increases and they are useful to estimate abundance distribution of tungsten ions in plasmas [2].

Several theoretical groups attempted to reproduce the UTA feature at 4.5-7 nm by constructing collisional-radiative (CR) models [2,5], but the UTA is not well reproduced yet. So far the recombination processes are not included in any CR models for tungsten and Pütterich et al. [5] suggested that dielectronic recombination (DR) processes in plasmas could contribute to the UTA structure. The recombination processes are also important for the tungsten transport study and the charge state distribution in plasmas. However, the theoretical studies on the DR rate coefficients of tungsten ions are limited for some charge states as summarized by Li et al. [6]. Atomic structures of tungsten ions with many electrons are complex, and the comprehensive study is not easy.

Generally a CR model calculates population densities of excited states with steady-state assumption and it can give radiative power loss and emission spectra. Effective ionization and recombination rates obtained by the CR model including density effect are useful to calculate charge state distribution. We have developed an algorithm-based CR model in which the set of atomic energy levels in the model is determined after systematic convergence studies [7,8]. This method allows us to construct more comprehensive atomic structure than those constructed by conventional ways. We apply this model to study the effective ionization and recombination rate coefficients of tungsten ions systematically and compare with rates obtained by other theoretical studies. Here in this report we focus on the effective recombination rate coefficients. In the following part, we introduce our CR model in section 2, and show some comparison of the effective recombination rates in section 3. In section 4 we discuss the difference and summarize the report.

2. Algorithm-based collisional-radiative model

Details of the algorithm-based CR model are described in [7,8], so brief description on the model is given here. In order to construct more comprehensive atomic structure of tungsten ions, we treat configuration averaged or *nl* averaged energy levels throughout the model. The atomic structure is constructed using the algorithm in the following way. A set of energy levels is created by adding one outermost electron *nl*, with *n* up to 8 and *l* up to 4, to the core states of one-charge higher ion. The core states are selected as the created levels contribute to the population kinetics through the DR process. Number of the core states is increased by including higher excited states and the convergence is checked with the mean charge state and the radiation power rate. The mean charge decreases and the radiative power rate increases with increasing number of the core states, and they converge with 30-50 core states, as described in ref. [7,8]. A set of the energy levels are determined recursively by descending the charge state with the same algorithm.

The atomic data used in the CR model is calculated as follows: The energy levels, radiative transition probabilities, and autoionization rates are calculated using the HULLAC code [9] without configuration interaction. The electron-impact ionization and excitation, and radiative recombination rate coefficients are

calculated using Lotz's [10], Mewe's [11], and Kramers' [12] empirical formulae, respectively. Three-body recombination rate coefficients are calculated as an inverse process of collisional ionization in detailed balance. The DR and excitation-autoionization processes for autoionizing states are intrinsically included in the CR model.

This CR model produces the effective ionization and recombination rates for given electron temperature and density, which are used to calculate the charge state distribution. Obtained distribution as a function of electron temperature is different from other works such as by Pütterich et al. [13], but the abundance ratio of W^{45+} to W^{44+} ions agrees well with the measurements in JT-60SA [14].

3. Effective recombination rate coefficients

We obtained the effective recombination rate coefficients using the algorithm-based CR model for tungsten ions with charges q = 11-63. In the model, we considered neighboring 7 ions and we assumed electron density as $10^{14}cm^{-3}$. The calculations were performed for electron temperature from 100eV to 5keV. The DR process is implicitly included as a combined process of the dielectronic capture and following radiative decay to a bound state.

Figure 1 shows examples of the effective recombination rates from W^{29+} to W^{28+} ions (Fig.1a) and from W^{28+} to W^{27+} ions (Fig.1b). The ground states of W^{29+} and W^{28+} ions are $4d^64d^9$ and $4d^64d^{10}$, respectively. For comparison, the effective recombination rates from ADAS database [15] (data file "acd50_w.dat") and the dielectronic recombination rates obtained by Li et al. [16] (W^{29+}) and Safronova et al. [17] (W^{28+}) are plotted. The ADAS recombination rate is originally modified ADPAK data [18] by Pütterich et al. [19] and processed in the ADAS's CR model. The recombination rate coefficients in ADPAK data were calculated with an averaged ion model and Pütterich et al. derived the modification factors for the recombination rate to fit to spectroscopic measurements in ASDEX Upgrade. Data of Li et al. (2012) and Safronova et al. (2011) are the calculated dielectronic recombination rate coefficients. Our recombination rates are about one-order of magnitude larger than the ADAS rates at ~100 eV, and become closer at ~5 keV. The both DR rates of Li et al. and Safronova et al. are much smaller by factor 2 – 10 or more at 100 eV - 5 keV. We did not obtain the rates at electron temperature below 100eV since configuration averaged levels in the model are not suitable to estimate the recombination rates for low energy region. In addition W^{28+} and W^{27+} ions are not expected to be abundant in such low temperature and the recombination rates of these ions would not be important in fusion plasmas.

4. Discussion and summary

The difference of the recombination rates comes mainly from the different atomic structure, i.e. energy levels used in the models. The autoionizing states included in the calculations are different. Figure 2 shows the lower parts of the energy levels included in the model for W^{28+} and W^{27+} ions. The dielectronic capture occurs to the autoionizing excited states above the threshold levels, $4d^9$ and $4d^{10}$ for W^{28+} and W^{27+} ions, respectively. For the case of the recombination from W^{29+} to W^{28+} ions (Figs. 1a and 2a), the DR process through the inner-shell excited states such as $4s4d^{10}nl$ and $4s4d^94fnl$ states are not considered in the model of Li et al., and the DR channels through such inner-shell excited states can enhance the DR rate. For the

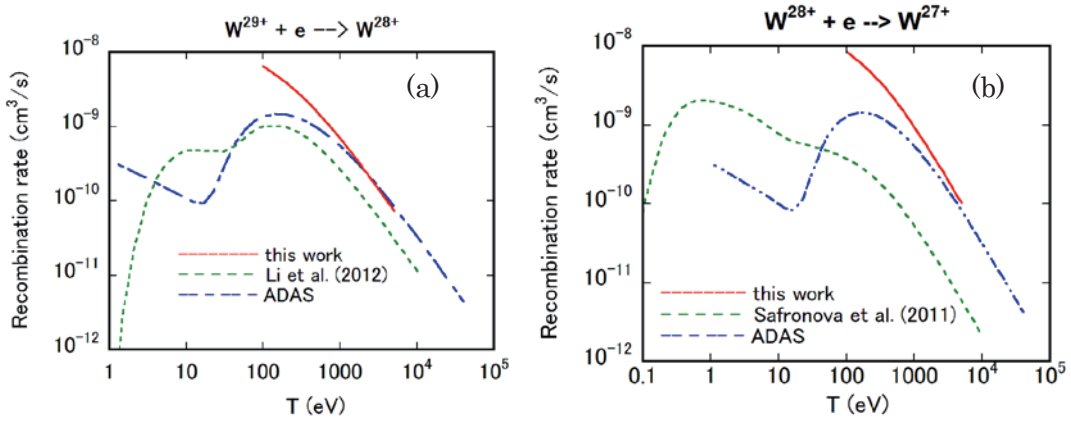

Figure 1. The effective recombination rate coefficients of this work (solid lines) and of ADAS (dot-dashed lines) for W^{29+} and W^{28+} ions. Dielectronic recombination rate coefficients calculated by Li et al. (W^{29+}) and by Safronova et al. (W^{28+}) are also plotted (dashed lines) for comparison.

case of recombination from W^{28+} to W^{27+} ions (Figs. 1b and 2b), the DR process through the inner-shell excited states such as $4p^64d^84f^2nl$, $4p^54d^{10}4fnl$, and $4s4p^64d^{10}4fnl$ are not considered in the model of Safronova et al. Lack of the DR channels through these inner-shell excited levels results in much lower DR rate than ours.

On the other hand, as seen in Fig.2, our model has big gaps below the core states in the energy level diagrams, since we only included outermost electron n up to 8. Li and Safronova included high n levels up to 1000 by using scaling law. The inclusion of such high n levels enhances the DR rate about factor 5 (W^{29+} case). We need to extend our model to include higher n levels for constructing more comprehensive atomic structure.

As a summary, we found that the algorithm-based CR model for tungsten ions is useful to construct more comprehensive atomic structure than those constructed using the conventional ways, and useful to estimate the effective recombination rate coefficients, since many DR channels through the inner-shell

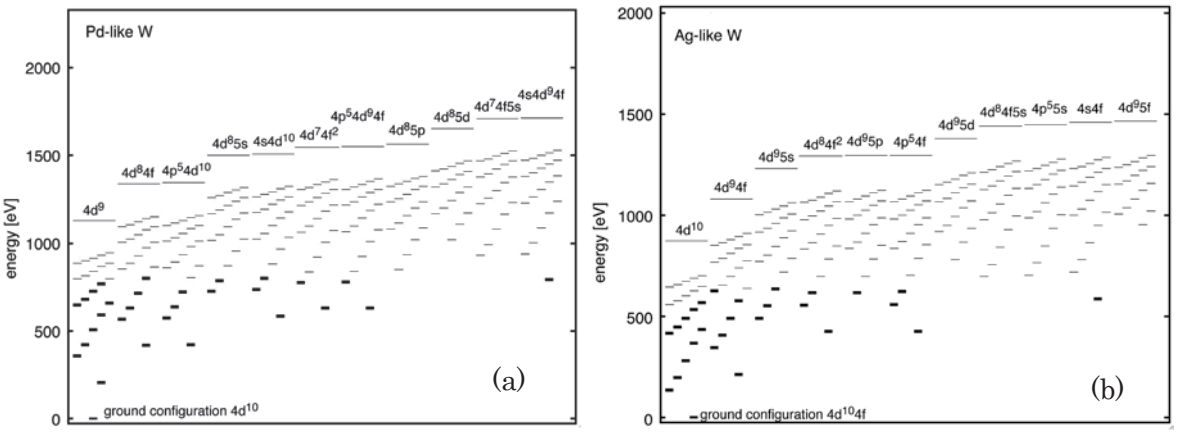

Figure 2. Part of energy level diagrams for W^{27+} and W^{28+} ions. The core states are indicated as longer bars and an outermost nl electron is added to construct an energy level which indicated as a short bar.

excited states can be included in the model. Such inner-shell excited states are not fully taken into account in the conventional models, which show much lower DR rate coefficients at electron temperature 100 eV – 1 keV. On the other hand, we did not include enough number of higher *n* levels which can also enhance the DR rates for lower temperature collisions. We need to extend our model to include such high *n* levels for future study.

Acknowledgements

This work was supported partly by KAKENHI (JSPS grant-in-aid for scientific research) (B) 23340185, (A) 23246165, and (B) 16H04623, and partly by the JSPS-NRF-NSFC A3 Foresight Program in the field of Plasma Physics (NSFC: No.11261140328, NRF: No.2012K2A2A6000443).

References

[1] C. S. Harte et al., J. Phys. B: At. Mol. Opt. Phys. **43** (2010) 205004.
[2] I. Murakami et al., Nuclear Fusion **55** (2015) 093016.
[3] S. Morita et al., AIP Conf. Proc. **1545** (2013) 143.
[4] H. A. Sakaue et al., AIP Conf. Proc. **1438** (2012) 91.
[5] T. Pütterich et al., AIP Conf. Proc. **1545** (2013) 132.
[6] M. Li et al., Plasma Sci. Tech. **16** (2014) 182.
[7] A. Sasaki, High Energy Density Phys. **9** (2013) 325.
[8] A. Sasaki and I. Murakami, J. Phys. B: At.Mol. Opt. Phys. **46** (2013) 175701.
[9] A.Bar-Shalom, M.Klapisch and J.Oreg, J.Quant.Spectr.Radiant.Trans. **71** (2001) 169.
[10] W. Lotz, Z. Phys. **216** (1968) 241.
[11] R. Mewe, Astron. Astrophys. **20** (1972) 215.
[12] H. Kramers, Philos. Mag. **46** (1923) 836.
[13] T. Pütterich et al., Nucl. Fusion **50** (2008) 085016.
[14] T. Nakano, and the JT-60 team, J. Nucl. Mater. **415** (2011) 5327.
[15] H. P. Summers, The ADAS Users Manual ver.2.6 (2004), http://www.adas.ac.uk/.
[16] B. W. Li et al, Phys. Rev. A **85** (2012) 052706.
[17] U. Safronova et al., J. Phys. B: At. Mol. Opt. Phys. **44**(2011) 035005
[18] D. Post et al., At. Data Nucl.Data Table **20** (1977) 397.
[19] T. Pütterich et al. Plasma Phys. Control. Fusion **50** (2008) 085016.

Fundamental Atomic Process in Source Development for Beyond EUV Lithography and other applications

B. Li [1], X. M. Chen [1], X. Y. Qiu[1], T. Higashiguchi [2], H. Ohashi[3], C. Z. Dong[4], P. Dunne[5] and G. O'Sullivan[2]

[1] School of Nuclear Science and Technology, Lanzhou University, Lanzhou 730000, China

[2] Department of Electrical and Electronic Engineering, Faculty of Engineering, Utsunomiya University, Yoto 7-1-2, Utsunomiya, Tochigi 321-8585, Japan

[3] Graduate School of Science and Engineering for Research, University of Toyama, Toyama, Toyama 930-8555, Japan

[4] Key laboratory of Atomic and Molecular Physics & Functional Materials of Gansu Province, College of Physics and Electronic Engineering, Northwest Normal University, Lanzhou, 730070, China

[5] School of Physics, University College Dublin, Belfield, Dublin 4, Ireland

Abstract

Development of EUV/SXR sources with emission at wavelengths less than 10 nm has moved from being a subject of interest for next generation semiconductor lithography to one for both nanoscale surface patterning and imaging. Systematic calculations for UTA positions were performed for elements with atomic number Z = 49–92, with the help of both laser produced plasmas (LPPS) and Large Helical Device (LHD) experimental measured spectra it was found that the peak such UTAs in optically thin plasmas in the extreme ultraviolet region follows a quasi-Moseley's law.

We carried out a detailed calculation on dielectronic recombination rate coefficients of Ne-, Rh-, Pd- and Ag-like W [7]. Excellent agreement has been found for Ne-like W while a large discrepancy was found for Pd-like W, which implies that more *ab initio* calculations and experimental measurements are badly needed.

Keywords: EUV, UTA, tungsten, dielectronic recombination

1. Introduction

The behavior of the highly-charged ion (HCI) in heavy ion element plasmas in the extreme ultraviolet (EUV) or soft x-ray (SXR) spectral regions is currently of major interest and has been motivated by their application in a number of high profile areas of science and technology, such as W-inclusion as plasma-facing components (PFCs) in magnetic confinement fusion, Tin (Sn) and gadolinium (Gd) LPPs are proposed for 13.5-nm and 6.x-nm EUV lithography as well as laboratory plasma light sources for x-ray microscopy in the water window, 2.3–4.4 nm, and the carbon window, 4.4–5.0 nm [1]. These sources exploit the advantage that $4p^6 4d^N$-$4p^6 4d^{N-1} 4f$+$4p^5 4d^{N+1}$ (n = 4–n = 4, Δn = 0) unresolved transition arrays (UTAs) in several charge states appear at almost same wavelength [2] in spectra from LPPs of these elements. Systematic calculations for UTA positions were performed for elements with atomic number Z = 49–92 that enabled the peak wavelength of the 4d-4f and 4p-4d component transitions of the 4-4 UTAs to be

estimated. For a complete understanding of plasma emission, reliable atomic data are needed. Of particular, reliable dielectronic recombination (DR) rate coefficients are crucial for the modeling of the ionization balance in plasmas. We carried out a detailed calculation on dielectronic recombination rate coefficients of Ne-, Rh-, Pd- and Ag-like W [3,4].

2. Variation of UTAs with Z

As earlier studies on W and Tb [5] demonstrated that for n = 4 - n = 4 transitions the emission is dominated by Pd-, Ag- and Rh-like lines, i.e. the spectra containing fewest lines where the emission is not divided amongst many transitions. Figure 1 show measured emission spectra of Bi, Pb and Au in LHD plasmas associated with calculated weighted transition probabilities using Cowan code.

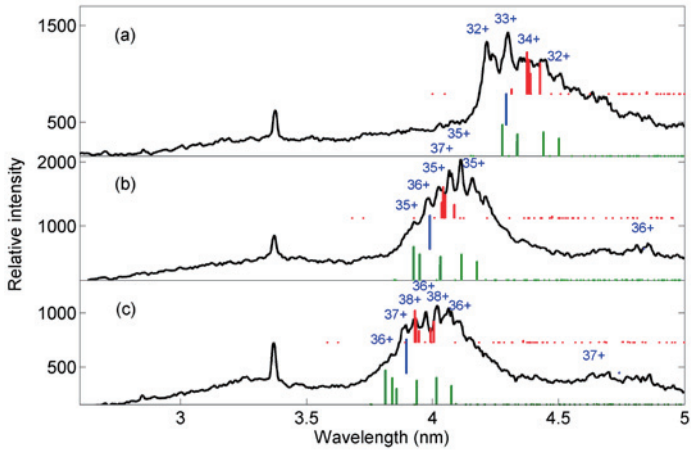

Figure 1. Comparisons of (a) Au, (b) Pb and (c) Bi LHD spectra with calculated weighted transition probabilities using Cowan code for Ag- (green), Pd- (blue) and Rh-like (red) ions in n=4 – n=4 UTAs. Prominent transitions are labeled by the charge state [6].

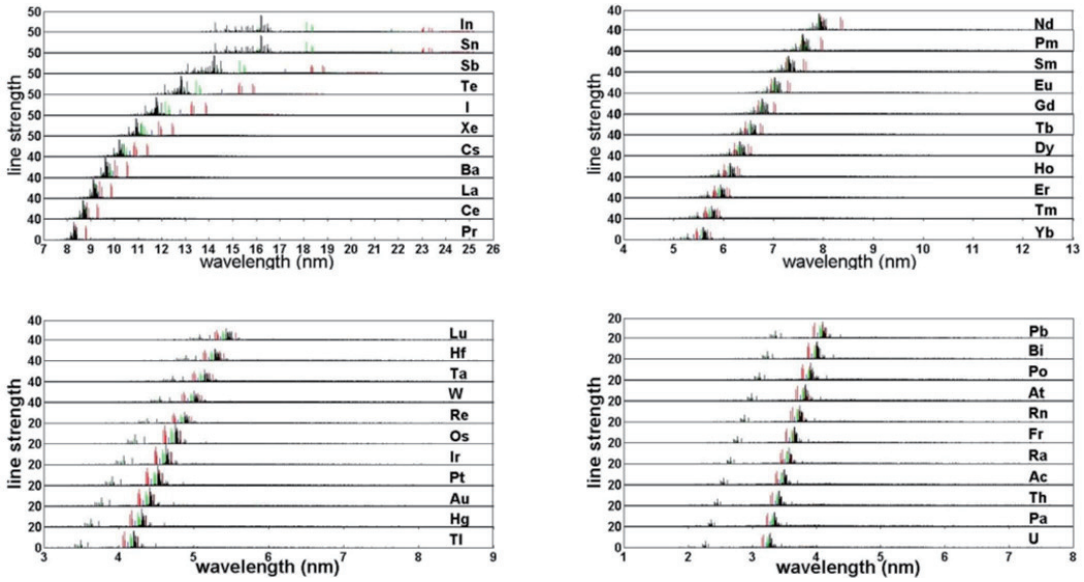

Figure 2. Calculated position of n=4 – n=4 transitions in key ions in elements from indium (Z=49) to uranium (Z=92) [7].

Figure 2 shows the calculated positions of the strongest n=4 – n=4 transitions for four stages of each element corresponding to Ru-like (red), Rh-like (blue), Pd-like (green) and Ag-like (black) ions. From this plot it is clear that maximum overlap between emission from different stages occurs in the lanthanides and

corresponds, from an atomic physics viewpoint, to the localization of the 4f wavefunction in the ionic core where its overlap with the 4d changes little with ion stage. For Lower Z elements the emission extends over a broader energy range due to differing degrees of 4f localization while the 4p spin orbit splitting causes the emission to diverge to form two emission regions at the higher Z end. The discrete line emission is dominated by Ag-, Pd- and Th-like ions. For the Hartree-Fock with configuration interaction calculations, the electrostatic Slater-Condon F^k, G^k, and R^k parameters were reduced by 10% while the spin orbit integrals were left unchanged. With the help of both laser produced plasmas (LPPS) and Large Helical Device (LHD) experimental measured spectra, Ohashi and co-workers [8] found that the peak such UTAs in optically thin plasmas in the extreme ultraviolet region follows a quasi-Moseley's law (figure 3).

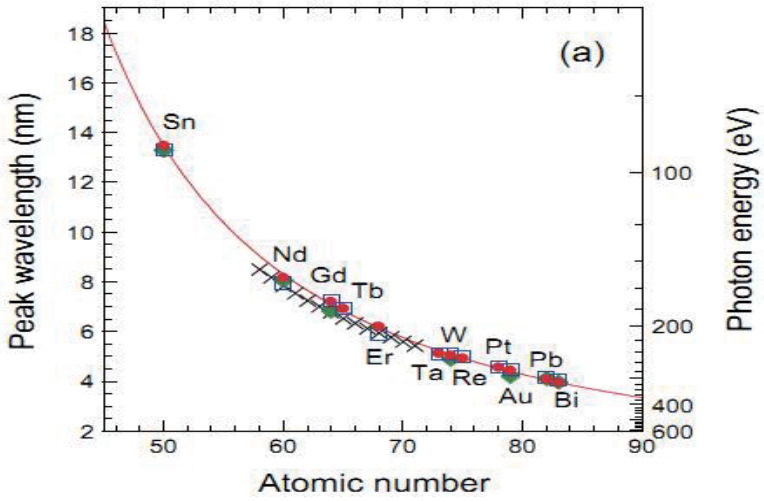

Figure 3. Atomic number dependence of the peak wavelength of n=4 – n=4 UTAs in ps-LPP (red), ns-LPP (blue) and LHD (green) spectra. Calculated peak wavelengths with GRASP are also shown (black). The solid line is an approximated curve for n=4 – n=4 UTAs in ps-LPPs with a power-law scaling, $\lambda = (21.86 \pm 12.09) \times R_\infty^{-1} \left(Z - (23.23 \pm 2.87)\right)^{-(1.52 \pm 0.12)}$ [8].

3. Dielectronic recombination of W ions

The DR process plays an important role in high-temperature plasmas, where it affects both the ionization balance and radiative energy losses. A significant number of publications on computational DR rate coefficients of W ions have appeared for tungsten during the past dacade. However, due to the complexity of the calculations as ions with open 4d and 4f shells are involved, very few *ab initio* level-by-level DR calculations are available for ionic stages lower than W^{34+}. Therefore, DR rate coefficients from the atomic data and analysis structure (ADAS) databases are currently the most widely used to model various fusion plasmas in the nuclear fusion community. The computations of such DR rate coefficients are based on the semiempirical Burgess-Merts formulas and the generalized collisional-radiative framework. The accurancy of such rates is another problem.

We carried out a detailed calculation on dielectronic recombination rate coefficients of Ne-, Rh-, Pd- and Ag-like W. The calculated DR cross section as well as rate coefficients are presented in figure 4(a) and (b), respectively. Very good agreement has been found between experimental measurements and various theoretical predictions.

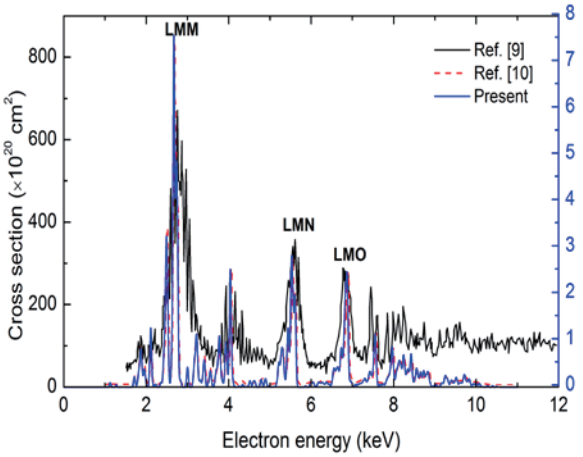

Figure 4(a). Comparison between the present calculated total DR cross section of Ne-like W (solid line) and calculation with the HULLAC code [10] (dashed line) and experimental measurement [9].

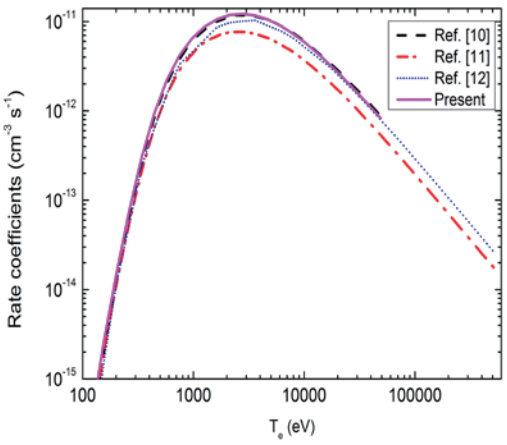

Figure 4 (b) Comparison between present calculated total DR rate coefficients of Ne-like W and other calculations with the HULLAC code [10, 11] and Autostructure code [12].

Present calculated total DR rate coefficients are plotted together with Safronova's result [13] as well as calculations by Foster [14], Pütterich *et al.* [15] and the FLYCHK [16] code in figure 5 (a). Calculated radiative recombination (RR) rate coefficient by Trzhaskovskaya *et al*. [17] are also presented for comparison. However, unlike the Ne-like W case, very big discrepancies are found between the various results. While the only *ab initio* calculation was by Safronova *et al*., further calculations were made to find the possible reasons for the discrepancy of their with our results and the outcome is summarized in figure 5 (b). We carried out four kinds of calculations: model 1: calculation including all doubly excited, non-autoionizing states, model 2: calculation with the same decay channel as Safronova *et al*. but omitting configuration interaction (CI), model 3: same as model 2 but with configuration interaction included, model 4: present calculation with doubly excited autoionzing states $4d^9$4f7g, $4d^9$4f8g, $4d^9$4f9g, $4d^9$6s6p, $4d^9$6s6f, $4d^9$6p6d, $4d^9$6p6f, $4d^9$6p6g, $4d^9$6d6f, $4d^9$6d6g, $4d^9$4f6g and non-autoionizing states $4d^9$4f6g. From figure 5 (b), firstly, we can see that configuration interaction has a big influence on total rate coefficients when T_e is smaller than 10 eV where, as we already k now, DR rate coefficients are sensitive to near-threshold resonances for lower temperature since they depends on $\exp\left(-E_{ij}/kT_e\right)$. Therefore, the present calculated DR rates are less accurate when T_e is below 10 eV. However, CI effects can be ignored for T_e greater than 100 eV. Secondly, inclusion of the omitted states improves the total rate coefficients by around 20%. Thirdly, in Safronova *et al*.'s calculation, for the non-resonant stabilization(NRS) decay channel they only included $4d^9$4fnl, $4d^9$5l5l'and $4d^9$5s6l, while in the present calculations we included all of the doubly excited non-autoionizing states. These decay channels significantly improved the total rate coefficient. We did not include further doubly excited autoionizing states, which will be followed by radiative decay cascade (DAC) transitions into NRS decay channel, as Behar *et al*. [18] have demonstrated that the DR rates are less affected by DAC for heavy elements and thus can be neglected for most applications.

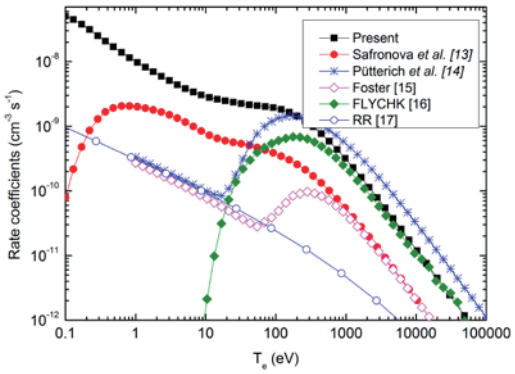

Figure 5(a). Total DR rate coefficients as a function of Te in Pd-like W.

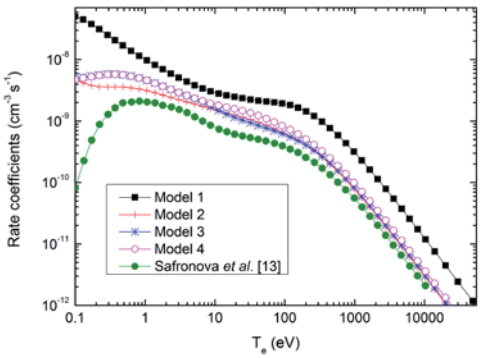

Figure 5(b). Comparison of total DR rate coefficients as a function of Te in Pd-like W by different calculation models.

Considering the current status of these discrepancies, further benchmarking from experimental measurement is of major importance.

Acknowledgements

The LZU group acknowledges support from the Fundamental Research Funds for the Central Universities Grant Nos. lzujbky-2014-9 and lzujbky-2015-71 International scientific collaboration program by Gansu Provincial Science and Technology Department Grant No. 144WCGA163 and National Natural Science Foundation of China Grant Nos. 11404152 and 11505087.

References

[1] G. O'Sullivan, B. Li, P. Dunne, et al., Phys. Scr. **90** (2015) 054002.

[2] G. O'Sullivan and R. Faulkner, Opt. Eng. **33** (1994) 3978.

[3] B. Li, G. O'Sullivan, Y. B. Fu and C. Z. Dong, Phys. Rev. A **85**(2012)012712

[4] B. Li, X. M. Chen, G. O'Sullivan and C. Z. Dong, J. Phys. B **49** (2016) 155201

[5] C. Harte, et al., J. Phys. B **43** (2010) 205004; B. Li, et al., Appl. Phys. Lett. **101** (2012) 013112

[6] H. Ohashi, et al., J. Phys. B **48** (2015) 144011

[7] B. Li, et al., Proc. SPIE **8139** (2010) 81390P

[8] H. Ohashi, et al., Appl. Phys. Lett. **104** (2014) 234107, Appl. Phys. Lett. **106** (2015) 169903

[9] H. Watanabe, et al., Plasma and Fusion Research **2** (2007)027

[10] E. Behar, et al., Phys. Rev. A **59** (1999) 2787

[11] U. I. Safronova, *et al.*, *At. Data Nuc. Data Tables* **95** (2009) 751

[12] S. Preval, *et al.*, *Phys. Rev. A* **93** (2016) 042703

[13] U. I. Safronova, *et al.*, J. Phys. B **44** (2011) 035005

[14] A. Foster, PhD thesis, University of Strathclyde, 2008.

[15] T. Pütterich, R. Neu, R. Dux, *et al.*, Plasma Phys. Control. Fusion **50** (2008) 085016.

[16] http://www.hydkin.de/plotform/index_tungsten.html?submit=W

[17] M. B. Trzhaskovskaya and V. K. Nikulin *At. Data Nucl. Data Table* **99** (2013) 249.

[18] E. Behar, et al., Phys. Rev. A **52** (1995) 3770

Collisional-radiative models for ground-state M1 line emission of highly charged tungsten ions in the LHD

D. Kato[1,2], K. Fujii[3], M. Goto[1,2], T. Oishi[1,2], H.A. Sakaue[1], I. Murakami[1,2], N. Nakamura[4], X.-B. Ding[5], C.-Z. Dong[5], S. Morita[1,2] and LHD Experimental group

[1]National Institute for Fusion Science, Toki 509-5292, Gifu, Japan

[2]Department of Fusion Science, SOKENDAI (Graduate University for Advanced Studies), Toki 509-5292, Gifu, Japan

[3]Graduate School of Engineering, Kyoto University, Kyoto 615-8540, Japan

[4]Institue for Laser Science, The University of Electro-Communications, Tokyo 182-8585, Japan

[5]Colledge of Phys. and Electronic Eng., Northwest Normal University, Lanzhou, 730070, China

Abstract

A collisional-radiative (CR) model is developed to analyze magnetic-dipole (M1) lines emitted by W^{q+} ions in the ground state ($4d^{10}4f^{k}$). Proton collision effects on the M1 line intensities are investigated theoretically with the CR model. In the present study, it is predicted that the proton collision facilitates radiative decay of the sub-valence excited configuration ($4d^{9}4f^{k+1}$) to the ground state, resulting in an enhancement of the M1 line intensity. Based on the present calculations, W^{27+} ion densities in core plasmas of Large Helical Device (LHD) are obtained from experimentally measured intensity profiles of the M1 line.

Keywords: tungsten, visible forbidden line, CR model, proton collision

1. Introduction

Magnetic-dipole (M1) lines of ground-state highly charged tungsten ions in near-UV and visible ranges have diagnostic usefulness for D-T burning ITER plasmas. M1 lines in these wavelength ranges enable the use of fiber optics, and absolute intensity calibration of spectrometers is facilitated with standard lamps. A large number of previously unreported visible emission lines of tungsten ions W^{q+} ($q = 8 - 28$) are measured by using low-energy electron beam ion traps [1,2]. Some of them are identified as the ground-state M1 lines of W^{q+} in accord with theoretical predictions. We succeeded in observing an M1 line at 389.4 nm of ground-state W^{26+} ions ($4f^2\ {}^3H_5 - {}^3H_4$) produced in Large Helical Device (LHD) [3]. Since then, a number of near-UV and visible M1 line emission from W^{q+} ($q = 23 - 28$) have been observed at the LHD [4].

In high-temperature hydrogen plasmas, proton collisions play a role in population of fine-structure levels. Due to the lack of available data, however, it has been neglected in modeling for the tungsten spectra. In the present study, a collisional-radiative (CR) model including proton collision induced (de)excitation in the fine-structure levels is developed to analyze M1 lines emitted by W^{q+} ions in the ground state ($4d^{10}4f^{k}$). Base on the CR model, the proton collision effects on the M1 line intensities are investigated theoretically.

2. Semi-classical perturbation calculations of proton collision cross sections

Effective strength of Coulomb repulsive interaction between W^{q+} and a proton of an impact velocity v is represented by a characteristic parameter: $\mu = qe^2/\hbar v$, where e is the elementary charge and $\hbar$ the reduced planck constant. In cases that $\mu \gg 1$, since the proton cannot penetrate in the vicinity of the target ion, perturbation methods can be used to calculate proton induced excitation cross sections of the target ion. The electric quadruple component is the primary electrostatic proton-W^{q+} interaction which induces transitions in fine-structure levels of the target ion. In a semi-classical perturbation approximation (SCPT-E2), the cross section σ is expressed simply by the electric quadruple transition rate of isolate W^{q+} ions, $B(E2)$,

$$\sigma = \left(\frac{e}{\hbar v_\mathrm{i}}\right)^2 a^{-2} B(E2) f_{E2}(\xi),$$

$$a = \frac{qe^2}{\mu v_\mathrm{i} v_\mathrm{f}}, \qquad \xi = \frac{qe^2}{\hbar}\left(\frac{1}{v_\mathrm{f}} - \frac{1}{v_\mathrm{i}}\right), \tag{1}$$

where μ is the reduced mass of a proton and a target ion, and $v_{\mathrm{i,f}}$ are velocities of incident and scattered protons, respectively. $f_{E2}(\xi)$ is a function given by assuming hyperbolic orbit for the proton in the Coulomb filed centered at the nucleus of W^{q+} [5]. The electric quadruple transition rates are calculated using HULLAC code [6].

Excitation rate coefficients in Fe^{13+} 3p doublet state are calculated and compared with recommended data [7] (Fig. 1). SCPT-E2 cross sections give rate coefficients which coincide with the recommended values

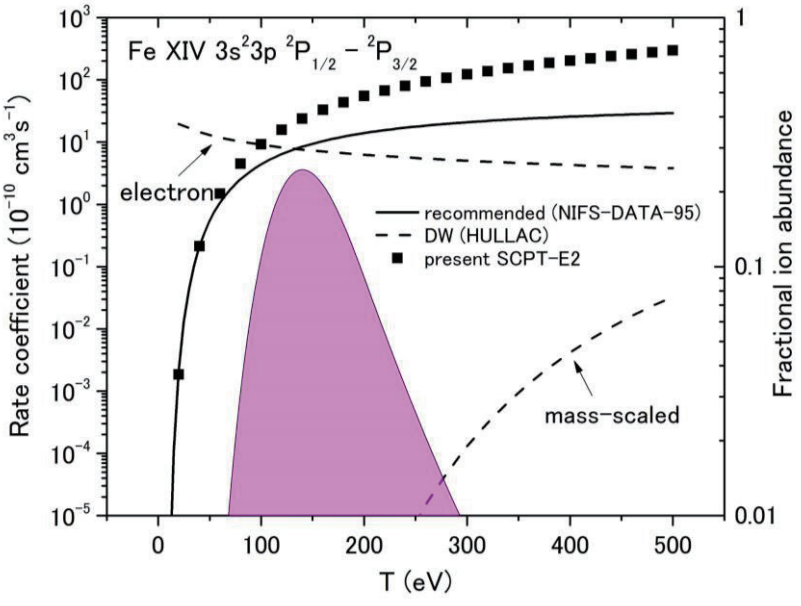

Fig.1 Excitation rate coefficient of Fe^{13+} $3s^2 3p\ {}^2P_{1/2} - {}^2P_{3/2}$. Solid squares are SCPT-E2 results, the solid curve recommended values [7] and dashed curves distorted wave results calculated by using HULLAC code [6]. Ionization equilibrium fractional abundance of Fe^{13+} is also shown in the figure.

at low temperatures but overshoot at high temperatures. About factor of 3 larger at the peak temperature of the equilibrium ion abundance. It is noted that simple mass-scaling of electron distorted-wave cross sections underestimates the rate coefficients by many orders of magnitudes.

3. Fractional population distribution of excited levels and ground-state M1 line intensity of W^{27+}

Fractional populations of excited levels are calculated by the CR model including the proton collision induced (de)excitation. As shown in Fig. 2, the fractional population distribution is drastically changed by proton collision effects. The proton collision facilitates redistribution in populations of quasi-degenerate excited levels in single configurations, which causes depopulation of meta-stable levels in the sub-valence excited $4d^9 4f^2$ configuration. Fractional populations of the ground state are, therefore, increased via $4f - 4d$ allowed transitions from the excited configuration resulting in an enhancement of the ground-state M1 line intensity. It is noted that the $4f - 4d$ EUV emission line intensities are also increased.

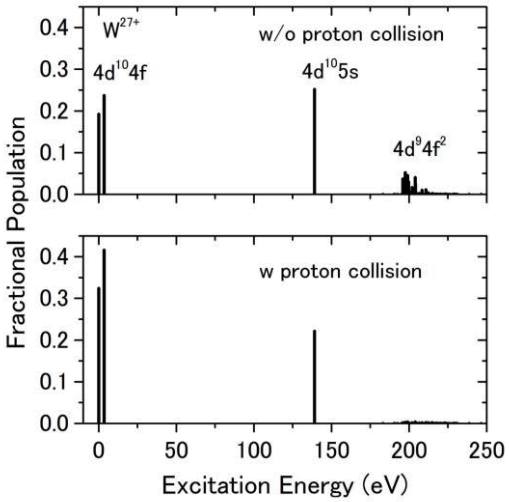

Fig.2 Fractional populations of W^{27+} levels. $n_e = n_p = 10^{13}$ cm^{-3} and $T_e = T_p = 1$ keV are assumed.

Figure 3 shows temperature and density dependences of an M1 line intensity for ground-state W^{27+} ions ($4f\ ^2F_{7/2} - {}^2F_{5/2}$ at 337.7 nm). Remarkable enhancement of the intensity with proton collisions is seen in the figure. Above 700 eV, proton collision rate coefficients among levels in the excited states ($4d^9 4f^2$) exceed electron collision excitation rate coefficients of the upper level of the M1 transition ($4f\ ^2F_{7/2}$), which causes the opposite temperature dependence of the intensity between the lower temperature (electron

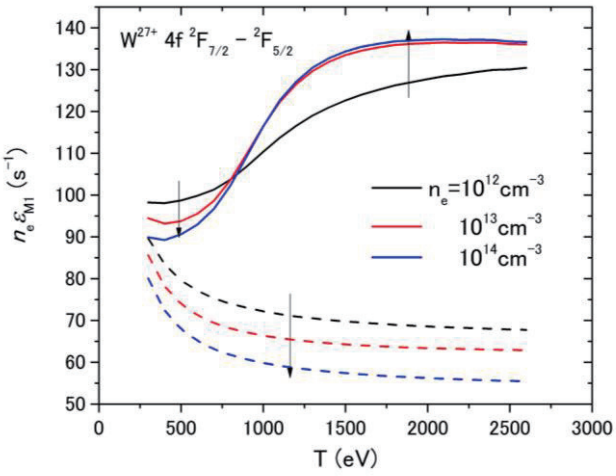

Fig.3 Temperature and density dependences of M1 line intensity of W^{27+} $4f\ ^2F_{7/2} - {}^2F_{5/2}$ at 337.7 nm. Dashed lines are calculations without proton collision.

collision dominant) and higher temperature (proton collision dominant) regions. The M1 intensity is saturated above 10^{13} cm^{-3} in the higher temperature region.

4. Vertical distributions of an M1 line intensity and ion density distribution of W^{27+} ions in LHD

Local line intensities at an effective minor radius r_{eff} on a poloidal cross section are expressed for a given local electron temperature T_{e}, density n_{e}, ion fractional abundance n_q and W density n_{W} as,

$$I_{\mathrm{M1}}(r_{\mathrm{eff}}) = \varepsilon_{\mathrm{M1}}(T_{\mathrm{e}}, n_{\mathrm{e}}) n_{\mathrm{e}} n_q n_{\mathrm{W}}. \qquad (2)$$

In the present calculations, n_q are ionization equilibrium values at the given T_{e} and n_{e}. Figure 4 shows a comparison of the present calculations and experimental measurements. In the measurement, a polyethylene tube containing a tungsten wire (0.6 mm long and 0.15 mm diameter which reads N_{W} about 6.6×10^{17} /pellet) was injected in a LHD discharge. Line emission was observed at 44 lines of sight along the horizontal axis of a horizontally elongated poloidal cross section of the LHD. T_{e} and n_{e} profiles on the poloidal cross section were also measured by Thomson scattering. The present model gives the vertical profiles of good agreements with the measured profile. The proton collision effect increases fractional population of the ground state, which results in an enhancement of the M1 line intensity by 40 - 50 %.

Radial distribution of W^{27+} ions and W density are deduced based on the measured vertical profile (Fig. 5). The initial ion density distribution has a maximum at $r_{\mathrm{eff}} = 0.3$ m. The ionization equilibrium abundance of W^{27+} becomes the maximum at the local electron temperature (about 1.0 keV). The peak position of the radial distribution moves toward the plasma center ($r_{\mathrm{eff}} = 0$) as the temperature at the plasma center decreases with

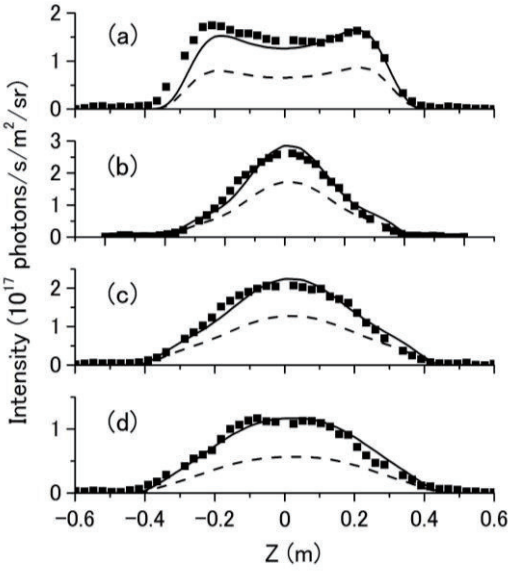

Fig. 4 Vertical distributions of W^{27+} M1 line intensities at (a) t = 4.1, (b) 4.3, (c) 5.0 and (d) 5.6 s. Tungsten pellet is injected at 4.0 s. Solid squares indicate measurement and solid curves calculations, respectively. Dashed lines are the calculation neglecting proton collision effect.

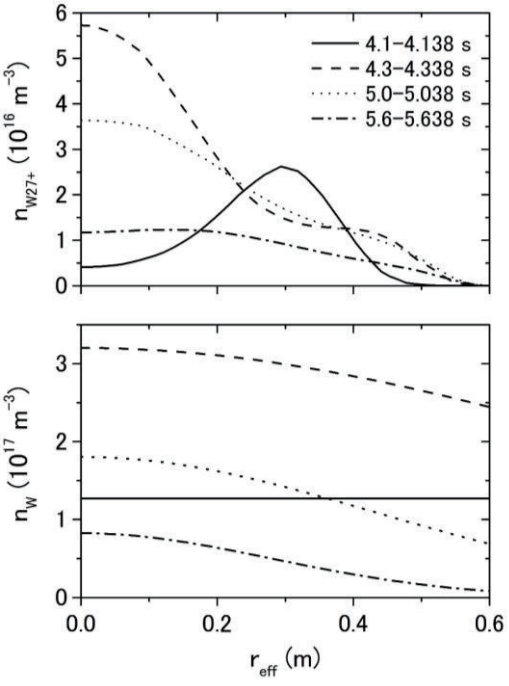

Fig. 5 Radial profile of W^{27+} ion distribution (upper) and W density (lower) deduced from vertical profiles of the M1 line intensity in Fig. 3. Peak temperatures at the plasma center are 2.0, 1.0, 1.0, and 1.2 keV at 4.1, 4.3, 5.0 and 5.6 s, respectively.

time. The time variation of the W^{27+} ion distribution indicates that ion transport effects on charge state distributions should be small in core plasmas. The W density in the core plasma is initially increased after the pellet injection (4.1 – 4.3 s) accompanying a temperature drop and a density rise. Since the temperature and density are stable in later times (5.0 – 5.6 s), the apparent decrease in the W density at the core plasma indicates diffusion of the tungsten ions after confinement in the plasma center.

Acknowledgements

DK is grateful to KAKENHI (15H04235). This work was partly supported by the JSPS-NRF-NSFC A3 Foresight Program in the field of Plasma Physics (NSFC: No.11261140328, NRF: No.2012K2A2A6000443).

References

[1] A. Komatsu et al, Phys. Scr. T**144**, (2011) 014012; Plasma and Fusion Res. **7** (2012) 1201158.

[2] Z. Fei et al, Phys. Rev. A **90** (2014) 052517.

[3] D. Kato et al, Phys. Scr. T**156** (2013) 014081.

[4] K. Fujii, D. Kato et al, submitted to Plasma Phys. Control. Fusion.

[5] K. Alder et al, Rev. Mod. Phys. **28** (1956) 432.

[6] A. Bar-Shalom, M. Klapisch and J. Oreg, J. Quant. Spectrosc. Radiat. Transfer **71** (2001) 169.

[7] I. Skobelev, I. Murakami and T. Kato, NIFS-DATA-**95** (Jan. 2006).

SOLPS simulations of EAST radiation divertor with N and Ar seeding

X.J. Liu[1,*], G. Deng[1], S. Liu, J. Huang[1], C. Wu[1], L. Zhang[1], X. Gao[1], and EAST Team[1]

[1]Institute of Plasma Physics, Chinese Academy of Sciences, P.O. 1126, 230031 Hefei, Anhui, China
*Eamil:julie1982@ipp.ac.cn

Abstract

A critical issue for EAST and future tokamak machines such as ITER and China Fusion Engineering Testing Reactor (CFETR) is the elimination of excessive heat load on the divertor target plates. As a means of actively reducing and controlling the power fluxes to the target plates, localized impurity (N, Ar) gas puffing from lower dome is investigated by using SOLPS5.0 on EAST with double null configuration. The radiative efficiency and distribution of the two gases are compared. The effect of N and Ar seeding on target power loading and the confinement is also presented. The simulation results indicate that both N and Ar puffing can effectively reduce the peak heat flux load and electron temperature Te at divertor targets similarly. N seeding can reach a higher radiative loss fraction (~85%) than Ar case (~75%), and N radiates power in divertor region mianly, while the radiative power inside separatrix for Ar seeding is also significant. Ar impurity puffing results in a faster decrease of the power across the sepatratrix, it seems unfavourable for plasma performance with the heating power close to the L-H transition threshold power.

Keywords: EAST, radiative divertor, SOLPS, impurity seeding

1. Introduction

The mitigation of divertor heat flux is an active topic of inverstigation on present tokamaks. It's also a critical issue for EAST to explore a long pulse and high heating power operation. This problem may become more crucial if carbon has to be avoided as a plasma facing material for ITER and China Fusion Engineering Testing Reactor (CFETR) due to high co-deposition of tritium [1]. One promising approach is seeding impurity gases with high radiative loss rate to enhance the radiation from both inside and outside the last closed flux surface (LCFS), to convert plasma thermal energy to radiation spread over a much larger surface area and eventually to reduce the target heat load. This technique has been investigated on a number of tokamaks in both L- and H-mode [2-5]. In order to optimize the choice and puffing rate of impurity seeded, detailed modeling and analysis is necessary to understand well the radiative distribution and their effect on heat load on divertor targets and core performance.

In this paper, we use the SOLPS5.0 code package [6] for the simulations of scrape-off layer (SOL) and divertor plasma. SOLPS mainly consists of two coupled codes: B2.5 is a fluid code that solves Braginskii-like equations for the ions (D, C, He, N, Ar) and electrons. Eirene is a Monte-Carlo code that describes kinetic neutrals [7]. Both codes are coupled via source terms for particle, momentum and energy. As we known, the atomic physics model and database are significant in determining the plasma constituents and the interaction among them. Since ADAS (Atomic Data and Analysis Structure) database [8] is actively maintained and upgraded, the mainly atomic processes included in this work, for example, ionization, excitation, dissociation, charge exchange and elastic collisions are from ADAS database. The accuracy of the data is mostly considered to be about 10-20%.

Detailed modeling studies of divertor target power loading and radiative distribution in EAST, as well as the consequence for core confinement with N and Ar seeding are presented by using SOLPS5.0. In section 2 we briefly describe the EAST divertor geometry and computational mesh, as well as the modeling setups. The modeling results and discussions with N and Ar seeding are presented in section 3, followed by a summary in section 4.

2. Simulation parameters

2.1. Geometry and computational grid

A grid is constructed for double null shot 41383 at 4.5 s shown as Fig. 1. Equilibrium is provided by equilibrium fitting (EFIT) code. The computational region includes the 'core' region (a small segment of the region with closed field lines, i.e., the area between core edge interface (CEI) and separatrix), left SOL region and right SOL and the private flux regions (PFR), including upper and lower PFR. The grid has 98 poloidal including the guard cells at four targets and 36 radial cells including the guard cells at the core and SOL boundaries, with the separatrix being located between cell number 18 and 19. It stretches radially from about -3.8 cm to 3.7 cm on either side of the separatrix at the midplane.

2.2. Boundary conditions and modeling assumptions

In modeling, the multi-fluid species includes D^0 neutrals, D^+ main ions and C impurities with neutral C^0 and all charged state ions and additional N^{0-7+} in N seeding case and Ar^{0-18+} instead in Ar seeding plasma. Carbon is produced self-consistently from physical and chemical sputtering and has zero recycling at targets, PFR, and SOL boundaries. The physical sputtering rates for both ions and neutrals are taken from the TRIM database [9]. Constant chemical sputtering rate 2% is used for carbon production. The transport of hydrocarbons is not included in this paper and the sputtered material and the seeded impurities (N and Ar) are treated as atom. The power across the CEI enter into the computational region is set to P_{CEI} =1.6 MW, which is calculated according to the energy balance by subtraction of ~20% radiation power (=0.4 MW) inside the CEI surface not accounted in this simulations from the total heating power. It is equally distributed between electrons and ions. The density of bulk ions D^+ is set to 1.0×10^{19} m^{-3} at the outer midplane separatrix and maintained by a feedback loop through D_2 gas puffing outside the SOL region (see Fig. 1). Normally, the anomalous cross-field transport coefficients are determined by fitting the upstream density (n_e) and temperature (T_e) profiles measured by RP (Reciprocating Probe) and edge TS (Thomson Scattering) system. However the upstream profiles for n_e and T_e are not available for this discharge, so we choose a typical empirical value $D_\perp$ =0.3 m^2s^{-1} and $\chi_e=\chi_i$=1.0 m^2s^{-1} for particle and ion and electron heat diffusivities respectively is this paper. The parallel plasma transport is flux limited, and no drifts are included in this simulation. The radial decay length λ_T for both electron and ion temperature and λ_n are set to 0.03 m. The recycling coefficients for D^0 and D^+ are set to 1.0 at the PFR and outer SOL edges. At the divertor target plates, the standard sheath boundary condition is applied. According to the Bohm criterion, the flow will be at least the sonic speed at the sheath entrance. The sheath heat transmission coefficients for electrons and ions are set to 4.5 and 2.5, respectively.

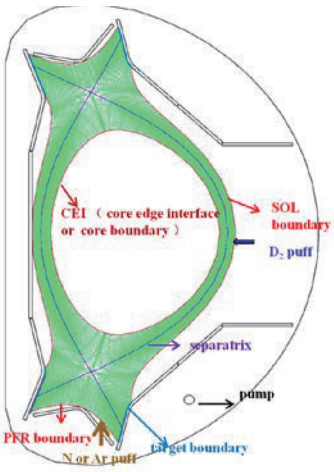

FIG 1. The 2D physical mesh for modeling in this paper is shown. The impurity gas (N and Ar) are injected from t h e lower dome and D_2 puffing for controlling the electron density at the outer midplane separatrix. The boundaries are pointed out with arrows.

3. Simulation results and discussions

3.1. The distribution of radiation power and its effect on divertor behavior

To detailed investigate the distribution and its effect on the heat flux load and temperature at divertor targets with N and Ar seeding, we have carried out an impurity puffing rate scan. The radiation power in edge including the SOL and divertor region ($P_{edge,rad}=P_{SOL,rad}+P_{div,rad}$), i.e., the whole area outside the separatrix and in core region which covers the entire area inside separatrix surface ($P_{core,rad}$=0.4MW+ $P_{core,SOLPS}$), as well as the peak electron temperature at lower outer divertor as a function of radiation power loss fraction (f_{rad}) for N and Ar seeding are shown in Fig. 2(a) and 2(b)

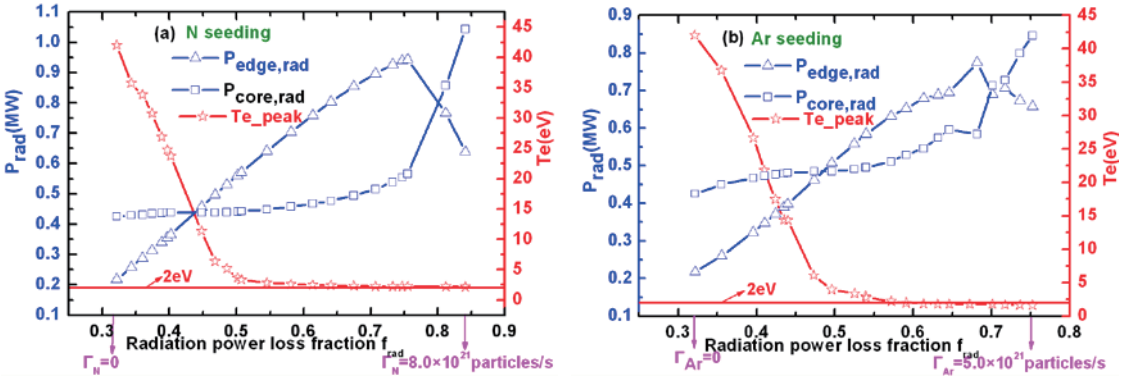

FIG 2. The radiation in edge (the whole area outside the separatrix) and in core region (including the radiation inside CEI surface), as well as the peak electron temperature at lower outer divertor against radiation power loss fraction for N seeding (a) and Ar seeding (b) are shown. The horizontal solid lines correspond to 2eV.

respectively. The horizontal solid lines correspond to 2eV. We can find that N seeding can reach a higher radiative loss fraction f_{rad} ~85% (corresponding to N puffing rate $\Gamma_N=8.0\times10^{21}$ particles/s) than Ar seeding f_{rad} ~75% (with Ar puffing rate $\Gamma_{Ar}=5.0\times10^{21}$ particles/s), and N radiates power in divertor region mianly, while the radiative power inside separatrix for Ar seeded discharge is also significant. For N seeding, $P_{edge,rad}$ increase as f_{rad} increasing and reach the maximum value at f_{rad} ~75%, while $P_{core,rad}$ is almost flat until f_{rad} >75%. When f_{rad} >75%,

the radiation power move into separatrix and exceed the radiative loss in edge at f_{rad}~80%. For Ar seeded case, both $P_{edge,\ rad}$ and $P_{core,\ rad}$ increase, and it increases faster in edge region than in core region when f_{rad}<65%, and the radiation in core region dominates when at f_{rad}>70%. Fig. 2 also shows that both N and Ar puffing can effectively reduce the peak electron temperature Te and heat flux load (not shown in Fig. 2) at divertor targets similarly. The divertor get detachment (Te_peak ~2eV) when the impurity gas puffing reach at a relatively high level of f_{rad}.

To make it clean, we plot the radiation power ratio of edge to core against f_{rad} with N and Ar seeding in Fig. 3. We can see that the ratio is totally higher for N seeding plasma than for Ar. It means that $P_{edge,\ rad}$ is higher for low-z N seeding than Ar. It also can be found that the ratio increases against f_{rad} and reach the maximum value, then drops for both N and Ar seeding, the maximum value reaches at f_{rad}~70% for N seeded and f_{rad}~60% for Ar. The ratio increases faster in N seeding plasma than in Ar case. It indicates that when seeding with N, the increased radiative power is mainly in edge region, while in Ar seeding case, power radiates in core region also significantly.

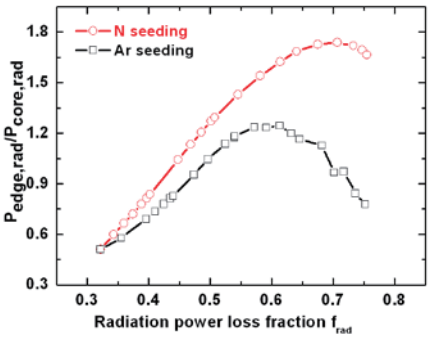

FIG 3. The radiative power ratio of edge to core is plotted as a function of radiation power loss fraction with N and Ar seeding.

3.2. The effect of impurity seeding on confinement

Beside the mitigation of divertor heat load, another crucial consideration for impurity seeding is to keep the compatibility with core performance. A strong positive correlation between normalized energy confinement factor H_{98} (which is an indicator of confinement) with the edge effective charge Zeff was found in [4, 10]. In Fig. 4, the effective charge at CEI (Z_{CEI}) as a function of the total radiative power fraction f_{rad} is illustrated. As can be seen, Z_{eff} at CEI is totally larger in N seeding than in Ar seeding at a fixed f_{rad}. We can deduce that N has a higher confinement than Ar from the relationship between H_{98} and Z_{eff} [10]. More detailed experimental validation on it will be performed in future. The results also show that Z_{eff} at CEI vary slightly with f_{rad} when f_{rad}<50%. It suggests that the divertor screening for impurities injected get weaker at a high level f_{rad}.

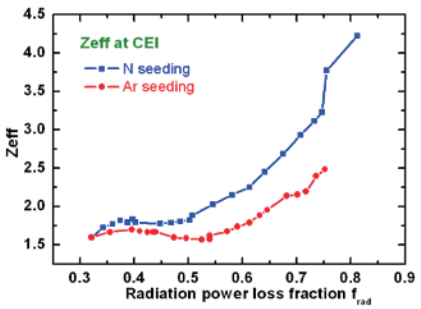

FIG 4. The effective charge at CEI against f_{rad} with N and Ar seeding.

The effect of different impurities seeding on the energy confinement has been investigated on experiments [2, 11]. The results show that H_{98} is to a large degree independent of radiating impurity when the power across the separatrix entering into SOL (P_{sep}) is larger than the threshold power of L-H mode transition (P_{th}). It means H_{98} depends strongly on the different between input power and the radiated power inside the LCFS. So we plot P_{sep} with N and Ar seeding case against the radiated fraction f_{rad} in Fig. 5. The horizontal solid line indicates the predicted L-H transition threshold power P_{th} (~1.55 MW) for this discharge by using the formula in [12], which is in proximity to P_{sep} without any impurity seeding of this simulated discharge. It appears that P_{sep} decreases faster with Ar seeding than N. It indicates that Ar is not a good radiator when the heating power is close to P_{th}, it may induces the degradation of H_{98}.

3.3. Discussions

In fact, all the differences between N and Ar seeded plasma are attributed to their different radiation characteristics. Fig 6 shows the radiative power loss rate L_z of some important elements in tokamak plasma as a function of temperature at a fixed n_e (~$10^{20}m^{-3}$) calculated from the non-local thermodynamic equilibrium (NLTE) collisional radiative (CR) model by FLYCHK code [13].We can see that N radiation peak is at Te ~10-30eV, it's a good divertor radiator for EAST. The first radiation peak of Ar is almost at the same Te with N, and there is another higher radiation peak at Te ~ 100-500eV. That suggests Ar is a good radiator for both divertor and core region simultaneously, it may be suitable for ITER or DEMO to reduce the power enter into SOL region. We also can find that N has the similar L_z with C, it seems to be a C-like radiator. That would be the reason why N seeding can recover some or all the loss of H_{98} in metallic wall

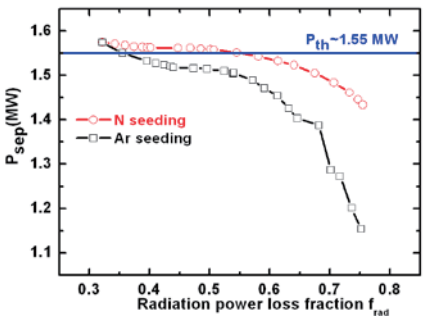

FIG 5. The radiative power ratio of edge to core is plotted as a function of radiation power loss fraction with N and Ar seeding.

tokamaks to the level of C wall observed in ASDEX-U and JET [4, 14].

4. Conclusions

We have simulated an L-mode double null discharge with N and Ar seeding from lower dome. The simulations indicate that both N and Ar puffing can effectively reduce the peak heat flux load and electron temperature Te at divertor targets similarly. N seeding can reach a higher radiative loss fraction (~85%) than Ar case (~75%), and N radiates power in divertor region mianly, while the radiative power inside separatrix for Ar seeding is also significant. The maximum radiation power loss fraction f_{rad} ($=P_{rad,tot}/P_{in}$) ~85% in N seeding is higher than in Ar case with f_{rad} ~75%. N radiates power in divertor region mianly, while the radiative power inside separatrix for Ar seeding is also significant. For both N and Ar seeding, the radiation ratio of edge to core region increases as the total radiation increasing, and reach the max value and then the radiation region move into the separatrix. The divertor get detachment when the impurity gas puffing reach a high level for both N and Ar seeding. We also found that Z_{eff} at CEI is totally larger in N seeding than in Ar seeding at a fixed f_{rad}, and Ar impurity puffing results in a faster decrease of P_{sep} than N. Those indicate that Ar may be not a good radiator for confinement with the heating power close to the L-H transition threshold. It seems N is well suited and even better than Ar for current discharge parameters. This may because that the majority of radiative peak for N is at lower temperature which corresponds to divertor region. Further studies of the compatibility and mechanism of high confinement with impurity seeding will be performed to optimize the choice of radiators.

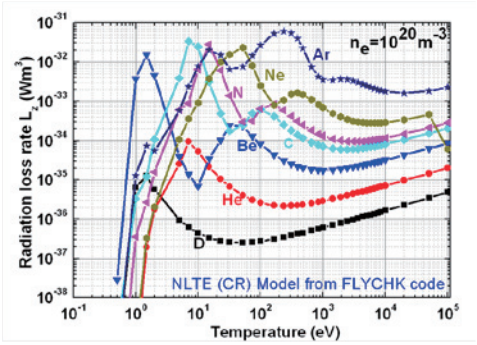

FIG 6. The radiative power loss rate L_z of some important elements in tokamak as a function of temperature at a fixed ne.

Acknowledgements

This work is supported by National Magnetic Confinement Fusion Science Program of China under contract no. 2014GB106005, 2015GB101003, 2015GB101000; National Nature Science Foundation of China under contract no. 11275231, no. 11305206, no.11405213 and no.11575244, and partly supported by the JSPS-NRF-NSFC A3 Foresight Program in the field of Plasma Physics (NSFC: No.11261140328, NRF: No.2012K2A2A6000443).

References

[1] G. Janeschitz, et al., Nucl. Fusion 42, 14 (2002)
[2] M. L. Reinke, J. W. Hughes, A. Loarte, D. Brunner, I. H. Hutchinson et al., J. Nucl. Mater. **415**, S340 (2011)
[3] G. L. Jackson, M. Murakami, D. R. Baker, R. Budny et al., Plasma Phys. Control. Fusion **44**,1893 (2002)
[4] J. Schweinzer, A. C. C. Sips, G. Tardini, P. A. Schneider et al., Nucl. Fusion 51, 113003 (2011)
[5] A. Kallenbach, M. Bernert, R. Dux, L. Casali, T. Eich et al., Plasma Phys. Control. Fusion **55**,124041 (2013)
[6] R. Schneider, X. Bonnin, K.Borras, D. P. Coster et al., Contrib. Plasma Phys. 46(1-2), 3-191 (2006)
[7] D. Reiter, M. Baelmans, P. Börner, Fusion Science and Technology. 47(2), 172-186 (2005)
[8] H. P. Summers, http://www.adas.ac.uk./manual.php, 2004
[9]W. Echstein and D. B. Heifetz, J. Nucl. Mater. **145-147**, 332(1987)
[10] S. K. Rathgeber, R. Fischer, S. Fietz, A. Kallenbach *et al*, Plasma Phys. Control. Fusion **52**,095008 (2010)
[11] A. Loarte, J. W. Hughes, M. L. Reinke, J. L. Terry *et al*, Phys. Plasmas **18**,056105 (2011)
[12] C. B. Huang, X. Gao, Z. Liu, X. Han, T. Zhang *et al*, Plasma Phys. Control. Fusion 52,075005 (2016)
[13] http://adas.phys.strath.ac.uk/.
[14] C. Giround, G. P. Maddison, S. Jachmich, F. Rimini *et al*, Nucl. Fusion **53**,113025 (2013)

Isotope effect in dissociation processes of deuterated molecules from doubly excited states

Yasuhiro Sakai [1,2], Karin Takahashi [1], Toru Hasegawa [1], Naoya Miyauchi [1], Daiji Kato [3,4], Izumi Murakami [3,4], and Hiroyuki A. Sakaue[3]

[1]Dept. of Physics, Toho University, Funabashi 274-8510, Chiba, Japan

[2]Research Center for Materials with Integrated Properties, Toho Univ., Funabashi 274-8510, Chiba, Japan

[3]National Institute for Fusion Science, Toki 509-5292, Gifu, Japan

[4]SOKENDAI (Graduate University for Advanced Studies), Toki 509-5292, Gifu, Japan

Abstract

To study an isotope effect in dissociation processes of deuterated molecules from doubly excited states, scattered electron-ion coincidence experiments were performed. The total generalized oscillator strength distribution (GOSD) and the ionic GOSDs of molecular deuterium (D_2) under 200 eV incident electron energy at a scattering angle of 6 degree were determined and were compared with those of molecular hydrogen (H_2). The total GOSD of D_2 was similar to that of H_2, and there is also little difference between both ionic GOSDs. However, the D^+ formation by dissociative ionization was completely different from that of H^+. The partial ionic GOSD of D^+ was half of that of H^+ in magnitude. Besides, it was found that the estimated ratios of the dissociative ionization to neutral dissociation have much difference. When doubly excited molecules were decayed by dissociation from the $Q_1{}^1\Sigma_g^+(1)$ state, the ratio of the dissociative ionization to neutral dissociation in the case of H_2 was 3:7, while that of D_2 was 1:9. It seems that this is so-called isotope effect.

Keywords: electron scattering, doubly excited states, dissociative recombination, dissociative ionization, neutral dissociation, isotope effects, hydrogen, deuterium, generalized oscillator strength, cross sections

1. Introduction

Dissociative recombination(DR) processes which are one of the important process in divertor plasma originate from doubly excited states produced by electron capture with low energy electron-molecular ion collision. In general, doubly excited states are dissociated by either the neutral dissociation or the dissociative ionization. In these dissociation processes, it is expected that isotope effects are observed. Information on isotope effects is very important for predicting the performance of the future fusion reactor. Therefore, it is necessary to know how doubly excited molecules dissociate; i.e. branching ratios and cross sections. We chose molecular deuterium (D_2) among deuterated molecules as the first step for the study of an isotope effect in dissociation processes.

The potential curves on the molecular hydrogen (H_2) involving both the doubly excited states of Q_1 and Q_2 are shown in Fig.1. Their potential curves are the results calculated by Sharp [1] and Sánchez et al. [2] Within the Franck-Condon region, the doubly excited states lie above the first ionization threshold. The Q_1

and Q_2 doubly excited series of states converge to the first and second excited states of H_2^+ and have the electronic configuration of $(2p\sigma_u)(nl)$ and $(2p\pi_u)(nl)$, respectively. In the case of D_2, although its potential curves are the same as those of H_2, the Franck-Condon region is slightly narrow (~16%).

Most of the experimental studies on the doubly excited states of H_2 have involved photo-impact experiments, there were few experimental studies performed by electron impact except for the Co-EELS experiments by Odagiri et al. [3].

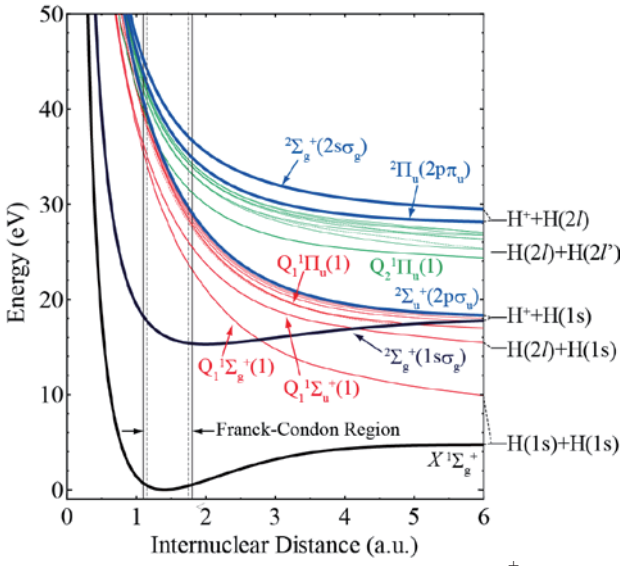

Fig.1 Potential curves of H_2 and H_2^+ [1,2].

In this study, the total generalized oscillator strength distribution (GOSD) and the ionic GOSDs of D_2 were determined by the scattered electron-ion coincidence (SEICO) experiment, and were compared with our previous results of H_2 [4], to investigate an isotope effect in dissociation processes of D_2 from doubly excited states.

2. Experimental set-up and procedure

The electron-ion coincidence spectrometer used in this experiment [4,5]. Briefly, the spectrometer consisted of a pulsed electron gun, an electron energy analyzer, and two Willy–McLaren time-of-flight (TOF) mass spectrometers, as shown in Fig.2. One of the mass spectrometer was a long system with high (mass) resolution, while the other was a short system with high collection efficiency for fragmented ions. However, we used only the short TOF mass spectrometer for this study. The duration of the electron beam pulses was 100 ns, and the repetition rate was 200 kHz. After the scattered electrons passed through the collision region, the resulting ions were extracted to the TOF mass spectrometer using a pulsed electric field (pulse intensity: 100 V/cm ; pulse rate: 200 kHz; pulse width: 3.4 μs). The extracted ions were then accelerated in a secondary region using a dc-electric field of 470 V/cm, and the ions travelled through a free drift region, before being detected using a microchannel plate (MCP) detector, where their mass was determined based on the flight time. Scattered electrons were analyzed with the electron-energy analyzer,

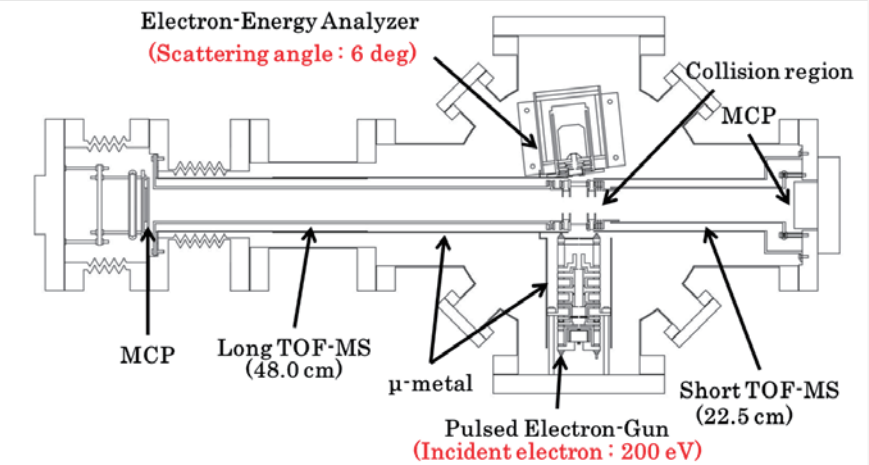

Fig.2 Schematic of the scattered electron-ion coincidence spectrometer

and the excitation energy of target molecules were selected every collision event.

To determine the GOSDs, we used a mixed gas method [5, 6]. In the mixed gas method, helium (He) was used as a standard reference gas in a certain ratio and mixed with the target gas. An electron energy-loss spectrum of He showed a remarkable 2^1P peak that corresponded to the transition from $(1s)^2$ to (1s)(2p) at 21.2 eV under a few hundred eV electron impact and small scattering angle. The spectra observed by experiments involving H_2 and D_2 had no structures around that region and showed a continuum state, because their ionization energies were generally below 15 eV. Therefore, the 2^1P excitation peak overlapped on the continuum state of the target atoms and molecules, in the He mixed gas spectrum. Because the differential cross section (DCS) is well known, we can use the excitation peak of He as a normalization standard to obtain the DCS of an excitation target of interest. A mixture of 51.6 % D_2 and 48.4 % He was used.

3. Results and Discussions

The total GOSDs of H_2 and D_2 determined for a 200 eV incident electron energy and a scattering angle of 6 degrees are shown in Fig.3(a). The magnitude of the momentum transfer, K^2, for the given experimental conditions is shown in the upper horizontal axis. The large peak around 12eV was associated with excitations mainly from $(1s\sigma_g)^{-1}(2p\sigma_u)$ and $(1s\sigma_g)^{-1}(2p\pi_u)$, corresponding to the $B^1\Sigma^+_u$ and $C^1\Pi_u$ states, respectively. Although the GOSD of D_2 around $(1s\sigma_g)^{-1}$ ionization threshold was slightly smaller than that of H_2, the behavior against the electron energy-loss was almost similar.

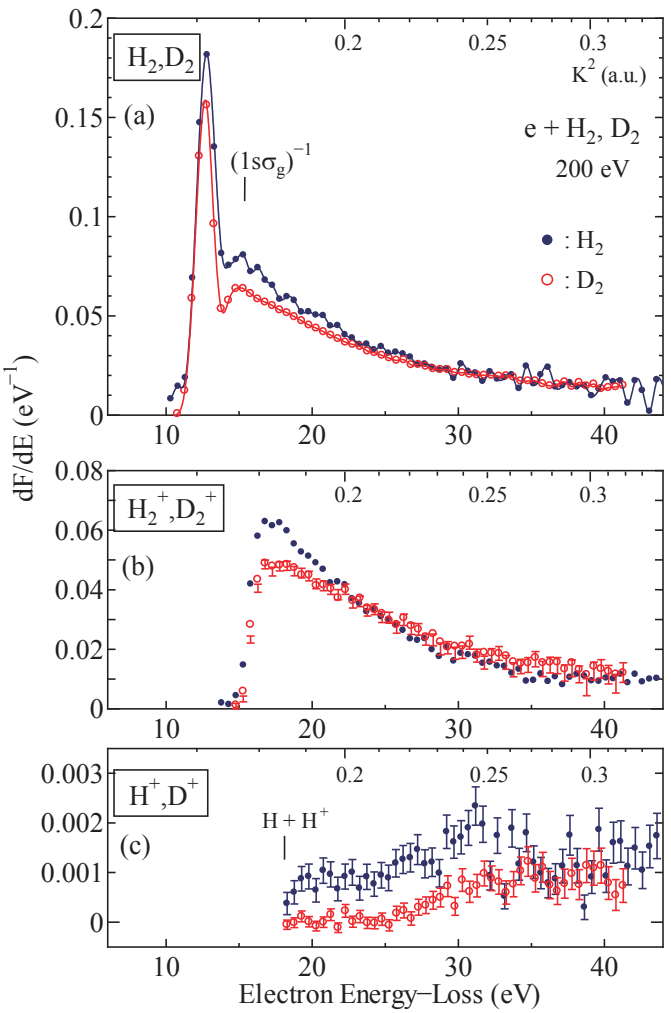

Fig.3. (a) The absolute total generalized oscillator strength distributions(GOSDs) of H_2 and D_2, (b) the partial ionic GOSDs of H_2^+ and D_2^+, (c) the partial ionic GOSDs of H^+ and D^+, respectively.

The partial ionic GOSDs of H_2^+ and D_2^+ are shown in Fig.3(b). Both GOSDs increased from the first ionization threshold $(1s\sigma_g)^{-1}$ at 15.4 eV, which has a maximum value at about 18 eV. After the energy-loss value exceeded the peak, both the ionic GOSD decreased gradually with further increase in the energy-loss values. There was little difference in their ionic GOSDs. However, the D^+ formation by dissociative ionization was completely different from that of H^+, as can be seen from Fig.3(c). The partial

ionic GOSD of D^+ was half of the H^+ one in magnitude. In particular, the GOSD of D^+ was very small in the energy-loss region of 18 to 22e V. This mechanism is being considered at present.

Figure 4 shows the ratios of of H^+/H_2^+ and D^+/D_2^+, respectively. Although the threshold energy of D^+ formation is 18.16 eV, molecular ion formation is dominant and the D^+ fragment were rarely observed in energy-loss region from threshold to about 25 eV. The GOSD of H^+ formation from the $Q_1{}^1\Sigma_g{}^+(1)$ state was about 8×10^{-4} eV^{-1}, whole that of D^+ was about 2×10^{-4} eV^{-1}, at around 28 eV. We estimated the ratio of the dissociative ionization to neutral dissociation, from these results and ionization efficiency. When doubly excited molecules were decayed by dissociation from the $Q_1{}^1\Sigma g^+(1)$ state, the ratio in the case of H_2 was 3:7, while that of D_2 was 1:9.

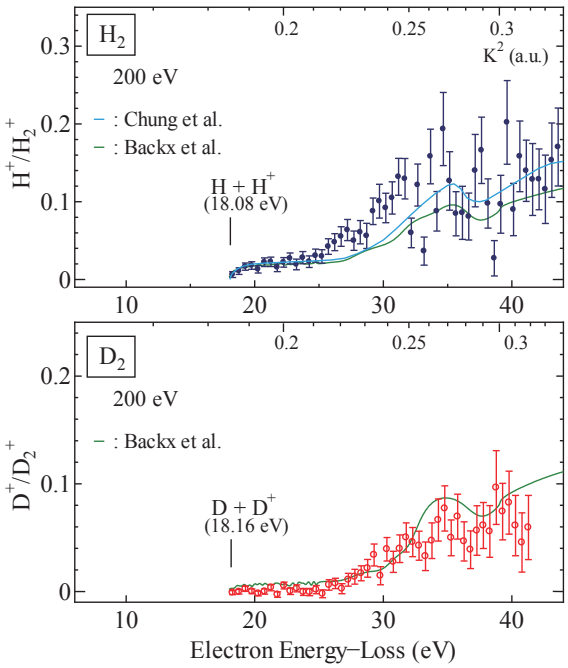

Fig.4 Ratios of H^+/H_2^+ and D^+/D_2^+

4. Conclusions

The absolute GOSDs of D_2, D_2^+, and D^+ were obtained by the scattered electron-ion coincidence measurements for 200 eV incident electron energy and a scattering angle of 6 degrees, and were compared with the case of H_2. As a result, we found that an isotope effect appeared in dissociation processes on D_2. In particular, when doubly excited molecules were decayed by dissociation from the $Q_1{}^1\Sigma g^+(1)$ state, the neutral dissociation was more dominant than that of dissociative ionization in the D_2 case.

Acknowledgements

This work was partly supported by a LHD Project Collaboration Research between NIFS and Toho University, and by the JSPS-NRF-NSFC A3 Foresight Program in the field of Plasma Physics (NSFC: No.11261140328, NRF: No.2012K2A2A6000443). This work was also supported by the JSPS KAKENHI Grant-in-Aid for Scientific Research (C) (26400536), and the Research Center for Materials with Integrated Properties, Toho University.

References

[1] T. E. Sharp, Atomic Data, **2** (1971) 119..

[2] I. Sánchez et al. J. Chem. Phys. **106** (1997) 7720, **110** (1999) 6702.

[3] T. Odagiri et al. J. Phys. B, **28** (1995) L465.

[4] K.Takahashi et al., Eur.Phys.J., D, **68** (2014) 83.

[5] K.Yamamoto and Y.Sakai, J.Phys.B, **48** (2012) 055201.

[6] K.Takahashi et al., J.Phys.Conf. Series, **288** (2011) 012013.

Optical oscillator strengths of valence-shell excitations of atoms and molecules determined by the newly developed dipole (γ, γ) method

Lin-Fan Zhu[1,2], Long-Quan Xu[1,2], Xu Kang[1,2], Ya-Wei Liu[1,2], Dong-Dong Ni[1,2], Ke Yang[3], N. Hiraoka[4] and K. D. Tsuei[4]

[1]Hefei National Laboratory for Physical Sciences at Microscale and Department of Modern Physics, University of Science and Technology of China, Hefei, Anhui 230026, People's Republic of China

[2]Synergetic Innovation Center of Quantum Information and Quantum Physics, University of Science and Technology of China, Hefei, Anhui 230026, People's Republic of China

[3]Shanghai Institute of Applied Physics, Chinese Academy of Sciences, Shanghai 201204, People's Republic of China

[4]National Synchrotron Radiation Research Center, Hsinchu 30076, Taiwan, Republic of China

Abstract

The dipole (γ, γ) method, which is the inelastic x-ray scattering operated at a negligibly small momentum transfer, is newly developed to determine the absolute optical oscillator strengths of the valence-shell excitations of atoms and molecules. This new method is free from the line saturation effect, and the Bethe-Born conversion factor of the dipole (γ, γ) method varies much more slowly with the excitation energy than that of the dipole (e, e) method. Thus the dipole (γ, γ) method provides a reliable approach to obtain the benchmark optical oscillator strengths of the valence-shell excitations for gaseous atoms and molecules, and it is demonstrated by the measurements of absolute optical oscillator strengths for gaseous helium, argon, nitrogen and carbon monoxide.

Keywords: optical oscillator strength, photoabsorption cross section, dipole (γ, γ) method

1. Introduction

The absolute optical oscillator strength (OOS), or the equivalent quantity of photoabsorption cross section, of an atom or molecule represents the transition probability between initial and final states and is essential in describing and understanding the physical processes involving the photon absorption and emission, which widely exist in plasma, interstellar space, planetary atmosphere, and energy deposition. Meanwhile, the precise experimental OOSs can be used to test the theoretical models and calculational codes rigorously.

Many experimental techniques, including the photoabsorption method [1], electron energy loss spectroscopy (EELS) [2], dipole (e, e) method [3], lifetime method [4], self-absorption [5] and etc, have been used to measure the absolute OOSs of atoms and molecules. Among them, the photoabsorption method and the dipole (e, e) method are most commonly used. However, the photoabsorption method is influenced by the line saturation effect which can seriously limit the accuracies of the measured OOSs for the discrete excitations. Although the dipole (e, e) method is free from the line saturation effect, the rapid variation of its Bethe-Born conversion factor may bring considerable uncertainties. Therefore, developing

new general experimental technique and cross-checking the OOSs determined by different methods are valuable, and can promote the corresponding fields greatly.

Recently, the nonresonant inelastic x-ray scattering (IXS) technique, which is extensively used in condensed matter physics, was extended to measure the dynamic parameters in momentum space for gaseous atoms and molecules [6,7]. The very low cross section of the IXS was partly resolved by increasing the target's density for gaseous atoms and molecules by utilizing the high penetrating power of hard x-ray. When the IXS is operated at the negligible momentum transfer, i.e., $q^2 \approx 0$ which is the so-called dipole approximation condition, it can be used to simulate the photoabsorption process as well as to measure the OOSs of atoms and molecules, and we call this method as dipole (γ, γ) method [8]. As a new experimental method to determine the OOSs of atoms and molecules, the dipole (γ, γ) method is realized by our group for the first time [8]. Then the OOSs of the valence discrete excitations of gaseous helium, argon, nitrogen and carbon monoxide were determined by this method [8-11].

2. Experimental method

The dipole (γ, γ) method was realized by using the Taiwan Beamline BL12XU at SPring-8. In brief, a Si (333) monochromator and a Si (555) spherical analyzer were applied to achieve a high energy resolution of about 70 meV. During the experiment, the analyzer energy of the scattered photon was fixed at about 9900 eV, while the incident photon energy varied, from which the energy loss can be easily determined. The target and the helium samples were sealed in a gas cell with Kapton windows and put on the experimental platform for the measurement in turn, herein the helium sample was used for normalization. The pressures in the gas cell were maintained at about 1 MPa relying on the samples. In addition, the actual transmissivities of two sample gases were measured and all the spectra of helium and target were measured at room temperature.

From the measured experimental spectra, the OOSs of the target were absolutized by referencing the OOS of the 2^1P of helium which has been investigated with a high accuracy both experimentally and theoretically. The details of the normalization procedure can be found in Refs. [8-11].

The experimental errors of the OOSs determined by dipole (γ, γ) method come from the contributions of the Bethe–Born conversion factors, the statistical counts, the transmissivity and the pressures of both target and helium, as well as the OOS of the 2^1P of helium. Among them the main contribution of the experimental errors is due to the statistical counts which depending on the definite transition. This statistical error can, in principle, be greatly reduced by accumulating the counts although it is hard to obtain a long beam time. The contributions from other sources is negligibly small [8-11]. To the best of our knowledge, the dipole (γ, γ) is free from any systematic error.

3. Results and Discussions

Considering that helium is the simplest multi-electron system and its calculated OOSs of the valence-shell excitations have reached a very high accuracy，we choose the helium to demonstrate the validity of the presently proposed dipole (γ, γ) method. The OOSs of the excitations of $1s^2\,{}^1S_0 \rightarrow 1snp\,{}^1P_1$ series (n= 3 – 7) of helium were measured by the dipole (γ, γ) method and shown in Fig. 1 along with the

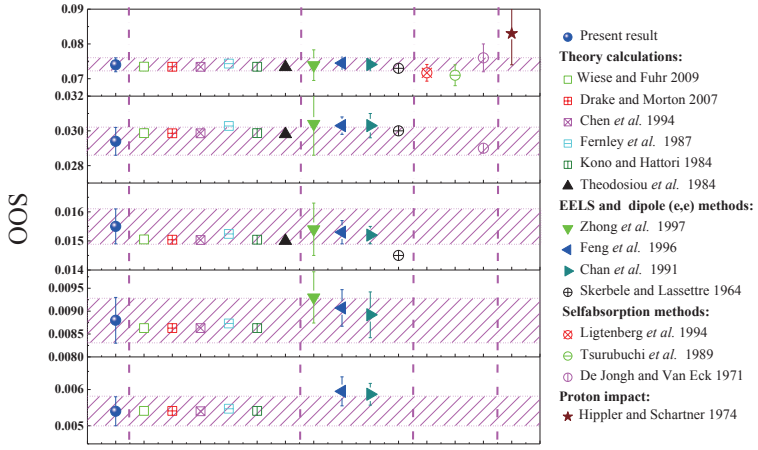

Fig. 1 The OOSs of the n^1P_1 (n= 3 – 7 from up to down) of helium measured by the present dipole (γ, γ) method along with the previous experimental and theoretical results [8].

previous experimental and theoretical OOSs. It is clear from Fig. 1 that most of the latest calculations give nearly identical results, and the present OOSs determined by the dipole (γ, γ) method agree excellently with these sophisticated calculations. Within the experimental errors, all of the present dipole (γ, γ) results are in excellent agreement with those measured by the dipole (e, e) method and EELS method as well as the selfabsorption results. The present results provide a rigorous test of the theoretical methods and confirm the validity of the high resolution dipole (γ, γ) method.

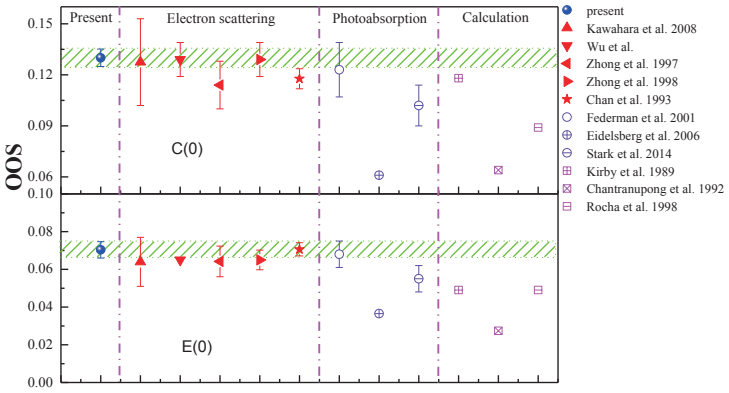

Fig. 2 The OOSs of C(0) and E(0) of carbon monoxide measured by the present dipole (γ, γ) method along with the previous experimental and theoretical results [11].

After the demonstration of the validity of the dipole (γ, γ) method, it is used to measure the experimental benchmark OOSs of argon, nitrogen and carbon monoxide which have extensive applications in astrophysics [9-11]. As an example, the OOSs of the C(0) and E(0) transitions of carbon monoxide are shown in Fig. 2. Generally speaking, the OOSs determined by the dipole (γ, γ) method are in good agreement with the previous EELS and dipole (e,e) results, while the photoabsorption method give lower values, especially for the strong discrete transitions, which is the typical line saturation behavior.

The cross-check of the oscillator strengths measured by the present dipole (γ,γ) method, the dipole (e,e) method, and the extrapolating method based on the EELS give us confidence that the dipole (γ,γ) OOSs can serve as benchmark data because the experimental techniques, experimental conditions, and normalization procedures used are distinctly different. For example, the target pressure in the present dipole (γ,γ) method are about 1 MPa, while it is about 0.01 Pa in the dipole (e,e) method and the EELS. We use the OOS of the 2^1P of helium to absolutize OOSs of the target, while the dipole (e,e) method uses the TRK sum rule to normalize their data. The good agreement of the dipole (γ,γ) results and those of the dipole (e,e) and the

extrapolating methods excludes the possibility of any systematic error. Therefore, it is reasonable to think that the lower OOSs of the strong transitions determined by the photoabsorption method are influenced by the line-saturation effect.

4. Summary and Conclusion

The dipole (γ,γ) method is proposed and realized based on the third generation synchrotron radiation, and its validity is demonstrated by the OOS measurement of helium. The benchmark OOSs of the valence-shell excitations of argon, nitrogen and carbon monoxide have been determined by the dipole (γ,γ) method. It is worth mentioning that every experimental technique has its own merits and demerits. Although for the strong transitions the photoabsorption method is influenced by the line-saturation effect, it has the highest energy resolution to determine the oscillator strengths of the rotational states. Although the present dipole (γ,γ) method, the dipole (e,e) method, and the extrapolating method with the moderate energy resolution of tens of meV can only measure the OOSs of the vibronic states at the present stage, they are free from the line-saturation effect. The dipole (e, e) method has the advantage of a large cross section, which can achieve a good signal-to-noise ratio and a good statistical count, while the rapid variation of its Bethe-Born conversion factor may bring some uncertainties. The accurate Bethe-Born conversion factor of the dipole (γ,γ) method can avoid this problem, and the only limitation of the dipole (γ,γ) method is its low cross section, which results in the poor statistical counts for the weak transitions. However, the dipole (γ,γ) method is free from any systematic error, to the best of our knowledge. Thus it is possible to achieve a higher precision for the oscillator strengths with the dramatic progress of the third generation synchrotron radiation and the free electron laser.

Acknowledgements

This work was partly supported by National Natural Science Foundation of China (Nos. U 1332204 and 11274291) and the JSPS-NRF-NSFC A3 Foresight Program in the field of Plasma Physics (NSFC: No.11261140328, NRF: No.2012K2A2A6000443).

References

[1] G. Stark, A. N. Heays, J. R. Lyons, et al., Astrophys. J. **788** (2014) 67.

[2] H. Kawahara, D. Suzuki, H. Kato, et al., J. Chem. Phys. **131** (2009) 114307.

[3] W. F. Chan, G. Cooper & C. E. Brion Phys. Rev. A **44** (1991) 186.

[4] E. Krishnakumar & S. K. Srivastava Astrophys. J. **307** (1986) 795.

[5] R. C. G. Ligtenberg, P. J. M. Van Der Burgt, S. P. Renwick, et al., Phys. Rev. A **49** (1994) 2363.

[6] B. P. Xie, L. F. Zhu, K. Yang, et al., Phys. Rev. A **82**(2010)032501.

[7] L. F. Zhu, L. S. Wang, B. P. Xie, et al., J. Phys. B: At. Mol. Opt. Phys. **44**(2011)025203.

[8] L. Q. Xu, Y. W. Liu, X. Kang, et al., Sci. Rep. **5** (2015) 18350.

[9] X. Xu, D. D. Ni, X. Kang, et al., J. Phys. B: At. Mol. Opt. Phys. **49** (2016) 064010.

[10] Y. W. Liu, X. Kang, L. Q. Xu, et al., Astrophys. J. **819** (2016) 142.

[11] X. Kang, Y. W. Liu, L. Q. Xu, et al., Astrophys. J. **807** (2015) 96.

Observation of resonant excitation of Fe^{14+}

TSUDA Takashi[a], SHIMIZU Erina[a], Safdar ALI[a], SAKAUE Hiroyuki A.[b], KATO Daiji[b,c], MURAKAMI Izumi[b,c], HARA Hirohisa[d,e], WATANABE Tetsuya[d,e], and NAKAMURA Nobuyuki[a]

[a] Inst. for Laser Science, The Univ. of Electro-Communications, Tokyo 182-8585, Japan

[b] National Institute for Fusion Science, Gifu 509-5292, Japan

[c] Department of Fusion Science, SOKENDAI, Gifu 509-5292, Japan

[d] National Astronomical Observatory of Japan, Tokyo 181-8588, Japan

[e] Department of Astronomical Science, SOKENDAI, Tokyo 181-8588, Japan

Abstract

We present extreme ultraviolet spectra of highly charged Fe ions observed with a compact electron beam ion trap as a function of monoenergetic electron beam energy. For $3s3p$ - $3s3d$ lines in Fe XV, strong intensity enhancement at a specific electron energy is confirmed. The enhancement is assigned as the resonant excitation via dielectronic capture followed by autoionization. The resonance contribution to line intensity ratio, which is important for the diagnostics of astrophysical plasmas, is discussed.

Keywords: EBIT, iron ions, EUV spectroscopy, resonant excitation

1.Introduction

Spectra of highly charged Fe ions in the extreme ultraviolet (EUV) range are important for the spectroscopic diagnostics of astrophysical hot plasmas such as solar corona [1]. In such diagnostics, plasma parameters, such as electron temperature and density, are determined through the comparison between the observed spectra and theoretical spectra calculated with a collisional radiative (CR) model. For accurate diagnostics, the model spectra should thus be examined by laboratory benchmark spectra obtained with a well-defined condition. We have been studying EUV spectra of highly charged Fe ions with an electron beam ion trap (EBIT), which can realize well-defined plasma consisting of a quasi-monoenergetic electron beam and trapped ions with a narrow charge state distribution [2, 3, 4]. In our previous study [3], the electron density dependence of the intensity ratio was measured for several density-sensitive emission lines in Fe XIII, XIV, and XV with a compact EBIT called CoBIT [5]. Although good quantitative agreement was obtained between the experiment and our model calculation for Fe XIII and XIV, a significant discrepancy was found for the intensity ratio between the $3s3p\ ^3P_2$ - $3s3d\ ^3D_3$ (233.9 Å) and $3s3p\ ^1P_1$ - $3s3d\ ^1D_2$ (243.8 Å) transitions in Fe XV. The discrepancy for this line ratio has also been found so far from solar observations (for example, see Ref. [6]),

and line blending has often been pointed out as the origin of the discrepancy [6, 7, 8]. However, the possibility of line blending has been ruled out by high resolution observation in our previous study [4]. In this paper, we study the electron energy dependence of the line ratio whereas the density dependence was the main subject of interest in the previous studies. Resonant excitation contribution to the line ratio is also observed and discussed.

2. Experiment

Experiment was performed with a compact EBIT, called CoBIT [5]. Highly charged Fe ions were produced by successive ionization of iron injected as a vapor of ferrosen ($Fe(C_5H_5)_2$ by a 500 eV electron beam. After a "cooking" time of 1600 ms, the electron energy was swept between 400 and 500 eV for 10 ms (probing time), and kept at 500 eV for 10 ms (keeping time) for preserving the charge distribution. After the probing and keeping time was repeated 100 times, the ions were dumped and the cycle was started again from the cooking time. The electron beam current was 10 mA throughout the measurement.

The EUV emission from the trapped Fe ions was observed with a grazing incidence flat field grating spectrometer [9] employing a 1200 gr/mm concave grating with 13450 mm radius of curvature (Hitachi 001-0660). The diffracted EUV photon was detected by a position sensitive detector (PSD) consisting of five micro channel plates and a resistive anode (Quantar Technology Inc. model 3391). The front of the micro channel plate was coated by CsI for enhancing the sensitivity. When a photon was detected, the position on the PSD, pulse height, and the electron energy were recorded on PC in list mode.

3. Results and discussion

A result of about 80 hrs data acquisition is shown in Fig. 1. In this wavelength range, lines from Fe XIII to XV were observed with a few lines from impurity ions. Fe XV lines of present interest are $3s3p\,{}^3P_2$ - $3s3d\,{}^3D_3$ at 234 Å and $3s3p\,{}^1P_1$ - $3s3d\,{}^1D_2$ at 244 Å. As seen in the figure, intensity enhancement was observed at an electron energy of 420 eV for both the lines whereas no energy dependence was confirmed for almost all the other lines in the present electron energy and wavelength ranges. This enhancement is considered to be due to excitation realized by dielectronic capture followed by autoionization:

$$\mathrm{e} + \mathrm{Fe}^{14+}\,(3s^2) \rightarrow \mathrm{Fe}^{13+}\,2p^{-1}3s^2 3p3d \rightarrow \mathrm{Fe}^{14+}\,3s3d + \mathrm{e}. \qquad (1)$$

This is a resonant process that have a sharp dependence on electron energy. Except for

the resonant energy at 420 eV, there can be found no strong energy dependence even for the lines of interest.

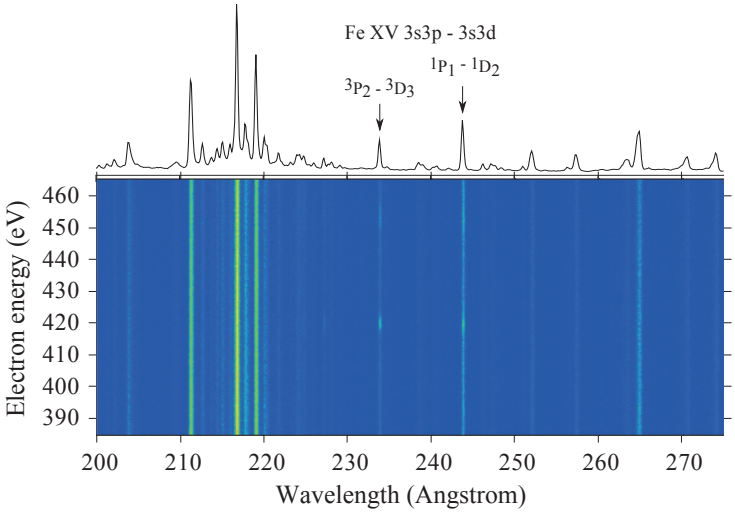

Figure 1: EUV spectra of highly charged Fe ions observed with a compact EBIT as a function of electron energy. The intensity is represented by color (blue to red). The wavelength scale was calibrated with well-known Fe lines, and the electron energy was calibrated with the theoretical resonance energy calculated with HULLAC [10]. The spectrum integrated for whole electron energy range is shown in the upper panel.

It is noted that the electron energy scale was calibrated with the theoretical resonance energy calculated with HULLAC [10]. The electron beam energy in an EBIT is primarily determined by the potential difference between the electron gun and the middle electrode of the ion trap. However, the actual interaction energy between the electron and the trapped ions is affected by the space charge potential, which is generally difficult to know experimentally. In the present study, the difference between the energy estimated from the potential difference and the calibrated energy was about 15 eV, which may be due to the space charge potential.

Figure 2 shows a closeup view for the lines of present interest at the electron energy range where the resonance was observed. Spectra at on- and off-resonance energies are also shown. The observed intensity ratio of 234 Å to 244 Å lines is 0.5 and 0.9 (preliminary) at off- and on-resonance, respectively. As confirmed in this example, not only intensity but also intensity ratio is strongly affected by the resonance. It is thus important to take the resonance contribution into account for estimating the ratio by CR model calculation. However, the resonance contribution cannot account for the discrepancy between the experiment and the model found in the previous study [3]. The observation in the previous study was done at the electron energy corresponding to the present cooking energy, which

is well above the resonance. In the present study, it is confirmed that the line ratio for the off-resonance region is 0.5 - 0.6 almost independently of electron energy for the 400 - 500 eV range and thus higher than the CR model ratio, which is 0.3 [3], obtained for the typical electron density of CoBIT (10^{10} cm^{-3}).

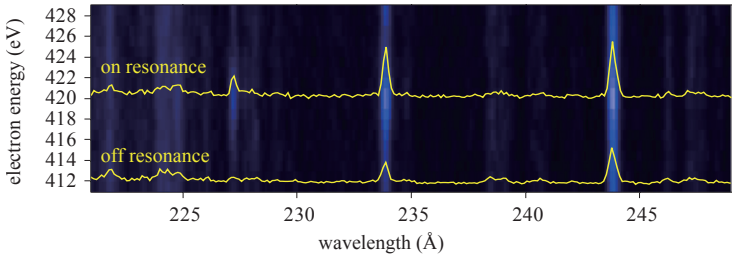

Figure 2: Similar to Fig. 1 but for the wavelength and energy ranges of present interest. The yellow lines represent the on-resonance spectrum at 420 eV and the off resonance spectrum at 412 eV.

The amount of intensity enhancement at the resonance should be proportional to the resonant excitation cross section. Although it is rather difficult to obtain absolute cross section, relative cross section can be deduced from the present observation. The analysis for the cross section is in progress, and will be published elsewhere.

Acknowledgement

This work was performed under the Research Cooperation Program in the National Institutes of Natural Sciences (NINS).

References

[1] T. Watanabe, J. Phys.: Conf. Ser. **163**, 012002 (2009).
[2] H. A. Sakaue *et al.*, J. Appl. Phys. **109**, 073304 (2011).
[3] N. Nakamura *et al.*, The Astrophysical Journal **739**, 17 (2011).
[4] E. Shimizu *et al.*, J. Phys.: Conf. Ser. **583**, 012019 (2015).
[5] N. Nakamura *et al.*, Rev. Sci. Instrum. **79**, 063104 (2008).
[6] P. L. Dufton *et al.*, Astrophysical Journal **353**, 323 (1990).
[7] S. O. Kastner and A. K. Bhatia, Astrophysical Journal **553**, 421 (2001).
[8] F. P. Keenan *et al.*, Astronomy & Astrophys. **449**, 1203 (2006).
[9] H. Ohashi *et al.*, Rev. Sci. Instrum. **82**, 083103 (2011).
[10] A. Bar-Shalom, M. Klapisch, W. H. Goldstein, and J. Oreg, *"The HULLAC package computer set of codes for atomic structure and processes in plasmas"*, unpublished.

Tungsten Spectra Measurement on EAST and Requirement of Atomic Data for Its Quantitative Analysis

L. Zhang[1], S. Morita[2,3], X. D. Yang[1], Z. Xu[1], T. Ohishi[2,3], P. F. Zhang[1], J. Huang[1], W. Gao[1], Y. M. Duan[1], Y. J. Chen[1], J. L. Chen[1], Z. W. Wu[1], L. Q. Hu[1] and EAST team

[1] Institute of Plasma Physics Chinese Academy of Sciences, Hefei 230026, China
[2]National Institute for Fusion Science, Toki 509-5292, Gifu, Japan
[3] SOKENDAI (Graduate University for Advanced Studies), Toki 509-5292, Gifu, Japan

Abstract

EAST tokamak has been equipped with upper tungsten divertor since 2014 to improve the divertor heat load capability. In order to study the tungsten behavior in long pulse discharges, tungsten spectra have been measured at 20-140Å with a newly installed extreme ultraviolet (EUV) spectrometer fulfilled a fast time response charge-coupled detector (CCD) of 5ms/frame. It is found that emission lines from highly ionized W ions of W^{40+} to W^{45+} can be easily observed with strong intensities in longer wavelength range of 120-140 Å when the central electron temperature exceeds 2.5keV. In this work, the isolated line from W^{45+} ($3d^{10}4s\ ^2S_{1/2} - 3\ d^{10}4p\ ^2P_{1/2}$) at 126.998Å is used for the quantitative evaluation based on the absolute intensity measurement. The tungsten concentration is also evaluated from tungsten radiation power coefficient based on the total radiation loss measurement. The requirement of atomic data is described and results are compared between the two approaches.

Keywords: EAST tokamak, tungsten, EUV spectroscopy, ADAS database

1. Introduction

ITER has adopted tungsten as the divertor material for the D-T operation. In order to improve the divertor heat load capability, the tungsten mono-block has been equipped on upper divertor of EAST tokamak at 2014 [1]. The tungsten accumulation has been often observed in NBI-heated H-mode discharges suggesting a sufficient improvement of tungsten ion confinement [2], which is one of the critical issues to achieve long pulse H-mode discharges. Then, a quantitative analysis on the tungsten behavior is urgently desired for maintaining high-performance plasmas in EAST.

In order to study the tungsten behavior in long pulse discharges, tungsten spectra have been measured at 20-140Å with a newly installed extreme ultraviolet (EUV) spectrometer fulfilled a fast time response CCD of 5ms/frame [3]. In 2014 and 2015 campaigns, the tungsten spectra, e.g. unresolved transition array (UTA) at 45-70 Å, were always observed with strong intensity during H-mode phase in NBI-heated discharges, whereas EAST was operated with lower single null (LSN) configuration. The density profile

during H-mode phase is peaked due to an improved particle confinement, while the central electron temperature is relatively low, e.g., $T_e(0)$<2.0keV. It was then difficult to observe highly ionized tungsten ions of W^{43+} -W^{45+}. In 2016 spring campaign, EAST has been operated with upper single null (USN) configuration to improve the divertor heat load capability. Additionally installed 4.6GHz LHW and ECRH heating systems contribute to increase the T_e up to 4keV. Then, highly ionized tungsten ions of W^{40+} to W^{45+} can be easily measured with strong intensity. An isolated line from W^{45+} ($3d^{10}4s\ ^2S_{1/2} - 3\ d^{10}4p\ ^2P_{1/2}$) at 126.998Å is used for the quantitative evaluation based on the absolute intensity measurement. The tungsten concentration is also evaluated from tungsten radiation power coefficient based on the total radiation loss measurement.

2. Methods for evaluation of W concentration and required atomic data

2.1 Method 1: qualitative analysis based on line intensity measurement

Figure 1 shows a cross section of EAST tokamak and line of sight (LOS) of the EUV spectrometer. The chord-integrated line intensity of W ions in ionization stage of q is written by equation (1). The W concentration, $c_{W,}$ can be evaluated from equation (2). Here, the value of c_W is defined as a ratio of the total number of tungsten particles to electrons.

$$\begin{aligned} I^{W^{q+}} &= \int n_{W^{q+}}(l)\mathrm{PEC}^{W^{q+}}(l)n_e(l)\mathrm{d}l \\ &= \int c_W(l)n_e(l)FA^{W^{q+}}(l)\cdot PEC^{W^{q+}}(l)n_e(l)dl \\ &= \int c_W f_{c_W}(l)n_e(l)FA^{W^{q+}}(l)\cdot PEC^{W^{q+}}(l)n_e(l)dl \end{aligned} \quad (1)$$

$$c_W = I^{W^{q+}} / \int f_{c_W}(l)FA^{W^{q+}}(l)PEC^{W^{q+}}(l)n_e^2(l)\mathrm{d}l \quad , (2)$$

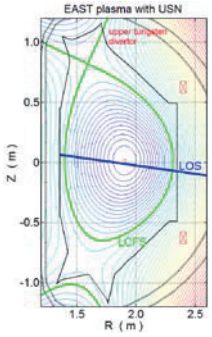

Fig. 1. EAST cross section and LOS of EUV spectrometer.

where I^{Wq+}, n_{Wq+}, PEC^{Wq+}, c_W (r), f_{Cw} and FA^{Wq+} are the chord-integrated line intensity from W^{q+} , the density of W^{q+}, the photon emissivity coefficient of line from W^{q+}, the density profile of W, the normalized density profile of W and the fractional abundance of W^{q+} under ionization equilibrium (see Figure 2), respectively. In the analysis the PEC of W line and FA of W ions are utilized as the atomic data. In practice, the effective ionization and recombination coefficients from Atomic Data and Analysis Structure (ADAS) database are used in a set of rate equations to calculate the FA in EAST parameters including electron temperature and density and their profiles. An effect of the impurity transport is also considered. Meanwhile, the PEC is directly obtained from ADAS database (arf40_ic series) and compared with that from HULLAC as shown in Figure.3.

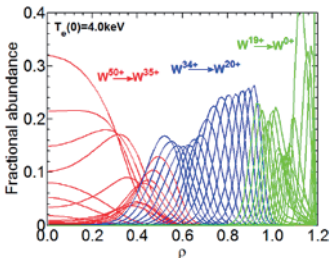

Fig. 2. Example of calculated FA of W ions in EAST plasmas.

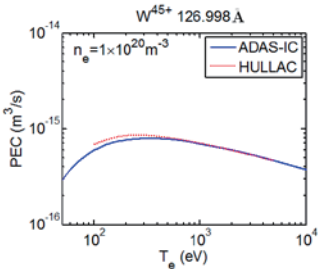

Fig. 3. PEC of W^{45+} at 126.998Å from ADAS and HULLAC databases.

2.2 Method 2: qualitative analysis based on total radiation loss measurement

The cooling rate, L_W, is calculated with equation (3). The radiation power loss from W ions can be then evaluated from equation (4), in which L_w^{q+} is the radiation power coefficient of W^{q+} calculated from ADAS database. The L_W calculated with L_w^{q+} from average ion model [4] and ADAS database [5] are compared in Figure 4. The calculated L_w is then compared with experimentally obtained ones in Ref. [6].

$$L_W(T_e, n_e) = \sum_q L_W^{q+}(T_e, n_e) N_{W^{q+}}/N_W \quad (3)$$

$$P_W = \int L_W(T_e, n_e) n_e(r)\, n_W(r) \mathrm{d}V \quad (4)$$

When the c_w is analyzed with this method for a target shot, another calibration shot with similar T_e profile to the target shot is required, and a sudden increase in the radiation power loss caused by the c_w increase in the calibration shot. Radiation power loss is experimentally measured by bolometer system [7]. For the calibration shot, the cooling rate calibrated from the power loss is calculated with equation (5). The ΔP_{rad} and $\Delta I_{W\text{-}UTA}/n_e$ are shown in Figure 5. For the target shot, the radiation power loss caused by W can be described by equation (6). The c_W can be then evaluated with equation (7).

$$L_W^{Cali} = \Delta P_{rad}^{Cali} / (\Delta I_{W-UTA}^{Cali}/n_e) \quad (5).$$

$$P_W = L_W^{Cali} \cdot (I_{W-UTA}/n_e) = \int L_W(T_e, n_e) n_e(r)\, n_W(r) \mathrm{d}V = \int L_W(T_e, n_e) n_e^2(r)\, c_W f_{c_W}(r) \mathrm{d}V \quad (6)$$

$$c_W = L_W^{Cali} \cdot (I_{W-UTA}/n_e) / \int L_W(T_e, n_e) n_e^2(r)\, f_{c_W}(r) \mathrm{d}V \quad (7)$$

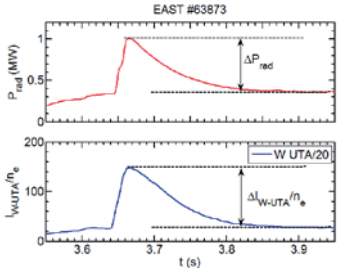

Fig. 5. Sudden increase in radiation power loss caused by W

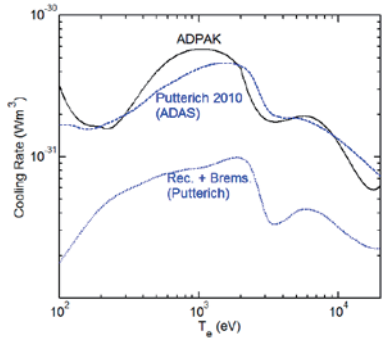

Fig. 4. Comparison of L_W calculated with L_w^{q+} from average ion model and ADAS database.

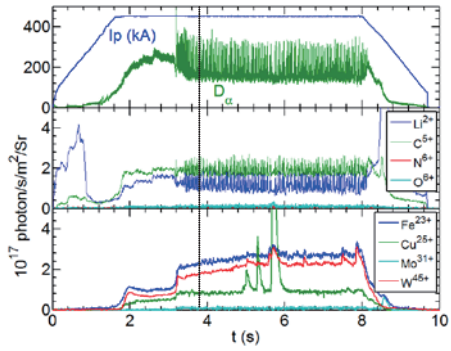

Fig. 6. Time evolution of absolute intensity of emission lines from Li^{2+}, C^{5+}, N^{6+}, O^{6+}, Fe^{22+}, Cu^{25+}, Mo^{31+} and W^{45+} at 134.99 Å, 33.73 Å, 24.78 Å, 21.6 Å, 132.85 Å, 111.186 Å, 127.868 Å and 126.998Å, respectively. The vertical dashed line indicates t=3.8s.

3. Results

The time evolution of absolute intensity of several emission lines for shot #62946 is plotted in Figure 6. In the analysis, the c_W is evaluated at 3.8s during steady state H-mode phase. The T_e and n_e profiles are obtained experimentally as shown in Figure 7. The profiles of W transport coefficients are assumed as shown in Figure 8. The calculated profiles of W ion density with the method in Sec. 2.1 are plotted in

Figure 9. The comparison of evaluated c_W with the two methods is shown in Table 1. It is found that during the steady state H-mode phase in this shot, the c_w is in the order of 10^{-5}, and the c_w evaluated with W cooling rate is 4 times higher than that evaluated with PEC.

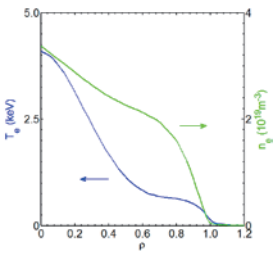

Fig. 7. T_e and n_e profiles.

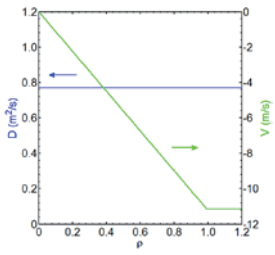

Fig. 8. Assumed profiles of W transport coefficients.

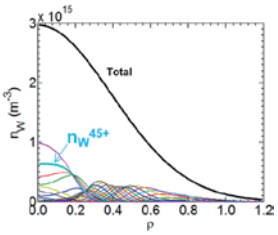

Fig. 9. Calculated profiles of density of W ions using PEC.

Table 1. Results of evaluated c_W

Method	$n_W(0)/n_e(0)$	N_W/N_e
PEC of W^{45+} (ADAS)	0.0019%	0.0012%
Cooling rate (ADPAK)	0.0080%	0.0056%

4. Summary

Tungsten spectra have been measured in EAST discharges using newly installed EUV spectrometers. The tungsten behavior has been studied with quantitative analysis. Methods for evaluation of c_w based on the cooling rate of tungsten ions and the PEC at 126.998Å of W^{45+} ions are introduced with required atomic data. It is found that the c_w from W cooling rate is roughly 4 times bigger than that from PEC. It suggests further detailed work is necessary for the quantitative evaluation of tungsten ion density.

Acknowledgements

This work was supported by the National Magnetic Confinement Fusion Science Program of China (Grant Nos.2014GB124006, 2013GB105003,2015GB101000), National Natural Science Foundation of China (Grant Nos. 11575244, 11275231, 11305207), and was partly supported by the JSPS-NRF-NSFC A3 Foresight Program in the field of Plasma Physics (NSFC: No. 11261140328, NRF : No. 2012K2A2A6000443)

References

[1] B. N. Wan, et al., Nucl. Fusion **55** (2015)104015.

[2] L. Zhang, et al., submitted to Nucl. Mat. Energy.

[3] L. Zhang, et al., Rev. Sci. Instrum. **86** (2015)123509.

[4] D Post, et al., At. Data Nucl. Data Tables **20** (1977) 397.

[5] T Pütterich, et al., Nucl. Fusion **50** (2010) 025021.

[6] I Murakami et al., Nucl. Fusion **55** (2015) 093016.

[7] Y. M. Duan, et al., Plasma Sci. Technol. **13** (2011) 546.

VUV spectroscopy for tungsten WIV-WVII line emissions in Large Helical Device

T. Oishi[1,2], S. Morita[1,2], X. L. Huang[1], H. M. Zhang[2], Y. Liu[2], M. Goto[1,2] and the LHD Experiment Group[1]

[1]National Institute for Fusion Science, National Institutes of Natural Sciences, Toki 509-5292, Gifu, Japan
[2]Department of Fusion Science, SOKENDAI (Graduate University for Advanced Studies), Toki 509-5292, Gifu, Japan

Abstract

Spectroscopy diagnostics is conducted to measure spectra of emissions released from tungsten ions in Large Helical Device (LHD) for steady state operations of current-free plasma discharges. The tungsten ions are introduced in the LHD plasma by injecting a coaxial tungsten impurity pellet. VUV spectroscopy using a high-resolution 3 m normal incidence spectrometer has been applied to measure VUV lines from tungsten ions at lower ionization stages. Many tungsten lines of WIV-WVII are successfully observed just after the tungsten pellet injection as the first observation of line emissions from low-ionized tungsten ions in magnetically-confined fusion plasma experiments. Five WVI lines at 605.93 Å (5d-6p), 639.68 Å (5d-6p), 677.72 Å (5d-6p), 1168.15 Å (6s-6p) and 1467.96 Å (6s-6p) have the highest intensity and are entirely isolated from other intrinsic impurity lines.

Keywords: plasma spectroscopy, vacuum ultraviolet, magnetically confined fusion, impurity transport, tungsten ions in lower ionization stages

1. Introduction

Tungsten is regarded as a leading candidate material for the plasma facing components (PFCs) in ITER and future fusion reactors because of its high melting point, low sputtering yield, and low tritium retention. One of major concerns on the tungsten PFC is that the tungsten ion causes a large radiation loss due to its large atomic number of Z = 74 when it is contaminated into plasmas. Considering transport processes of tungsten impurity in plasma confinement devices with tungsten PFCs, firstly neutral tungsten atoms are sputtered and released from the divertor plates. A line emission from the tungsten neutrals has been measured using visible spectroscopies as an indicator of the sputtering yield. On the other hand, tungsten ions at higher ionization stages are distributed in a core region of high-temperature plasmas. Their emissinons in the wavelength range of extreme ultraviolet (EUV) and soft X-ray (SX) have been most intensively measured to evaluate core tungsten accumulation phenomena. However, diagnostics for tungsten ions at lower ionization stages which are expected to be distributed in edge and divertor plasmas is quite insufficient even though it is necessary for accurate evaluation of tungsten influx and comprehensive understanding of the tungsten impurity transport in high temperature plasmas. In this study, vacuum ultraviolet (VUV) spectra of emissions released from tungsten ions are measured in the Large Helical Device (LHD) for contribution to the tungsten transport study in edge plasmas of ITER and other tungsten-divertor fusion devices and for the expansion of experimental database of tungsten line emissions.

2. Tungsten pellet injection experiments in LHD

Tungsten ions are distributed in the LHD plasma by injecting a pellet consisting of a small piece of tungsten metal wire enclosed by a carbon or polyethylene tube. The length and diameter of a W wire can be selected in ranges of 0.5 ~ 1.0 mm and 0.02 ~ 0.2 mm, respectively. Then a pellet is made up of approximately $1 \times 10^{16} \sim 2 \times 10^{18}$ W atoms and accelerated by pressurized He gas of 10 ~ 20 atm. The pellet injection orbit is located on the midplane of the plasma having a 12° angle from the normal to the toroidal magnetic axis. Figure 1(a) shows a typical waveform of the tungsten pellet injection experiment with hydrogen discharge with magnetic axis position, R_{ax}, of 3.60 m at toroidal magnetic field of B_t, of −2.75 T. Here, the minus sign of B_t means inverse direction, i.e., counter-clockwise direction. The plasma was initiated by the electron cyclotron heating, and further heated by the neutral hydrogen beams. At the timing of the tungsten pellet injection of 4.0 s, the total port-through power of the neutral beam injection (NBI) for heating, P_{NBI}, is 12 MW and the central electron density, n_{e0}, is 2×10^{13} cm^{-3}. After the pellet injection, the central electron temperature, T_{e0}, and the plasma stored energy evaluated from the kinetic energy of electrons, W_{pe}, quickly decrease, while n_{e0} increases. After T_{e0} reaches the minimum value around 0.2 keV, T_{e0} and W_{pe} start to recover due to continuous neutral beam heating. We have found that plasmas can be survive after the tungsten pellet injection with high P_{NBI} and low n_{e0} as shown in Fig. 1 (a) (so-called "OK" shots). However, depending on experimental conditions, plasmas collapse suddenly just after the pellet injection (so-called "collapse" shots). Figures 1 (b) and (c) shows waveforms of "collapse" shots with high n_{e0} of 4×10^{13} cm^{-3} and low P_{NBI} of 6 MW at the pellet injection, respectively. In these cases, the neutral beam heating cannot afford to sustain plasmas with high power loss by ionization, excitation, and radiation due to high electron density.

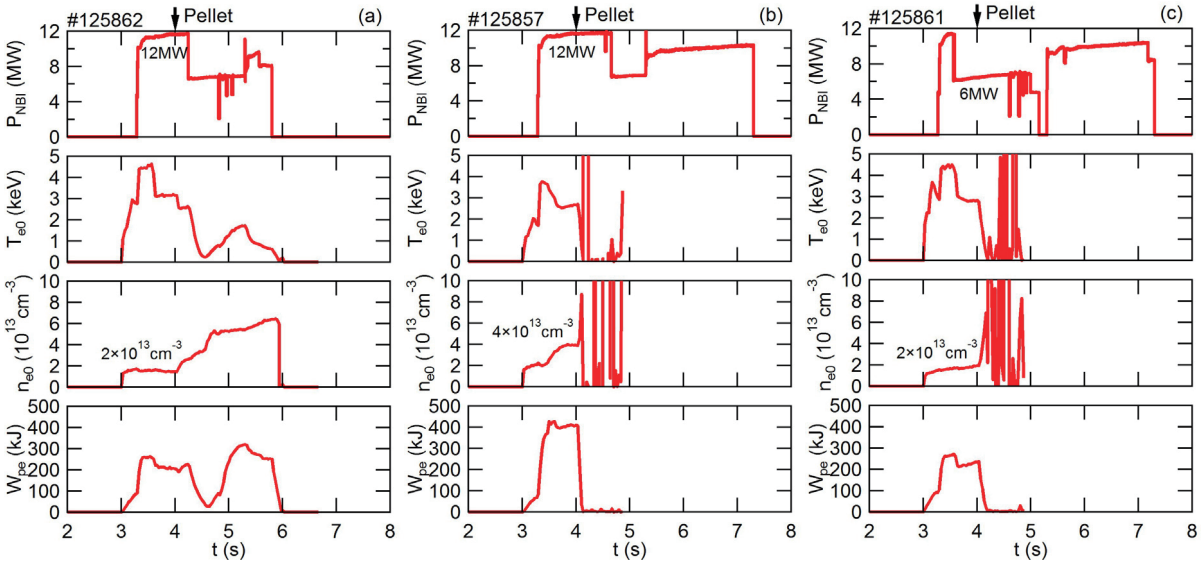

Figure 1. Port-trough NBI power, P_{NBI}, central electron temperature, T_{e0}, central electron density, n_{e0}, and electron kinetic energy, W_{pe}, in typical waveforms of W pellet injection experiments in LHD. (a) "OK" shot in which plasmas can be survive after the tungsten pellet injection with high P_{NBI} and low n_{e0}. Plasmas collapse just after the pellet injection due to (b) high n_{e0} and (c) low P_{NBI} at the pellet injection, respectively, which are called "Collapse" shots.

As shown in Fig. 1, success in the tungsten pellet injection depends on both the NBI heating power and the electron density. Figure 2 shows the results of the pellet injection as "OK" or "collapse" as a function of P_{NBI} and the averaged electron density, n_e. We can select the number of atoms enclosed in a pellet, N_W, by changing the size of the pellet. In Fig. 2, open circle and closed circle means "OK" and "collapse" shot, respectively, and the size of circles corresponds N_W. Figure 2 (a) shows the result with R_{ax} = 3.60 m. The pellet injection successes in the range of high P_{NBI} and low n_e while it fails in the range of low P_{NBI} and high n_e. When n_W is small, plasma can survive in low P_{NBI} and high n_e range. We conducted the experiments with three kinds of R_{ax} of 3.60 m, 3.75 m, and 3.90 m. Large R_{ax} value means that a position of the magnetic axis is shifted outward. Figures 2 (b) and (c) shows the "OK" and "collapse" plot with R_{ax} = 3.75 m and 3.90 m, respectively. Parameter space for "OK" shot is limited to lower n_e range in more outward-shifted configuration. It means that robustness against tungsten injection depends on the magnetic configurations.

3. VUV diagnostics for tungsten line emissions

A 3m normal incidence VUV spectrometer (McPherson model 2253) is installed on an outboard midplane diagnostic port which is the same as the impurity pellet injector [1]. A back-illuminated CCD detector (Andor model DO435-BN: 1024 × 1024 pixels) is placed at the position of the exit slit of the spectrometer. A high wavelength dispersion of 0.037 Å/pixel enables measurements of the Doppler profiles of the impurity lines in the working wavelength range of 300-3200 Å. The viewing angle covers entire vertical region of LHD plasma at a horizontally-elongated poloidal cross section. In this study, the "full-binning" measurement was employed for detailed observations of spectra of line emissions in which time resolution is 50 ms and all 1024 vertical pixels are replaced by single channel. We conducted VUV measurements by scanning the wavelength shot by shot between the wavelength ranges of 495-1475 Å.

Figure 3 shows examples of tungsten spectra measured in the time frame just after the tungsten pellet injection in hydrogen discharge in LHD. Observed tungsten lines are indicated by solid arrows in this figure. Among many tungsten lines of WIV - WVII observed in this experiment, it was found that WVI

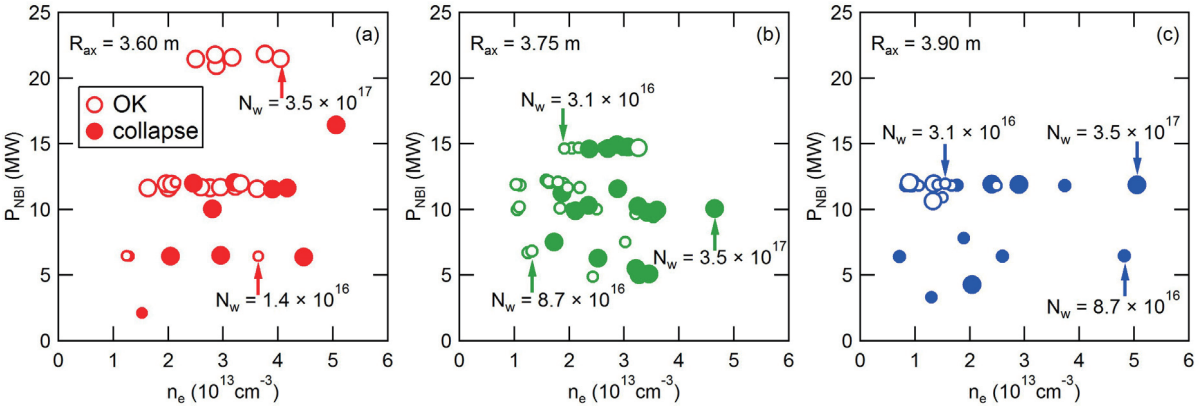

Figure 2. Results of the pellet injection as "OK" or "collapse" as a function of P_{NBI} and the averaged electron density, n_e, with R_{ax} = (a) 3.60 m, (b) 3.75 m, (c) 3.90 m. The size of circles corresponds the number of atoms in a pellet, N_W. Open and closed circle means "OK" and "collapse" shot, respectively.

lines emitted with the brightest intensities. We successfully observed five bright WVI lines at 605.93 Å (5d-6p), 639.68 Å (5d-6p), 677.72 Å (5d-6p), 1168.15 Å (6s-6p) and 1467.96 Å which were entirely isolated from other intrinsic impurity lines [2]. In addition, WV lines were observed in a wide wavelength range of 715-1370 Å.

4. Summary

VUV spectroscopy using a high-resolution 3 m normal incidence spectrometer has been applied to measure VUV lines from tungsten ions at lower ionization stages in LHD. We successfully observed several bright WVI lines. The result strongly suggests that those lines will be useful for the spectroscopic study in ITER and other tungsten-divertor devices.

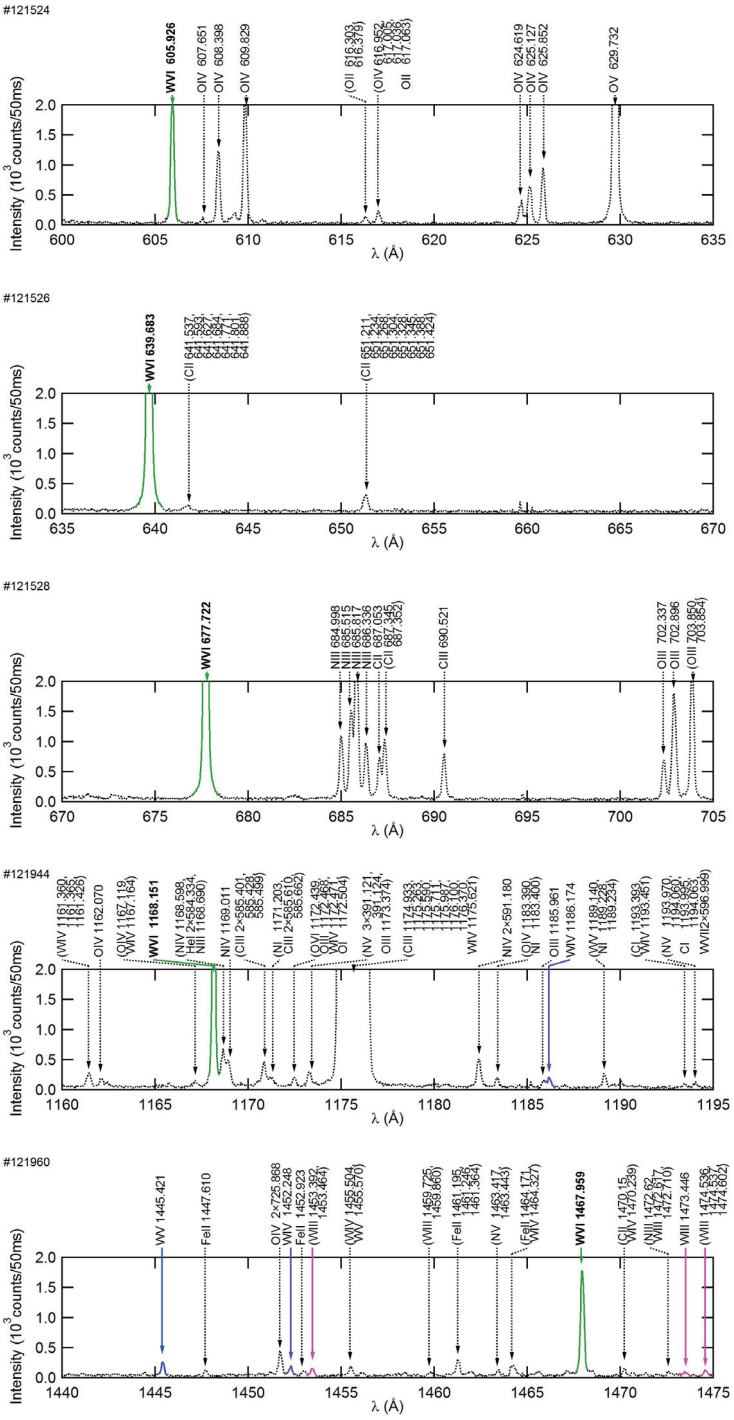

Figure 3. VUV spectra including WVI emission lines.

Acknowledgements

The authors thank all the members of the LHD team for their cooperation with the LHD operation. This work is partially conducted under the LHD project financial support (NIFS14ULPP010). This work was also supported by Grant-in-Aid for Young Scientists (B) 26800282 and partially supported by the JSPS-NRF-NSFC A3 Foresight Program in the Field of Plasma Physics (NSFC: No.11261140328, NRF: No.2012K2A2A6000443).

References

[1] T. Oishi, S. Morita, C. F. Dong *et al.*, Applied Optics **53** (2014) 6900.

[2] T. Oishi, S. Morita, X. L. Huang *et al.*, Physica Scripta **91** (2016) 025602.

Direct observation of the M1 transition between the ground state fine structure splitting of W VIII

MITA Momoe and NAKAMURA Nobuyuki
Inst. for Laser Science, The Univ. of Electro-Communications, Tokyo 182-8585, Japan

Abstract

We present direct observation of the M1 transition between the fine structure splitting in the $4f^{13}5s^25p^6\ ^2F$ ground state of W VIII. The observed wavelength 574.44 ± 0.05 nm (air) (preliminary), which corresponds to the fine structure splitting of 17403 ± 2 cm^{-1} (preliminary), shows reasonable agreement with the previously reported value 17410 ± 5 cm^{-1} obtained indirectly through the analysis of EUV spectra [Ryabtsev *et al.*, Atoms **3** (2015) 273].

Keywords: EBIT, tungsten ions, visible spectroscopy, plasma diagnostics

1.Introduction

Tungsten will be used as a plasma-facing material in ITER, and thus is considered to be the main impurity ions in the ITER plasma [1]. In order to suppress the radiation loss due to the emission of the impurity tungsten ions, it is important to understand the influx and the charge evolution of tungsten ions in the plasma through spectroscopic diagnostics. There is thus a strong demand for spectroscopic data of tungsten ions. In particular, it has been recently pointed out that the diagnostics and control of the edge plasma are extremely important for steady state operation of high-temperature plasmas. Thus the atomic data of relatively low charged tungsten ions are growing significance in the ITER plasma diagnostics [2].

Recently, Ryabtsev and co-workers [3, 4, 5] observed EUV spectra of W VIII excited in vacuum spark and made detail analysis of the spectra with the aid of a line identification program [6, 7]. Through their efforts, it has been confirmed that the ground state configuration of W VIII is $4f^{13}5s^25p^6$, which had been uncertain in the previous experimental [8] and theoretical [9, 10] studies due to the competition with $4f^{14}5s^25p^5$. They also determined the fine structure splitting in the ground state ($^2F_{5/2}$ and $^2F_{7/2}$) to be 17410 ± 5 cm^{-1}.

We have been using an electron beam ion trap (EBIT) to observe previously unreported lines of tungsten ions [11, 12]. An EBIT produces highly charged ions through successive ionization of trapped ions by a quasi-monoenergetic electron beam. It is thus possible to produce selected charge state ions by tuning the electron beam energy, and thus to obtain simple spectra which are useful to identify previously unreported lines. In this paper, we

present observation of the M1 transition between fine structure splitting in the ground state $4f^{13}5s^25p^6\ ^2F$ of W VIII.

2. Experiment

The experimental setup and the method of the present measurements were essentially the same as those used in our previous studies [13, 12]. Multiply charged tungsten ions were produced with a compact electron beam ion trap (called CoBIT) at the University of Electro-Communications in Tokyo. The detailed description on the device is given in the previous paper [14]. In the present study, tungsten was introduced into the trap through a gas injector as a vapor of $W(CO)_6$. Visible emission was observed with a commercial Czerny-Turner type of visible spectrometer. A biconvex lens was used to focus the emission on the entrance slit of the spectrometer. The diffracted light was detected with a liquid-nitrogen-cooled back-illuminated CCD. The wavelength was calibrated using emission lines from several standard lamps placed outside CoBIT. The uncertainty of the wavelength calibration was estimated to be 0.05 nm (preliminary) including systematics. Emission in the EUV range was also observed to help the identification of visible lines. A grazing-incidence flat-field spectrometer [15] consisting of a 1200 g/mm concave grating and a Peltier-cooled back-illuminated CCD was used.

3. Results and discussion

Figure 1 shows the visible and EUV spectra obtained simultaneously at electron energies of 90, 100, 115, and 130 eV. In the previous study with the Livermore EBIT, the EUV spectra of tungsten ions were observed with wavelength and electron energy ranges similar to the present study, and the several transitions of W VII and VIII were identified [2]. Our spectra shown in Fig. 1 are generally consistent with their spectra; thus, through the comparison with their spectra the lines of W VII and VIII can be identified as shown in the figure. Based on the energy dependence, a cluster of lines near 19nm can be assigned to W IX although there were not identified in the previous Livermore spectra.

In the visible spectra, the line observed at 574 nm shows the same electron energy dependence as the W VIII lines in the EUV spectra. Thus it can be assigned to the transition between the fine structure splitting of the ^2F ground state in W VIII. The wavelength is consistent with the energy interval 17410 cm^{-1} previously obtained from the high resolution EUV spectra of vacuum spark [3]. The visible spectra shown in Fig. 1 were observed with a low dispersion grating (300 g/mm brazed at 500 nm) to cover a

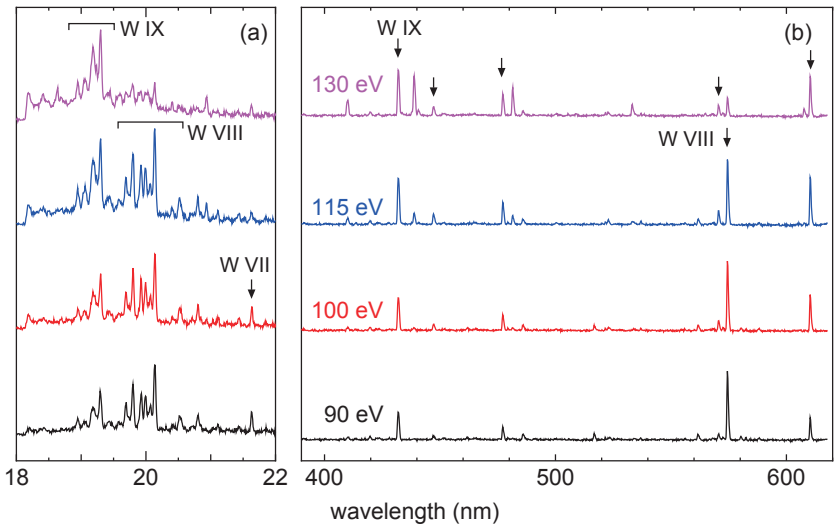

Figure 1: Spectra of tungsten ions in (a) the EUV range and (b) the visible range, obtained simultaneously at electron energies of 90 (black), 100 (red), 115 (blue), and 130 eV (magenta).

wide visible wavelength range (350 to 620 nm). We have confirmed that in the observed wavelength range, the line at 574 nm is the only prominent line that can be assigned to W VIII. It is reasonable considering the energy level of W VIII. According to the calculation by Ryabtsev *et al.* (See Fig. 2 of Ref. [3]), the two configurations $4f^{14}5p^5$ and $4f^{13}5p^6$ compete for the ground state, and the other configurations have excitation energies of larger than 300,000 cm^{-1}, which would make transitions in the EUV range. The two lowest configurations both have a doublet structure ($^2P_{1/2,3/2}$ for $4f^{14}5p^5$ and $^2F_{5/2,7/2}$ for $4f^{13}5p^6$), but the energy splitting for $4f^{14}5p^5$ ^2P is too large to be observed in the visible range, so that the transition between the doublet levels of $4f^{13}5p^6$ ^2F is considered to be the only transition that fall in the visible range. It may also be possible to have more visible transitions if we can observe transitions between high excited levels. However, there is less chance to observe such transitions in the low density EBIT plasma.

In order to obtain the transition wavelength, we have observed the visible spectrum with a higher resolution using a 1200 g/mm grating brazed at 400 nm. The experimental wavelength obtained from the higher resolution observation is 574.44 ± 0.05 nm (air) (preliminary), which corresponds to a fine structure splitting of 17403 ± 2 cm^{-1} (preliminary). Our present value shows reasonable agreement with the previous experimental value by Ryabtsev *et al.* [3]. It is noted that the Ryabtsev value was obtained through the analysis of the EUV spectrum containing a lot of transitions arising from highly excited states to

the ground configurations. On the other hand, the present experiment is the first direct observation of the transition between the fine structure splitting. The present result has confirmed the reliability of the analysis done by Ryabtsev *et al.*

Acknowledgement

This work was supported by JSPS KAKENHI Grant Numbers 16H04623, 16H04028, and partly supported by the JSPS-NRF-NSFC A3 Foresight Program in the field of Plasma Physics (NSFC: No.11261140328, NRF: No.2012K2A2A6000443).

References

[1] Y. Ralchenko, Plasma Fusion Res. **8**, 2503024 (2013).
[2] J. Clementson, T. Lennartsson, and P. Beiersdorfer, Atoms **3**, 407 (2015).
[3] A. Ryabtsev *et al.* , Atoms **3**, 273 (2015).
[4] A. Ryabtsev *et al.* , Optics and Spectroscopy **113**, 109 (2012).
[5] A. Ryabtsev *et al.* , Physica Scripta **87**, 045303 (2013).
[6] V. Azarov, Physica Scripta **44**, 528 (1991).
[7] V. Azarov, Physica Scripta **48**, 656 (1993).
[8] G. Veres *et al.* , J. Quant. Spectrosc. Radiat. Transfer **56**, 295 (1996).
[9] T. A. Carlson *et al.* , Atomic Data and Nuclear Data Tables **2**, 63 (1970).
[10] J. Sugar and V. Kaufman, Physical Review A **12**, 994 (1975).
[11] A. Komatsu *et al.* , Plasma Fusion Res. **7**, 1201158 (2012).
[12] Y. Kobayashi *et al.*, Physical Review A **92**, 022510 (2015).
[13] Y. Kobayashi *et al.* , Phys. Rev. A **89**, 010501(R) (2014).
[14] N. Nakamura *et al.* , Rev. Sci. Instrum. **79**, 063104 (2008).
[15] H. Ohashi *et al.* , Rev. Sci. Instrum. **82**, 083103 (2011).

Current progress of a NIFS project: spectroscopic measurements and database development for highly charged rare earth elements

F. Koike*
Department of Materials and Life Sciences, Sophia University, 7-1 Kioi-cho, Chiyoda-ku, Tokyo, 102-8554 Japan
C. Suzuki, I. Murakami, H. A. Sakaue, M. Goto, D. Kato, T. Kato, S. Morita, H. Funaba
National Institute for Fusion Science, Toki, Gifu 509-5292, Japan
A. Sasaki
Quantum Beam Science Directorate, Japan Atomic Energy Agency, 8-1 Umemidai, Kizugawa, Kyoto 619-0215, Japan
**e-mail: koikef@sophia.ac.jp*

Abstract

The extreme ultra violet (EUV) optical transitions of lanthanide highly charged ions have been observed in LHD plasmas as one of the NIFS collaborative research projects. The structure of unresolved transition array (UTA) from the inter sub-shell transitions in N-shell open ions has been investigated theoretically to facilitate their comparison to the data. Atomic structures and optical transition rates have been calculated by using GRASP92 and RATIP including the interactions between the configurations $4p^5 4d^{w+1}$ and $4p^6 4d^{w-1} 4f$ in the excited states with $w = 2$ to 9.

Keywords: MCDF, EUV, lanthanide ions, UTA

1 Introduction

The spectral data and the knowledge on the dynamics of extreme ultraviolet (EUV) optical emissions from highly charged heavy ions are of recently growing needs in a variety of fields such as the development of shorter wavelength light sources for semiconductor lithography [1], the development of microscopes using shorter wavelength light sources [2], or the exploration of tools for the diagnostics of nuclear fusion plasmas [3] in magnetic confinement as well as inertial confinement fusion reactors.

Generally speaking, the valence shells of highly charged atomic ions are mostly of partially filled open shells regardless if they are in the ground or excited states. In the case of N, open sub-shells, $dd - pf$ type configuration interaction is significant. In N sub-shells, the binding energies of single electron orbitals are larger in the order of $4s$, $4p$, $4d$, $4f$. If we replace a $4d$ electron by a $4p$ electron with oposite parity and larger binding energy and another $4d$ electron by a $4f$ electron with oposite parity and smaller binding energy at the same time in a $4d^2$ configuration, we may have a $4p4f$ configuration that has the same total symmetry with small difference of total binding energy in unperturbed orbital energy basis. We may expect that the interactions between these two configurations are substantially strong to modify the states, which may cause the drastic change of the spectral feature in the EUV region for highly charged heavy atomic ions.

Extensive studies of EUV emissions from lanthanide ions have been performed in laser produced plasmas [4–6], in vacuum spark discharges [4, 7], and in tokamak [8–11]. Recently systematic studies on EUV spectra from highly charged heavy ions have been carried out in the Large Helical Device (LHD) plasmas at National Institute for Fusion Science (NIFS) by our

group [3, 12–17]. And, further on, charge-separated spectroscopy measurements for Gd and Dy ions have recently been carried out in electron beam ion traps (EBIT) [18–20].

The wavelengths of the $4d - 4f$ transitions are reported to be, for example, 7.9 nm for Nd ($Z = 60$), 7.0 nm for Eu ($Z = 63$) , and 6.8 nm for Gd ($Z = 64$) [21]. The $4d - 4f$ transitions of Tb ($Z = 65$) at 6.5 nm has been investigated theoretically by Sasaki et al [22]. To study the EUV light emissions from highly charged heavy ions in connection to their atomic structures, it is quite effective to investigate in thin plasma conditions. We have proposed the use of the LHD plasmas for the spectral measurement of lanthanide elements. We have presently covered almost the whole range of the atomic number in lanthanide atoms, say, for atoms with $Z = 58, 60, 62, 64, 65, 66, 67, 68, 69, 70, 71$, and 72 [3, 23]. The present accumulation of the spectral data is now enabling our investigation on the Z-dependence of the spectral features in lanthanide elements. We are continuing the spectral analysis using the available data. We have made elaborate atomic structure calculations based on a Multi-Configuration Dirac-Fock (MCDF) approximation to compare the results with the experimental data.

We describe the theory and the method of numerical procedure in the next section. In section 3, we describe and discuss the representative results of the present calculation. And finally, in section 4, we give concluding remarks.

2 Theory and numerical procedure

We carry out the Multi-Configuration Dirac-Fock (MCDF) calculations of electronic state structures of the ions with wide range of charge states $q+$ for heavy atomic ions A^{q+}; in those ions the N-shells are mostly partially filled in their ground states and this causes the complexity of the electronic structures. We take the following Dirac-Coulomb Hamiltonian H_{DC} to perform the MCDF procedure; that is

$$H_{DC} \;=\; \sum_i h_i \;+\; \sum_{i>j} \frac{1}{r_{ij}}, \tag{1}$$

where, h_i is the Dirac Hamiltonian of a single electron atomic ion for the i'th electron, and r_{ij} is the distance between the electrons i and j. We use the atomic units $e = m = \hbar = 1$ throughout the paper unless otherwise specified. In MCDF calculations, we optimize the individual single electron atomic orbitals in ASF, Ψ, which consists of the linear combination of CSF's, Φ_α, numerically by means of the self-consistent field (SCF) iterative procedure, where α is the set of quantum numbers to specify the configuration. The Breit interaction and the QED corrections are included as perturbation using the results of MCDF calculation. The ASF Ψ is represented by

$$\Psi \;=\; \sum_\alpha c_\alpha \Phi_\alpha, \tag{2}$$

where, c_α is the expansion coefficient, which reflects the interactions between the CSF's, and can be called the mixing coefficient due to the configuration interactions (CI). Both the mixing coefficients c_α and the single electron orbitals are optimized simultaneously in the MCDF procedure. We may find the optimum shape of the single electron atomic orbitals that fits to the multi-configuration state under consideration. We can avoid the excessive expansion of ASF in terms of many CSF's which contain the variety of single electron orbitals; this feature gives us the chance to implement the realistic physical characteristics to the individual single electron orbitals.

We employed the General purpose Relativistic Atomic Structure Program 92 (GRASP92) [24] for the electronic structure, and the Relativistic Atomic Transition and Ionization Properties (RATIP) code [25, 26] for transition wavelengths and strengths. We have made the MCDF calculations for all the lanthanide atomic species for ions with the number of electrons from 27 to 59. In the present calculations, we included all the CSF's with one electron excitations to the sub-shell orbitals in the N-shell from the N-shell orbitals in the ground states. For instance, to calculate $Gd^{26+}1s^22s^22p^63s^23p^63d^{10}4s^24p^64d^2$ = [Ni]$4s^24p^64d^2$, we considered all the possible one electron excitations from $4s^24p^64d^2$ to $4d$ and $4f$ orbitals. We calculate wavelengths and the strengths of electric dipole (E1) transitions for all the possible combinations of the ASF's that are obtained by the MCDF procedure. In the case of Gd^{26+} ions, for instance, we calculate the transitions to the ground states $4s^24p^64d^2 - 4s^24p^64d4f$, and $4s^24p^64d^2 - 4s^24p^54d^3$, as well as between the excited states $4s^24p^64d4f - 4s^24p^54d^24f$, $4s^24p^54d^3 - 4s4p^64d^3$, $4s^24p^54d^24f - 4s4p^64d^24f$, $4s^24p^54d^24f - 4s^24p^54d^3$, and $4s4p^64d^24f - 4s4p^64d^3$. Although we can consider the orbital relaxations in RATIP, we adopt the common basis orbital sets in both the states before and after the optical transitions. The accuracy requirement is not as high as to urge us to adopt such a sophisticated method. And further on, by using the common basis orbitals, we can avoid the risk to face at large errors in the energy offset that come from the core electrons.

3 Numerical results and discussion

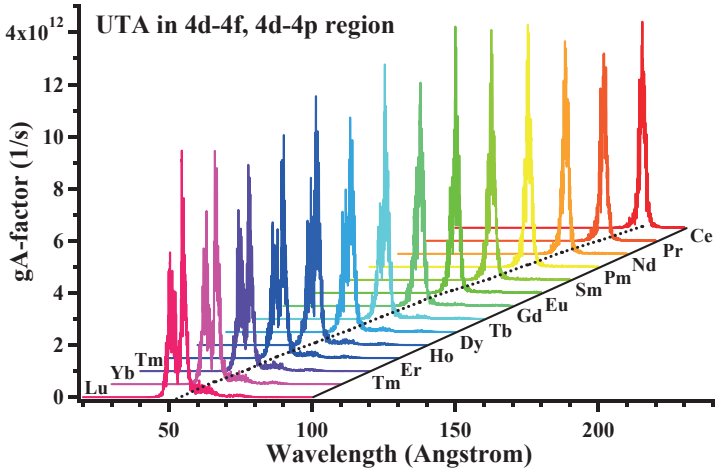

Figure 1: (color on line) Synthesized EUV photoemission spectra of Lanthanide atomic ions for the region of $4p - 4d$,$4d - 4f$ UTA. The distribution of weighted Einstein coefficients (gA-factors) for transitions between N sub-shell states of Ce ($Z = 58$) to Lu ($Z = 71$) for ions with a configuration [Ni]$4s^24p^64d^w (w = 2 \sim 8)$ in the ground state. Holizontal axis: Wavelength of the emitted photons in units of Å. Vertical axis: Sums of the weighted Einstein coefficients in units of $1/s$. The sums of all the calculated gA-factors have been convoluted by the Lorentzian function of full width at half maximum (FWHM) 0.10 Å and the triangular function of FWHM 0.10 Å. The dotted line under the curves indicate the wavelengths of the spectral peak position.

Fig.1 shows the distribution of weighted Einstein coefficients, i.e., gA-factors, for transitions between N sub-shell states of cerium (Ce, $Z = 58$) through lutetium (Lu, $Z = 71$) for

ions with a configuration [Ni]$4s^2 4p^6 4d^w$ in the ground state, where, w runs from 2 to 8. The sums of all the calculated gA-factors have been convoluted by the Lorentzian function of full width at half maximum (FWHM) 0.10 Å and the triangular function of FWHM 0.10 Å to synthesize the actual UTA emission spectra in plasmas or other media. Although the kinetic population analyses are desirable to compare the theoretical atomic structure calculations to the experimental spectra, the simple sum of gA-factors is still comparable if the plasmas are thin enough. We can see, in Fig.1, that the UTA spectral peaks are enough narrow compared to the term splittings of the excited states; the spread of the gA-factor distribution has been suppressed due to the interference between the $4p-4d$ and $4d-4f$ simultaneous transitions. The dotted line under the curves in Fig.1 indicate the wavelengths of the spectral peak position. We find that the wavelength that gives spectral peak position shifts towards the shorter wavelength region. Ohashi et al [27] has recently pointed out that the peak position obeys the Moseley type formula. We secondly give the numerical results of Yb ($Z = 70$) ions. In Fig.2, we illustrate

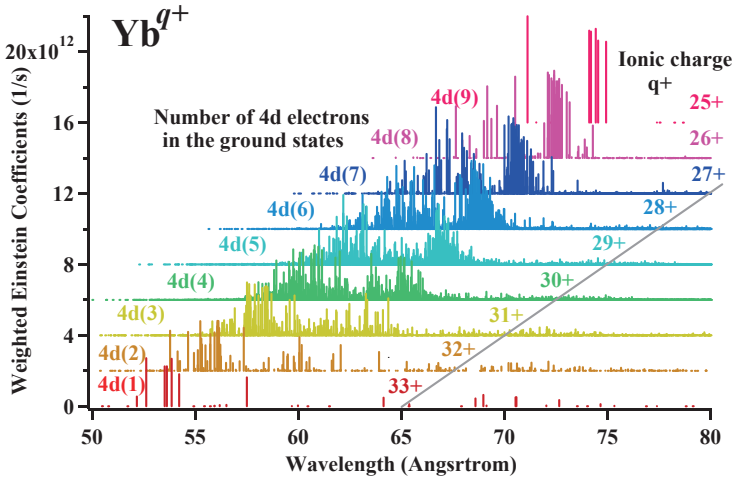

Figure 2: (color on line) Ionic charge dependence of the distribution of gA-factors in Yb ions. Vertical bars: the weighted Einstein coefficients for $4d - 4f$ and $4p - 4d$ transitions for individual ionic charges from Yb^{25+} with $4d^9$ to Yb^{33+} with $4d^1$. Horizontal axis: wavelength of emitted photons in units of Å. Vertical axis: weighted Einstein coefficients in units of $1/s$.

ionic charge dependence of the distribution of gA-factors by bar diagrams for each Yb^{q+} ion with $q = 25$ to 33. On the right hand side of each spectral entry, the charge state $q+$ is indicated and the corresponding occupation number of $4d$ electrons is given on the left hand side. The spectral profiles clearly shows doubly peaked nature especially near to the ions with half filled $4d$ sub-shells such as $4d^5$ or $4d^6$. The distance between the double peaks is about 10 Å and it stays almost constant for all the ionic charge states. The spectral profile shifts towards the shorter wavelength region by about 3 Å from $q = 33$ to 25. Then we may expect that the doubly peaked spectral nature will not be smeared out by their superposition over the different charge states. It would also be noteworthy that the spectral features at longer wavelength side are prominent at lower charge states whereas the shorter wavelength side are rather predominant at higher charge states. We will be suggested from this feature, that the $4d - 4f$ and $4p - 4d$ UTA spectrum may show up a shift of the appearance of the spectral peak position depending on the temperature of the source plasmas.

4 Conclusion

The accurate theoretical calculations of the atomic structures and dynamics that include the relativistic effects and the electron correlation effects provide us with a good base for precision analysis of highly charged atomic ions in plasmas or other media. To investigate the EUV optical emissions of lanthanide highly charged ions in the region of intra N shell UTA spectrum, we have carried out the MCDF calculations using the smallest possible numbers of atomic orbitals, which allow us to discuss the effect of electron correlations in the UTA spectrum on the basis of the characteristics of the single electron atomic orbitals. The detailed comparisons of the present numerical calculations to the existing experimental data are seriously desired, which will be issued in our forthcoming papers.

Acknowledgements

This work has been carried out with the support and under the auspices of the NIFS collaboration research program (NIFS12KLPF025). This work was partly supported by the JSPS-NRF-NSFC A3 Foresight Program in the field of Plasma Physics (NSFC: No. 11261140328, NRF: No. 2012K2A2A6000443).

References

[1] J. D. Gillaspy *EUV Sources for Lithography Edited by V. Bakshi, SPIE Press* 47 (2006).
[2] P. A. C. Takman, H. Stollberg, G. A. Johansson, A. Holmberg, M. Lindblom, and H. M. Hertz, *J. Microsc.* **226**, 175 (2007).
[3] C. Suzuki et al, *J. Phys.* **B45**, 135002 (2012).
[4] S. S. Churilov, R. R. Kildiyarova, A. N. Ryabtsev, and S. V. Sadovsky *Phys. Scr.* **80**, 045303 (2009).
[5] P. K. Carroll and G. OSullivan*Phys. Rev. A***2**5, 275 (1982).
[6] G. M. Zeng, H. Daido, T. Nishikawa, H. Takabe, S. Nakayama, H. Aritome, K. Murai, Y. Kato, M. Nakatsuka, and S. Nakai *J. Appl. Phys.* **7**5, 1923 (1994).
[7] P. Mandelbaum, M. Finkenthal, J. L. Schwob and M. Klapisch, *Phys. Rev.* **A 35** 5051(1987).
[8] M. Finkenthal et al *J. Appl. Phys.* **59**, 3644 (1986).
[9] M. Finkenthal, H. W. Moos, A. Bar-Shalom, N. Spector, A. Zigler, and E. Yarkoni *Phys. Rev.* **A38**, 288 (1988).
[10] M. Finkenthal, S. Lippmann, L. K. Huang, H. W. Moos, Y. T. Lee, N. Spector, A. Zigler, and E. Yarkoni *Phys. Scr.* **41**, 445 (1990).
[11] M. Fournier, W. H. Goldstein, A. Osterheld, M. Finkenthal, S. Lippmann, L. K. Huang, H. W. Moos, and N. Spector *Phys. Rev.* **A50**, 2248 (1994)
[12] T. Kato et al *J. Phys. B: At. Mol. Opt. Phys.* **41**, 035703 (2008).
[13] C. Suzuki et al *J. Phys. Conf. Ser.* **163** 012019 (2009).
[14] C. Suzuki C *J. Phys. B: At. Mol. Opt. Phys.* **43**, 074027 (2010).
[15] C. S. Harte et al *J. Phys. B: At. Mol. Opt. Phys.* **43** 205004 (2010).
[16] C. Suzuki C et al *J. Phys. B: At. Mol. Opt. Phys.* **44** 175004 (2011).
[17] C. Suzuki C et al, *J. Phys. B: At. Mol. Opt. Phys.* **48**, 144012 (2015).
[18] D. Kilbane, G. OSullivan, J. D. Gillaspy, Yu. Ralchenko, and J. Reader *Phys. Rev.* **A86**, 042503 (2012).

[19] H. Ohashi, H. A. Sakaue, and N. Nakamura *Phys. Scr.* **T156**, 014013 (2013).
[20] D. Kilbane, G. OSullivan, Y. A. Podpaly, J. D. Gillaspy, J. Reader, and Yu. Ralchenko *Eur. Phys. J.* **D68**, 222 (2014).
[21] O'Sullivan, et al, *J. Opt. Soc. America*, **71**, 227(1981).
[22] A. Sasaki, et al, *Appl. Phys. Lett.* **97**, 231501 (2010).
[23] F. Koike et al, *Proceedings of ICAMDATA* 6 (2013).
[24] F. A. Parpia, C. F. Fischer, and I. P. Grant, *Commpt. Phys. Commun.*, **94**, 249 (1996).
[25] S. Fritzsche, *J. Elec. Spec. Rel. Phenom.* , **114** –**116**, 1155 (2001).
[26] S. Fritzsche, *Comput. Phys. Commun.* **183**, 1525 (2012).
[27] H. Ohashi, T. Higashiguchi, et al, *Applied Physics Letters* **1**04 234107 (2014).

Charge exchange spectroscopy for multiply charged ions of high *Z* elements

H. Tanuma[1], N. Numadate[1], Y. Uchikura[1], K. Shimada[1], T. Akutsu[1], E. Long[2], and G. O'Sullivan[2]

[1]Department of Physics, Tokyo Metropolitan University, Hachioji, Tokyo 192-0397, Japan

[2] Department of Physics, University College Dublin, Belfield, Dublin 4, Ireland

Abstract

We have performed the ion beam collision experiments using multiply charged tantalum ions and observed EUV (extremely ultra-violet) emission spectra in collision of ions with molecular targets, namely N_2 and O_2. The broad UTAs (un-resolved transition arrays) from multiply charged Ta ions and the sharp emission lines from multiply charged fragment atomic ions are observed for the first time. The mechanism of the multiply charged fragment atoms are discussed.

Keywords: tantalum, EUV, charge exchange, UTA, ion-molecule collision, molecular dissociation

1. Introduction

Tungsten will be used as a component of plasma-facing devices in the International Thermonuclear Experimental Reactor (ITER). For the plasma diagnostic with the spectroscopic method and the understanding of impurity transport in the plasma, spectroscopic data of multiply charged tungsten is necessary indeed. However, as the review articles on the available data for tungsten emission lines has pointed out, the spectroscopic data for W IX – W XXVII ions are quite poor [1-3]. Therefore, a number of both experimental and theoretical studies for spectroscopic properties of highly charged tungsten ions have been reported in this decade. For example, extremely ultra-violet (EUV) emission spectra from W VIII – W XXVIII ions in the 20 nm region have been observed in the Large Helical Device (LHD) at the National Institute for Fusion Science (NIFS) following pellet injection into the plasma [4].

Charge exchange spectroscopy (CXS) is a powerful method used to observe emission lines of highly charged ions and to measure charge transfer cross sections in collisions of highly charged ions with neutral atoms/molecules. We had performed this type of spectroscopy on multiply charged Xe and Sn ions to provide the atomic data for the next-generation of semiconductor lithography [5, 6]. Through the series of experiments and theoretical analysis, we are convinced that the CXS is useful to observe not only the resonance transitions, which are the transitions from the excited states to the ground state, but also optical transitions between excited states.

In this work, we report new emission spectral date in charge exchange spectroscopy in collisions of multiply charged Ta ions with neutral gases. As tungsten has five isotopes of the mass numbers from 180 to 186, it is not suitable for the ion beam experiment with charge state separation after an analyzing by a dipole magnet. On the other hand, tantalum has Ta-181 with the natural abundance of 99.988%, then almost single isotope should be considered for tantalum. Because the atomic number of tungsten is 74 and that of

tantalum is 73, we can regard that the electronic structure and transitions are extremely similar between two of them. Therefore, we have decided to use Ta ions instead of W ions in our experiments.

2. Experiments

We had inserted a Ta sheet into a plasma chamber of a 14.25 GHz electron cyclotron resonance ion source (ECRIS) where an oxygen plasma of about 10^6 K had been confined by a magnetic field. Produced multiply charged Ta ions in the plasma were extracted with an electric potential of 15 kV, and the charge-state of ions was selected by using a double-focusing dipole magnet. The ion beam with single charge state was introduced into a collision cell filled with a target gas, and photon emissions from the collision cell in an EUV region were observed at the magic angle. A typical ion beam intensity was 1-10 nA at the most down-stream of the beam line, and a gas pressure in the cell was kept around $2x10^{-2}$ Pa. EUV emission spectra were measured by a compact grazing-incident spectrometer equipped with a gold-plated cylindrical mirror for light condensing and a variable-line-spacing (ca. 1200 lines/mm) grating. A CCD camera with a Peltier cooling system was installed in the spectrometer to observe emissions in the wavelength region of 5-30 nm. Because of the extremely weak intensity of EUV emissions, exposure times were 120 min.

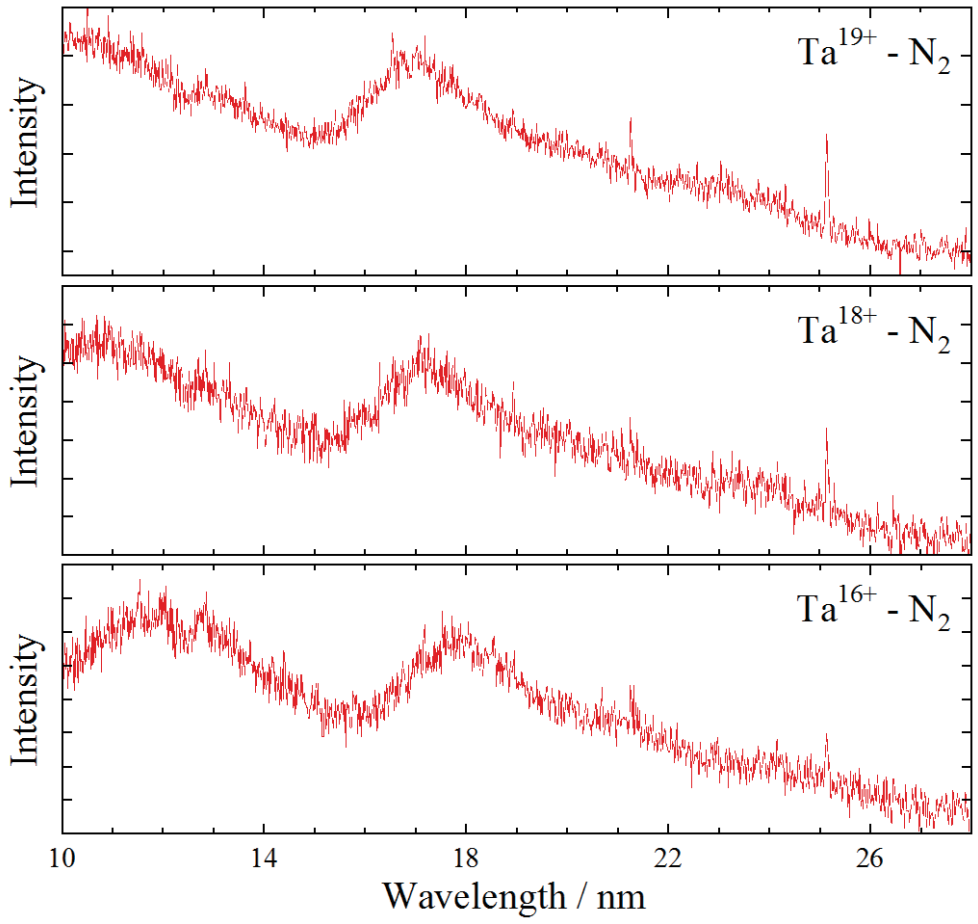

Fig. 1. EUV emission spectra observed in collisions of multiply Ta ions with N_2 target.

3. Results and Discussion

Fig. 1 shows typical EUV emission spectra observed in collisions of multiply charged Ta ions with N_2 gas target in the wavelength from 10 to 27 nm. We can see very broad unresolved transition arrays around 17-18 nm. As the single electron capture is generally dominant in collisions of multiply charged ions with neutral targets, the charge state of emitting ions might be one smaller than that of the incident ions. The peak positions of the UTAs depend on the charge states, and the wavelengths are shorter for higher charge states. This tendency is quite familiar for the UTAs of highly charged ions. The electronic configuration of the ground state Ta^{q+} ion is $[Kr]4d^{10}4f^{27-q}$ for q = 16-26. Therefore, the UTA might correspond to the 4f - 5d and/or 4f - 5g transitions. To make the identification definite, we need theoretical calculations with atomic structure code.

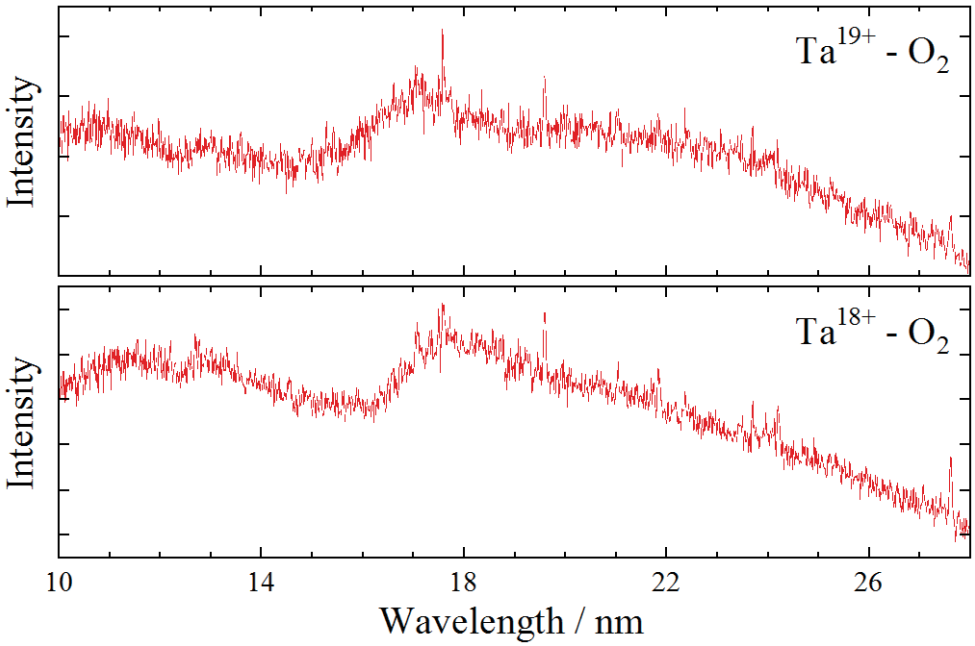

Fig. 2. EUV emission spectra observed in collisions of multiply Ta ions with O_2 target.

Not only the broad UTAs but also sharp emission lines have been observed in these spectra. The wavelengths of these lines are 20.9 and 24.7 nm are independent on the charge states of the incident ions. Therefore, these might be due to the emissions from the targets. EUV emission spectra in collisions of Ta ions with O_2 target have been shown in Fig. 2. As can be seen in these spectra, UTAs are quite similar for the cases of N_2 target. But, the sharp lines at 17.3 and 19.3 nm are completely different transitions from those observed in collisions with N_2. After the comparisons with the atomic spectra database, these line emissions can be regarded as N V 2s-3p (20.9 nm), N IV $2s^2$-2s3p (24.7 nm), O VI 2p-3d (17.3 nm), and O V 2s2p-2s3d (19.3 nm) transitions. Production of highly charged fragment ions by ion collisions have been reported [7-9]. In these previous works, they have measured kinetic energy release (KER) spectra for each fragmentation channel. However, as far as I know, this is the first time of the observation of EUV photo emissions from fragment atoms in collisions of multiply charged ions with molecular targets. Usually, in slow collisions of highly charged ions, multiply electron capture has extremely small cross sections.

Therefore, we must consider the possibility of an inner-shell ionization, because the cross sections of the inner-shell electron capture are also negligibly small. On the other hand, in the experiments of the inner-shell ionization of N_2 molecules by the synchrotron radiation facility, they observed only lower charge states of fragment atomic ions [10]. Therefore, we consider that the multiply charged atomic fragment ions might be produced in an inner-shell ionization and outer-shell capture by close collisions of highly charged ions.

4. Conclusion

We observed UTAs of highly charges Ta ions. However, at present, the identification of each transition have not been performed yet. We will identify the transitions corresponding to observed emission of transitions in the EUV region of multiply charged tantalum ions after the comparison with theoretical calculations as the same as Sn and Xe ions. And we believe such data is useful to understanding of the transitions of tungsten ions for the fusion plasma research.

Acknowledgements

This work was partly supported by the JSPS-NRF-NSFC A3 Foresight Program in the field of Plasma Physics (NSFC: No.11261140328, NRF: No.2012K2A2A6000443) and a grant-in-aid for Scientific Research (A) from the Ministry of Education, Culture, Sports, Science and Technology (MEXT).

References

[1] A. E. Kramida and T. Shirai, J. Phys. Chem. Ref. Data **35** (2006) 423.
[2] A. E. Kramida and T. Shirai, At. Data Nucl. Data Tables **95** (2009) 305.
[3] A. E. Kramida, Can. J. Phys. **89** (2011) 551.
[4] C. Suzuki *et al*., J. Phys. B: At. Mol. Opt. Phys. **44** (2011) 175004.
[5] H. Ohashi *et al*., J. Phys. B: At. Mol. Opt. Phys. **43** (2011) 065204.
[6] R. D'Arcy *et al*., Phys. Rev. A **85** (2012) 062513.
[7] A. Remscheid *et al*., J. Phys. B: At. Mol. Opt. Phys. **29** (1996) 515.
[8] B. Siegmann *et al*., Phys. Rev. A **62** (2000) 022718.
[9] J. Rajput *et al*., Phys. Rev. **74** (2006) 032701.
[10] T. Kaneyasu *et al*., J. Phys. B: At. Mol. Opt. Phys. **41** (2008) 135101.

Towards time-resolved imaging of electron and atomic motions in momentum space

Masahiko Takahashi

Institute of Multidisciplinary Research for Advanced Materials, Tohoku University, Sendai 980-8577, Japan

Abstract

We report the current status of our two ongoing projects using high-energy electron projectile. One is development of an experimental technique that is called time-resolved electron momentum spectroscopy (TR-EMS) and aims to take a series of snapshots of molecular orbitals, in momentum space, changing rapidly during a chemical reaction. The other is development of an experimental technique that is called time-resolved atomic momentum spectroscopy (TR-AMS) and aims to measure in real time how and how much change of atomic motions in a transient species are brought about by the preceding change of electron motion. It is discussed that a joint use of TR-EMS and TR-AMS would be a completely new, momentum space approach to studying ultrafast chemical reaction dynamics.

Keywords: electron momentum spectroscopy, atomic momentum spectroscopy, chemical reaction dynamics, ultrafast pump and probe technique, high-energy electron collision

1. Introduction

One of the goals in the field of chemical reaction dynamics is to watch reaction in real time. Indeed there have been a number of proposals and even some excellent experiments that seek to observe real time chemical reactions. For instance, the time resolved electron/X-ray diffraction technique [1, 2] has made it possible to visualize the structural dynamics during chemical reaction. The experiments can now show the decisive moments in the life of molecules, that is, the breaking and formation of chemical bonds between atoms. Nevertheless, there still remains the challenge to explore why the atoms are dancing in such a way. Since chemical reactions are driven by the change of electron motion, one may desire to have a pair of new experimental techniques. Namely, one is a technique that takes a series of snapshots of molecular orbitals changing rapidly during chemical reaction. The other is its complementary technique to measure in real time how and how much change of atomic motions in transient species are brought about by the preceding change of electron motion. These new techniques could be developed by advancing electron momentum spectroscopy and atomic momentum spectroscopy respectively, as discussed in the following sections.

2. Time-resolved electron momentum spectroscopy

Time-resolved electron momentum spectroscopy (TR-EMS), an advanced form of EMS, employs ultrashort laser and electron pulses in a pump-probe scheme. Basically, EMS is a sort of (e, $2e$) spectroscopy and involves coincident detection of the two outgoing electrons produced by impact ionization of a continuous beam of electrons having 1 keV or higher energy at large momentum transfer, so that it enables one to look at individual molecular orbitals in momentum space [3, 4].

The experimental set-up of TR-EMS [5] is schematically shown in Fig. 1. Briefly, the 800 nm output from the 5-kHz femtosecond laser is split into a pump path and an electron-generation path. 90% of the output is used to yield the pump laser pulse, which excites the molecule in the target gas beam to initiate a photo-induced unimolecular chemical reaction, after the 5-kHz repetition rate being halved by an optical chopper. On the other hand, 10% of the output is frequency tripled to produce electron pulses via the photoelectric effect. The photocathode is made of a silver film that is negatively biased to accelerate the electron pulses up to 1.2 keV. The resulting electron pulses of 1 ps temporal width are then used to induce EMS scattering. The EMS events are detected by an EMS spectrometer for which an exceptionally large spherical analyzer is employed.

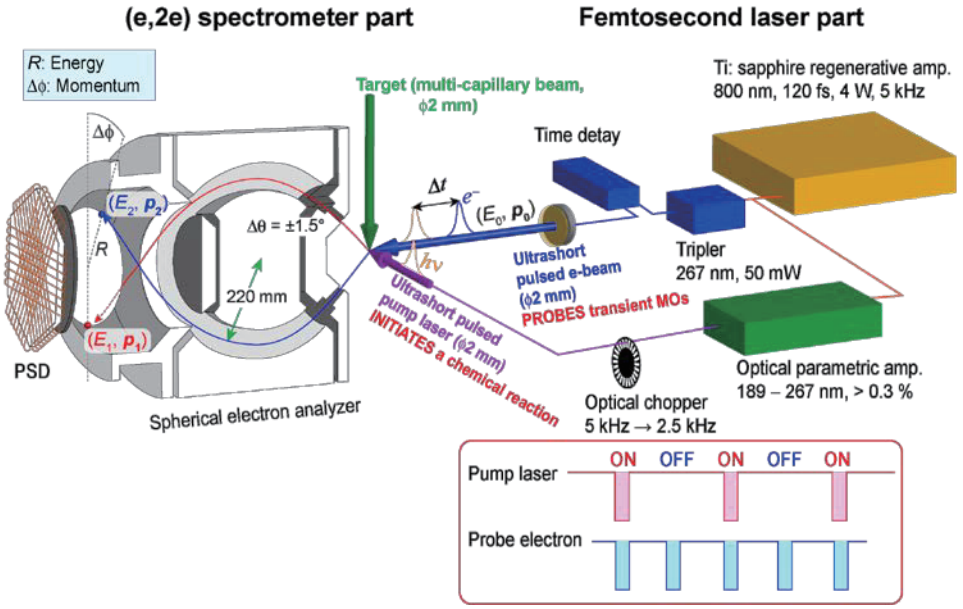

Fig.1 A schematic representation of a time-resolved electron momentum spectroscopy apparatus. Abbreviations are: PSD for position sensitive detector, E_j and $\boldsymbol{p}_j$ (j = 0, 1 and 2) for the kinetic energies and momenta of the incident, inelastically-scattered and ejected electrons, respectively.

The first TR-EMS experiment has been reported in 2015 [6], for the outermost, 3*s* Rydberg orbital of deuterated acetone molecule in its second excited singlet, S_2 (n, 3*s*) state with a lifetime of 13.5 ps [7]. Although the data quality was low, this work has been recognized as the first to demonstrate that EMS experiments on short-lived transient species are feasible, opening the door to time-resolved orbital imaging in momentum space [8, 9]. The second TR-EMS experiment has recently been conducted for the toluene molecule in its S_1 (π, π^*) state. Since the lifetime of the toluene S_1 state is 86 ns [10] and is much longer than the current experimental time resolution of ±35 ps, a TR-EMS experiment without any contributions of the following intramolecular relaxation processes [11] has been made while the whole valence electronic structure being covered. Although statistics of the experimental data leave much to be desired again, this work has shown through comparisons with molecular calculations that TR-EMS has an inherent capability to observe spatial distributions, in momentum space, of not only the outermost orbital but also all other, more tightly bound orbitals of a molecular excited state [12].

3. Time-resolved atomic momentum spectroscopy

Measurements of atomic motions in a molecule can be made by using electron-induced atomic momentum spectroscopy (AMS). It is the complete electron analog for better-known neutron Compton scattering, as has beautifully been developed and demonstrated by Maarten Vos and his colleagues [13]. Here, the measurement of the energy distribution of keV electrons backscattered elastically from molecules reveals one or more peaks. These peaks are at nonzero energy loss and have an intrinsic width. The usual interpretation of these measurements is attractively simple. It assumes a billiard-like collision takes place between the electron and a specific atom in the molecule and the scattering atom behaves as a free particle. The peak position is then related to the mass of the scattering atom, and its width is a Compton profile of the momentum distribution of this atom in the molecule.

In order to attempt a real-time measurement of atomic motions in chemical reactions, however, higher instrumental sensitivity would be desired. We have therefore developed a multi-channel AMS apparatus [14]. Briefly, a continuous incident electron beam of 2-keV collides with a gaseous target from a gas nozzle. Outgoing electrons making a scattering angle of 135° are dispersed by a spherical analyzer and detected by one large-area position-sensitive detector.

We have conducted an experiment on the CF_4 molecule by using the developed AMS apparatus, and compared with the results in literature [15]. It has been found that although our energy resolution is a little bit poor compared to the existing AMS apparatus, the signal count rate, normalized in terms of energy resolution, incident electron beam current and data accumulation time, has been improved by a factor of 2000 or more [14]. This value may be considered large enough to go towards time-resolved AMS (TR-AMS) measurements in a pump-probe scheme.

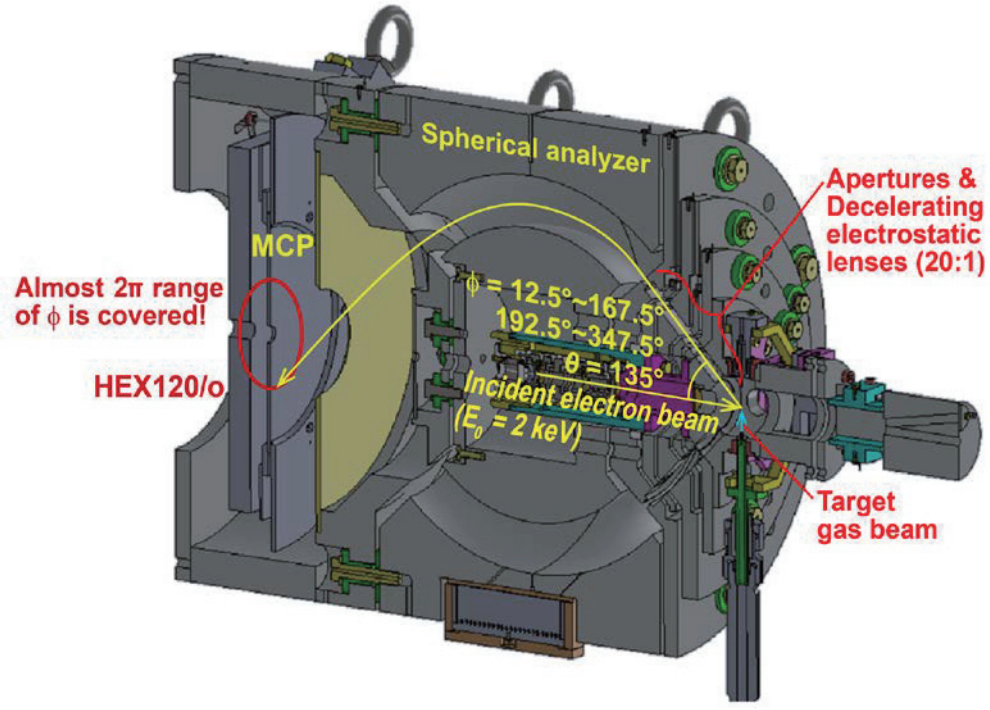

Fig.2 A schematic representation of a highly-sensitive atomic momentum spectroscopy apparatus.

4. Summary

The TR-EMS experiments on the acetone and toluene excited molecules have represented the first time that measurements of electron momentum densities for short-lived molecular excited states are feasible, opening the door to time-resolved orbital imaging in momentum space or filming a molecular orbital movie that makes it possible to directly access the driving force behind chemical reaction. In addition, we have successfully developed a multichannel AMS spectrometer. The instrumental sensitivity achieved may be considered high enough to extend the use of this technique for time-resolved measurements of atomic motions in a decaying system. We believe a joint use of TR-EMS and TR-AMS would provide a completely new, momentum-space approach to studying chemical reaction dynamics.

Acknowledgements

The author would thank all of his colleagues, whom he have had the greatest pleasure of working with, for their contributions to the subjects described herein. In particular, he would acknowledge Dr. Masakazu Yamazaki at his research group and Prof. Chaoyuan Zhu at National Chiao-Tung University, Taiwan for their great experimental and theoretical contributions. This work was partially supported by Scientific Research Grants (Nos. 20225001, 25248002, and 15K13615) from the MEXT of Japan, as well as by the Management Expenses Grants for National Universities Cooperation. This work was also partly supported by the JSPS-NRF-NSFC A3 Foresight Program in the field of Plasma Physics (NSFC: No.11261140328, NRF: No.2012K2A2A6000443).

References

[1] A. H. Zewail, Annu. Rev. Phys. Chem. **57** (2006) 65.

[2] J. Kim, K. H. Kim, J. H. Lee, and H. Ihee, *Acta Cryst. A* **66** (2010) 270.

[3] E. Weigold and I. E. McCarthy, *Electron Momentum Spectroscopy* (Kluwer/Plenum, New York, 1999).

[4] M. Takahashi, *Bull. Chem. Soc. Jpn*. **82** (2009) 751.

[5] M. Yamazaki, Y. Kasai, K. Oishi, H. Nakazawa, and M. Takahashi, *Rev. Sci. Instrum*. **84** (2013) 063105.

[6] M. Yamazaki, K. Oishi, H. Nakazawa, C.Y. Zhu, and M. Takahashi, *Phys. Rev. Lett.* **114** (2015) 103005.

[7] J. C. Owrutsky and A. P. Baronavski, *J. Chem. Phys.* **110** (1999) 11206.

[8] T. Wogan, *Physics* **8** (2015) 23.

[9] Research Highlights, *Nature* **519** (2015) 392.

[10] C. G. Hickman, J. R. Gascooke, and W. D. Lawrance, *J. Chem. Phys*. **104** (1996) 4887.

[11] *Modern Trend in Chemical Reaction Dynamics: Experiment and Theory, Part II*, ed. X. Yan and K. Liu (World Scientific, Singapore, 2004).

[12] M. Yamazaki, Y. Tang, and M. Takahashi, *submitted*.

[13] M. Vos, M. R. Went, G. Cooper, and C.A. Chatzidimitriou-Dreismannatoms, *J. Phys. B* **41** (2008) 135204.

[14] M. Yamazaki, M. Hosono, Y. Tang, and M. Takahashi, *in preparation*.

[15] M. Vos, *J. Chem Phys*. **132** (2010) 074306.

Observation of forbidden transitions from highly charged ions in a Kingdon trap

N. Numadate[1], H. Shimaya[1], T. Ishida[1], K. Okada[2], N. Nakamura[3], and H. Tanuma[1]

[1]Department of Physics, Tokyo Metropolitan University, Hachioji, Tokyo 192-0397, Japan

[2]Department of Physics, Sophia University, Chiyoda, Tokyo 102-8554, Japan

[3]Institute of Laser Science, University of Electro-Communications, Chofu, Tokyo 182-0021, Japan

Abstract

We have reproduced the solar wind charge exchange collision of hydrogen-like O^{7+} ions with He gas at collision energies of 42 keV in the laboratory. According to the classical over barrier model, the dominant electron capture level in the collision of O^{7+} with He is the principal quantum number $n = 4$. The populations of 1s2s and 1s2p states become large due to cascades from the higher excited states, so the main emission lines following the charge exchange are short-lived allowed transition of $1s^2\ ^1S_0$ - $1s2p\ ^1P_1$ and long-lived forbidden transition of $1s^2\ ^1S_0$ - $1s2s\ ^3S_1$. By using a Kingdon ion trap, we succeeded in observing of the forbidden transitions from the helium-like O^{6+} ions produced by single electron capture. The measured X-ray spectrum had a peak at 560 eV which correspond to the forbidden emission of $1s^2\ ^1S_0$ - $1s2s\ ^3S_1$ in O^{6+} ion.

Keywords: solar wind charge exchange, forbidden transitions, soft X-ray, ECR ion source, Kingdon trap

1. Introduction

In 1994, the soft X-ray emission whose intensity varied in cycles of several days was observed by an observatory satellite, ROSAT (ROntgen SATellit, an X-ray observatory launched in 1990) [1]. This emission came from where there was no particular hot object, so it remained mysterious. In 1996, the soft X-ray emission from Comet Hyakutake was observed by also the ROSAT [2]. It was also mysterious and surprising that the comet which composed mainly of ice and dust emitted the soft X-ray. Following this observation, soft X-ray emissions were observed from various comets and it was suggested that these emissions were caused by charge exchange reactions between highly charged ions included in the solar wind and cometary neutrals [3]. Now it has been recognized that a part of soft X-ray background emissions stems from the charge exchange collision of the solar wind ions with the neutrals in the heliosphere, and this phenomenon is called Solar Wind Charge eXchange (SWCX).

According to the observation by the Suzaku satellite, it proved that the forbidden transitions ($1s^2\ ^1S_0$ - $1s2s\ ^3S_1$) in metastable O^{6+} ions produced by the charge exchange were main emissions in the SWCX [4, 5]. The absolute values of emission cross sections are needed for astrophysics in order to analyze the X-ray spectra, but the forbidden lines following the charge exchange reactions with the energy of tens of keV have not been observed yet in the beam-based experiments due to the long lifetimes of the excited states. In our laboratory, we have observed the soft X-ray emissions in the SWCX process for the electric dipole allowed transitions with very short lifetime [6, 7]. In this time, we succeeded in the laboratory observation

of the long-lived forbidden transitions by trapping of metastable O^{6+} ions after the SWCX reaction of $O^{7+}(1s) + He \rightarrow O^{6+}(1snl) + He$.

2. Experimental setup

The highly charged O^{q+} ions were produced with a 14.25 GHz electron cyclotron resonance ion source (ECRIS) with the introduction of O_2 gas into a plasma chamber [8]. They were extracted by an electric potential of 6 kV and then only hydrogen-like O^{7+} ions were selected with a 110° double focusing dipole magnet. After the charge-state separation, the ion beam profile was optimized with adjustable x-y slits, an einzel lens, and an electric quadrupole lens. With a switching magnet, the ions were provided to a spectroscopy beam-line and fed into a collision gas cell. The target He gas was introduced into a collision cell and the absolute He pressure in the collision cell was kept approximately 5.3×10^{-3} Pa, which was measured with a capacitance manometer. Two pairs of electrostatic lenses were mounted in the collision cell in order to prevent the ion beam from diffusing. By applying high voltage to the collision cell, we can achieve the solar wind ion speed (0.2 - 4.2 keV/u). A trap chamber was located behind the collision chamber. We installed a microchannel plate (MCP) and a silicon drift detector (SDD) in order to detect the trapped ions and the soft X-ray emission from the trapped metastable ions, respectively. Our SDD was a window-less type, so we didn't need to take the transmission into account. The DC O^{7+} ion beam current of about 5 nA was obtained from the ECRIS, which was measured with a faraday cup located at the most downstream of the beam-line.

The details of the Kingdon ion trap and the experimental technique used in the ion trapping measurements have been previously described [9], so only brief description is given in this paper. The Kingdon ion trap consists of a central wire electrode, a cylinder electrode, and two end-cap electrodes. Ions are trapped in a logarithmic and a harmonic potentials produced by the electrodes. The cylinder electrode has four apertures for ion passing and soft X-ray observation. For reducing the disturbance of the electric field, the apertures were covered with a gold coating tungsten mesh.

A timing sequence of the ion trapping experiment is shown in figure 1. The ion beam was injected into the Kingdon ion trap when the wire electrode was biased to higher potential than the other electrodes. Then the wire potential was rapidly switched to lower potential than others by a high voltage push-pull switching unit. At the same time, the ion beam was turned off with a deflector to avoid colliding with the trapped ions. The timing of the switching of the wire potential and the beam-off was a start for a storage time of the ions, and while trapping the ions the soft X-ray from the metastable ions was observed with the SDD. Just after the start of the trapping measurement, the ions trapped in unstable trajectories lost quickly and collided with the electrodes. This collision caused the background emissions with the broad energy range in the forbidden line measurements, so the detection of soft X-ray started with a delay to reduce the background. After a pre-determined storage time, the trapped ions were ejected by raising the wire potential. A fraction of the ejected ions was detected with the MCP.

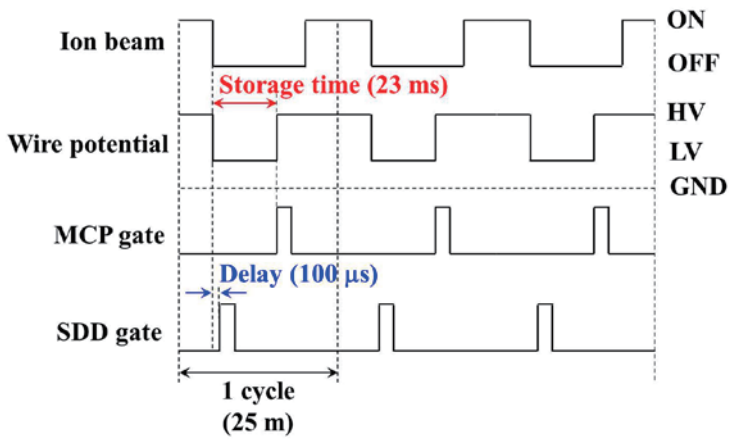

Fig.1 A timing sequence of the ion trapping experiment and the forbidden emission observation. The observation time of the soft X-ray in one cycle was set to 2 ms, and the net accumulation time was 1.92 hours.

3. Soft X-ray spectra of He-like oxygen

The forbidden line spectra in collisions of O^{7+} ions with He gas at collision energy of 42 keV is shown in figure 2(a). The peak at 560 eV corresponds to $1s^2\ ^1S_0$ - $1s2s\ ^3S_1$ transitions of O^{6+} ions. High energy tail and a part of low energy tail are background signals caused by collisions of the trapped ions with the trap electrodes. The other part of low energy tail is due to background signals caused by the soft X-ray detector. As the low energy tail is the sum of the two kinds of background signals, the spectrum has an asymmetric structure.

The resonance line spectra in collisions of O^{7+} with H_2 gas at the same collision energies as the forbidden line measurements is shown in figure 2(b). During the resonance line measurement, the H_2 gas pressure in the trap chamber was kept 3.0×10^{-2} Pa, and DC O^{7+} ion beam was injected. We didn't operate the ion trap in this measurement, so only short-lived allowed emissions following the charge exchange were observed. This spectrum consists of a dominant peak and two small peaks. They correspond to three transitions of $1s^2$ - 1s2p (574 eV), $1s^2$ - 1s3p (666 eV), and $1s^2$ - 1s4p (698 eV), and it can be distinguished by deconvolution using Gaussian functions with a full-width at half-maximum of 73 eV for each transition. The transitions of $1s^2$ - 1s2p might include not only the resonance line ($1s^2$ - $1s2p\ ^1P_1$, 574 eV) but also the inter-combination line ($1s^2$ - $1s2p\ ^3P_1$, 569 eV), but the contribution of the inter-combination line can be neglected because of the long lifetime of μs. As well as the forbidden line observations, the low energy tail is due to the background signal derived from collisions of the ions with the wire electrode. Figure 2(c) shows the comparison of the forbidden and the resonance line spectra. As the counting rate of the resonance emission was much greater than that of the forbidden transitions, the spectra are normalized with their peak intensities obtained by Gaussian fittings. We can find significant and reasonable difference between two peak positions.

According to the classical over barrier model [10] and the two-center atomic orbital close coupling method [11], the dominant electron capture level in collisions of O^{7+} with He is the principal quantum number $n = 4$. By the cascade from the upper states to the lower states, the populations of 1s2s and 1s2p

states become large, and then the main emission lines following the charge exchange are the transitions of $1s^2$ - 1s2s/1s2p.

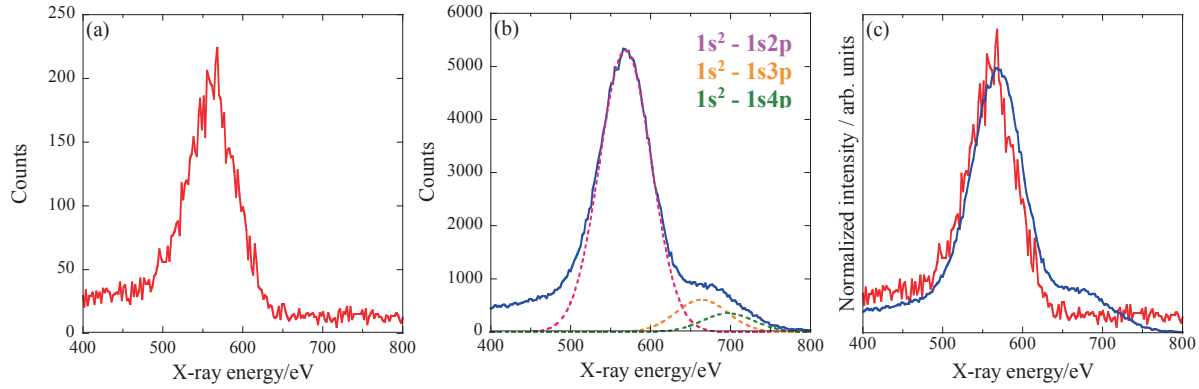

Fig.2 Soft X-ray emission spectra of (a) Forbidden transition, (b) Resonance transitions and (c) both for comparison. In the (c) spectra, their intensities are normalized.

Acknowledgements

This work was partly supported by the JSPS-NRF-NSFC A3 Foresight Program in the field of Plasma Physics (NSFC: No.11261140328, NRF: No.2012K2A2A6000443) and a grant-in-aid for Scientific Research (A) from the Ministry of Education, Culture, Sports, Science and Technology (MEXT).

References

[1] S. L. Snowden *et al*., Astrophys. J. **424** (1994) 714.

[2] C. M. Lisse *et al*., Science **274** (1996) 205.

[3] T. E. Cravens *et al*., Astrophys. J. **532** (2000) L153.

[4] R. Fujimoto *et al*., Publ. Astron. Soc. Jpn. **59** (2007) S133.

[5] Y. Ezoe *et al*., Publ. Astron. Soc. Jpn. **63** (2011) S691.

[6] T. Kanda *et al*. Phys. Scr. **T144** (2011) 014025.

[7] H. Shimaya *et al*. Phys. Scr. **T156** (2013) 014002.

[8] H. Tanuma *et al*., J. Chin. Chem. Soc. **48** (2001) 389.

[9] N. Numadate *et al*., Rev. Sci. Instrum. **85** (2014) 103119.

[10] A. Niehaus, Nucl. Instrum. Methods B **31** (1988) 359.

[11] L. Liu, *et al*., J. Phys. B **45** (2011) 015202.

Intensity and polarization measurements of Hα radiation from backscattered H* atoms by proton impact on polycrystalline tungsten surface

Hiroyuki. A. Sakaue[1], Daiji Kato[1,2], Izumi Murakami[1,2], Shouta Mineta[3], Kenji Motohashi[4] and Yasuhiro Sakai[3]

[1]National Institute for Fusion Science, National Institutes of Natural Sciences,
322-6 Oroshi-cho, Toki 509-5292, Japan
[2]Department of Fusion Science, SOKENDAI (The Graduate University for Advanced Studies),
322-6 Oroshi-cho, Toki, Gifu 509-5292, Japan
[3]Department of Physics, Toho University, 2-2-1 Miyama, Funabashi, Chiba 274-8510, Japan
[4]Department of Biomedical Engineering, Faculty of Science and Engineering, Toyo University,
2100 Kujirai, Kawagoe, Saitama 350-8585, Japan

Abstract

We observed Hα line from the reflected hydrogen atoms when the protons were irradiated to the polycrystalline tungsten surface at 35keV. The spatial intensity distribution and polarization degree of Hα line from reflected H* were observed. From these experimental results, it was shown that Hα line is aligned to the reflected direction of hydrogen atom.

Keywords: Hα, tungsten, polarization

1. Introduction

Tungsten is planned to use as material for the divertor plates in ITER because of the high sputtering threshold energy for light ion bombardment, the highest melting point among all the elements, and less tritium retention compared with carbon-based materials [1-3]. Divertor plates in a fusion device are exposed to high intensity heat fluxes of energetic particles. Many experiments indicate that tungsten retains tritium and deuterium due to their bombardment of hydrogen isotope plasma. The resultant retentions of the isotopes raise to the safety and economic problems, and should be minimizes for future fusion reactor operations. Thus, many efforts are being made to predict hydrogen isotopes retention in various forms of tungsten under the actual fusion reactor condition. The retention, reflection, recycling, sputtering of hydrogen isotope atom in tungsten surface attracts extensive attention from the viewpoint of estimating the inventory of tritium atoms in a nuclear fusion device. We paid attention to the reflection processes of the hydrogen atoms by the proton irradiation to the tungsten surface, and then we measured spatial intensity distribution of the Hα line from reflected hydrogen and the degree of polarization distribution.

2. Experimental apparatus

The experiment was performed in a beam line connected with a medium-current ion implanter (ULVAC IM-200MH-FB) at the National Institute for Fusion Science (NIFS), as shown in figure 1. Details of the ion source and beam line are described elsewhere [4]; hence, they will be only briefly explained here. The H^+ ion beam, accelerated to 35 keV, was introduced into a vacuum chamber after mass/charge separation. The ion beam transmitted through a 5-mm-diameter aperture hole entered normally on a polycrystalline tungsten surface, supported by a linear-motion manipulator. A bias voltage of ~100 V was applied to the disk, with the aperture hole used to retard secondary electrons emitted from the tungsten surface. The pressure of the vacuum chamber was maintained at $\sim 1 \times 10^{-6}$ Pa without introducing the ion beam, whereas it reached $\sim 3 \times 10^{-5}$ Pa under ion-beam irradiation of the tungsten surface. The ion beam entered perpendicular onto the tungsten surface. The polarizer was installed between quartz window and Hα band-pass filter. After passing through a quartz window, Hα band-pass filter and condenser lens, the Hα image from the reflected H* atoms was projected on the two-dimensional (2D) charge coupled device (CCD).

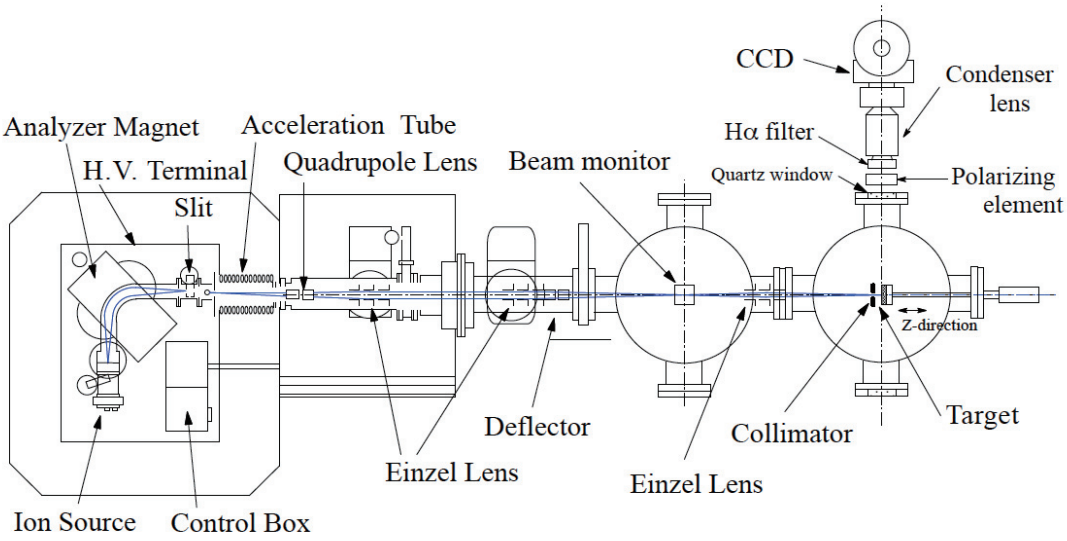

Fig.1. Experimental apparatus

3. Result and discussion

We measured the spatial distribution of Hα line intensity from reflected H* atoms under irradiation of H^+ ion-beam (35keV). Figure 2 shows the two-dimensional spatial Hα line intensity distributions. The polycrystalline tungsten surface is located at Z = 650 (pixel). Reflected hydrogen atoms which emit Hα are strongly reflected in the direction of 180 degrees with respect to the incident protons.

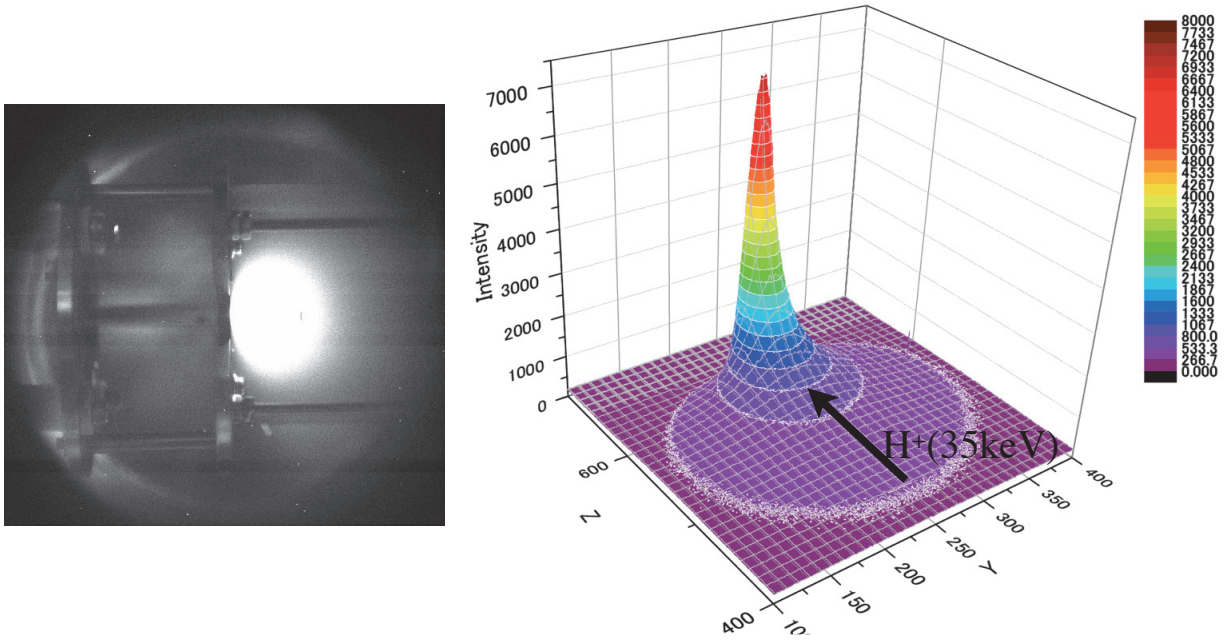

Fig.2. The spatial intensity distribution of Hα radiation from reflected H* atoms.

Using the analysis of decay curve, we estimated the mean vertical velocity component in direction normal to the surface. The intensity decay follows the well-known relation,

$$I = \sum_k I_{0k} \exp\left(- \frac{z}{< v_\perp > \tau_k} \right) \quad .$$

Where I_{ok} is the intensity from a particular transition k at the surface (z =0), $v_\perp$ is the vertical velocity component normal to the surface, τ k is the lifetime of the excited state. Figure 3 shows the decay curve of Hα line intensity. From this decay curve, the mean vertical velocity was estimated at 775.4km/s (3.14keV).

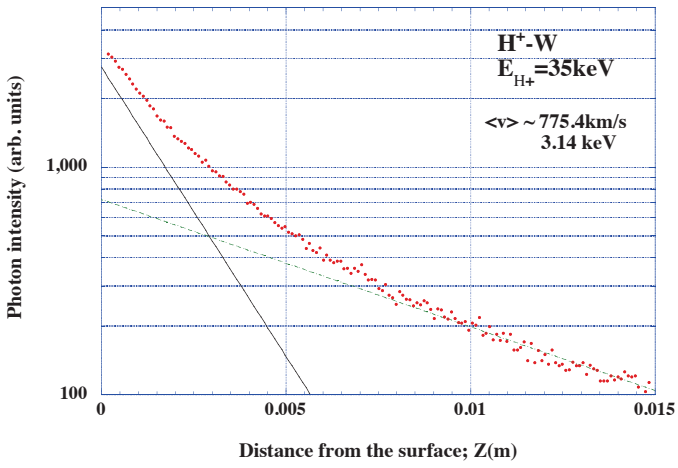

Fig.3. The decay curve of Hα line intensity.

Next, we measured the polarization degrees of Hα line from reflected H* atoms. The polarization with respect to surface is expressed as,

$$P = \frac{I_{\parallel} - I_{\perp}}{I_{\parallel} + I_{\perp}} \quad ,$$

where $I \parallel$ and $I \perp$ are Hα line intensities polarized along the surface and perpendicular to the surface, respectively. In fig.4, we show the polarization degrees of Hα line at Z=644, with emission lines intensities $I \parallel$ and $I \perp$. The degree of polarization of Hα line from the hydrogen atom, which is reflected in the direction perpendicular to the tungsten surface, becomes negative. And, as for the Hα line from reflected H* atoms which have a parallel velocity component to the tungsten surface, the degree of polarization becomes positive value. In other word, this experimental result shows that the Hα lines are aligned to the reflected direction of H* atoms.

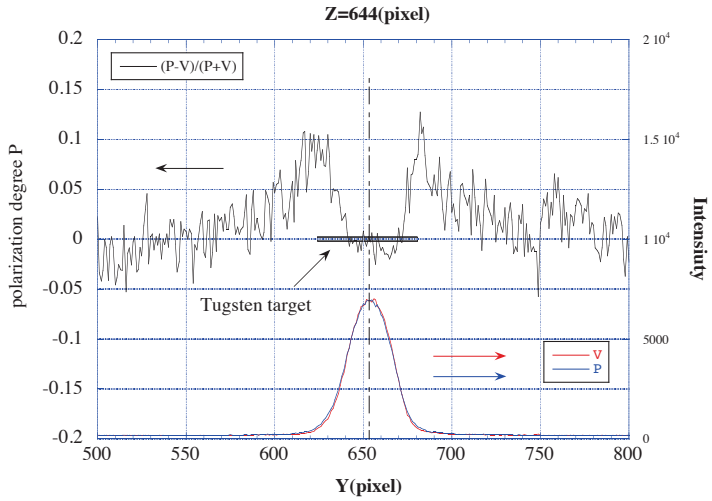

Fig.4. The polarization degrees P and intensity of Hα radiation from reflected H* atoms at z=644 (pixels).

Acknowledgements

This work was partly supported by the JSPS-NRF-NSFC A3 Foresight Program in the field of Plasma Physics (NSFC: No.11261140328, NRF: No.2012K2A2A6000443).

References

[1] .J.Roth, E.Tsitrone, A.Loarte, et al., J. Nucl. Mater. **390-391** (2009) 1-9

[2] Z.Tian, J.W.Davis, A.A.Haasz, J. Nucl. Mater. **399** (2010) 101-107.

[3] K.Ohya, J.Kawata, T.Tanabe, et al., J. Nucl. Mater. **258-263** (1998) 1055-1059

[4] K.Motohashi, K.Nogami, Y.Sakai, H.A.Sakaue, D.Kato and T. Kenmotsu: NIMB **283** (2012) 59-62.

Characterization of material ablation with intense extreme ultraviolet (EUV) light generated with laser

H. Nishimura[1], N. Tanaka[1], R. Deguchi[1], N. Wada[1], A. Sunahara[2], M. Murakami[1] and A. Yogo[1]

[1]Institute of Laser Engineering, Osaka University, Suita, Osaka, Japan
[2]Institute for Laser Technology, Suita, Osaka, Japan

Abstract

We present a comparative study on the hydrodynamic behavior of plasmas generated by material ablation by the irradiation of nanosecond extreme ultraviolet (EUV or XUV) or infrared laser pulses on solid samples. It was clarified that the difference in the photon energy deposition and following material heating mechanism between these two lights result in the difference in the plasma parameters and plasma expansion characteristics. Silicon plate was ablated by either focused intense EUV pulse (λ=9–25 nm, 10 ns) or laser pulse (λ=1064 nm, 10 ns), both with an intensity of ~ 10^9 W/cm^2. Both the angular distributions and energy spectra of the expanding ions revealed that the photo-ionized plasma generated by the EUV light differs significantly from that produced by the laser. The laser-generated plasma undergoes spherical expansion, whereas the EUV-generated plasma undergoes planar expansion in a comparatively narrow angular range. It is presumed that the EUV radiation is transmitted through the expanding plasma and directly photo-ionizes the samples in the solid phase, consequently forming a high-density and high-pressure plasma. Due to a steep pressure gradient along the direction of the target normal, the EUV plasma expands straightforward resulting in the narrower angular distribution observed.

Keywords: laser plasma source, EUV, ablation

1. Introduction

Recent progress on extreme ultraviolet (EUV) light sources enables us to utilize shorter wavelength of few to few tens of nanometer for micro machining of materials [1]. Since EUV photon energy exceeds 100 eV and corresponding photon energy is beyond the solid density, the ablation behavior, due to difference in energy deposition mechanism, is quite different from that of laser ablation in such a way that EUV light penetrates through ablation plasma and directly heats material of original density by photo-ionizing the inner orbit electrons. Although differences in ablation characteristics in EUV and laser ablation are reported [2], many aspects in the physics of EUV energy deposition and transportation remain unclear.

Material ablation by infrared (IR), visible, or ultraviolet (UV) lasers has been widely used for several industrial applications such as surface machining, pulsed laser deposition (PLD), and material analysis. Furthermore, the mechanisms and characteristics of ablation have been investigated. For example, Russo et al. extensively studied influences of wavelength on material ablation used for inductively coupled plasma mass spectrometry [3]. The process of material heating with a conventional long wavelength (UV to IR) laser can

be explained as follows: First, a shallow material surface is partially ionized due to Ohmic heating via energetic electrons accelerated by a laser field or multi-photon absorption processes. The laser field then further accelerates these free electrons (inverse bremsstrahlung absorption), and the acquired kinetic energy is transferred to other electrons and ions via Coulomb collisions. The absorption is followed by energy relaxation to orbital electrons, thermal diffusion, and energy transfer to the lattice as a result of electron phonon coupling. Due to heating of the material, the surface plasma expands toward the low-pressure side, forming an ablation plasma. Because the critical density for a Nd:YAG laser (λ=1064 nm) is 9.9×10^{20} cm^3 (well below that of solid material), the laser absorption region also expands away from the surface of the material. Therefore, material ablation from the solid region is maintained by thermal conduction from the absorption region to the ablation front. However, the mechanisms of material ablation are expected to be completely different in the case of EUV. The atoms or molecules are photoionized by the EUV radiation. The photo-ionized electrons or subsequently generated Auger electrons then transfer their energy to neighboring electrons (free or bound electrons). During expansion of the ablation plasma, although the EUV light is partially absorbed by the bound electrons of the expanding ions, most of the EUV radiation is transmitted to the high-density region due to the critical density for EUV wavelength region that exceeds the solid density. In order to validate these steps in the described ablation mechanisms, the ablation behavior of both laser- and EUV heated matter was investigated. The goals of this study are: (1) to improve understanding of the EUV ablation mechanism, and (2) to characterize EUV ablation by comparing it to laser ablation.

2. Experiments and analysis

An intense laser produced plasma EUV source at ILE Osaka University was used in the experiments (see Fig. 1). EUV emission from a solid xenon target ranging 11-20 nm was focused onto the sample material with an intensity of ~5 x 10^9 W/cm^2. A Nd:YAG laser was used for laser ablation experiments [4].

A charge collector array with four charge collectors was used to measure the angular distribution of ion number and energy spectra. The species of expanding particles were measured by the Thomson parabola mass and charge analyzer. The experimental results showed noticeable difference between EUV and laser ablation in the angular distribution, energy spectra, and abundance of ionization stages [5]. The spectrum

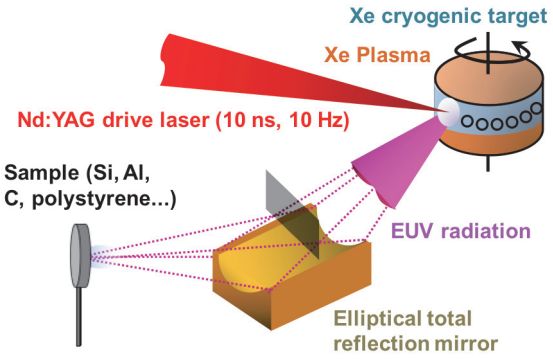

Fig. 1 EUV irradiation system. EUV light from the Xe plasma generated with Nd:YAG laser is focused on a sample with an elliptically toroidal mirror [4].

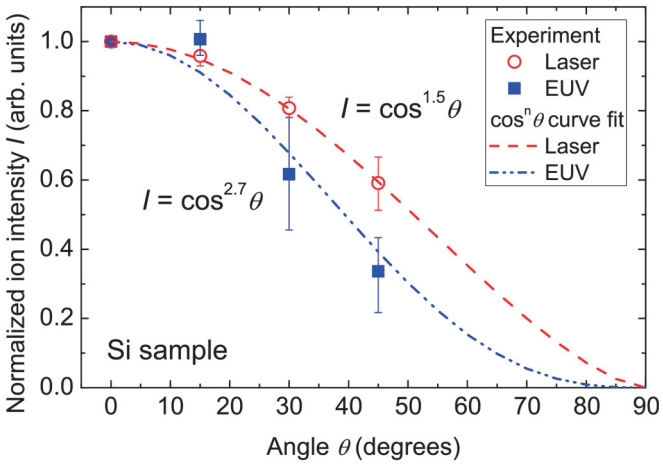

Fig. 2. A normalized angular distributions of expanding Si ions for EUV and laser plasmas. A narrower distribution is seen for the case of extreme ultraviolet (EUV) ablation [5].

for EUV ablation followed exponential decay curve having high kinetic energy component, and that for laser ablation showed convex spectrum having drastic cut off near 100 eV. The angular distribution of expanding ions from EUV ablation plasma shows narrower distribution than that from laser ablation plasma. The time-of-flight (TOF) spectrum of the ions in the expanding plasma was measured by a charge collector array consisting of four charge collectors located 210 mm away from the ablation spot at angles θ of 0, 15, 30, and 45 degrees from the sample surface normal. The time evolution of the ion current flowing into each charge collector (i.e., the TOF spectrum) was measured and converted into an energy distribution dN/dE . The expanding ions were also measured separately by a Thomson parabola mass-charge ion analyzer. It was confirmed that singly charged ions were the dominant ionic species present for both the Si and Al samples regardless of EUV or laser ablations. Angular- and energy-resolved measurements of the expanding ions were performed for both EUV and laser ablation. As shown in Fig. 2, the angular distribution of the Si ions produced by EUV ablation is narrower than that of ions produced by laser ablation. The angular distributions were well fitted with a $\cos^n\theta$ distribution. The multipliers n are n=1.5 for laser ablation and n=2.7 for EUV ablation. The results clearly show forward directed expansion in EUV ablation. The dN /dE energy spectra (N is the ion number density per unit energy, and E is ion kinetic energy) at the target normal angle for the Si sample are shown in Fig. 3. These spectra were compared with an isothermal expansion model [6] given as $\frac{dN}{dE} \propto \left(\frac{E}{E_0}\right)^{\frac{\alpha-2}{2}} \exp\left(-\frac{E}{E_0}\right)/\Gamma\left(\frac{\alpha}{2}\right)$ where α represents the geometry of expansion; α =1 corresponds to one-dimensional (1D) planar expansion, α=2 to 1D cylindrical expansion, and α=3 to 1D spherical expansion. In the equation above, α expresses the geometrical influence on the plasma cooling rate, while ε_0 is the characteristic energy that determines ion expansion property. In the case of EUV ablation, the energy spectrum is described well by a planar or cylinder expansion, while for laser ablation at 1064 nm it is more closely described by a spherical expansion.

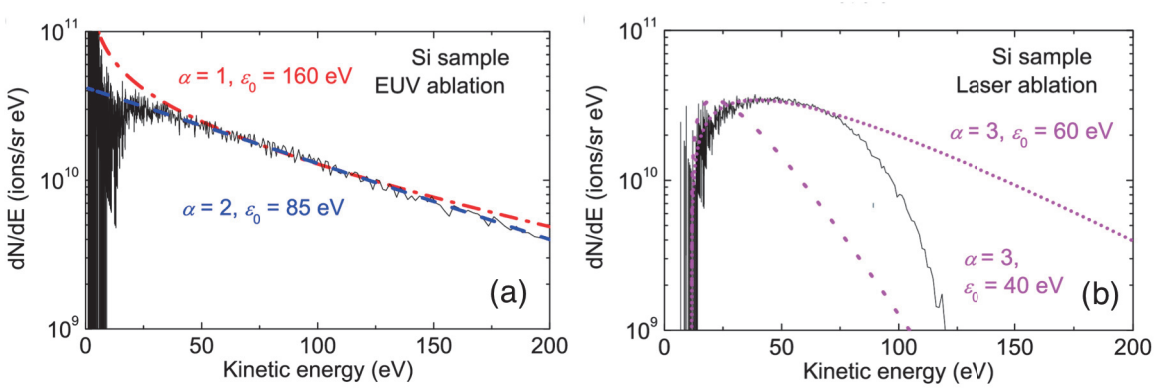

Fig. 3. Energy spectra of expanding Si ions for (a) EUV and (b) laser ablations at the target normal [5]. They are compared with theoretical predictions [6].

The results were also compared and discussed using ablation parameters simulated by STAR 1D code [7]. The ablation process is considered to take place in three steps; material heating by the photon-matter interaction, plasma formation associated with plasma heating, and plasma cooling via expansion. In the case of EUV ablation, the radiation passes through a low density expanding plasma; therefore, the EUV energy is transferred primarily to the high-density plasma or solid material, resulting in more ion formation. Due to the steep pressure gradient, the disc-shaped plasma expands along the target normal into vacuum resulting in straightforward expansion. Furthermore, because the EUV plasma expansion is one dimensional, the plasma cooling is slow, and the kinetic energy tends to be high. However, in the case of laser ablation, the "outer" low-density region of the plasma is heated due to inverse Bremsstrahlung absorption along the pathway of the incident laser, and the plasma expands spherically along the radial direction.

Acknowledgements

This work was partly supported by JSPS Grant-in-Aid for Young Scientists (B) number 25800303, Grant-in-Aid for Scientific Research (B) number 22340172, and MEXT Project for Creation of Research Platforms and Sharing of Advanced Research Infrastructure" opening up a new photonics industry through high-intensity lasers". And also This work was partly supported by the JSPS-NRF-NSFC A3 Foresight Program in the field of Plasma Physics (NSFC: No.11261140328, NRF: No.2012K2A2A6000443).

References

[1] T. Makimura et. al, Journal of Physic Conference Series, 59, 279 (2007).

[2] M. Berrill, et. al., J. Opt. Soc. Am. B 25, 32 (2008).

[3] R. E. Russo, X. L. Mao, O. V. Borisov, and H. Liu, J. Anal. At. Spectrom.15, 1115 (2000).

[4] M. Masuda et. al., Appl. Phys. B 119, 421 (2015).

[5] N. Tanaka, et al., Appl. Phys. Lett. 107, 114101 (2015).

[6] M. Murakami et. al, Physics Plasmas 12, 062706 (2005).

[7] A. Sunahara and K. A. Tanaka, Fusion Engineering and Design, 85, 935 (2010).

The 6th China- Japan-Korea Joint Seminar on Atomic and Molecular Processes in Plasma (AMPP2016)
Scientific Program

25 July 2016 (Monday)
Registration: 14:00-20:00

26 July (Tuesday)

Opening Ceremony **Chair:** **Z. Y. Cui** **(SWIP)**	09:00	Z. Y. Cui (SWIP)	**Opening**
	09:05	X. R. Duan (SWIP) J. M. Li (SJTU) S. Morita (NIFS) C. Z. Dong (NWNU)	**Welcome speech**
Session 1 Chair: J. M. Li (SJTU)	09:25	Z. Y. Cui (SWIP)	Fusion Research Activities at SWIP
	09:50	S. Morita (NIFS)	Evaluation of poloidal distribution of edge electron temperature in stochastic magnetic field layer of LHD using intensity ratio among impurity line emissions
Photo and Coffee Break 10:15-10:40			
Session 2 Chair: C. Z. Dong (NWNU)	10:40	J. S. Yoon (NFRI)	A+M Data evaluation for fusion and low temperature plasma
	11:05	X. Gao (CSRC)	Theories for precision atomic structures and electronic scattering
	11:30	J. M. Yang (CAEP)	Absorption and Emission X-ray Spectra of Plasmas Driven By Intense Radiation on High Power Laser Facilities
	11:55	D. X. Sun (NWNU)	Laser produced plasma spectroscopy and its application on elemental detection
Lunch Break12:20-14:00			
Session 3 Chair: N. Nakamura (UEC)	14:00	I. Murakami (NIFS)	Effective Recombination rates for tungsten ions derived with a Collsional-Radiative Model
	14:25	B. W. Li (LZU)	Fundamental Atomic Process in Source Development for Beyond EUV Lithography and other applications
	14:50	D. Kato (NIFS)	Collisional-radiative models for ground-state M1 line emission of highly charged tungsten ions in the LHD
	15:15	C. R. Wu (ASIPP)	Signatures of recombination in the EAST upper tungsten divertor
	15:35	M. G. Su (NWNU)	Investigation of temporal-spatially resolved spectra and radiation dynamics properties of highly charged ions in laser-produced plasma
Coffee Break 16: 00-16:20			
Session 4 Chair: J. M. Yang (CAEP)	16:20	B. He (IAPCM)	Inelastic process and stopping power in Al and Be plasmas
	16:45	M. Y. Song (NFRI)	A+M Data Center Activities in National Fusion Research Institute
	17:10	C. Gao (NUDT)	Inner-shell resonant absorption and double Auger decay on population dynamics of neon plasma in interaction with ultra-intense x-ray pulses
	17:35	X. J. Liu (ASIPP)	SOLPS simulations of EAST radiation divertor with N_2 and Ar seeding
Bus 18:00			

27 July (Wednesday)			
Session 5 Chair: I. Murakami (NIFS)	09:00	S. X. Tian (USTC)	Anion velocity imaging study of dissociative electron attachments to CO_2
	09:25	Y. Sakai (Toho Univ.)	Isotope effect in dissociation processes of deuterated molecules from doubly excited states
	09:50	D. L. Yu (SWIP)	Status of neutral beam aided diagnostics on HL-2A
	10:15	L. Y. Xie (NWNU)	Dielectronic recombination of the highly charged Ar^{15+}, Xe^{51+} and Ba^{51+}-Ba^{55+} ions
Coffee Break 10:40 - 11:00			
Session 6 Chair: J. S. Yoon (NFRI)	11:00	L. F. Zhu (USTC)	Optical oscillator strengths of valence-shell excitations of atoms and molecules determined by the newly developed dipole (γ,γ) method
	11:25	F. Y. Long (IAPCM)	A new model to calculate electron-electron coulomb energy based on electron density
	11:50	Y. M. Yu (IPHY,CAS)	Finite field calculation of static polarizabilities and hyperpolarizabilities of In^+ and Sr
Lunch Break 12:15 – 14:00			
Session 7 Chair: S. Morita (NIFS)	14:00	N. Nakamura (UEC)	Observation of resonant excitation of Fe^{14+}
	14:25	L. Zhang (ASIPP)	Tungsten spectra measurement on EAST and the requirement of atomic data for its quantitative analysis
	14:45	T. Oishi (NIFS)	VUV spectroscopy for tungsten WIV-WVII line emissions in Large Helical Device
	15:10	M. Mita (UEC)	Observation of visible and EUV emission of Tungsten ions
	15:30	F. Koike (Sophia Univ.)	Characteristics of EUV spectra from N-open shell lanthanide ions in LHD plasmas
Coffee Break 15:55-16:15			
Session 8 Chair: J. L. Zeng (NUDT)	16:15	H. Tanuma (TMU)	Charge exchange spectroscopy for multiply charged ions of high Z elements
	16:40	M. Takahashi (Tohoku Univ.)	Towards time-resolved imaging of electron and nuclear motions in momentum space
	17:05	N. Numatate (TMU)	Observation of forbidden transitions from highly charged ions in a Kingdon trap
	17:25	Y. Yang (Fudan Univ.)	Simulating a Maxwell-Boltzmann Energy distribution in SH-HtscEBIT for temperature diagnostics of divertor-like plasma
	17:50	K. Ma (Huangshan Univ.)	Theoretical calculation on the photoelectron angular distribution of sodium-like ions
Bus 18:15			

28 July (Thursday)			
Session 9 Chair: H. Nishimura (Osaka Univ.)	09:00	Z. M. Hu (CAEP)	Dielectronic Recombination Studies Related to Fusion Plasma
	09:25	H. A. Sakaue (NIFS)	Intensity and Polarization measurements of Ha radiation from backscattered H* atoms by proton impact on polycrystalline tungsten surface
	09:50	W. Gao (ASIPP)	Study of the Zeeman effect on the Dα spectra in EAST tokamak
	10:10	M. Lv (Sichuan Univ.)	Atomic processes in ultra-intense X-ray atoms interaction
Coffee Break 10:35 - 10:55			
Session 10 Chair: L. F. Zhu (USTC)	10:55	H. Nishimura (Osaka Univ.)	Characterization of material ablation with intense extreme ultraviolet (EUV) light generated with laser
	11:20	Z. Xu (ASIPP)	Analysis of tungsten spectra in extreme ultraviolet spectral region on EAST
	11:40	Y. Y. Qi (Jiaxing Univ.)	The atomic dynamic process in quantum plasma
Summary of the Seminar			
Lunch Break 12:20 – 13:40			
Session 11 **Chair:** Z. Y. Cui (SWIP) S. Morita (NIFS) C. Z. Dong (NWNU)	13:40-14:00 Visiting HL-2A device 14:20-18:00 Discussions on next seminar and workshop plans Education of young scientists Discussion on coordinator meeting Discussions on on-going and future studies in Atomic and Molecular Processes in Plasma Discussions with PHD students, Post-doctoral researchers and young scientists		

Collection of Abstracts in AMPP2016

Evaluation of poloidal distribution of edge electron temperature in stochastic magnetic field layer of LHD using intensity ratio among impurity line emissions

S.Morita*,†,[1], E.H.Wang#,[2], H.M.Zhang†,[3], I.Murakami*,†,[4], T.Oishi*,†,[5], X.L.Huang*,[6], Y.Liu†,[7] and M.Goto*,†,[8]

* National Institute for Fusion Science, Toki 509-5292, Gifu, Japan
† Department of Fusion Science, The Graduate University for Advanced Studies, Toki 509-5292, Gifu, Japan
#Institute of Plasma Physics Chinese Academy of Sciences, Hefei 230026, Anhui, China

The helical device is typically characterized by the presence of stochastic magnetic field layer in the plasma edge, which has fully three-dimensional magnetic field structure. Large Helical Device (LHD) has the stochastic magnetic field layer outside the last-closed-flux surface (LCFS) which is defined the core plasma. In the stochastic magnetic layer all the plasma parameters such as temperature and density have three-dimensional structure. Therefore, it is very important for the transport study to evaluate the temperature and density as a function of poloidal direction in the stochastic magnetic field layer.

Two-dimensional distribution of impurity lines emitted from the stochastic magnetic field layer in LHD has been observed using a space-resolved extreme ultraviolet (EUV) spectrometer. The density and temperature in the stochastic magnetic field layer typically range in $10^{13} \leq n_e \leq 10^{14}$ cm^{-3} and $10 \leq T_e \leq 500$eV. The two-dimensional electron temperature distribution in the stochastic magnetic field layer is successfully measured using the line intensity ratio of Li-like NeVIII 2s-3p ($^2S_{1/2}$-$^2P_{3/2}$: 88.09 Å, $^2S_{1/2}$-$^2P_{1/2}$: 88.13 Å) to 2p-3s ($^2P_{1/2}$-$^2S_{1/2}$: 102.91 Å, $^2P_{3/2}$-$^2S_{1/2}$: 103.09 Å) transitions emitted from radial location near LCFS. The intensity ratio analyzed with ADAS code shows no dependence on the electron density below 10^{14} cm^{-3}. The result indicates a little higher temperature, i.e., 220 eV, in the poloidal location at high-field side near helical coils called O-point compared to the temperature near X-point, i.e., 170 eV. The electron temperature profile is also measured at the edge boundary of ergodic layer using the line intensity ratio of Li-like CIV 2p-3d ($^2P_{1/2}$-$^2D_{3/2}$: 384.03 Å, $^2P_{3/2}$-$^2D_{5/2}$: 384.18 Å) to 2p-3s ($^2P_{1/2}$-$^2S_{1/2}$: 419.53 Å, $^2P_{3/2}$-$^2S_{1/2}$: 419.71 Å) transitions. The intensity ratio analyzed with CHIANTI, ADAS and T.Kawachi's codes shows a slightly higher temperature near O-point, i.e., 25 eV for CHIANTI, 21 eV for ADAS and 11 eV for Kawachi's codes, compared to the temperature at X-point ranging in 15-21 eV for CHIANTI, 9-15 eV for ADAS and 6-9 eV for Kawachi's codes.

The present result clearly indicates that the three-dimensional effect in the stochastic magnetic field layer is very important not only in the plasma parameter but also in the transport coefficient.

References

[1] E.H.Wang, S.Morita, M.Kobayashi, I. Murakami, M.Goto and C.F.Dong, 2012 *Rev.Sci.Instrum.*: **83** 10E509.
[2] E.H.Wang, S.Morita, C.F.Dong, M.Goto, I. Murakami and T.Oishi, 2013 *Plasma Fus. Res.:* **8** 2402176.

[1] E-mail: morita@nifs.ac.jp
[2] E-mail: erhui@ipp.ac.cn
[3] E-mail: zhang.hongming@nifs.ac.jp
[4] E-mail: mizumi@nifs.ac.jp
[5] E-mail: oishi@nifs.ac.jp
[6] E-mail: huang.xianli@nifs.ac.jp
[7] E-mail: liu.yang@nifs.ac.jp
[8] E-mail: goto@nifs.ac.jp

A+M data evaluation for fusion and low temperature plasmas

Jung-Sik Yoon[1]

Plasma Technology Research Center, National Fusion Research Institute,
37, Dongjangsan-ro, Gunsan, Jeollabuk-Do, 573-540, Korea

As interest has increased in the interaction between plasma and materials, the role of modeling and simulation of low temperature plasmas has become important in understanding the effects of charged particles and radicals in plasma applications. Also, in fusion plasma and in fusion plasma diagnostics, plasma-material interaction (PMI) processes determine the erosion rate and lifetime of plasma-facing materials. Therefore there is a continuing need for better understanding and improved data for atomic, molecular and plasma-material interaction processes and properties in fusion devices and plasma processing, especially in semiconductor manufacturing.

In fusion plasma community, the principal constituents of fusion plasma are ions of H (H, D, T) and He and electrons. The most basic data needs are those for a plasma of H and He, inculding data for the transition to neutral gas. Then come data needs for impurities and their collision processes with (H, He, e^-) and finally we may need data for some collision processes among impurities. Thus, a number of different and increasingly sophisticated databases are available or are bing developed. For ITER and to ensure data consistency in the analysis of the experimental results, it is desirable to move towards production of validated and internationally recommended standard database that combines the best features of the available databases.

In early development of plasma reactors in low temperature plasma, processing has been achieved through trial and error. However, increasing demand to shrink the feature dimensions and demand for diminished defect density, it is now generally accepted that the traditional method of meeting these requirements by trial and error has reached the point of diminishing returns. Thus, plasma process modeling now becomes a necessary engineering tool in the design of new semiconductor equipment and in process control, and also, the high cost of developing both the plasma equipment and processes has motivated development of less-empirical methods, and modeling/simulation in particular, to speed the time to market and to reduce costs. Such plasma are complex environments in which a multitude of atomic and molecular processes occur and many of these processes are initiated by electron impact and an understanding of these precursor reactions is critical to a broader understanding of the dynamics of the discharge.

Absolute electron scattering cross sections for molecular targets, including their daughter radicals, are important in developing models of plasma reactors and testing the efficacy of various plasma processing gases. Low-energy electron collision data for these gases are generally quite sparse and, in many cases, only a limited range of cross section data is available. This is particularly the case for many of the important reactions e.g., dissociation, dissociative attachment , which lead directly to the production of those reactive species in the plasma which are responsible for the surface modification or deposition. As an important aspect of the operation and development of plasma processing reactors is the ability to model the atomic and molecular processes that take place, we must inevitably draw upon scattering theory, in many cases, to provide the important collision data.

The plasma community is a rapacious user of atomic and molecular data but is increasingly faced with a deficit of data necessary to both interpret observations and build models that can be used to develop the next-generation plasma tools that will continue the scientific and technological progress of the late 20th and early 21st century. It is therefore necessary to both compile and curate the A&M data we do have and thence identify missing data needed by the plasma community (and other user communities). Such data may then be acquired using a mixture of benchmarking experiments and theoretical formalisms.

[1]E-mail: jsyoon@nfri.re.kr

Theories for precision atomic structures and electronic scattering

Xiang Gao*[,1], Jia-Ming Li[†,2]

[*] Beijing Computational Science Research Center, Beijing, 100193, China
[†] Key Laboratory for Laser Plasmas (Ministry of Education) and Department of Physics and Astronomy, Shanghai Jiao Tong University, Shanghai, China, 200240; Department of Physics and Center for Atomic and Molecular Nanosciences, Tsinghua University, Beijing, 100084, China; Collaborative Innovation Center of Quantum Matter, Beijing, 100084, China

An extended atomic data with sufficiently high precision in energy levels and transition / collision rates is required for satellite observation in astrophysics studies and the energy development research in inertial confinement fusion (ICF) and magnetic confinement fusion (MCF). In this talk we will present a scenario to perform calculations leading to such large scale atomic data with high precision based on analytical continuation properties of the scattering matrices, connecting spectroscopy and collisions. More specifically, an excited atomic system, which consists of infinite bound states and adjacent continuum states, can be regarded as an atomic ion with various degrees of excitations and an excited channel electron either in bound orbitals or continuum orbitals. Such an excited atomic system can be calculated precisely by variational methods within a reaction zone where the ion and the channel electron coupling strongly, such as close-coupling methods, R-matrix methods etc. The dynamical properties of the electron-ion complex can be described by scattering matrices. The eigenvalues and the corresponding eigenvectors of the scattering matrices are related to the eigen quantum defects μ_α and the transformation matrices $U_{i\alpha}$ in the multichannel quantum defect theory (MQDT). In our scenario, the scattering matrices (i.e., MQDT parameters) in both bound and continuum energy ranges can be calculated directly with enough accuracies by our recent developed codes, REigen code (Eigen-channel based on non-relativistic R-matrix method) and R-REigen code (Eigen-channel based on relativistic R-matrix method) [1-5]. Applying the MQDT, we can calculate and predict all energy level positions up to fine-structures in discrete energy regions (i.e., bound state energy regions) without missing any lines. On the other hand, the scattering matrices in the discrete energy regions can be examined stringently by precise spectroscopic data determined by experimental measurements. Therefore, accuracies of the MQDT parameters (i.e., scattering matrices) in bound energy ranges can be readily ascertained. Through analytical properties of scattering matrices, the accuracies of scattering matrices in continuum energy regions can also be obtained with desired accuracies. One can obtain various relevant cross sections for electron-ion collision processes with adequate accuracy. Note that since the physical parameters (μ_α, $U_{i\alpha}$) vary smoothly with energies due to the analytical properties of scattering matrices, thus, they only need to be calculated in a few energy points over the energy regions of interest. Applications of our methods in a few atomic systems will be presented to demonstrate the advantage enjoyed by this approach, which can meet the requirements in stages of precision physics for astrophysics and energy researches.

References

[1] X. Gao, J. M. Li, 2012 *Chin. Phys. Lett.* **29** 033101.
[2] X. Gao, J. M. Li, 2014 Phys. Rev. A **89** 022710.
[3] T. N. Chang, T. K. Fang and Xiang Gao, 2015 *Phys. Rev. A* **91** 023403.
[4] D. L. Zeng, X. Gao, X. Y. Han and J. M. Li, 2015 *Phys. Rev. A* **91** 022707.
[5] X. Gao, R. Jin, D. L. Zeng, X. Y. Han, J. Yan and J. M. Li, 2015 *Phys. Rev. A* **92** 052712.

[1] E-mail: xgao@csrc.ac.cn
[2] E-mail: jmli@tsinghua.edu.cn

Absorption and Emission X-ray Spectra of Plasmas Driven by Intense Radiation on High Power Laser Facilities

Jiamin Yang[*, 1], Jiyan Zhang[*], Yang Zhao[*], Chengwu Huang[*], Gang Xiong[*], Bo Qing[*], Zhimin Hu[*], Jun Yan[†], Zeqing Wu[†], Cheng Gao[‡], Jiaolong Zeng[‡], Jianmin Yuan[‡]

[*]Research Center of Laser Fusion, China Academy of Engineering Physics, Mianyang 621900, China
[†]Beijing Institute of Applied Physics and Computational Mathematics, Beijing 100088, China
[‡]National University of Defense Technology, Changsha, China

X-ray absorption and emission properties of hot/warm dense plasmas have important roles in inertial confinement fusion, magnetic confinement fusion and astrophysics. A series of experiment studies on the x-ray absorption and emission spectra of hot/warm plasmas using the intense x-ray radiation generated by laser-plasma interactions have been presented, which include radiative opacity of hot plasma, K-shell absorption spectrum of warm dense matter and x-ray spectra of plasmas in intense radiation field. For the opacity experiment, the opacity of Fe plasma of about 75eV has been measured and compared with simulations of several models, such as STA, DCA and DTA [1]. It is shown that the DTA model gives better calculations for the 2p-3d absorptions due to its inclusion of configuration interactions. For the K-shell absorption spectrum experiment, the K-shell absorption edge shifts and broadening of a warm dense matter with ion-ion couple parameter of about 65 were achieved by using a specific target design and were compared with the simulations. Both the temperature derived from the measured K-edge broadening and the observed K-edge shifts are in agreement with the simulations [2, 3]. For the x-ray emission experiment, high resolution x-ray spectra of the Al plasmas in intense radiation have been measured. It was shown that the satellites *q*, *r* and *a-d* of the He-α resonance line is much higher than the satellite *j*, *k*, *l*. The x-ray spectra were also simulated and compared with the simulations. It was found that the large ratio of the satellites q, r and a-d to *j*, *k*, *l* caused by the intense radiation rather than the high plasma density [4-6].

References

[1] Jiyan Zhang et al., 2011 *Phys. Plasmas* **18**, 113301; Jiyan Zhang et al., 2012 *Phys. Plasmas* **19**, 113302
[2] Yang Zhao, Jiamin Yang*, Jiyan Zhang et al., 2013 *Phys. Rev. Lett.* **111**, 155003
[3] E. G. Hill, S. J. Rose, 2012 *High Energy Density Physics* **10**, 1016
[4] Lihua Bao et al., 2011 *Phys. Plasmas* **18**, 023301
[5] V. L. Jacobs, M. Blaha, 1980 *Phys. Rev. A* **21**, 525
[6] A. Saemon et al., 1999 *Phys. Rev. Lett.* **82**, 4843

[1] E-mail: yjm70018@sina.com

Effective Recombination Rates for Tungsten Ions Derived with a Collisional-Radiative Model

Izumi Murakami*†,[1], Akira Sasaki‡,[2]

* National Institute for Fusion Science, National Institutes of Natural Sciences, Toki, Gifu 509-5292, Japan
† SOKENDAI (The Graduate University of Advanced Studies), Toki, Gifu 509-5292, Japan
‡ Kansai Photon Science Institute, National Institutes of Quantum and Radiological Science and Technology, Kizugawa, Kyoto, 619-0215, Japan

Tungsten is one of the most plausible plasma-facing materials and used for wall and divertor plates in fusion devices. Even though the sputtering yield of tungsten by proton is low, tungsten is sputtered by impurity ions and transported into plasma. For examining tungsten behavior in plasma, the ionization and recombination rates of tungsten ions are highly required to solve impurity transport equations. There are some studies carried out to obtain the ionization and recombination rates (e.g. [1,2]), however, all charge states are not covered yet because of the complexity of electron structures of tungsten ions.

We constructed a collisional-radiative (CR) model for tungsten ions of which electron states were determined by a computer algorithm [3, 4]. A set of electron states is generated systematically descending the charge state. For example, the excited states of Pd-like ion (W^{28+}) are generated by adding one electron to the excited states of Rh-like ion (W^{29+}), which have a significant population and are expected to contribute to the dielectronic recombination (DR) process. Using this CR model, we calculated the fractional ion abundance of tungsten ions and the mean charge in ionization equilibrium [4]. The calculated abundance ratio of W^{45+} and W^{44+} ions agreed with the measurements in JT-60U [5].

We use this CR model to obtain effective ionization and recombination rate coefficients of tungsten ions with charge q = 11-63. Atomic data used in the CR model are calculated using the HULLAC code [6] and empirical formulae. Details of the model are described in Ref. [3,4]. Dielectronic capture, autoionization, and radiative decay for autoionizing states are explicitly included in the model. Here, we considered neighboring 7 ions in the model to solve the rate equations to obtain effective ionization and recombination rates.

Figure 1 shows the effective recombination rate for W^{29+} ion as a function of electron temperature with electron density 10^{14}cm^{-3} and other available rates are plotted for comparison. ADAS [7] has the effective recombination rates, acd50_w.dat, obtained from their CR model and original recombination rates in the model are modified ADPAK data by Pütterich et al. [8]. The DR rate obtained by Li et al. [9] is also plotted. Difference between these data is mainly due to different sets of electron states considered in the model.

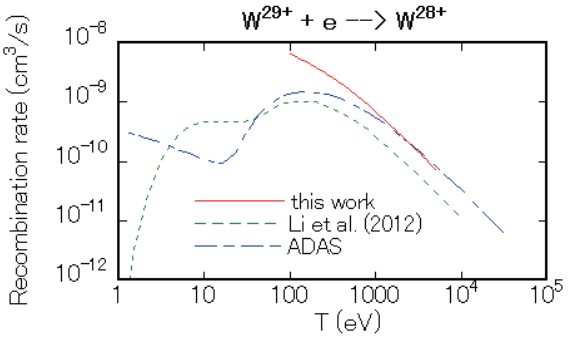

Fig. 1. Effective recombination rates for W^{29+} ion with electron density 10^{14}cm^{-3} of this work (solid line) and ADAS (long dashed line) [7], and DR rate by Li et al. [9].

Acknowledgements This work is carried out partly supported by the JSPS KAKENHI No. 23340185, 23246165, and 16H04623.

References

[1] S. D. Loch et al., 2005 *Phys. Rev. A* **72** 052716
[2] M. Li et al., 2014 *Plasma Sci. Tech.* **16** 182
[3] A. Sasaki, 2013 *High Energy Density Phys.* **9** 325
[4] A. Sasaki and I. Murakami, 2013 *J. Phys. B: At.Mol. Opt. Phys.* **46** 175701
[5] T. Nakano, 2011 *J. Nucl. Mater.* **415** S327
[6] A. Bar-Shalom et al., 2001, *J. Quant. Spectrosc. Radiat. Transfer* **71** 169
[7] H. P. Summers, 2004 The ADAS User Manual, http://www.adas.ac.uk
[8] T. Pütterich et al., 2008 *Plasma Phys. Control. Fusion* **50** 085016
[9] B. W. Li et al., 2012 *Phys. Rev. A* **85**, 052706

[1] E-mail: murakami.izumi@nifs.ac.jp
[2] E-mail: sasaki.akira@qst.go.jp

Fundamental Atomic Process in Source Development for Beyond EUV Lithography and other applications

Bowen Li*[,1], Ximeng Chen* Takeshi Higashiguchi[†], Hayato Ohashi[‡], Chenzhong Dong[€], Padraig Dunne[$], and Gerry O'Sullivan[$]

[*] School of Nuclear Science and Technology, Lanzhou University, Lanzhou 730000, China
[†] Department of Electrical and Electronic Engineering, Faculty of Engineering, Utsunomiya University, Yoto 7-1-2, Utsunomiya, Tochigi 321-8585, Japan
[‡]Graduate School of Science and Engineering for Research, University of Toyama, Toyama, Toyama 930-8555, Japan
[€]Key laboratory of Atomic and Molecular Physics & Functional Materials of Gansu Province, College of Physics and Electronic Engineering, Northwest Normal University, Lanzhou, 730070, China
[$] School of Physics, University College Dublin, Belfield, Dublin 4, Ireland

The behavior of the highly-charged ion (HCI) in heavy ion element plasmas is currently of major interest and has been motivated by their application in a number of high profile areas of science and technology, such as W-inclusion as plasma-facing components (PFCs) in magnetic confinement fusion, plasmas as source for EUV lithography as well as laboratory plasma light sources [1]. After two decades of research, the semiconductor industry is about to introduce lithography sources operating at an EUV wavelength of λ =13.5 nm that have sufficient in-band power for high-volume manufacturing (HVM). These sources are based on emission from resonance 4p-4d and 4d-4f transitions in tin (Sn) laser produced plasmas (LPPs) in stages from Sn^{9+}-Sn^{13+}whose emission is optimized at a plasma electron temperature of T_e = 30–50eV. Higashiguchi and coworkers demonstrate that an in-band EUV source diameter as low as 18μm was produced due to short scale length of the sub-ns duration laser-produced plasma (LPP) [2].

Development of EUV/SXR sources with emission at wavelengths less than 10 nm has moved from being a subject of interest for next generation semiconductor lithography to one for both nanoscale surface patterning and imaging. From studies of rare earth spectra, it is well known that the same transitions emit strongly near 6.7 nm in Gd and Tb [3]. For 1.06 μm irradiation, a conversion efficiency (CE) of 0.6% of laser pulse energy into 'in-band' EUV emission at 6.76 nm was observed from a Gd plasma source [4]. Subsequently, a highermeasured CE of 0.8% into 0.6% bandwidth at the same wavelength was obtained by multi-beam irradiation [5]. Alternatively, we report on the usefulness of germanium (Ge) and gallium (Ga) plasmas as potential extreme ultraviolet (EUV) sources at both 6.x and 13.5nm [6].

We carried out a detailed calculation on dielectronic recombination rate coefficients of Ne-, Rh-, Pd- and Ag-like W [7]. Excellent agreement has been found for Ne-like W while a large discrepancy was found for Pd-like W, which implies that more *ab initio* calculations and experimental measurements are badly needed.

References

[1] G. O'Sullivan, *et al.* 2015 J. Phys. B 48, 144025
[2] T. Dinh, *et al.* 2014 Rev. Sci. Instrum. 85,116104
[3] S. S. Churilov *et al*. 2009 Phys. Scr. 80, 045303
[4] T. Higashiguchi *et al.* 2013 Opt. Express 21, 31837
[5] K. Yoshida *et al.* 2014 *Appl. Phys. Express*7, 086202
[6] B. Li *et al.* 2015 J. Appl. Phys. 118, 073302
[7] B. Li *et al.* 2016 J. Phys. B (in press)

[1] E-mail: libw@lzu.edu.cn

Collisional-radiative models for ground-state M1 line emission of highly charged tungsten ions in the LHD

Daiji Kato[*,†,1]

[*] National Institute for Fusion Science, National Institutes of Natural Sciences, Gifu 509-5292, Japan
[†] Department of Fusion Science, The Graduate University for Advanced Studies SOKENDAI, Gifu 509-5292, Japan

Magnetic-dipole (M1) lines of ground-state highly charged tungsten ions in near-UV and visible ranges have diagnostic usefulness for D-T burning ITER plasmas. M1 lines in these wavelength ranges enable the use of fiber optics, and absolute intensity calibration of spectrometers is facilitated with standard lamps. A large number of previously unreported visible emission lines of tungsten ions W^{q+} $(q = 8 - 28)$ are measured by using low-energy electron beam ion traps [1,2]. Some of them are identified as the ground-state M1 lines of W^{q+} in accord with theoretical predictions. We succeeded in observing an M1 line at 389.4 nm of ground-state W^{26+} ions ($4f^2\ {}^3H_5 - {}^3H_4$) produced in Large Helical Device (LHD) [3]. Since then, a number of near-UV and visible M1 line emission from W^{q+} $(q = 23 - 28)$ have been observed at the LHD [4].

A collisional-radiative (CR) model is developed to calculate the M1 line spectra. HULLAC code is used to generate atomic data (energy levels, radiative transition rates, electron collision strengths). In the present study, proton collision effects on the line spectra are investigated theoretically. The electric quadruple approximation is used for calculations of proton collision (de)excitation rate coefficients of W^{q+} ions. In this approximation, polarization of target ions induced by the proton is neglected at all, and the cross section σ is expressed simply by the electric quadruple transition rate of isolate W^{q+} ions, $B(E2)$,

$$\sigma = \left(\frac{e}{\hbar v_\mathrm{i}}\right)^2 a^{-2} B(E2) f_{E2}(\xi),$$

$$a = \frac{qe^2}{\mu v_\mathrm{i} v_\mathrm{f}}, \qquad \xi = \frac{qe^2}{\hbar}\left(\frac{1}{v_\mathrm{f}} - \frac{1}{v_\mathrm{i}}\right),$$

where μ is the reduced mass of a proton and a target ion, and $v_{\mathrm{i,f}}$ are velocities of incident and scattered protons, respectively. $f_{E2}(\xi)$ is a function given by assuming hyperbolic orbit for the proton in the Coulomb filed centered at the nucleus of W^{q+} [5]. The electric quadruple transition rates are calculated using HULLAC code.

In the present study, it is found that fractional population distributions are drastically changed by proton collision effects (see Fig. 1). The proton collision facilitates redistribution in populations of quasi-degenerate excited levels in single configurations, which causes depopulation of meta-stable levels in the sub-valence excited $4d^9 4f^{k+1}$ configuration. Fractional populations of the ground state are, therefore, increased via $4f - 4d$ allowed transitions from the excited configuration resulting in an enhancement of the ground-state M1 line intensities. It is noted that the $4f - 4d$ EUV emission line intensities are also increased. Based on the present calculations, W^{q+} ion densities in LHD core plasmas are obtained from experimental measurements of the M1 line intensities.

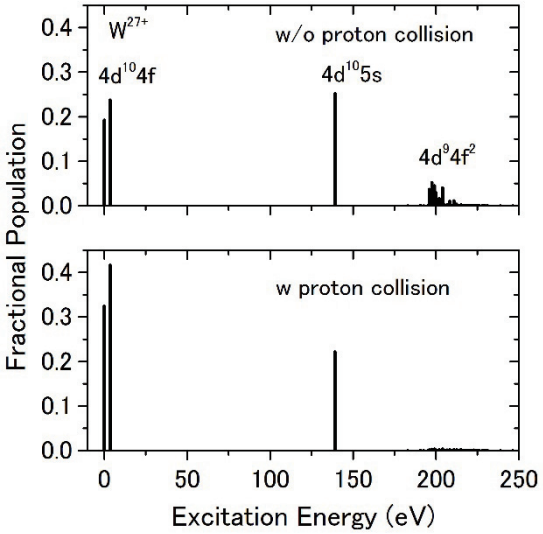

Fig. 1. Fractional populations of W^{27+} levels. $n_\mathrm{e} = n_\mathrm{p} = 10^{13}$ cm^{-3} and $T_\mathrm{e} = T_\mathrm{p} = 1$ keV are assumed.

References

[1] A. Komatsu et al, 2011 *Phys. Scr.* **T144**, 014012; 2012 *Plasma and Fusion Res.* **7**, 1201158.
[2] Z. Fei et al, 2014 *Phys. Rev. A* **90**, 052517.
[3] D. Kato et al, 2013 *Phys. Scr.* **T156**, 014081.
[4] K. Fujii, D. Kato et al, submitted to *Plasma Phys. Control. Fusion*.
[5] K. Alder et al, 1956 *Rev. Mod. Phys.* **28**, 432.

[1] E-mail: kato.daiji@nifs.ac.jp

Signatures of recombination in the EAST upper tungsten divertor

C. R. Wu[*, †], J. Huang[*, †, 1], Z. Jin[*, †], W. Gao[*], W. Gao[*], Z. Xu[*, †], J.F. Chang[*], Y. M. Hou[*], P. F. Zhang[*, †], Y. J. Chen[*], L. Zhang[*], Z. W. Wu[*], J. G. Li[*] and EAST Team[*]

*Institute of Plasma Physics, Chinese Academy of Sciences, P.O. 1126, 230031 Hefei, Anhui, China
† Science Island Branch of Graduate School, University of Science and Technology of China, 230031 Hefei, Anhui, China

Recombination has been found to be a significant fraction of the total ion sink towards plates under detached divertor conditions[1-7]. The recombination occurs in regions where $T_e \sim 1$ eV and $n_e \geq 10^{20}$ m^{-3}. The distribution of the populations of excited states of deuterium in a plasma depends on both excitation and recombination processes. Excitation tends to preferentially populate the low lying excited states and recombination the high lying ones. Thus, the process of recombination may be identified from the ratio of the excited state populations, particularly in the Balmer series[8]. Currently, the upper graphite divertor on EAST have been replaced with ITER-like tungsten monoblock divertor to support higher divertor heat flux up to 10 MW/m^2. During 2015 campaign, in the upper single null geometry, detachment was obtained during L-mode density ramp discharges. Measurements of the spatial distribution of the recombination are presented. There are two OSMA spectrometers used to measuring deuterium Balmer series line emissions, D_α, D_β, D_γ, D_δ, etc. The start of recombination is closely correlated with the onset of detachment. The spatial distribution of the D_γ/D_α ratios indicate that the recombination takes place close to the separatrix strike point.

References

[1] J. L. Terry, et al., 1998 Phys. Plasmas **5 1759**.
[2] G. M. McCracken, et al., 1998 Nucl. Fusion **38 619**.
[3] R. C. Isler, et al., 1997 Phys. Plasmas **4 2989**.
[4] G. D. Porter, et al., 1996 Phys. Plasmas **3 1967**.
[5] F. Wising, et al., 1996 Contrib. Plasm. Phys. **36 136**.
[6] S. I. Krasheninnikov, et al., 1997 Phys. Plasmas. **4 1638**.
[7] A. Loarte, 1997 J. Nucl. Mater. **241 118**.
[8] D. Lumma, et al., 1997 Phys. Plasmas **4 2555**.

[1] E-mail: juan.huang@ipp.ac.cn

Temporal-spatially Resolved Measurement and Analysis of Extreme Ultraviolet Emission Spectra from Laser-Produced Al Plasmas

Mao-Gen Su*[1],Shi-Quan Cao*, Qi Min*, Dui-Xiong Sun*[2] and Chen-Zhong Dong*[3]

*Key Laboratory of Atomic and Molecular Physics and Functional Material of Gansu Province, College of Physics and Electronic Engineering, Northwest Normal University, Lanzhou, 730070, China

High-resolution spectral measurement for laser produced plasma is a powerful tool for studying the atomic structures of highly charged ions and radiation hydrodynamics in plasma. A clear understanding of evolution laws related to the ionization stages and plasma parameters in laser produced plasma is important for the construction of a spectral model in the field of astrophysics and laboratory plasma diagnostics and x-ray source applications.

In this Letter, Temporal evolution of extreme ultraviolet emission from laser-produced aluminum (Al) plasma has been experimentally and theoretically investigated. Fig. 1 shows the normalized measured and simulated spectra for several time delays.

In order to quickly diagnose the plasma, the assumptions of a normalized Boltzmann distribution among the excited states and a steady-state collisional-radiative model are used to estimate the values of electron temperature and electron density in plasma. We succeeded in reproducing the simulated spectra related to the different time delays, which are in good agreement with experiments.

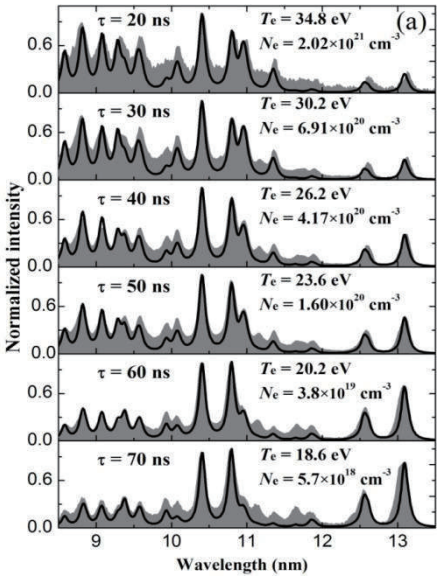

Fig.1. Comparisons between the measured (gray fill) and simulated (black lines) spectra for various time delays.

References

1.Shi-Quan Cao, Mao-Gen Su, Dui-Xiong Sun, Qi Min and Chen-Zhong Dong, 2016 *Chin. Phys. Lett.* **33**, 045201

2. M. G. Su, S. Q. Cao, D. X. Sun, Q. Min, and C.Z. Dong, 2013 *Phys. Plasmas* **20**, 113302.

[1]E-mail: sumg@nwnu.edu.cn

[2]E-mail:sundx@nwnu.edu.cn

[3]E-mail:dongcz@nwnu.edu.cn

Inelastic process and stopping power in Al and Be plasmas

Bin He[1], **Jian-Guo Wang** [2]

Data center for high energy density physics research,
Institute of Applied Physics and Computational Mathematics, Beijing 100088, P.R. China

The plasmas are usually in partially ionized states for most experiments of the stopping power for ions in plasmas. As far as we know, the first relevant experiment was done more than 30 years ago [1], where the stopping of 1MeV deuterons in warm Al plasmas was measured and found enhanced compared with the cold targets. Last year [2] the energy loss of 15MeV protons in both cold and warm dense Be matters were measured in high accuracy, which showed an increasing relative to cold matter. The related theoretical investigation was started about 36 years ago [3] for fast protons in hot Au target. After that some phenomenal models [4] were suggested to estimate the stopping power for energetic ions in intermediate or high-Z plasmas. In recent time an *ab initio* model [5] was developed by us to study the problem based on the average atomic model (AA model) [6], where some bound electrons may distribute at excited states in hot plasmas so that the excitation and ionization as well as their reverse processes have contribution to the inelastic stopping.

In the present talk we will introduce some of our recent progresses in the field mainly focusing on the influence of inelastic process upon the stopping power in partially ionized plasmas, which is also called as inelastic stopping. The method for the calculation is first-order relativistic plane wave Born approximation with all the possible transitions considered. It is found to work well for the projectile energy $E_p \geqslant$ 100keV/u of deuterons by comparison of excitation cross sections of Al ions from solving the time-dependent Schrödinger equation.

First it is found that the inelastic stopping is considerably weakened due to the strong influence from the reverse processes of the excitation and ionization in Al plasmas. The Bethe equation is found to overestimate the inelastic stopping by at least 10%. Comparison of some different models indicates that our model is totally in good agreement with the experiment [1] and the main reason for this is that our results for the inelastic processes should be the most reliable**.** Since the isolated ion model where all the bound electrons are assumed in ground state also agrees well with the experiment [7], the inelastic stopping is studied for deuterons in the Al plasmas with a fixed density at 7 different charge states, where the comparison of the isolated ion model with ours is made and a new experiment is suggested to verify which model is more reliable.

For both cold solid Be and warm dense matter Be only 1s state is occupied by the bound electrons where excitation by projectile is forbidden. The stopping powers of proton with very high velocity in cold and warm Be matters are obtained which are in good agreement with the experiment [2] and recommended data by Ziegler's[8]. For cold matter we consider both ionization of bound electrons and elastic collision of free electrons. For warm matter included are both ionization and plasma wave of free electrons.

Acknowledgement: Bin He acknowledges the useful discussions with Prof. Claude Deutsch. This work was supported by the Science and Technology Foundation of Chinese Academy of Engeering Physics under grant No. 2014B09036, the Chinese National Foundation of Sciences (Grants Nos. 111574034, U1530142, 11474031, and 11371218).

References

[1] F.C. Young *et al.*, 1982 *Phys. Rev. Lett.* **45** 549
[2] A.B. Zylstra *et al.*, 2015 *Phys. Rev. Lett.* **114** 215002
[3] E. Nard *et al* 1977 *Phys. Fluids* **21,** 574
[4] T.M. Mehlhorn 1981 *J. Appl. Phys.* **52** 652;
P. Wang *et al* 1998 Phys. Plasmas **5** 2977
[5] B. He and J.G. Wang 2013 *Nuclear Fusion* 53 093009
[6] Balazs F. Rozsnayai 1972 *Phys. Rev. A*. **5** 1137
[7] D.Casas *et al.*, 2013 *Phys. Rev.E*. **88** 033102
[8] J.F. Ziegler, 1977 Hydrogen-Stopping power and Ranges in all elements, Pergamon press Inc.

[1] E-mail: Hebin-rc@163.com

[2] E-mail: Wang_jianguo@iapcm.ac.cn

A+M Data Center Activities in National Fusion Research Institute

Mi-Young*, [1], Deuk-Chul Kwon*,Sang-Young Chung*, Hee-Chol Choi*, Hyonu Chang*, Won-Seok Chang*,Jun-Hyoung Park*,Sun Min Han*, Kiyong Lee*, Young Rock Kim*,Dhanoj Gupta*,Young-Woo Kim*, Dae-Chul Kim*, Jongsik Kim*, Yonghyun Kim*

* Plasma Fundamental Technology Research team, Core Technology Research Division, Plasma Technology Research Center, National Fusion Research Institute,37 Dongjangsan-ro, Gunsan, Jeollabuk-do, 54004, Republic of Korea

A+M Data play an important role in a variety of systems ranging from gas discharge, electron beam lasers, and plasma processing devices to aurora and solar plasma. Low-temperature plasmas are used in the semiconductor industry for etching, depositing materials and cleaning reaction chambers. The electron impact cross section data for molecules and atoms relevant to such environments would give a better understanding and insight regarding the different phenomena occurring in these areas of sciences. In this presentation, I would like to introduce the main activities of four field of the A+M Data Center in National Fusion Research Insstitute.

The first field of research is generated the collision data of atomic and molecular and the physical and chemical properties of the molecules required for plasma data analysis. I will show our experimental system and theoretical method to obtain data. The second field of research is the development of simulators for plasma analysis and process analysis[2].

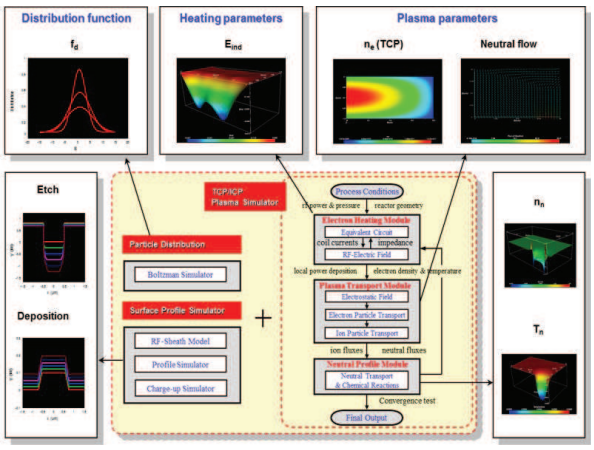

Fig. 1. The plasma simulator concept

The third field of research is to diagnose the characteristics of the plasma generated in a variety of conditions.

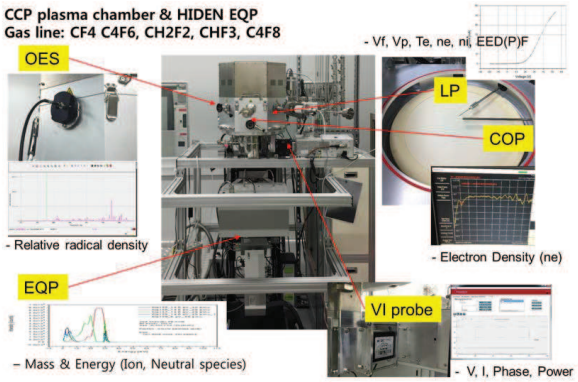

Fig. 2. Plasma diagnostics

The last field of research is to establish a platform for data dissemination and to evaluate data[1] for user. we already establish electron collision for atomic and molecular 26,514 recode.

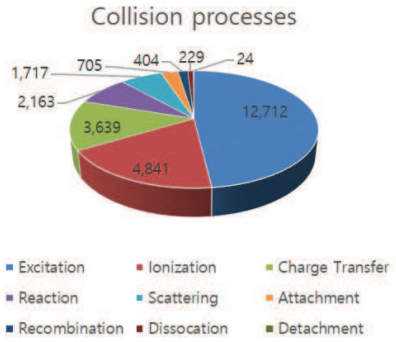

Fig. 3. Plasma DB

References

[1] Mi-Young Song, Jung-Sik Yoon, Hyuck Cho, Yukikazu Itikawa, Grzegorz P. Karwasz, Viatcheslav Kokoouline, Yoshiharu Nakamura, and Jonathan Tennyson, 2015 *J. Phys. Chem. Ref. Data* **44** 023101.

[2] Deuk-Chul Kwon, Mi-Young Song and Jung-Sik Yoon, 2013 *J. Phys. D: Appl. Phys.* **46** 025202.

[1]E-mail: mysong@nfri.re.kr

Inner-shell resonant absorption and double Auger decay on population dynamics of neon plasmas in interaction with ultraintense x-ray pulses

Cheng Gao[*,1], **Jiaolong Zeng**[*2], **Jianmin Yuan**[*,†]

[*] Department of Physics, College of Science, National University of Defense Technology, Changsha Hunan 410073, P. R. China [†] IFSA Collaborative Innovation Center, Shanghai Jiao Tong University, Shanghai 200240, P. R. China

With the application of x-ray free electron lasers (XFEL) such as the Linac Coherent Light Source (LCLS) and SACLA, which are expanding the light-matter interaction from long-wavelength to short-wavelength region [1]. Irradiated by such high intense hard x-rays, the inner shell electrons of atoms are easily excited or ionized leading to the formation of core hole states, which are followed mainly by Auger decay and different charge states are formed consequently.

We developed a model to simulate the dynamics of level populations and charge state distributions of neon plasmas interacting with ultraintense x-ray pulses by solving a time-dependent rate equation (TDRE) in the detailed level-accounting (DLA) approximation [2, 3, 4]. It is shown that:

1. Inner-shell resonant absorption (IRA) can play an important role on the population dynamics [5]. Take neon and an x-ray pulse with photon energy of 1050 eV as an example. The 1050 eV photon can not ionize $1s$ electron of Ne^{6+} and higher charge stages. However, it can be effectively resonantly absorbed by $1s \rightarrow 4p$ of Ne^{6+} and $1s \rightarrow 3p$ of Ne^{7+} leaving a K hole which can further decay. Only when the IRA effects are properly taken into account can we correctly explain the experimental CSD [1].

2. In the framework of the DLA formalism, we studied the effects of double Auger decay (DAD) on charge state distribution. The DAD rates are obtained by using the developed method under the assumption of shake off and knock out processes [6, 7]. After the $1s$ photoionization of neon atom, the DAD processes give accessible decay channels from the K-shell hole state of Ne^{+} to levels of Ne^{3+}, resulting in an increase of the population fraction of Ne^{3+} and a decrease of that of Ne^{2+}. Compared with the results without considering the DAD effects, better agreement is obtained between theory and experiment.

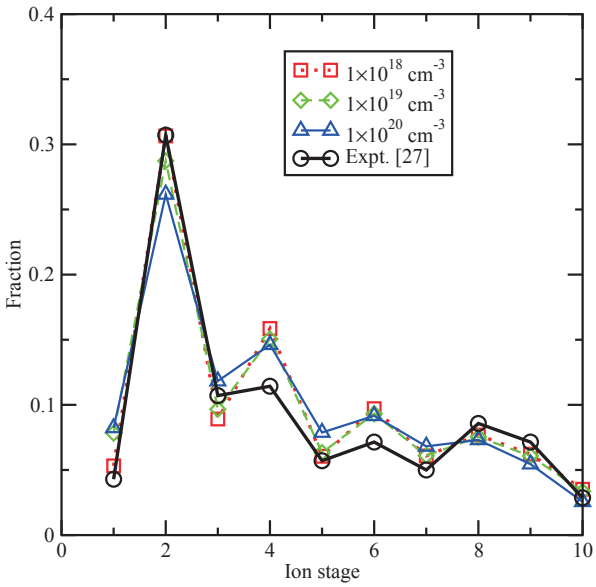

Fig. 1. Charge state distribution of neon plasma at ion density of 10^{18}, 10^{19} and 10^{20} cm^{-3}: comparison with experiment [1].

References

[1] L. Young *et al.*, 2010 Nature (London) **466** 56.

[2] C. Gao, J.L. Zeng, Y.Q. Li, F.T. Jin, and J.M. Yuan, 2013 High Energy Density Phys. **9** 583.

[3] C. Gao, J.L. Zeng, and J.M. Yuan, 2015 Contrib. Plasma Phys. **55** 123.

[4] C. Gao, J.L. Zeng, and J.M. Yuan, 2016 J. Phys. B: At. Mol. Opt. Phys., **49** 044001.

[5] W.J. Xiang, C. Gao, Y.S. Fu, J.L. Zeng, and J.M. Yuan, 2012 Phys. Rev. A **86** 061401(R).

[6] J.L. Zeng, P.F. Liu, W.J. Xiang and J.M. Yuan, 2013 Phys. Rev. A, **87** 033419.

[7] P.F. Liu, J.L. Zeng, A. Borovik, Jr., S. Schippers and A. Muller, 2015 Phys. Rev. A, **92** 012701.

[1]E-mail: gaocheng@nudt.edu.cn
[2]E-mail: jlzeng@nudt.edu.cn

SOLPS simulations of EAST radiation divertor with N2 and Ar seeding

X.J.Liu[*,1], G.Z.Deng[*], C. R. Wu[*], J. Huang[*], L.Wang[*], L. Zhang[*], X. Gao[*], and EAST Team[*]

*Institute of Plasma Physics, Chinese Academy of Sciences, P.O. 1126, 230031 Hefei, Anhui, China
† Science Island Branch of Graduate School, University of Science and Technology of China, 230031 Hefei, Anhui, China

A critical issue for fusion tokamak experimental device is excessive heat load on divertor targets. Impurity seeding has been considered a promising means to enhance the radiation from the plasma edge and eventually to reduce the target heat load. It may become more crucial if carbon has to be avoided as a plasma facing material for ITER and CFETR due to high co-deposition of tritium [1]. So the radiation characters of different gas radiator (N2 and Ar) have been studied by using SOLPS5.0 (B2.5-EIRENE) code package. The atomic and molecular physics model determines the interaction of the plasma constituents, and eventually affect the power dispersal and momentum losses in edge plasma modeling. We have simulated an L-mode discharge with N2 and Ar seeding. In our modelling, all used reaction rates are from the ADAS database[2]. The simulations show that the maximum radiation power loss fraction f_{rad} ($=P_{rad,tot}/P_{in}$) can reach ~85% for N seeding, and ~75% for Ar seeding. The propotion of edge radiation increases as the total radiation increases, and reach the max value, then the radiation region move into the separatrix. The divertor get detachment when f_{rad}~70% for N, and f_{rad}~65% for Ar. The simulation results indicate Ar and N2 seeding are both highly effective in mitigation of the divertor peak heat flux. However, It seems N2 is well suited and even better than Ar for current discharge parameters. This may be that the majority of radiation for N2 seeding case is in the SOL and divertor region rather than inside the last closed flux surface. Further studies of the compatibility of high confinement with impurity seeding will be performed to optimize the choice of radiators.

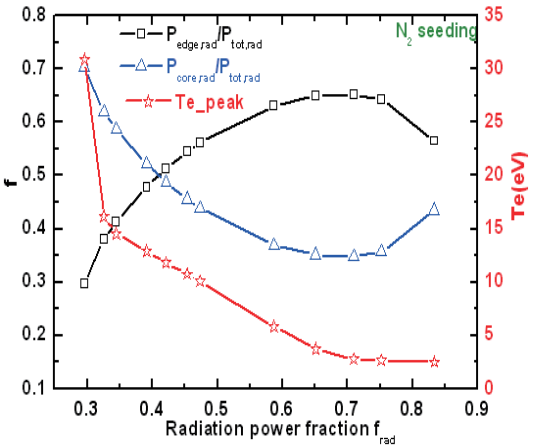

Fig.1 Electron temperature and radiation distribution in core and edge region for N2 seeding plasma.

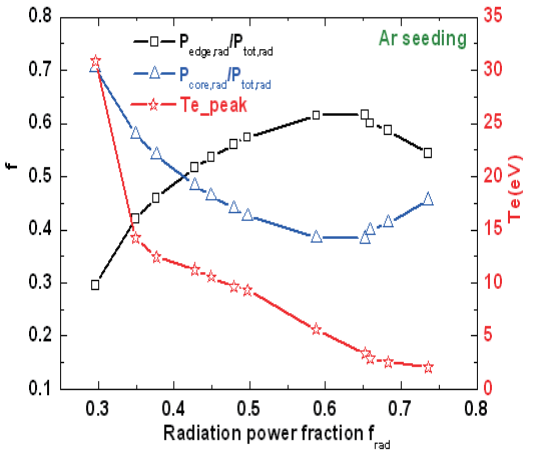

Fig.2 Electron temperature and radiation distribution in core and edge region for N2 seeding plasma.

References

[1] G. Janeschitz, et al., 2002 Nucl. Fusion **42, 14.**
[2] H. P. Summers, http://www.adas.ac.uk./manual.php, 2004.

[1] E-mail: julie1982@ipp.ac.cn

Anion velocity imaging study of dissociative electron attachments to CO_2

Shan X. Tian

Department of Chemical Physics, University of Science and Technology of China, Hefei, 230026, China

Dissociative electron attachments to CO_2 were investigated by using our home-made anion time-sliced velocity map imaging apparatus [1]. Anion velocity imaging, as the state-of-the-art technique, enabled us to have more insights into the dissociation dynamics of CO_2^- at different resonant states [2,3] than that obtained with a traditional turn-table experimental arrangement. Around the electron attachment energy of 8.2 eV, the gradual change of the angular distributions of the fragment O^- produced in $CO_2^-(^2\Pi_g) \rightarrow CO(^1\Sigma^+) + O^-(^2P)$ was due to a dynamic Renner-Teller effect [2]. Three-body [$CO_2^- \rightarrow 2O + C^-$] and two-body [$CO_2^- \rightarrow O_2 + C^-$] dissociations were observed in the electron attachment energy range 15.9-19.0 eV, in which the two-body fragmentation process was proposed to be a new reaction pathway to molecular oxygen in Earth's prebiotic primitive atmosphere [3].

Considering the large quantities of low-energy electrons in interstellar space and the upper atmosphere, we suggest that the present two-and three-body pathways for generating molecular O_2 and the free O atoms should be incorporated into a general circulation model of atmospheric chemistry.

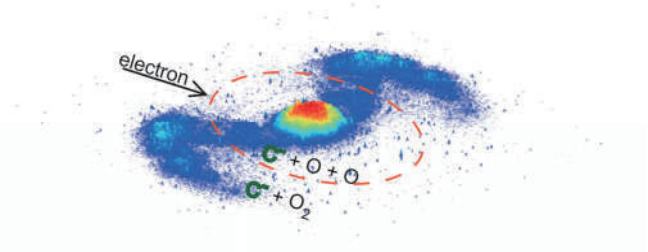

Fig. 1. C^- time-sliced velocity image recorded at 15.9 eV.

Acknowledgments: This work has the supports of Natural Science Foundation of China (Grant No. 21273213), the Ministry of Science and Technology of China (Grant No. 2013CB834602) and Hefei Science Center of Chinese Academy of Sciences.

References

[1] B. Wu, L. Xia, H.-K. Li, X.-J. Zeng and S. X. Tian, 2012 *Rev. Sci. Instrum.* 83 013108.
[2] B. Wu, L. Xia, Y.-F. Wang, H.-K. Li, X.-J. Zeng and S. X. Tian, 2012 *Phys. Rev. A* 85 052709.
[3] X.-D. Wang, X.-F. Gao, C.-J. Xuan and S. X. Tian, 2016 *Nature Chem.* 8 258-263.

E-mail: sxtian@ustc.edu.cn

Isotope effect in dissociation processes of deuterated molecules from doubly excited states

Yasuhiro Sakai*,†,[1], Karin Takahashi*, Toru Hasegawa*, Naoya Miyauchi*, Daiji Kato[#,$], Izumi Murakami[#,$], and Hiroyuki A. Sakaue[#]

[*] Dept. of Physics, Toho University, Funabashi, Chiba 274-8510, Japan
[†] Research Center for Materials with Integrated Properties, Toho University, Funabashi, Chiba 274-8510, Japan
[#] National Institute for Fusion Science, National Institutes of Natural Sciences, Toki, Gifu 509-5292, Japan
[$] Dept. of Fusion Science, SOKENDAI (The Graduate University for Advanced Studies), Toki, Gifu 509-5292, Japan

Dissociative recombination(DR) processes which are one of the important process in divertor plasma originate from doubly excited states produced by electron capture with low energy electron-molecular ion collision. In general, doubly excited states are dissociated by either the neutral dissociation or the dissociative ionization. In these dissociation processes, it is expected that isotope effects are observed. Information on isotope effects is very important for predicting the performance of the future fusion reactor. Therefore, it is necessary to know how doubly excited molecules dissociate; i.e. branching ratios and cross sections.

In this study, absolute generalized oscillator strength distributions(GOSDs), total and partial ionic GOSDs of hydrogen(H_2) and deuterium(D_2) were investigated. The experiments were performed with the scattered electron ion coincidence (SEICO) spectrometer in our laboratory[1,2]. The total GOSDs of H_2 and D_2 determined for a 200 eV incident electron energy and a scattering angle of 6 degrees are shown in Fig.1(a). The magnitude of the momentum transfer, K^2, for the given experimental conditions in shown in the upper horizontal axis. The large peak around 12eV was associated with excitations mainly from $(1s\sigma_g)^{-1}(2p\sigma_u)$ and $(1s\sigma_g)^{-1}(2p\pi_u)$, corresponding to the $B^1\Sigma^+_u$ and $C^1\Pi_u$ states, respectively. Although the GOSD of D_2 around $(1s\sigma_g)^{-1}$ ionization threshold was slightly smaller than that of H_2, the behavior against the electron energy-loss was almost similar.

The partial ionic GOSDs of H_2^+ and D_2^+ are shown in Fig.1(b). Both GOSDs increased from the first ionization threshold $(1s\sigma_g)^{-1}$ at 15.4 eV, which has a maximum value at about 18 eV. After the energy-loss value exceeded the peak, both the ionic GOSD decreased gradually with further increase in the energy-loss values. There was little difference in their ionic GOSDs. However, the D^+ formation by dissociative ionization was completely different from that of H^+, as can be seen from Fig.1(c). The partial ionic GOSD of D^+ was half of the H^+ one in magnitude. In particular, the GOSD of D^+ was very small in the energy-loss region of 18 to 22e V. This mechanism is being considered at present. Besides,

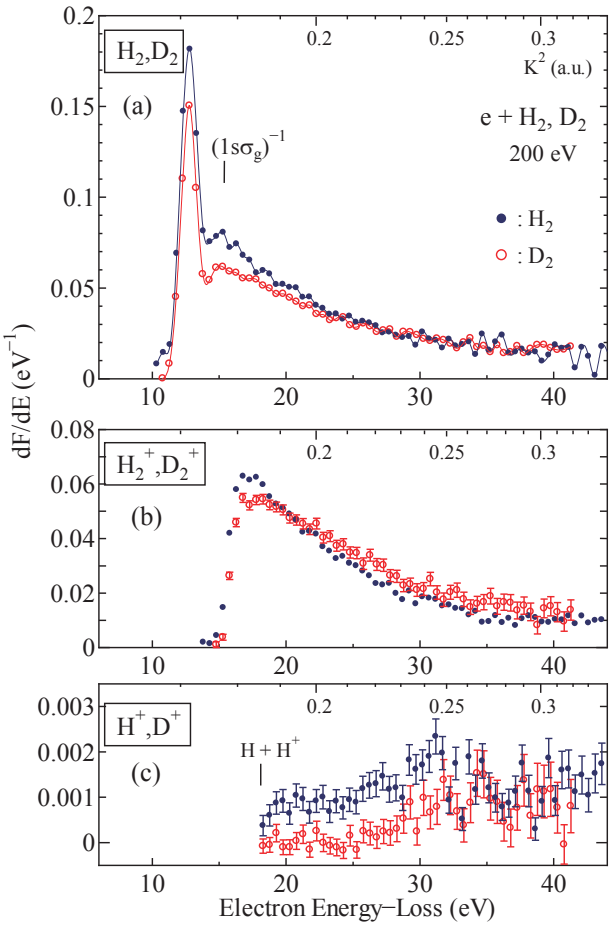

Fig. 1. (a)The absolute total generalized oscillator strength distributions(GOSDs) of H_2 and D_2, (b) the partial ionic GOSDs of H_2^+ and D_2^+, (c)the partial ionic GOSDs of H^+ and D^+, respectively.

we estimated the ratio of the dissociative ionization to neutral dissociation. When doubly excited molecules were decayed by dissociation from the $Q_1{}^1\Sigma g^+(1)$ state, the ratio in the case of H_2 was 3:7, while that of D_2 was 1:9. It seems that this is so-called isotope effect.

References

[1] K. Yamamoto and Y. Sakai, 2012 *J. Phys. B: At.Mol. Opt. Phys,* **45**, 055201.
[2] K. Takahashi *et al.*, 2014 *Eur. Phys. J. D,* **68**, 83.

[†,1] E-mail: sakai@ph.sci.toho-u.ac.jp

KLL-dielectronic recombination and polarization of X-ray emissions of H-like to B-like barium ions

Q. Q. Man *, L. Y. Xie*,[1], H. Y. Cui *, J. Jiang* , D. H. Zhang*, C.Z.Dong*

* Key laboratory of Atomic and Molecular Physics & Functional Materials of Gansu Province, College of Physics and Electronic Engineering, Northwest Normal University, Lanzhou, 730070, China

Dielectronic recombination (DR) is an important process in collision of electrons with highly charged ions. The DR process exists widely in hot astrophysical, laboratory and fusion plasmas where it strongly affects both the charge-state distribution and the x-ray spectrum. Accurate knowledge of DR cross sections is therefore needed for modeling of astrophysical and fusion plasmas. The x-ray radiations from the DR process can provide information on the directionality of the electron currents and the orientation of the magnetic-field lines, and anisotropy of the electron energy distributions in plasmas, and can also be used as a diagnostic tool [1] .

KLL DR processes and the polarization of emitted x-rays are attracted much interesting for highly charged ions with few electrons in recently [2]. In this report, we calculated the resonance energies, resonance width, and corresponding radiative and auger transition rates for all of individual KLL resonance state of the highly charged H-like to B-like barium ions using the Multi-configuration Dirac-Fock method[3], and obtained the DR resonance strengths and linear polarization degree of X-ray emissions[4] for each of the ions mentioned above. In the calculations, the electron correlation effects, QED effects, and Breit interactions are well considered. And the influence of Breit interactions on Auger rates, DR resonance strengths and polarization of X-ray are analyzed and discussed. Partly of the present results for the differential cross sections and a comparison with the EBIT experimental measurements are plotted in Fig.1 and 2, good consistency is obtained.

This work is partly supported by the National Basic Research Program of China (973 Program) (Grant No. 2013CB922200), and the National Natural Science Foundation of China (Grant Nos. U1331122,U1330117,U1332206,U153014,11464404 2,11564036)。

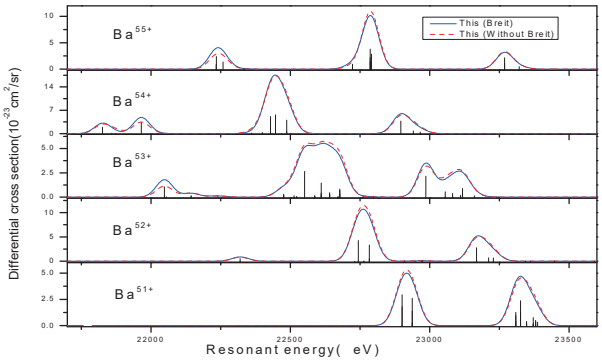

Fig. 1. Resonance strengths and differential cross sections (convolved with a Gaussian of FWHM=70eV） for the H-like to B-like barium ions .

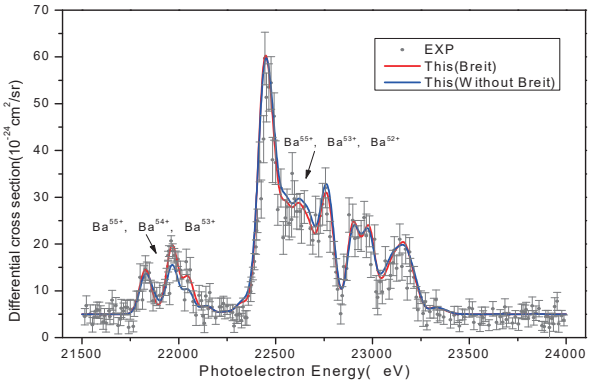

Fig. 2. The present calculated differential cross section (convolved with a Gaussian of FWHM=70eV) with considering Breit interactions (red line) and without Breit interactions (blue line) for H-like to B-like Barium ions (the ratio of the relative proportion ofBa^{54+}:Ba^{53+}:Ba^{52+}:B^{51+}=30.11%:42.99%:23.76%:3.14%), and compared with EBIT experimental results [5].

References

[1] H. Jörg, Z.M.Hu, H. Bekker et al. 2015 *Phys. Rev. A* **91** 042705.

[2] S. Fritzsche, A. Surzhykov, and Th. Stöhlker, 2009 *Phys. Rev.Lett.* **103** 113001.

[3] P. Jönsson , G. Gaigalas, J. Bieroń et al., 2013 *Comput. Phys. Commun.* **184** 2197.

[4] Z. Hu, X. Han, Y.Li et al., 2012 *Phys. Rev. Lett.* **108** 073002.

[5] D.A. Knapp, R.E. Marrs, M. B. Schneider, 1993 *Phys Rev. A* **47** 2039.

[1] E-mail: xiely@nwnu.edu.cnu

Theoretical study of Dielectronic Recombination of Li-Like Ar^{15+} and Xe^{51+} Ions

L. J. Dou[*, ξ, †], L. Y. Xie[†, 1], Z. K. Huang[*, ξ], C. Z. Dong[†], and X. W. Ma[*, 2]

[*] Institute of Modern Physics, Chinese Academy of Sciences, Lanzhou, 730000, China
[ξ] University of Chinese Academy of Sciences, Beijing 100049, China
[†] College of Physics and Electronic Engineering, NWNU, Lanzhou, 730070, China

Dielectronic recombination (DR) of Li-like ions has attracted much interest both in experimental and theoretical studies due to its signification in modeling astrophysics and fusion plasmas, and in testing atomic structure and collision theories in recent years [1]. We performed a detailed calculations for the $\Delta n = 0$ transition of Li-like Ar^{15+} and obtained the DR rate coefficients by using the Flexible Atomic Code (FAC) [2] based on the relativistic configuration interaction method. The resonance positions and strengths for the $2p_{1/2}nl$, $2p_{3/2}nl$ (n=10-17) doubly excited states of Ar^{14+} ion are presented. For the higher Rydberg resonances with n>17 close to thresholds, the resonances are obtained by extrapolation in combination with quantum defect theory (QDT) [3]. Our calculated rate coefficients (black line) are illustrated in Fig.1 and compared with the experimental results by employing the electron-ion merged-beams technique at the heavy ion storage ring CSRm at IMP [4].

The same method was used to calculate the DR process of middle-Z Li-like Xe^{51+} ions. All DR resonances associated with the two Rydberg resonance series $(2p_{1/2}nl_j)_J$ (n=18-32) and $(2p_{3/2}n'l_j)_J$ (n'=9-27) was considered in the calculations. The contributions from higher Rydberg resonances with n>32 and n'>27 throughout to thresholds are obtained by extrapolation based on QDT. Fig.2 shows the calculated DR spectrum (black line) for the $(2p_{3/2}9l_j)_J$ resonance manifolds compared with the recent experimental results at the heavy-ion storage ring ESR by Bernhardt et al. [5]. Good agreement is obtained.

This work is partly supported by the National Natural Science Foundation of China (Grant Nos. U1331122, U1330117, U1332206, 11320101003, U1530142), and the External Cooperation Program of the CAS, No. GJHZ1305).

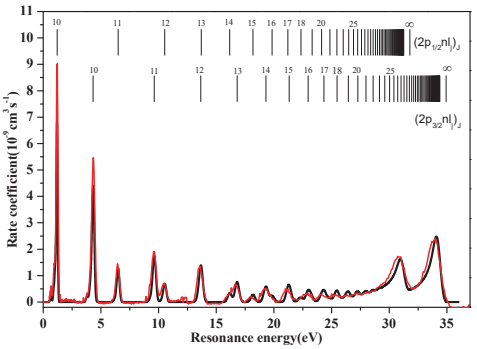

Fig. 1. Comparision of the theoretical (black line) and experimental (red line) rate coefficients for Ar^{15+} ions. The theoretical rates are cut off at n_{cut}=75. The rate coefficients are obtained from the theoretical resonance strengths convoluted with the experimental electron beam temperatures (40 meV/k_B transverse and 0.8 meV/k_B longitudinal).

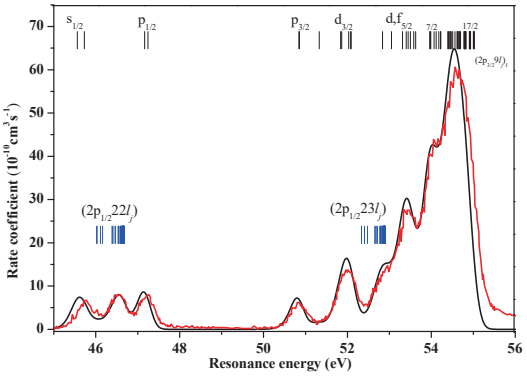

Fig. 2. Comparision of the theoretical (black line) and experimental (red line) rate coefficients for Xe^{51+} DR spectrum in the energy range of the $2s+e\rightarrow(2p_{3/2}9l_j)_J$ resonance groups. Totally 64 individual resonances are included for the $(2p_{3/2}9l_j)_J$ manifold, which are blended by $(2p_{1/2}nl_j)_J$ with n = 22 and n = 23 manifolds (blue vertical bars). The rates are obtained from the theoretical resonance strengths folded with transverse (120 meV/k_B) and longitudinal (0.2 meV/k_B) temperatures.

References

[1] J. Colgan et al., 2004 *A&A* **417** 1183
[2] M. F. Gu, 2008 *Can. J. Phys* **86** 675
[3] Y. Hahn, 1985 *Adv. At. Mol. Phys* **21** 123
[4] Z. K. Huang et al., 2015 *Phys. Scr* **T166** 014023
[5] D. Bernhardt et al., 2015 *Phys. Rev. A* **91** 012710

[1]E-mail: xiely@nwnu.edu
[2]E-mail: x.ma@impcas.ac.cn

Optical oscillator strengths of valence-shell excitations of atoms and molecules determined by the newly developed dipole (γ, γ) method

Lin-Fan Zhu[*,†,1] **Xu Kang**[*,†], **Long-Quan Xu**[*,†], **Ya-Wei Liu**[*,†], **Ke Yang**[‡], **N. Hiraoka**[§], **and K. D. Tsuei**[§]

[*] Hefei National Laboratory for Physical Sciences at Microscale and Department of Modern Physics, University of Science and Technology of China, Hefei, Anhui 230026, People's Republic of China

[†] Synergetic Innovation Center of Quantum Information and Quantum Physics, University of Science and Technology of China, Hefei, Anhui 230026, People's Republic of China

[‡] Shanghai Institute of Applied Physics, Chinese Academy of Sciences, Shanghai 201204, P. R. China

[§] National Synchrotron Radiation Research Center, Hsinchu 30076, Taiwan, Republic of China

The absolute optical oscillator strength (OOS), or the equivalent quantity of photoabsorption cross section, of an atom or molecule represents the transition probability between two quantum states and is essential in describing and understanding the physical processes involving the photon absorption and emission, which widely exist in plasma, interstellar space, planetary atmosphere, and energy deposition. Very resently, a new experimental method, i.e., the dipole (γ, γ) method, has been proposed and realized by our group to determine the OOSs of atoms and molecules. In the dipole (γ, γ) method, the high energy photon impact ($\sim$10 keV) at the dipole approximation condition of $q^2 \approx 0$ (i.e.,the small scattering angle) is used to simulate the photoabsorption process.

Using the dipole (γ, γ) method, the absolute OOSs of valence-shell excitations of helium, argon, nitrogen and carbon monoxide were determined and compared with the previous experimental and theoretical results [1, 2, 3, 4]. These results show that the dipole (γ, γ) method provides a reliable approach to obtain the benchmark data of the OOSs of the valence-shell excitations for gaseous atoms and molecules.

It is worth to mention that every experimental technique to determine OOSs of atoms and molecules has its own merits and demerits. The photoabsorption method is influenced by the line-saturation effect, at the same time, it has the highest energy resolution to determine the oscillator strengths of the rotational states. Considering the moderate energy resolution of tens of meV, the present dipole (γ, γ) method and the dipole (e, e) method can only measure the oscillator strengths of the vibronic states at the present stage, while they are free from the linesaturation effect. The dipole (e, e) method has the advantage of a large cross section, which can achieve a good signal-to-noise ratio and a good statistical count, but the rapid variation of its Bethe-Born conversion factor may bring considerable uncertainties. The Bethe-Born conversion factors of the dipole(γ, γ) method, which can be accurately determined by simulating the light path directly, can avoid this problem. Actually, the only shortage of the dipole (γ, γ) method is its low cross section and limited single-to-noise ratio, to some extent, it can be solved by improving the density of the target. Furthermore, the dipole (γ, γ) is free from any systematic error, to the best of our knowledge. Thus it is possible to achieve a higher precision for the oscillator strengths with the dramatic progress of the third generation synchrotron radiation and the free electron laser.

References

[1] L. Q. Xu, Y. W. Liu, X. Kang *et al* 2015 *Sci. Rep.* **5** 18350

[2] Y. W. Liu, X. Kang, L. Q. Xu *et al* 1991 *Astrophys. J.* **819** 412

[3] X. Xu, D. D. Ni, X. Kang *et al* 1994 *J. Phys. B* **49** 064010

[4] X. Kang, Y. W. Liu, L. Q. Xu *et al* 2009 *Astrophys. J.* **807** 96

[1] E-mail: lfzhu@ustc.edu.cn

A new model to calculate electron-electron coulomb energy based on electron density

LONG Feiyun*[,1], YAN Jun*[,2]

[*] Institute of Applied Physics and Computational Mathematics, Beijing 100088, China

Traditional density functional theory based on independent-electron approximation divides the Electron-electron coulomb energy into three parts: the Hartree term, the exchange term and the correlation term. The exact exchange term, originated from the antisymmetry of the wavefunction, demands accurate orbitals. And the correlation term, existed mainly in overlapping of the orbitals, is too complicated to describe. Both of the two terms are generally fitted from various data under known physical conditions [1].

Here we propose a new method to calculate the electron-electron coulomb energy with the conditional probability distribution, which is unique for the ground state. In coulomb system, the conditional probability distribution is generally continuous and differentiable， except at the boundaries. With the unique and continuous properties, the conditional probability is determined by the boundaries, which are profoundly related to the kinetic functionals.

Recently, three-dimensional spin-polarized homogeneous electron gas has been studied by quantum Monte Carlo method [2]. As a first step, we suppose and use their simulated radial distribution function for the boundary of inhomogeneous case. The conditional probability distribution is obtained by solving a set of integral equations. To test our method, we calculate the electron-electron coulomb energy of Be, Ne, Ar, Kr atoms from given electron density, and our results agree well with those of configuration-interaction method.

References

[1] Perdew J P, Kurth S. Density functionals for non-relativistic Coulomb systems in the new century[M]//A primer in density functional theory. *Springer Berlin Heidelberg,* 2003: 1-55.

[2] Spink G G, Needs R J, Drummond N D. Quantum Monte Carlo study of the three-dimensional spin-polarized homogeneous electron gas[J]. *Physical Review B, 2013,* 88(8): 085121.

[1] E-mail: supernova_1986@163.com
[2] E-mail: yan_jun@iapcm.ac.cn

Finite field calculations of static polarizabilities and hyperpolarizabilities of In^+, and Sr

Yan-mei Yu[*, 1], **Bing-bing Suo**[† 2]

[*] Beijing National Laboratory for Condensed Matter Physics, Institute of Physics, Chinese Academy of Sciences, Beijing 100190,China

[†] Institute of Modern Physics, Northwest University, Xi'an, Shanxi 710069, China

The dipole polarizabilities, dipole hyperpolarizabilities, quadrupole moments, and quadrupole polarizabilities of the $5s^2\ ^1S$ and $5s5p\ ^3P^o$ states of In^+ and Sr are calculated by using the finite field method. The electron correlation effect and the basis set convergence are investigated in the relativistic coupled-cluster and configuration interaction calculations in order to obtain polarizabilities of high accuracy. Comparative study of the fully and scalar relativistic calculations reveals the effect of the spin-orbit coupling on the dipole polarizabilities of In^+ and Sr. The blackbody-radiation shifts of the clock transition $5s^2\ ^1S_0$ - $5s5p\ ^3P_0^o$ due to the dipole polarizabilities, quadrupole polarizabilities, and dipole hyperpolarizabilities are evaluated to be 0.017, 8.33×10^{-10}, and 1.93×10^{-17} Hz for In^+ and 2.09 and 5.82×10^{-8}, and 1.69×10^{-15} Hz for Sr. The blackbody-radiation shifts from the quadrupole polarizabilities and dipole hyperpolarizabilities are significantly less than that from the dipole polarizabilities and therefore can be safely omitted for the quoted $\times10^{-18}$ uncertainty of the optical frequency standard of In^+ and Sr.

References

[1] Y. M Yu, B. B Suo, H. H. Feng, et. al., 2015 *Phys. Rev. A* **92** 052515.

[1] E-mail: ymyu@aphy.iphy.ac.cn
[2] E-mail: bsuo@nwu.edu.cn

Observation of resonant excitation of Fe^{14+}

TSUDA Takashi[a], SHIMIZU Erina[a], Safdar ALI[a], SAKAUE Hiroyuki A.[b], KATO Daiji[b,c], MURAKAMI Izumi[b,c], HARA Hirohisa[d,e], WATANABE Tetsuya[d,e], and NAKAMURA Nobuyuki[a,1]

[a] Institute for Laser Science, The University of Electro-Communications, Tokyo 182-8585, Japan
[b] National Institute for Fusion Science, Gifu 509-5292, Japan
[c] Department of Fusion Science, SOKENDAI, Gifu 509-5292, Japan
[d] National Astronomical Observatory of Japan, Tokyo 181-8588, Japan
[e] Department of Astronomical Science, SOKENDAI, Tokyo 181-8588, Japan

Spectra of highly charged Fe ions in the extreme ultraviolet (EUV) range are important for the spectroscopic diagnostics of astrophysical hot plasmas such as solar corona [1]. In such diagnostics, plasma parameters, such as electron temperature and density, are determined through the comparison between the observed spectra and theoretical spectra calculated with a collisional radiative (CR) model. For accurate diagnostics, the model spectra should thus be examined by laboratory benchmark spectra obtained with a well-defined condition. We have been studying EUV spectra of highly charged Fe ions with an electron beam ion trap (EBIT), which can realize a well-defined plasma consisting of a quasi-monoenergetic electron beam and trapped ions with a narrow charge state distribution. In the previous studies [2-3], the dependence on the electron density was the main subject of interest. On the other hand in the present study, the dependence on the electron energy is studied.

Experiment was performed with a compact EBIT, called CoBIT [4]. Highly charged Fe ions were produced by injecting a ferrocene gas into CoBIT with an electron beam energy of 500 eV. After a "cooking" time of 1600 ms, the electron energy was swept between 400 and 500 eV for 10 ms (probing time), and kept at 500 eV for 10 ms (keeping time) for preserving the charge distribution. A preliminary result is shown in Fig. 1, where the intensity enhancement due to resonant excitation is confirmed. Comparison between the experimental results and theoretical resonant emission cross sections is given.

References

[1] T. Watanabe, 2009 *J. Phys.: Conf. Ser.* **163** 012002.
[2] N. Nakamura et al., 2011 *ApJ* **739** 17.
[3] E. Shimizu et al., 2011 *J. Phys.: Conf. Ser.* **583** 012019.
[4] N. Nakamura et al., 2008 *Rev. Sci. Instrum.* **79** 063104.

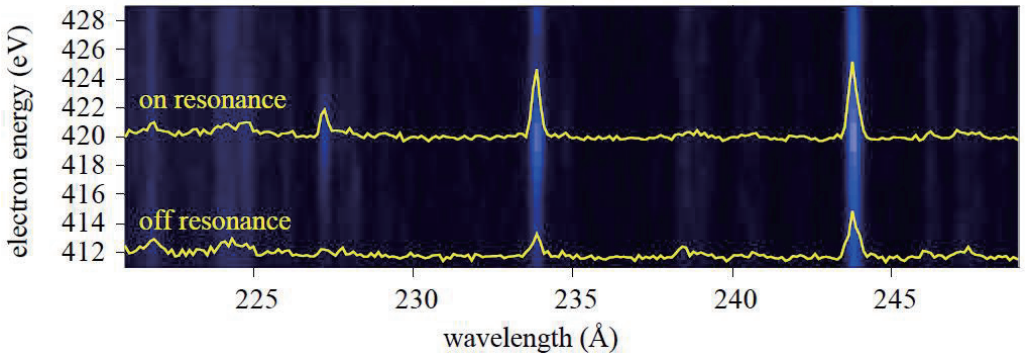

Fig. 1. Electron energy dependence of Fe XV $3s3p$ - $3s3d$ lines observed with CoBIT: $^3P_1$-$^3D_2$ (227 Å), $^3P_2$-$^3D_3$ (234 Å), and $^1P_1$–$^1D_2$ (244 Å).

E-mail: n_nakamu@ils.uec.ac.jp

Tungsten spectra measurement on EAST and the requirement of atomic data for its quantitative analysis

L. Zhang*[1], S. Morita[†‡], Z. Xu*, P. F. Zhang*, T. Oishi[†‡], X.D. Yang*, W. Gao*, J. Huang*, Y. J. Chen*, C. R. Wu*, Z. W. Wu*, J. L. Chen*, L. Q. Hu* and EAST team

[*] Institute of Plasma Physics, Chinese Academy of Science, Hefei 230031, China
[†] National Institute for Fusion Science, Toki, Gifu 509-5292, Japan
[‡]Department of Fusion Science, Graduate University for Advanced Studies, Toki, Gifu, 509-5292, Japa

Since the tungsten upper divertor was installed on EAST in 2014, three grazing incidence flat-field extreme ultraviolet (EUV) spectrometers have been developed [1-2] successively to measure tungsten spectrum, monitor the tungsten behavior and study the tungsten transport in EAST plasma. Two of them working at 10-130Å (EUV_Short) and 20-500 Å (EUV_Long) respectively measure the tungsten spectrum with fast time response of 5ms/frame, which have been operated routinely. The third one also working at 20-500 Å (EUV_Long2) measure space-resolved tungsten spectrum, which will finish its system commissioning until next EAST campaign.

In 2014 and 2015 campaign, EAST was operated with lower single null (LSN) configuration, tungsten spectra with strong intensity were measured during the H-mode phase heated by neutral beam injection (NBI) indicating the occurrence of central tungsten accumulation. However, in this case the density peaking combined with impurity accumulation resulted in the limitation of electron temperature (T_e) and the ionization stage of tungsten ions. In 2016 spring campaign, EAST was operated with upper single null (USN) configuration to improve its capability of power/particle handling in divertor, and tungsten spectra with strong intensity were measured during H-mode phase in multiple heating schemes, which provided the opportunities for measurement of the tungsten spectra at T_e up to 4keV and studying the tungsten behavior under wide-range conditions. At present, the line analysis of tungsten spectra are being carried on and the potential experimental approaches to suppress the tungsten accumulation are being explored [3].

More importantly, since tungsten accumulation during H-mode phase always caused a periodic disappearance of H-mode or even plasma disruption due to the large radiation power loss, the quantitative analysis of tungsten behavior is urgently desired in EAST discharges. Tungsten density evaluation is now being attempted [4] with two approaches by using tungsten cooling rate and combined with the measurement of radiation power loss and the photon emissivity coefficients (PECs) of line emission from W^{45+} (126.998Å) combined with the absolute measurement of emission intensity, respectively. The preliminary results show several times of different between each other and large uncertainties for themselves, thus the requirement of these atomic data is of high priority.

The potential collaboration between EAST experiment and atomic physics research in the near future could be considered on the following topics:

(1) Database of energy-resolved cooling rate as a function of T_e for tungsten and other metallic impurity.
(2) The achievement of accurate PECs for W^{45+} lines.
(3) The application of tungsten spectra measured in EBIT device to the decomposition and identification of tungsten spectra measured in EAST plasma.
(4) Measurement, identification and quantitative analysis of line emissions from tungsten ions with low ionization stages in EUV region, e.g. W^{6+}-W^{19+} .
(5) Measurement, identification and quantitative analysis of line emissions from tungsten ions with high ionization stages in EUV region, e.g. W^{46+}.
(6) Proposals on uncertainty assessment and benchmark experiments for atomic data.

References

[1] L. Zhang, et al., Rev. Sci. Instrum. 86, 123509 (2015)
[2] L. Zhang, et al., 30th ITPA Topical Group on Diagnostics, 21-24 June, 2016, Novosibirsk, Russia
[3] L. Zhang, et al., 26th IAEA FEC, EX/P7-11, 2016
[4] X. D. Yang, et al., A3 Foresight Program Workshop, 17-20 May 2016, Yinchuan, China

VUV spectroscopy for tungsten WIV-WVII line emissions in Large Helical Device

T. Oishi*,†,[1], S. Morita*,†,[2], X. L. Huang*,[3], H. M. Zhang†,[4], Y. Liu†,[5], M. Goto*,†,[6] and the LHD Experiment Group*

[*] National Institute for Fusion Science, National Institutes of Natural Sciences, Toki, Gifu 509-5292, Japan
[†]Department of Fusion Science, Graduate University for Advanced Studies, Toki, Gifu 509-5292, Japan

Tungsten is regarded as a leading candidate material for the plasma facing components in ITER and future fusion reactors. Considering tungsten impurity transport in ITER, the following three transport processes need to be evaluated: (1) release of neutral tungsten atoms from the divertor plates; (2) transport of tungsten ions at lower ionization stages in the edge plasmas; and (3) accumulation of tungsten ions at higher ionization stages in the core plasmas. However, tungsten ions in lower ionization stages have not been measured sufficiently even though it is necessary for accurate evaluation of tungsten influx and comprehensive understanding of the tungsten impurity transport. Therefore, we conducted spectroscopy diagnostics to measure spectra of emissions released from tungsten ions in Large Helical Device (LHD) with superconducting magnetic coils for steady state operations of current-free plasma discharges.

The tungsten ions are externally introduced in the LHD plasma by injecting a coaxial tungsten impurity pellet. VUV spectroscopy using a high-resolution 3 m normal incidence spectrometer has been applied to measure VUV lines from tungsten ions at lower ionization stages. Many tungsten lines of WIV-WVII are successfully observed just after the tungsten pellet injection as the first observation of line emissions from low-ionized tungsten ions in magnetically-confined fusion plasma experiments. As shown in Fig. 1, it is found that five WVI lines at 605.93 Å (5d-6p), 639.68 Å (5d-6p), 677.72 Å (5d-6p), 1168.15 Å (6s-6p) and 1467.96 Å (6s-6p) have the highest intensity and are entirely isolated from other intrinsic impurity lines [1]. The result strongly suggests that those lines will be useful for the spectroscopic study in ITER and other tungsten divertor devices.

This work was partially conducted under the LHD project financial support (NIFS14ULPP010), Grant-in-Aid for Young Scientists (B) 26800282, and the JSPS-NRF-NSFC A3 Foresight Program in the field of Plasma Physics (NSFC: No.11261140328, NRF: No.2012K2A2A6000443).

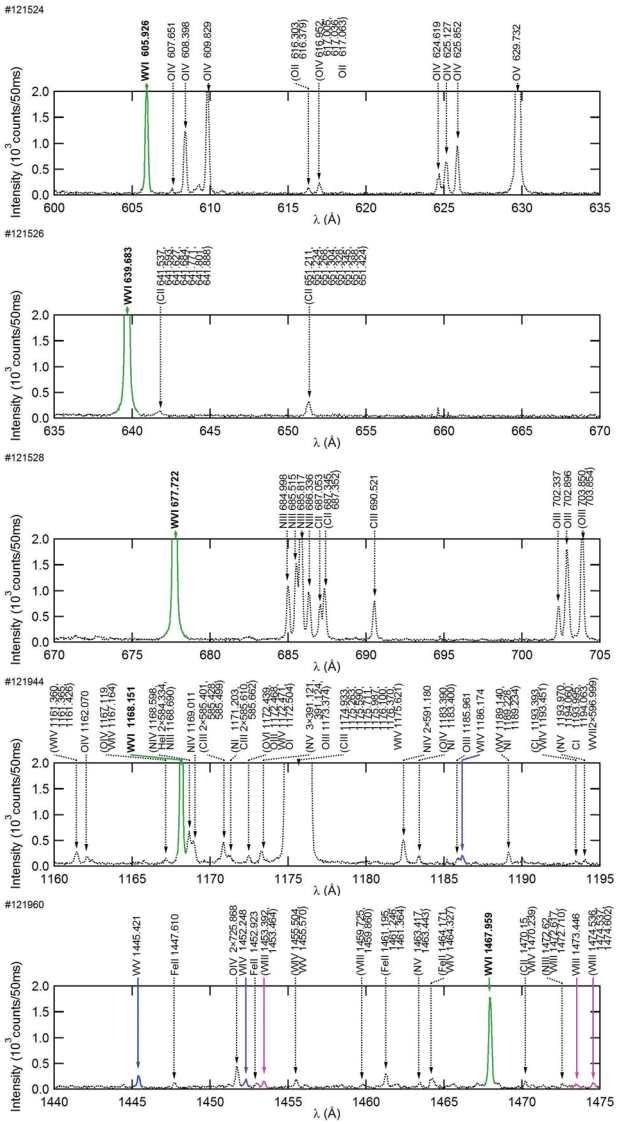

Fig. 1. VUV spectra including WVI emission lines observed in LHD.

References

[1] T. Oishi, S. Morita, X. L. Huang et.al., 2016 *Physica Scripta* **91** 025602

[1] E-mail: oishi@LHD.nifs.ac.jp
[2] E-mail: morita@nifs.ac.jp
[3] E-mail: huang.xianli@LHD.nifs.ac.jp
[4] E-mail: zhang.hongming@LHD.nifs.ac.jp
[5] E-mail: liu.yang@LHD.nifs.ac.jp
[6] E-mail: goto@nifs.ac.jp

Observation of visible and EUV emission spectra of tungsten ions

MITA Momoe, and NAKAMURA Nobuyuki[1]

Institute for Laser Science, The University of Electro-Communications, Tokyo 182-8585, Japan

Tungsten will be used as plasma facing material in ITER, and thus is considered to be the main impurity ions in the ITER plasma. In order to suppress the radiation loss due to the emission of the impurity tungsten ions, it is important to understand the influx and the charge evolution of tungsten ions in the plasma through spectroscopic diagnostics. The charge states span a wide range such as neutral or 1+ near the edge up to neonlike (64+) or higher near the core. There is thus strong demand for spectroscopic data of tungsten ions for a wide range of charge state.

We have been using an electron beam ion trap (EBIT) to observe previously unreported lines of tungsten ions [1]. An EBIT produces highly charged ions through successive ionization of trapped ions by a quasi-monoenergetic electron beam. It is thus possible to produce selected charge state ions by tuning the electron beam energy.

In this talk, we present visible and extreme ultraviolet (EUV) spectra of W^{5-8+}. These moderate charge states are important for the diagnostics of the ITER plasma near the edge. In particular, W^{6+} has a closed shell structure (Er-like, $4f^{14}5p^{6}$) so that its population is considered to be dominant for a wide area.

Furthermore, these ions attract attention also from the fundamental physics point of view. Recently, visible transitions in highly charged ions are suggested as potential candidates for a precise atomic clock that can be used to test the time variation of the fundamental physical constant, such as the fine structure constant [2]. Some transitions in W^{7+} and W^{8+} are also named as candidates in recent theoretical study by Berengut et al. [3]. However, it has not been identified yet by experiment.

Fig. 1 shows an example of EUV spectra obtained with an electron energy of 150 eV. Emission lines from W^{5-7+} can be identified as indicated in the figure based on the previous observation by Clementson et al. [4]. By comparing the energy dependence between simultaneously obtained visible and EUV spectra, we identify the emission charge state in visible spectra.

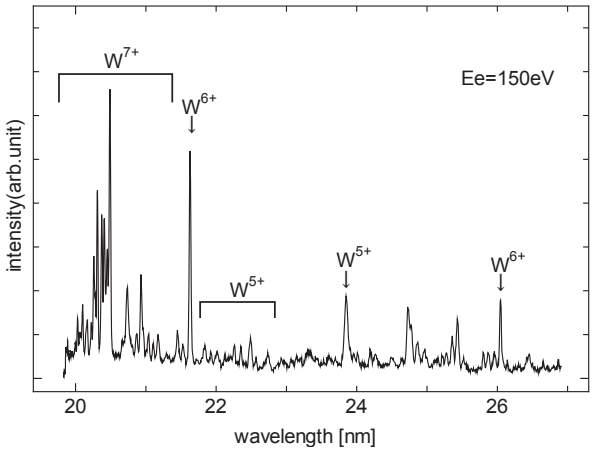

Fig. 1. An example of EUV spectra of tungsten ions obtained with CoBIT. The W^{5+} line at 23.8 nm may be blended with an impurity ion line.

References

[1] A. Komatsu et al., 2012 *Plasma Fusion Res.* **7** 1201158.
[2] J. C. Berengut et al., 2010 *Phys. Rev. Lett.* **105** 120801.
[3] J. C. Berengut et al., 2011 *Phys. Rev. Lett.* **106** 210802.
[4] J. Clementson et al., 2015 *Atoms* **3** 407.

E-mail: n_nakamu@ils.uec.ac.jp

Current progress of a NIFS project: spectroscopic measurements and database development for highly charged rare earth elements

F. Koike[1*], C. Suzuki[2], I. Murakami[2], H. A. Sakaue[2], M. Goto[2], D. Kato[2], T. Kato[2], S. Morita[2], H. Funaba[2], and A. Sasaki[3]

[1] Faculty of Science and Technology, Sophia University,
[2] National Institute for Fusion Science, Toki, Gifu 509-5292, Japan
[3]Japan Atomic Energy Agency

The spectra of photoemissions due to the transitions between sub-shell levels in N-sub-shell open atomic ions are of interest for the strong influence from the interactions between the electronic state configurations with different constituent orbitals. Modifications in unresolved transition array (UTA) spectral profile has been pointed out[1,2,3]. The wavelengths of the 4d - 4f transitions are reported to be, for example, 7.9 nm for Nd (Z=60), 7.0 nm for Eu (Z=63) , and 6.8 nm for Gd (Z=64)[4]. The 4d - 4f transitions of Tb (Z=65) at 6.5 nm has been investigated theoretically by Sasaki et al[5].

To study the EUV light emissions from highly charged heavy ions in connection to their atomic structures, it is quite effective to investigate in thin plasma conditions. We have proposed the use of the LHD plasmas for the spectral measurement of lanthanide elements. We have presently covered almost the whole range of the atomic number in lanthanide atoms, say, for atoms with Z=58, 60, 62, 64, 65, 66, 67, 68, 69, 70, 71, and 72[6,7]. The present accumulation of the spectral data is now enabling our investigation on the Z-dependence of the spectral features in lanthanide elements. We are continuing the spectral analysis using the available data.

We compared those spectra to our elaborate atomic structure calculations based on a Multi-Configuration Dirac-Fock (MCDF) approximation. We employed the General purpose Relativistic Atomic Structure Program 92 (GRASP92)[8] for the electronic structure, and the Relativistic Atomic Transition and Ionization Properties (RATIP) code[9] for transition wavelengths and strengths. We have made the MCDF calculations for all the lanthanide atomic species for ions with the number of electrons from 27 to 59.

One of the most interesting features in the distribution of the spectral structures is the modifications of 4d - 4f UTA. In the MCDF calculations, we optimize the individual single electron atomic orbitals in Atomic State Function (ASF), which consists of the linear combination of CSF's, numerically by means of the self-consistent field (SCF) iterative procedure, and the coefficients of CSF's are simultaneously evaluated. We may find the optimum shapes of the single electron atomic orbitals that fit to the multi-configuration state under consideration. We can avoid the excessive expansion of ASF in terms of many CSF's which contain the variety of single electron orbitals; this feature gives us the chance to implement the realistic physical characteristics to the individual single electron orbitals. By using the minimal basis sets, we may obtain a physically plausible set of single electron atomic orbitals; we may discuss the physical property of the atomic ions in connection with the character of single electron atomic orbitals. In the present calculations, we included all the CSF's with one electron excitations to the sub-shell orbitals in the N-shell from the N-shell orbitals in the ground states. For instance, to calculate Gd^{26+} $1s^22s^22p^63s^23p^63d^{10}4s^24p^64d^2$ = [Ni]$4s^24p^64d^2$, we considered all the possible one electron excitations from $4s^24p^64d^2$ to 4d and 4f orbitals. We considered the configurations $4s^24p^64d4f$, $4s^24p^54d^3$, $4s^24p^54d^24f$, $4s4p^64d^3$, and $4s4p^64d^24f$, and all the possible ASF's are optimized simultaneously, which gives us a set of atomic orbitals that are common throughout the ASF's. By using the Relativistic Atomic Transition and Ionization Property (RATIP) package[9], we calculate wavelengths and the strengths of electric dipole (E1) transitions for all the possible combinations of the ASF's that are obtained by the MCDF procedure. In the case of Gd^{26+} ions, for instance, we calculate the transitions to the ground states $4s^24p^64d^2$ -$4s^24p^64d4f$, and $4s^24p^64d^2$ - $4s^24p^54d^3$, as well as between the excited states $4s^24p^64d4f$ - $4s^24p^54d^24f$, $4s^24p^54d^3$ - $4s4p^64d^3$, $4s^24p^54d^24f$ - $4s4p^64d^24f$, $4s^24p^54d^24f$ - $4s^24p^54d^3$, and $4s4p^64d^24f$ - $4s4p^64d^3$.

Although we can consider the orbital relaxations in RATIP, we adopt the common basis orbital sets in both the states before and after the optical transitions. Tthe accuracy requirement is not as high as to urge us to adopt such sophisticated methods. And further on, by using the common basis orbitals, we can avoid the risk to face at large errors in the energy offset that come from the core electrons.

1) G. O'Sullivan et al, Opt. Eng. **33**, 3978 (1994).
2) J. Bauche et al, J. Phys. **B20**, 1443 (1987).
3) P. Mandelbaum et al, Phys. Rev. **A35**, 5051 (1987).
4) O'Sullivan, et al J. Opt. Soc. America, **71**, 227(1981).
5) A. Sasaki et al, Appl. Phys. Lett. **97**, 231501 (2010).
6) C. Suzuki et al, J. Phys. **B45**, 135002 (2012).
7) F. Koike et al, *Proceedings of ICAMDATA 6* (2013).
8) Parpia F A, Fischer C F and Grant I P 1996 Commpt. Phys. Commun. 94 249.
9) Fritzsche S 2012 Comput. Phys. Commun. 183 1525.

* E-mail: koikef@sophia.ac.jp

Charge exchange spectroscopy for multiply charged ions of high Z elements

Hajime Tanuma[*, 1], Naoki Numadate[*], Yoshiyuki Uchikura[*], Kento Shimada[*], Takuto Akutsu[*], Elaine Long[†], Gerry O'Sullivan[†]

[*] Department of Physics, Tokyo Metropolitan University, Hachioji, Tokyo 192-0397, Japan
[†] School of Physics, University College Dublin, Belfield, Dublin 4, Ireland

As tungsten will be used as a component of plasma-facing devices in the International Thermonuclear Experimental Reactor (ITER), a number of spectroscopic studies have been reported in this decade. The review articles on the available data for tungsten emission lines has pointed out that the spectroscopic data for W^{8+}–W^{26+} ions are relatively and quite poor [1, 2, 3]. Recently, EUV emission spectra from W^{7+}–W^{27+} ions in the 20 nm region have been reported in the Large Helical Device (LHD) at the National Institute for Fusion Science (NIFS) following pellet injection into the plasma [4].

In this work, we report new emission spectral date in charge exchange spectroscopy in collisions of multiply charged Ta ions with neutral gases. As tungsten has five isotopes of the mass numbers from 180 to 186, it is not suitable for the ion beam experiment with charge state separation after an analyzing by a dipole magnet. On the other hand, tantalum has 181-Ta with the natural abundance of 99.988%, then almost single isotope should be considered for tantalum. Because the atomic number of tungsten is 74 and that of tantalum is 73, we can regard that the electronic structure and transitions are extremely similar between two of them. Therefore we have decided to use Ta ions instead of W ions in our experiments.

We had inserted a Ta sheet into a plasma chamber of a 14.25 GHz electron cyclotron resonance ion source (ECRIS) and produced multiply charged Ta ions. After the charge-state separation, we had confirmed the production of Ta^{11+}–Ta^{24+} ions. The beam with one selected charge state was introduced into a collision cell filled with a target gas, and photon emissions from the collision cell in an extreme ultra-violet (EUV) region were observed by a compact glancing incident spectrometer equipped with a electrically cooled CCD camera.

Fig. 1 shows an typical EUV emission spectrum in the wavelength from 8 to 24 nm. We can see two strong unresolved transition arrays around 11 and 14 nm with many shape peaks. Widths of most of sharp peaks are much wider than the resolution of this spectrometer, 0.03 nm, then these sharp peaks are also overlapping of several line transitions.

We also observed similar spectra for different charge states of Ta ions. However, at present, the identification of each transition have not been performed yet. We will identify the transitions corresponding to observed emission of transitions in the EUV region of multiply charged tantalum ions after the comparison with theoretical calculations as the same as Sn and Xe ions [5, 6]. And we believe such data is useful to understanding of the transitions of tungsten ions for the fusion plasma research.

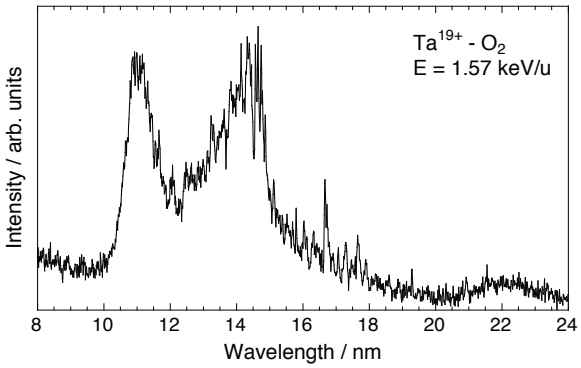

Fig. 1. EUV emission spectrum in collisions of Ta^{18+} ions with O_2 gas at energy of 1.57 keV/u.

References

[1] Kramida A E and Shirai T 2006 *J. Phys. Chem. Ref. Data***35** 423.

[2] Kramida A E and Shirai T 2009 *At. Data Nucl. Data Tables***95** 305.

[3] Kramida A E 2011 *Can. J. Phys.***89** 551.

[4] Suzuki C *et al.* 2011 *J. Phys. B: At. Mol. Opt. Phys.* **44** 175004.

[5] Ohashi H *et al.* 2011 *J. Phys. B: At. Mol. Opt. Phys.* **43** 065204.

[6] D'Arcy R *et al.* 2012 *Phys. Rev. A* **85** 062513.

[1] E-mail: tanuma@phys.se.tmu.ac.jp

Towards time-resolved imaging of electron and nuclear motions in momentum space

Masahiko Takahashi[1]

Institute of Multidisciplinary Research for Advanced Materials, Tohoku University, Sendai 980-8577, Japan

We have recently developed a new experimental technique, which is called time-resolved electron momentum spectroscopy (TR-EMS) and employs ultrashort laser (0.1 ps) and electron (1 ps) pulses in a pump-probe scheme [1]. This technique can be recognized as an advanced form of binary (e, 2e) spectroscopy or EMS that enables one to look at the spatial distributions of individual molecular orbitals in momentum space [2, 3]. Although there are ample rooms for improvement, the potential ability of TR-EMS has already been demonstrated through molecular orbital imaging of a short-lived (13.5 ps), second excited molecular state [4], an EMS study on the electronic structure of a relatively long-lived (80 ns), first excited molecular state [5], and an attempt at a product vibrational analysis of a photo-induced chemical reaction [6]. We are going further towards one of the goals of TR-EMS, that is, to film molecular orbital movies of chemical reactions, which would enable one to pierce straight to the heart of the reactions.

Under the above-mentioned circumstances, we are, in parallel, going to start or design two new projects. One is to develop a new experimental technique to afford a real-time measurement of nuclear motions in chemical reactions. The other is to extend the reach of TR-EMS from targets in field free space to those in external fields.

Measurements of nuclear motions in molecules can be made by using electron-induced atomic momentum spectroscopy (AMS). It is the complete electron analog for neutron Compton scattering, in which the nuclear motion causes a Doppler shift in the energy of elastically scattered electrons, as has beautifully been developed and demonstrated by Maarten Vos and his colleagues [7]. In order to attempt a real-time measurement of nuclear motions in chemical reactions, however, higher instrumental sensitivity would be desired. We have therefore developed a multi-channel AMS spectrometer [8], which has improved the instrumental sensitivity by a factor of 2000 or more compared to the existing spectrometer [7]. Our next step in this project is to develop, based on the achieved high sensitivity, time-resolved AMS (TR-AMS) with which one might be able to experimentally investigate how and how much the change in nuclear motions are brought about by the change in electron motion during chemical reactions.

Atoms and molecules in external fields also are one of the attractive targets in atomic and molecular science. For instance, we have theoretically found that the reaction coordinate dynamically switches to another coordinate with the increase in total energy of a system in crossed electric and magnetic fields [9]. Having such a different underlying motivation also, we have started examining the experimentally-feasible conditions for laser-assisted EMS (LA-EMS) that Konstantin Kouzakov and his colleagues have suggested and formulated theoretically [10, 11]. LA-EMS experiments would surely be possible if one can use the latest version of commercially available high power lasers.

References

[1] Yamazaki M, Kasai Y, Oishi K, Nakazawa H, Takahashi M 2013 *Rev. Sci. Instrum.* **84 063105**
[2] Weigold E and McCarthy I E 1999 *Electron Momentum Spectroscopy* (Kluwer/Plenum, New York)
[3] Takahashi M 2009 *Bull. Chem. Soc. Japan* **82 751**
[4] Yamazaki M, Oishi K, Nakazawa H, Zhu C, Takahashi M 2015 *Phys. Rev. Lett.* **114 103005**
[5] Yamazaki M, Tang Y, Takahashi M, *in preparation*
[6] Yamazaki M, Nakazawa H, Zhu C, Takahashi M 2015 *J. Phys. Conf. Ser.* **635 012010**
[7] *For example*, Vos M 2010 *J. Chem. Phys.* **132 074306**
[8] Yamazaki M, Hosono M, Tang Y, Takahashi M, *in preparation*
[9] Teramoto H, Toda M, Takahashi M, Kono H, Komatsuzaki T 2015 *Phys. Rev. Lett.* **115 093003**
[10] Kouzakov K A, Popov Yu V, Takahashi M 2010 *Phys. Rev. A* **82 023410**
[11] Bulychev A A and Kouzakov K A 2015 *Phys. Rev. A* **91 023413**

[1] E-mail: masahiko@tagen.tohoku.ac.jp

Observation of forbidden transitions from highly charged ions in a Kingdon trap

N. Numadate*,[1], T. Akutsu*, K. Shimada*, Y. Uchikura*, H. Shimaya*, T. Ishida*, K. Okada†, N. Nakamura‡, H. Tanuma*

*Department of Physics, Tokyo Metropolitan University, 1-1 Minami-Ohsawa, Hachioji, Tokyo 192-0397, Japan
†Department of Physics, Sophia University, 7-1 Kioicho, Chiyoda, Tokyo 102-8554, Japan
‡Institute for Laser Science, University of Electro-Communications, 1-5-1 Chofugaoka, Chofu, Tokyo 182-0021, Japan

In this 30 years, soft x-ray emissions have been observed by X-ray observatory satellites in the solar system [1]. Now it has been recognized that a part of these emissions stems from charge exchange collisions between highly charged ions in the solar wind and neutrals in the solar system [2]. These reactions are called solar wind charge exchange (SWCX). In the SWCX spectra, the forbidden transition from the metastable O^{6+} ($1s2s\ ^3S_1$) to the ground state ($1s^2\ ^1S_0$) has been observed as the main component [3]. In order to analyze the spectra quantitatively, absolute values of cross sections in the SWCX processes, in particular X-ray emission cross sections, are needed for astrophysics.

In those contexts, some SWCX processes have been reproduced in the laboratory, and X-ray emissions following them have been observed for the electric dipole allowed transitions [4,5]. However, it is very difficult to observe the forbidden transitions with a long lifetime of millisecond from the ions having the solar wind velocity of 300-900 km/s in the laboratory. Nonetheless we succeeded in the observation of the long-lived forbidden transition with ion trapping technique for the metastable O^{6+} ions after the charge exchange reactions of $O^{7+}(1s)$ + He → $O^{6+}(1snl)$ + He^+.

The hydrogen-like O^{7+} ion beam was produced by a 14.25 GHz electron cyclotron resonance ion source with an acceleration voltage of 6.0 kV, and injected into a collision cell filled with target helium gas. After the charge exchange collision, only O^{6+} were trapped in a Kingdon ion trap [6], and soft X-ray emissions from the metastable $O^{6+}(1s2s\ ^3S_1)$ ions were observed with a window-less silicon drift detector (SDD).

Figure 1 shows an observed forbidden transition (solid line). By fitting of the spectrum using the Gaussian function, the peak energy and the FWHM of the spectrum are determined. The FWHM of 73 eV was a typical value of the energy resolution of this SDD. The peak energy of 560 eV is corresponded to the transition of $1s^2\ ^1S_0$ - $1s2s\ ^3S_1$ of O^{6+} ions. We had also observed the resonance/intercombination lines of O^{6+} with the same set-up (dotted line). The peak energy is determined as 570 eV, which is corresponded to the transitions of $1s^2\ ^1S_0$ - $1s2p\ ^1P_1/^3P_1$. In this figure, the intensities are normalized at the peaks, and we can see the reasonable energy difference of about 10 eV between two peaks.

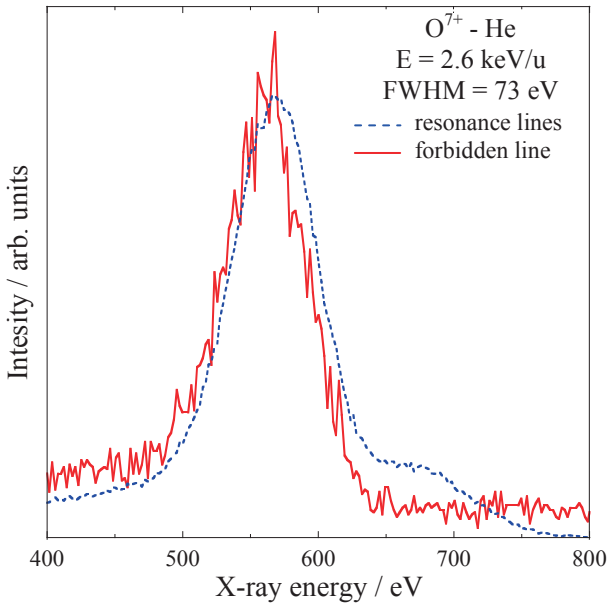

Fig. 1. Forbidden and resonance line spectra from O^{6+} ions.

References

[1] S. L. Snowden *et al.,* 1994 *Astrophys. J.* **424** 714.
[2] T. E. Cravens *et al.,*1997 *Geophys. Res. Lett.* **24** 105.
[3] R. Fujimoto *et al.,* 2007 *Publ. Astron. Soc. Japan* **59** S133.
[4] T. Kanda *et al.*, 2011 *Phys. Scr.* T **144** 014025.
[5] H. Shimaya *et al.*, 2013 *Phys. Scr.* T **156** 014002.
[6] N. Numadate *et al.*, 2014 *Rev. Sci. Instrum.* **85** 103119.

[1] E-mail: numadate-naoki@ed.tmu.ac.jp

Theoretical calculation on the photoelectron angular distribution of sodium-like ions

K. Ma*,[2], L. Y. Xie†, D. H. Zhang†, X. B Ding† and C. Z. Dong†,[1]

* School of Information Engineering, Huangshan University, Huangshan 245041, China
† Key Laboratory of Atomic and Molecular Physics & Functional Materials of Gansu Province, College of Physics and Electronic Engineering, northwest Normal University, Lanzhou 730070, China

In recent years, with the progress of light source, such as fourth generation synchrotron facilities or variously proposed free-electron lasers, and detection technology, especially in the aspect of the angle resolution detect, more and more attentions paid on the photoelectron angular distribution (PEAD). Compared with the traditional photoelectron spectrum, the PEAD is not only related to the amplitude of the photoionization channel, but also sensitive to the phase of these channels. As a result PEAD contains much more quantum information of the photoionization process and has been used to provide stringent tests of our understanding of basic physical processes underlying gas- and condensed-phase interaction with radiation, as well as a tool to probe physical and chemical structure in solids and surfaces.

For a long time, the dipole approximation is the basis in the study of the photoelectron angular distribution, but recently the non-dipole effect of the PEAD have been revealed in experimental measurement, especially in the low energy photon incident[1].

In this paper, the general formula of the PEAD has been derived by using the density matrix theory[2] and Racah algebra method. And then, the relativistic calculation program for PEAD has been further developed with the help of the program packages GRASP2K[3] and RATIP[4] which based on the multi-configuration Dirac-Fock (MCDF) method. By using this program, the dipole, non-dipole angular-distribution parameters and PEAD for sodium-like ions 2s and 2p have been calculated concretely. Fig.1 shows the $2p_{3/2}$ PEAD in the final state is $^3P_2$.

From the Fig.1 we can see that with the increase of PE energy, the PEAD has great changes. The results of dipole approximation and included non-dipole effects are similar at energy of v/c=0.1, but it has great difference at energy of v/c=0.4. In dipole approximation, the anisotropic properties of angle distribution will be decrease with the PE energy increase, the non-dipole effect and nuclear numbers will strengthen the angular distribution anisotropy.

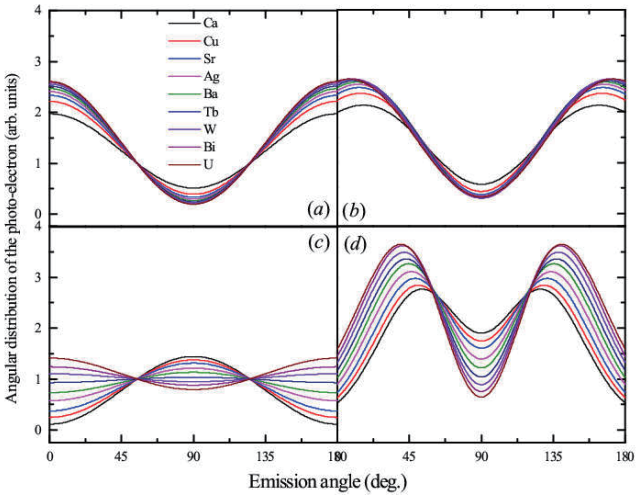

Fig. 1. Photoelectron angular distribution of $2p_{3/2}$ in sodium-like ions. (a) PE energy at v/c=0.1, dipole approximation; (b) PE energy at v/c=0.1, non-dipole effect have been included; (c) PE energy at v/c=0.4, dipole approximation; (b) PE energy at v/c=0.4, non-dipole effect have been included;

Project supported by the National Natural Science Foundation of China (Grant Nos. 11274254, U1332206, U1331122, 11464042, U1330117), by the Key Project for Young Talents in College of Anhui Province (Grant No. gxyqZD2016301), by the Natural Science Research Project of Anhui Province (Grant No. KJHS2015B01), and by the Natural Science Research Project of Huangshan University (Grant No. 2016xskq001)

References

[1] K. Ma, L. Y. Xie, D. H. Zhang et. al., 2016 *Acta Phys. Sin.* 65 083201.
[2] V. V. Balashov, A. N. Grum-Grahimailo, N. M. Kabachnik, 2000 Polarization and Correlation in Atomic Collisions (New York: Kluwer Academic/Plenum) pp45-97
[3] P. Jönsson, X. He, C. F. Fischer, et. al., 2007 *Comput. Phys. Commun.* **177** 597.
[4] S. Fritzsche 2012 *Comput. Phys. Commun.* **183** 1525.

[1] E-mail: dongcz@nwnu.edu.cn
[2] E-mail: makun0602@163.com

Dielectronic Recombination Studies Related to Fusion Plasmas

Zhimin Hu[1], **Jiamin Yang, Gang Xiong, Jiyan Zhang and Baohan Zhang**

Laser Fusion Research Center, China Academy of Engineering Physics, Mianyang 621900, China

Dielectronic recombination (DR) is a prominent process in collisions of electrons with highly charged ions. Due to the high intensity of DR resonances and their high strengths, this process often dominates the recombination rates in plasmas and generates intense x rays that effectively cool the plasmas. Normally, the DR process populates doubly excited states that decay via emission of DR satellite lines which are usually well resolved and have little contribution from other processes. The intensity ratio of a DR satellite line to the main line can be used for diagnostics of the plasma temperature. It is also sensitive to the plasmas density over a broad range of values. Moreover, qualitatively different information about the plasma state can be inferred from the linear polarization of the DR satellites, which is highly sensitive to the directionality of the recombining electrons. In fact, the directionality of anisotropic plasma electrons not only results in polarized DR lines, but also in anisotropic x-ray emission.

In this talk, we present the measurements of anisotropy [1, 2], resonance strength [3, 4] and linear polarization [5] of DR x-ray lines. Measurements of the DR resonant strength and the x-ray emission asymmetry identified strong contribution of the Breit interaction, especially in heavy gold ions, the Compton linear polarimetry gives a higher sensitivity to this intrinsically relativistic effect, even in the much lighter xenon ions. As demonstrated in the measurements at the EBITs, the Compton polarimetry work opens a large exploration space, in particular allowing one to access the quantum electrodynamics corrections of the generalized Breit interaction. Apart from the fundamental implications, our experimental results opens numerous possibilities for polarization diagnostics of hot anisotropic plasmas, which may reveal a presence of energetic directional electrons,

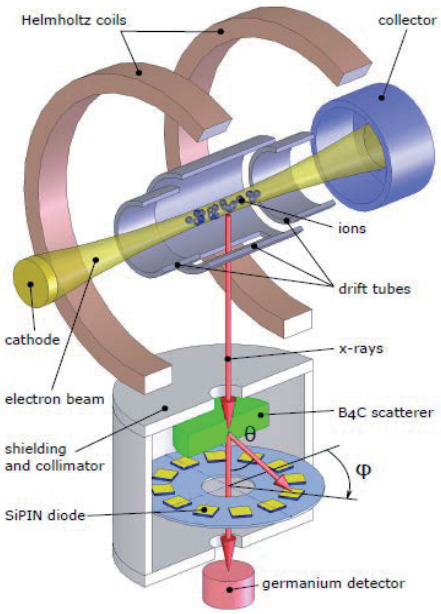

Fig. 1. Scheme of the polarization experiment on the Heidelberg electron beam ion trap.

for instance in relativistic jets of active galactic nuclei and laser-produced plasmas. Moreover, the polarization and anisotropy measurements may also be necessary for accurate temperature and density diagnostics of such plasmas.

References

[1] Z. M. Hu, X. Y. Han, Y. M. Li, et al., 2012 *Phys. Rev. Lett.* **108** 073002
[2] Z. M. Hu, Y. M. Li, X. Y. Han, et al., 2014 *Phys. Rev. A* **90**, 062702
[3] Z. M. Hu, Y. M. Li, N. Nakamura, 2013 *Phys. Rev. A* **87**, 052706
[4] G. Xiong, J. Y. Zhang, Z. M. Hu*, et al., 2013 *Phys. Rev. A* **88**, 042704
[5] J. Holger, Z. M. Hu, H. Bekker, et al., 2015 *Phys. Rev. A* **91**, 042705

[1] E-mail: zhimin.hu@caep.cn

Intensity and polarization measurements of Hα radiation from backscattered H* atoms by proton impact on polycrystalline tungsten surface

Hiroyuki. A. Sakaue[1], Daiji Kato[1,2], Izumi Murakami[1,2], Shouta Mineta[3], Kenji Motohashi[4] and Yasuhiro Sakai[3]

[1]National Institute for Fusion Science, National Institutes of Natural Sciences, 322-6 Oroshi-cho, Toki 509-5292, Japan
[2]Department of Fusion Science, SOKENDAI (The Graduate University for Advanced Studies), 322-6 Oroshi-cho, Toki, Gifu 509-5292, Japan
[3]Department of Physics, Toho University, 2-2-1 Miyama, Funabashi, Chiba 274-8510, Japan
[4]Department of Biomedical Engineering, Faculty of Science and Engineering, Toyo University, 2100 Kujirai, Kawagoe, Saitama 350-8585, Japan

Tungsten is planned to use as material for the divertor plates in ITER because of the high sputtering threshold energy for light ion bombardment, the highest melting point among all the elements, and less tritium retention compared with carbon-based materials [1-3]. Divertor plates in a fusion device are exposed to high intensity heat fluxes of energetic particles. Many experiments indicate that tungsten retains tritium and deuterium due to their bombardment of hydrogen isotope plasma. The resultant retentions of the isotopes raise to the safety and economic problems, and should be minimizes for future fusion reactor operations. Thus, many efforts are being made to predict hydrogen isotopes retention in various forms of tungsten under the actual fusion reactor condition. The retention, reflection, recycling, sputtering of hydrogen isotope atom in tungsten surface attracts extensive attention from the viewpoint of estimating the inventory of tritium atoms in a nuclear fusion device. We paid attention to the reflection processes of the hydrogen atoms by the proton irradiation to the tungsten surface, and then we measured spatial intensity and degree of polarization distributions of the Hα line from reflected hydrogen.

The experiment was performed in a beam line connected with a medium-current ion implanter (ULVAC IM-200MH-FB) at the National Institute for Fusion Science (NIFS), as shown in figure 1. Details of the ion source and beam line are described elsewhere [4]; hence, they will be only briefly explained here. The H^+ ion beam, accelerated to 35 keV, was introduced into a vacuum chamber after mass/charge separation. The ion beam transmitted through a 5-mm-diameter aperture hole entered normally on a polycrystalline tungsten surface, supported by a linear-motion manipulator. A bias voltage of ~100 V was applied to the disk, with the aperture hole used to retard secondary electrons emitted from the tungsten surface. The pressure of the vacuum chamber was maintained at $\sim 1 \times 10^{-6}$ Pa without introducing the ion beam, whereas it reached $\sim 3 \times 10^{-5}$ Pa under ion-beam irradiation of the tungsten surface. The ion beam entered perpendicular onto the tungsten surface. The polarizer was installed between quartz window and Hα band-pass filter. After passing through a quartz window, polarizer, Hα band-pass filter and condenser lens, the Hα image from the reflected H* atoms was projected on the two-dimensional (2D) charge coupled device (CCD).

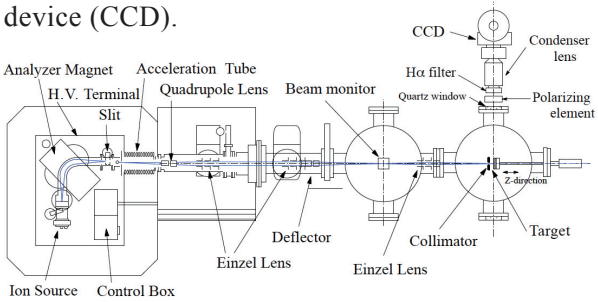

Fig.1. Experimental apparatus

We measured the spatial distribution of Hα line intensity from reflected H* atoms under irradiation of H^+ ion-beam (35keV). Using the analysis of the line intensity decay curve, we estimated the mean vertical velocity component in direction normal to the surface. And we measured the spatial distribution of Hα polarization degree. From these experimental results, it was shown that Hα line is aligned to the reflected direction of hydrogen atom. On this conference, the details of the spatial distribution of the intensity and polarization degree are explained.

References

[1] J.Roth et al., J. Nucl. Mater. **390-391** (2009) 1-9
[2] Z.Tian, J.W.Davis, A.A.Haasz, J. Nucl. Mater. **399** (2010) 101-107.
[3] K.Ohya et al., J. Nucl. Mater. **258-263** (1998) 1055-1059
[4] K.Motohashi, K.Nogami, Y.Sakai, H.A.Sakaue, D.Kato and T. Kenmotsu: NIMB **283** (2012) 59-62.

Study of the Zeeman effect on the D_α spectra in EAST tokamak

Wei Gao*[1], Juan Huang*[2], Chengri Wu*, Wei Gao*, Zong Xu*, Yumei Hou*, Zhao Jin*, Yingjie Chen*, Pengfei Zhang*, Ling Zhang*, Zhengwei Wu* and EAST Team*

* Institute of Plasma Physics, Chinese Academy of Sciences, P.O.Box 1126, Hefei, People's Republic of China 230031

The edge plasma determines the level of impurities in the core plasma and influences the core plasma confinement, which play a critical role in the fusion plasma[1-3]. Since the electron temperature and density decrease rapidly beside the scrape-off layer, the recycling processes are affected and dominated by atom and molecular processes in boundary region of the plasma which is mainly manifested in form of atom and molecular emission [4]. Therefore, it is important to study atomic and molecular spectrum in the boundary region. Based on the high resolution spectroscopy,D_α line shape was studied and to acquire more information of the local plasma. For the magnetic field, it can affect the atomic and molecular spectral shape, which is called Zeeman effect. Zeeman effect can be fully understood by quantum mechanics, and it has been investigated in many different ways on different fusion plasma[5-7].

Based on the passive spectroscopy, the D_α atomic emission spectra in boundary region of the plasma have been measured in EAST tokamak. The Zeeman splitting of the D_α spectral lines have been observed. A fitting procedure was developed by a nonlinear least squares method to fit and analyze the polarization π and $\pm\ \sigma$ of the D_α atomic spectra to get the information of the local plasma. In present work, the emission spectra were considered separately from different regions (low-field and high-field) along the viewing chord. The fitting result was shown in figure 1. By studying of the Zeeman effect of the emission spectra, emission position, magnetic field intensity and flow velocity of deuterium atom were determined.

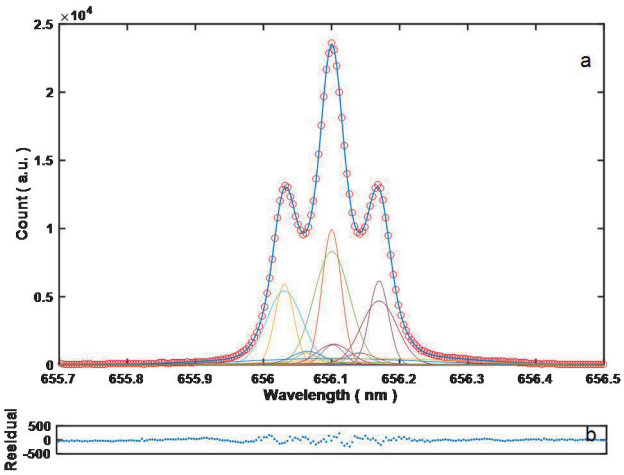

Fig. 1. D_α spectrum observed along the viewing chord and fitting results were shown in (a), the fitting data residuals was shown in (b). The open circles indicated the experimentally obtained spectra. The line indicated the fitting results and there different temperature components: cold, warm and hot.

References

[1] J Neuhauser, W Schneider, R Wunderlich and K Lackner 1984 *Nucl. Fusion* **24** 39
[2] P.C Stangeby and G.M McCracken 1990 *Nucl. Fusion* **30** 1225
[3] R.J Groebner 1993 *Phys. Fluids B* **5** 2343
[4] R Monk, A Loarte, A Chankin, S Clement, S.J Davies, J.K Ehrenberg, H.Y Guo, J Lingertat, G.F Matthews, M.F Stamp and P.C Stangeby 1997 *J. Nucl. Mater.* **241-243** 396
[5] J.D Hey, Y.T Lie, D Rusbüldt and E Hintz 1994 *Contrib. Plasma Phys*. **6** 725-747
[6] M Goto and S Morita 2002 *Phys. Rev. E* **65** 026401
[7] T Shikama, S Kado, H Zushi and S Tanaka 2004 *Phys. Plasmas* **11** 4701
[8] T Shikama, K Fujii, K Mizushiri, M Hasuo, S Kado and H Zushi 2009 *Plasma Phys. Control. Fusion* **51** 122001(9pp)

[1] E-mail: gaowei@ipp.ac.cn
[2] E-mail: juan.huang@ipp.ac.cn

Characterization of material ablation with intense extreme ultraviolet (EUV) light generated with laser

H. Nishimura*[1], N. Tanaka[1], R. Deguchi[1], N. Wada[1], A. Sunahara[2], M. Murakami[1] and A. Yogo[1]

[1]Institute of Laser Engineering, Osaka University, Suita, Osaka, Japan
[2]Institute for Laser Technology, Suita, Osaka, Japan

Recent progress on extreme ultraviolet (EUV) light sources enables us to utilize shorter wavelength of few to few tens of nanometer for micro machining of materials [1]. Since EUV photon energy exceeds 100 eV and corresponding photon energy is beyond the solid density, the ablation behavior, due to difference in energy deposition mechanism, is quite different from that of laser ablation in such a way that EUV light penetrates through ablation plasma and directly heats material of original density by photo-ionizing the inner orbit electrons. Although differences in ablation characteristics in EUV and laser ablation are reported [2], many aspects in the physics of EUV energy deposition and transportation remain unclear.

An effective approach to understand the material ablation is to study the expanding plasma because the energy spectrum of isothermal expansion during material heating is preserved even after the irradiation is stopped. This study aims 1) to understand the EUV ablation mechanism, and 2) to clarify the unique characteristics of EUV ablation by comparing with conventional laser ablation.

An intense laser produced plasma EUV source at ILE Osaka University [1] was used in the experiments(see Fig. 1) [3]. EUV emission from a solid xenon target ranging 11-20 nm was focused onto the sample material with an intensity of ~5 x 10^9 W/cm^2. A Nd:YAG laser (1064 nm) was used for laser ablation experiments. A charge collector array with four charge collectors was used to measure the angular distribution of ion number and energy spectra. The species of expanding particles were measured by the Thomson parabola mass and charge analyzer.

The experimental results showed noticeable difference between EUV and laser ablation in the angular distribution, energy spectra, and abundance of ionization stages. The spectrum for EUV ablation followed exponential decay curve having high kinetic energy component, and that for laser ablation showed convex spectrum having drastic cut off near 100 eV. The angular distribution of expanding ions from EUV ablation plasma shows narrower distribution than that from laser ablation plasma. The results were compared with a theoretical expansion model [4] and discussed using ablation parameters simulated by

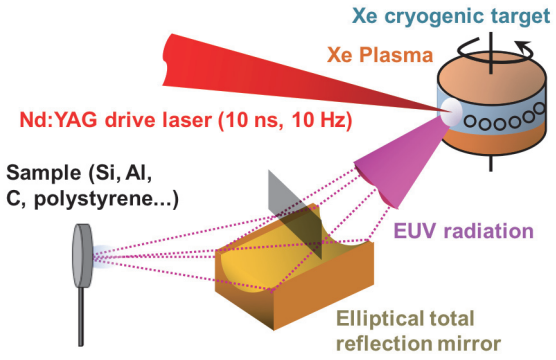

Fig. 1 EUV irradiation system. EUV light from the Xe plasma generated with Nd.YAG laser is focused on a sample with an elliptically toroidal mirror.

STAR 1D code [5]. Detailed discussion [6] and presumed ablation mechanisms will be presented in the presentation.

* This work was supported by JSPS Grant-in-Aid for Young Scientists (B) number 25800303, Grant-in-Aid for Scientific Research (B) number 22340172, and MEXT Project for Creation of Research Platforms and Sharing of Advanced Research Infrastructure" opening up a new photonics industry through high-intensity lasers".

[1] T. Makimura et.al, Journal of Physic Conference Series, **59**, 279 (2007)
[2] M. Berrill, et. al., J. Opt. Soc. Am. B **25**, 32 (2008)
[3] M. Masuda et. al., Appl. Phys. **B 119**, 421 (2015)
[4] A. Sunahara and K. A. Tanaka, Fusion Engineering and Design, **85**, 935 (2010).
[5] M. Murakami et. al, Physics Plasmas **12**, 062706 (2005).
[6] N. Tanaka, et al., Appl. Phys. Lett. **107**, 114101 (2015).

* nishimu@ile.osaka-u.ac.jp

Analysis of tungsten spectra in extreme ultraviolet spectral region on EAST

Z. Xu*,[1], Z. W. Wu*, L. Zhang*,[2], S. Morita†‡, T. Oishi†‡, W. Gao*, P. F. Zhang*, X.D. Yang*, J. Huang*, Y. J. Chen*, C. R. Wu*, J. L. Chen*, L. Q. Hu* and EAST team

* Institute of Plasma Physics, Chinese Academy of Science, Hefei 230031, China
† National Institute for Fusion Science, Toki, Gifu 509-5292, Japan
‡Department of Fusion Science, Graduate University for Advanced Studies, Toki, Gifu, 509-5292, Japan

Since the tungsten upper divertor has been installed on EAST in 2014, two fast-response extreme ultraviolet (EUV) spectrometers working at 10-130Å (EUV_Short) and 20-500 Å (EUV_Long) [1-2] respectively have been developed to measure tungsten spectra and monitor the tungsten behavior in plasma. The tungsten spectra with strong intensity were recorded during NBI H-mode phase with lower single null (LSN) configuration and H-mode phase in multiple heating schemes with upper single null (USN). The analysis of tungsten spectra is carried out as follows:

(1) The tungsten unresolved transition array (UTA) at 20-40 Å with high spectral resolution measured by EUV_Short is compared with the tungsten spectra measured from CoBIT device[3] as shown in Fig.1.

(2) The tungsten lines from W^{27+}-W^{45+} in UTA at 45-70 Å with low and high electron temperature (T_e) are identified based on NIST database as shown in Fig. 2(a).

(3) The 2nd order of tungsten lines from W^{27+}-W^{45+} in UTA at 90-140 Å at low and high electron temperature(T_e) are identified.

(4) The isolated W^{40+}-W^{45+} lines at 120-140 Å with high T_e are identified based on NIST database as shown in Fig. 2(b).

The time traces of line emission intensity from tungsten ions with different ionization stages during sawtooth and sudden impurity sputtering [4] events are plotted to check the results of identification of tungsten lines.

Finally, based on the results of tungsten line analysis, the temperature threshold for the appearance of tungsten ions with different ionization stages is investigated and compared with simulation result.

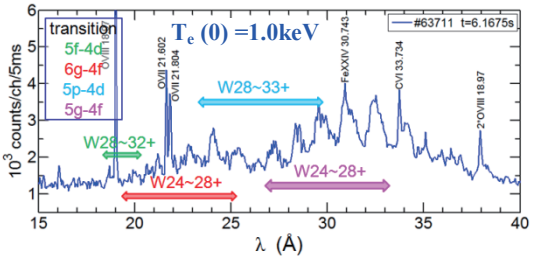

Fig.1. W-UTA at 20-40Å measured by EUV_Short

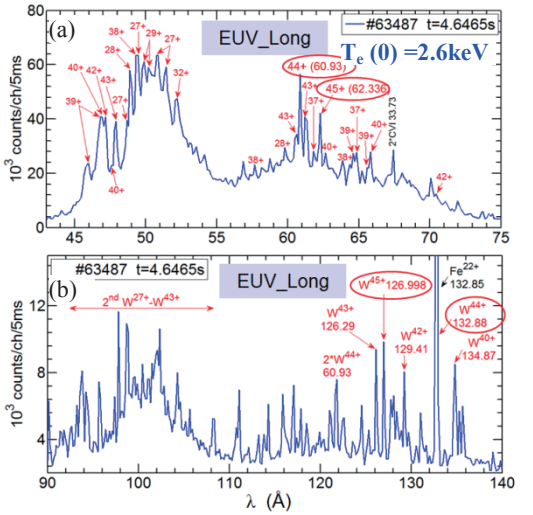

Fig.2. (a) W-UTA at 45-75 Å, (b) Isolated W lines at 120-140 Å, measured by EUV_Long

References

[1] L. Zhang, et al., Rev. Sci. Instrum. 86, 123509 (2015)
[2] L. Zhang, et al., 30th ITPA Topical Group on Diagnostics, 21-24 June, 2016, Novosibirsk, Russia
[3] S. Morita, et al., AIP Conf. Proc. 1545, 142-152 (2013)
[4] L. Zhang, et al., A3 Foresight Program Workshop, 17-20 May 2016, Yinchuan, China

[1] E-mail: xuzong@ipp.ac.cn
[2] E-mail: zhangling@ ipp.ac.cn

Fine-structure photoelectron spectra from the excited states $3p^5 3p$ of sodium atoms

X.B. Liu[*,1], **Y.L. Shi**[*], **and C.Z. Dong**[†2]

[*] Department of Physics, Tianshui Normal University, Tianshui, 741001, China
[†] Key laboratory of Atomic and Molecular Physics & Functional Materials of Gansu Province, College of Physics and Electronic Engineering, Northwest Normal University, Lanzhou, 730070, China

Photoionization is a fundamental atomic process in which an ion is formed as a result of the interaction of a photon with an atom. The unprecedented spectral capabilities and sensitivity of experimental highintensity have opened the door for quantitatively accurate studies of atomic structure and dynamics [1]. The main information about the observable universe is carried by photons, which can be detected by man-made orbital observatories. For example, the absorption lines of a neutral or ionized gas illuminated by a continuous background electromagnetic spectrum can provide detailed knowledge about the atomic abundances in the gas and about its density and temperature.

As quasi-one-electron systems with a single electron outside the closed-shell core, alkali atoms have proven to be an important and interesting testing ground for developing the many-electron theory of the photoionization process. In particular, medium and heavy alkali atoms are of interest for exploring correlation and relativistic effects in the photonelectron interaction and for use in photoelectric cells [2]. By utilizing the high resolution of electron spectrometers and the high brightness of third-generation synchrotron radiation sources, the fine structure of the photoelectron lines can be resolved. Recently, high-resolution photoelectron spectra from the ground and laser-excited states of sodium atoms were obtained experimentally [3]. Parallel to the experimental developments, theoretical investigations of the 2p photoionization processes have also been performed.

In the present paper, we demonstrate that the electron correlation of the 2p hole can clearly change the photoelectron spectra. The relativistic effects, which produce substantial change in the intensity distribution, are considerably less important for the corresponding photoionization thresholds. Furthermore, this study demonstrates the information that may be obtained regarding the relativistic effects in sub-valence photoionization processes, and the conclusions are by no means limited to excited sodium atoms.

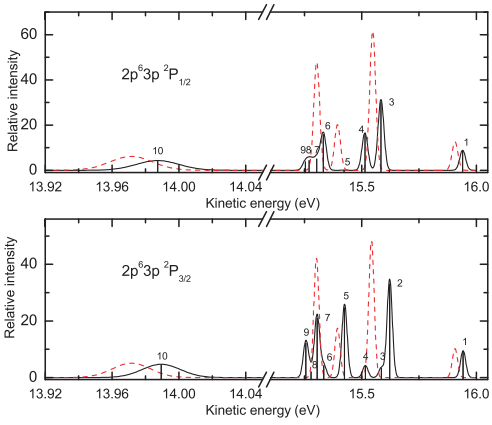

Fig. 1. The calculated $2p^5 3p$ photoelectron spectra with wave functions from the single-configuration approximation. The solid lines are the relativistic calculated spectra, and the (red) dashed lines are the nonrelativistic spectra.

This work has been supported by the National Natural Science Foundation of China (Grant Nos. 11264033 and 11464040), the Natural Science Foundation of Gansu Province (Grant No. 1506RJZE112) and the Scientific Research Foundation of Higher Education of Gansu Province (Grant No. 2014A-104).

References

[1] G.A. Alna'washi, M. Lu, M. Habibi *et. al.*, 2010 *Phys. Rev. A* **81** 053416.

[2] F.C. Chen, J.L. Wu, S.S. Yang *et. al.*, 2008 *J. Appl. Phys.* **103** 103721.

[3] D. Cubaynes, S. Guilbaud, F.J. Wuilleumier *et. al.*, 2009 *Phys. Rev. A* **80** 023410.

[1] E-mail: Liuxb_tstc@sohu.com
[2] E-mail: Dongcz@nwnu.edu.cn

Dielectronic recombination rate coefficients of W^{29+} ions

Yanbiao Fu, Rui Tian, Erlong Wei, Xudong Wang and Chenzhong Dong

Key laboratory of Atomic and Molecular Physics & Functional Materials of Gansu Province,
College of Physics and Electronic Engineering, Northwest Normal University, Lanzhou, 730070, China

In recent years, need for ITER research, the DR process of complex W ions with ground configuration 4d/4f subshell have been extensively pursued. In general, for calculation of DR with ground configuration 4d/4f subshell ions, resonant stabilizing transitions (RS) and nonresonant stabilizing (NRS) transitions from the resonant levels are included. The decays into autoionizing levels possibly followed by radiative cascades (DAC) from the resonant levels are neglected.

Theoretical calculations have been made for dielectronic recombination rate coefficients of W^{29+} ions using a flexible relativistic atomic code. Influence of excitation and radiation channels, configuration interactions, the effect of DAC are analyzed for DR rate coefficients. Firure 1 shows the DR and RR rate coefficients. The tags RS+NRS stand for the radiative transitions including resonant stabilizing transitions (RS) and nonresonant stabilizing (NRS) transitions, the tags DAC stand for the radiative transitions including RS, NRS and DAC, the tags NDAC stand for the radiative transition including all kinds of transitions except de-excitation cascade. Curves DR-DAC-4d and DR-DAC-4p are the DR rate coefficients for 4d and 4p subshell excitations including DAC transitions respectively. Curves DR-DAC-4d, DR-DAC-4p, DR-DAC, DR-RS+NRS and DR-NDAC are *ab initio* level-by-level DR rate coefficients for $j = (4p^6 4d^9)^{-1} nl\ n'l'$ (n = 4-6, n' = 4-23) using FAC. Curves DR- Ref. are DR rate coefficients of reference [1]. The DR rate coefficients from 4p subshell excitation are larger than 4d subshell excitation at $kT_e < 17$eV. The contributions through 4p subshell excitations to the total rate coefficient are 34%-63% in the whole temperature region. Hence the contributions from inner-shell electron excitation are very important. Comparison of the curve DR-DAC and DR-RS+NRS shows that the contributions from DAC transitions can be neglected at $kT_e < 20$ eV. The DAC transitions enlarges the total DR rate coefficients by a factor of about 1.21% at kT_e = 130 eV. The contributions from the DAC transitions increase smoothly with the increasing temperature and are about 9.7% at 1000 eV, 13.7% at 50000 eV. The contribution of DAC is evident. The curve DR-DAC-total (n'=4-1000) is total DR rate coefficients. The contributions from extrapolation DR-DAC(n'=24-1000) to the total DR rates are about 14.5% at 190 eV and 19.2% at 50000 eV. The total DR rate coefficients are greater than the RR rate coefficients for the case of electron temperature greater than 1 eV.

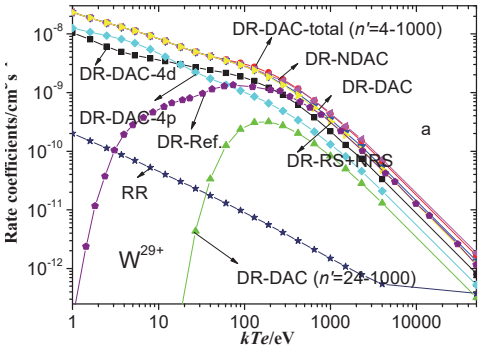

Figure 1: DR and RR rate coefficients for W^{29+} ions.

References

[1] Li B W, O'Sullivan G, Fu Y B, Dong C Z 2012 *Phys. Rev. A* 85 052706

E-mail: fuyb@nwnu.edu.cn

Influence of the magnetic interactions on angular distribution of electron emission from highly charged Be-like ions

Y. L. Shi[†,1], X. B. Liu[†], F. P. Lu[†], and C. Z. Dong[‡,2]

[†] Department of Physics, Tianshui Normal University, Tianshui 74101, China
[‡] Key Laboratory of Atomic and Molecular Physics & Functional Materials of Gansu Province, College of Physics and Electronic Engineering, Northwest Normal University, Lanzhou 730070, China

An atomic autoionizing state created by a beam of electron is aligned in the direction of the incident beam if the total angular momentum of the excited state is greater than 1/2. The alignment results from the fact that the excitation cross section has different values for different projections of the total angular momentum of the ion on the beam direction and independent of the sign [1-2]. The alignment of the ions can be revealed by studying its subsequent decay by ejection of the Auger electrons and characteristic x-ray emission. On the other hand, from the analysis of the Auger electron or photon, valuable information can be obtained for both the dynamical process and the magnetic sublevel population of the excited states, which is a very important supplement to the conventional observables [3].

The influence of the Breit interaction, typically appears as a relativistic correction to the Coulomb repulsion acting among the electrons, on the alignment (*i.e.* the population of the magnetic sublevels) and the angular distribution of electron emission from the excited state have been investigated systematically. Figure 1 shows the angular distribution for the electron emission of the $1s2s^22p_{3/2}\ ^3P_2 - 1s^22s\ ^2S_{1/2}$ autoionization of beryllium-like ions with projectile energies E_e = 2.0u, 4.0u, and 5.0u, following the electron-impact excitation from their $1s^22s^2\ ^1S_0$ ground state. Results are shown in the rest frame of three beryllium-like projectiles with charges Z = 54, 74 and 92 and in two approximations. Angular distributions with only the Coulomb repulsion incorporated into the Auger amplitudes (blue dashed lines, C only) are compared with those where the complete *e–e* interaction is taken into account (black solid lines, C+B). A rather strong interference between the Coulomb and the magnetic terms in the *e–e* interaction arises especially at low projectile energies, and gives rise to a double-peak structure in the angular distributions as well as to a 10% reduction of the electron yield in the forward direction if the nuclear charge of the projectiles is increased from Z = 54 to 92.

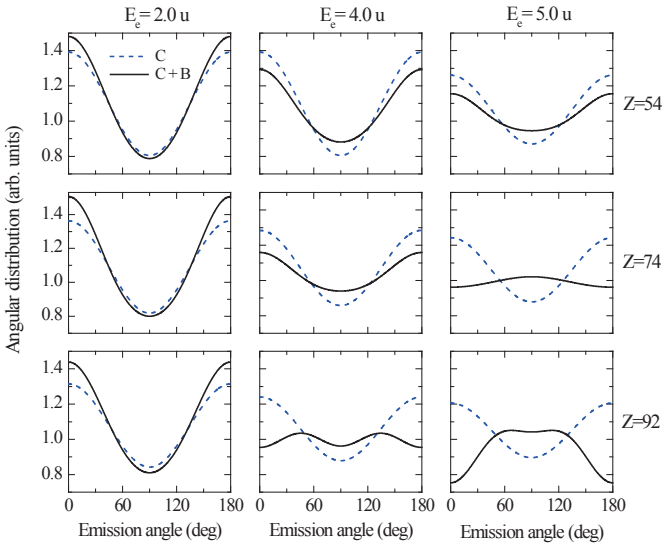

Fig.1. The angular distribution for the electron emission of the $1s2s^22p_{3/2}\ ^3P_2 - 1s^22s\ ^2S_{1/2}$ autoionization of beryllium-like ions with projectile energies E_e = 2.0u, 4.0u, and 5.0u, following the electron-impact excitation from their $1s^22s^2\ ^1S_0$ ground state.

This work has been supported by the National Natural Science Foundation of China (Grant Nos. 11464040 and 11264033), the Natural Science Foundation of Gansu Province (Grant No. 1506RJZE112) and the Scientific Research Foundation of Higher Education of Gansu Province (Grant No. 2014A-104).

References

[1] M. K. Inal and J. Dubau, 1987 *J. Phys. B* **20** 4221
[2] J. Eichler and Th. Stöhlker, 2007 *Phys. Rep.* **439** 1
[3] S. Fritzsche *et al*, 2012 *New J. Phys.* **14** 083018

[1] E-mail: shiyinglong331@163.com
[2] E-mail: dongcz@nwnu.edu.cn

Direct triple Auger decay of atoms and atomic ions: identifying the mechansim

Pengfei Liu*, Jiaolong Zeng*[1]

* College of Science, National University of Defense Technology, Changsha, Hunan 410073, China

A virtual sequential physical picture is proposed to investigate the direct triple Auger decy(DTAD) processes of atoms and atomic ions[1], which can be understood as a single Auger decay followed by a direct double impact ionization of the electron ejected in the first Auger process or equivalently as a direct double Auger decay (DDAD) followed by a single impact ionization by any one of the two electrons ejected in the DDAD process. The detailed computation scheme of the DTAD process is fulfilled basing on the explicit separation of dominant mechanisms for the DDAD and direct double electron-impact ionization processes. Such an idea is demonstrated by considering the DTAD processes of the lowest-energy K-vacancy resonances of C^{1+} $1s2s^22p^2$ 2D and 2P. The calculated probability density distribution of the three continuum electrons ejected in the DTAD process over the energies of any two electrons favors the scenario of a fast and two slow electrons. The DTAD rates for the dominant pathways are determined and the total rate explains a recent experiment.

Table 1. The decay rates of the dominant pathways for single, double, and triple Auger processes from initial terms of C^{1+} $1s2s^22p^2$ ^2D and ^2P.

TABLE I. The decay rates (s^{-1}) of the dominant pathways for the single, double and triple Auger (SA, DA, and TA) processes from initial terms of C^+ $1s2s^22p^2$ ^2D and ^2P. The intermediate terms of C^{2+} and C^{3+} are given to specify the route of DTAD process.

Initial C^{1+}	Intermediate C^{2+}	SA rate	Intermediate C^{3+}	DA rate	Final C^{4+}	TA rate
^2D	$1s^22s^2$	5.026[13]	$1s^22s_{1/2}$	1.341[12]	$1s^2$	4.640[9]
	$1s^2(2s_{1/2}2p_{3/2})_2$	7.641[12]	$1s^22s_{1/2}$	1.600[11]	$1s^2$	5.488[8]
	$1s^2(2s_{1/2}2p_{3/2})_2$		$1s^22p_{3/2}$	1.089[11]	$1s^2$	4.672[8]
	$1s^2(2s_{1/2}2p_{3/2})_1$	3.546[13]	$1s^22s_{1/2}$	7.328[11]	$1s^2$	2.492[9]
	$1s^2(2s_{1/2}2p_{3/2})_1$		$1s^22p_{1/2}$	1.826[11]	$1s^2$	7.724[8]
	$1s^2(2s_{1/2}2p_{3/2})_1$		$1s^22p_{3/2}$	3.660[11]	$1s^2$	1.548[9]
	$1s^22s^0(2p_{1/2}2p_{3/2})_2$	5.526[13]	$1s^22s_{1/2}$	1.883[11]	$1s^2$	6.365[8]
	$1s^22s^0(2p_{1/2}2p_{3/2})_2$		$1s^22p_{1/2}$	7.345[11]	$1s^2$	3.070[9]
	$1s^22s^0(2p_{1/2}2p_{3/2})_2$		$1s^22p_{3/2}$	1.493[12]	$1s^2$	6.241[9]
	total	1.557[14]	total	5.562[12]	total	2.042[10]
^2P	$1s^2(2s_{1/2}2p_{3/2})_1$	1.216[13]	$1s^22s_{1/2}$	2.510[11]	$1s^2$	8.534[8]
	$1s^2(2s_{1/2}2p_{3/2})_1$		$1s^22p_{1/2}$	6.256[10]	$1s^2$	2.646[8]
	$1s^2(2s_{1/2}2p_{3/2})_1$		$1s^22p_{3/2}$	1.254[11]	$1s^2$	5.442[8]
	$1s^22s^0(2p_{1/2}2p_{3/2})_1$	3.724[13]	$1s^22p_{1/2}$	7.848[11]	$1s^2$	3.330[9]
	$1s^22s^0(2p_{1/2}2p_{3/2})_1$		$1s^22p_{3/2}$	7.909[11]	$1s^2$	3.322[9]
	$1s^22s^0(2p_{3/2}^2)_2$	1.978[12]	$1s^22p_{3/2}$	6.939[10]	$1s^2$	2.914[8]
	$1s^22s^0(2p_{1/2}^2)_0$	1.882[13]	$1s^22p_{1/2}$	5.331[11]	$1s^2$	2.231[9]
	$1s^22s^0(2p_{1/2}^2)_0$		$1s^22p_{3/2}$	2.644[11]	$1s^2$	1.110[9]
	total	7.670[13]	total	2.987[12]	total	1.194[10]

References

[1] A. Müller *et al*, *Phys. Rev. Lett.* 2015 **114** 013002

E-mail: jlzeng@nudt.edu.cn

The realization of the dipole (γ,γ) method and its application to determine the absolute optical oscillator strengths of helium

Long-Quan Xu[*,†], **Ya-Wei Liu**[*,†], **Xu Kang**[*,†], **and Lin-Fan Zhu**[*,†,1]

[*] Hefei National Laboratory for Physical Sciences at Microscale and Department of Modern Physics, University of Science and Technology of China, Hefei, Anhui 230026, People's Republic of China

[†] Synergetic Innovation Center of Quantum Information and Quantum Physics, University of Science and Technology of China, Hefei, Anhui 230026, People's Republic of China

Absolute optical oscillator strength of atom or molecule has important applications in many fields such as plasma, interstellar space, and planetary atmosphere. Therefore, exploring new experimental method to determine OOS is very signaficant. Herein we proposed the dipole (γ,γ) method to determine the absolute OOSs of atoms and molecules with high accuracy for the first time. In the dipole (γ,γ) method, the high energy photon impact ($\sim$10 keV) at the dipole approximation condition of $q^2 \approx 0$ (i.e., at the small scattering angle) is used to simulate the photoabsorption process. The experimental arrangement is that a beam of monochromatic x-ray photon collide with gaseous atoms or molecules and the scattered photons are analysed by a spheric grating at the scattering angle of 2° to make sure that the squared momentum transfer satisfies the requirement of $q^2 < 10^{-2}$ a.u..

The experiment was carried out at Taiwan beamline in SPring-8, and the absolute OOSs of valence-shell excitations of atomic helium were determined by the present dipole (γ,γ) method and compared them with the previous experimental and theoretical results, which are shown in Table 1. It can be seen that the present high-resolution dipole (γ,γ) measurements are in excellent agreement with the results obtained by dipole (e, e) method and the ones of different theoretical calculations, while the photoabsorption method gives slightly lower value than present result of 2^1P transition. Thus the dipole (γ,γ) method provides a reliable approach to obtain the benchmark data of OOSs of valence-shell excitations for gaseous atoms and molecules.

Tab. 1. The OOSs of the $1s^2\,^1S_0 \rightarrow 1snp\,^1P_1$ transitions in helium.

$1^1S \rightarrow$	3^1P	4^1P	5^1P	6^1P
This work [1]	0.0740	0.0295	0.0156	0.0089
[2]	0.0739	0.0304	0.0154	0.0093
[3]	0.0741	0.0303	0.0152	0.0089
[4]	0.0717			
[5]	0.0731	0.0299	0.0151	0.0086

References

[1] L. Q. Xu, Y. W. Liu, X. Kang *et al* 2015 *Sci. Rep.* **5** 18350

[2] Z. P. Zhong *et al* 1997 *J. Phys. B: At. Mol. Opt. Phys.* **30** 5305

[3] W. F. Chan *et al* 1991 *Phys. Rev. A* **44** 186

[4] R. C. G. Ligtenberg *et al* 1994 *Phys. Rev. A* **49** 2363

[5] W. L. Wiese *et al* 2009 *J. Phys. Chem. Ref. Data* **38** 565

[1] E-mail: lfzhu@ustc.edu.cn

The magnetic quadrupole contribution to the polarization properties following electron-impact excitation and dielectronic recombination of highly charged ions

Z. B. Chen*,[1], J. L. Zeng*, and C. Z. Dong†

* College of Science, National University of Defense Technology, Changsha, Hunan 410073, China
†Key laboratory of Atomic and Molecular Physics & Functional Materials of Gansu Province, College of Physics and Electronic Engineering, Northwest Normal University, Lanzhou, 730070, China

Apart from its fundamental importance, electron-impact excitation (EIE) /dielectronic recombination (DR) is responsible for the vast majority of X-ray radiation produced in kinds of plasmas. In the past, the studies have mainly dealt with the total cross sections and rate coefficients. Much of today's interest, in contrast, is focused on the polarization properties of X-ray emission From the detailed analysis of the polarization, valuable information can be obtained about both the magnetic sublevels population of the excited states and the dynamical process. These properties have become indispensable tools for the diagnosis of plasma state and the analysis of complex spectra formation mechanism.

In this work, we calculated the linear polarization and angular distribution of the x-ray radiation of highly charged He-like and Li-like uranium ions following electron-impact excitation and dielectronic recombination processes using a relativistic distorted-wave method[1]. We investigated the contribution of the magnetic quadropole (*M2*) term to the subsequent characteristic x-ray emission from the above two processes. We found that while the *M*2 term as a slightly effect on the angular distribution and linear polarization of electron-impact excitation, it gives a substantially contribution for the same properties of dielectronic recombination.

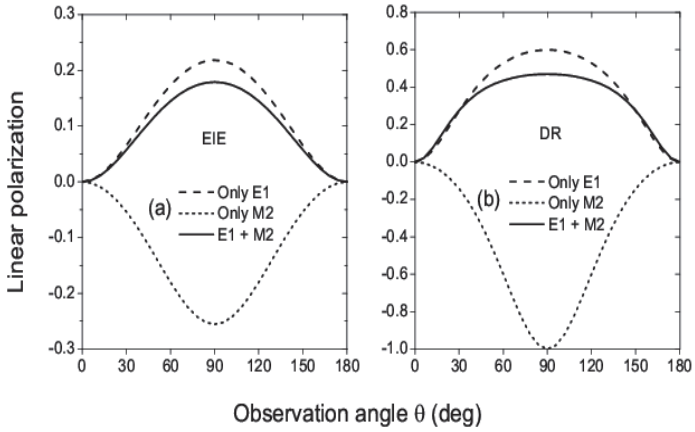

Fig. 1. The linear polarization of the $1s_{1/2}2s_{1/2}2p_{3/2}$ (J =3/2)→$1s^2 2s_{1/2}$ (J =1/2) transition for Li-like U^{89+} ions following EIE (left) and DR (right) processes as a function of the observation angle. E1 represents inclusion of only the electric-dipole approximation, M2 represents inclusion of only the magnetic-quadrupole approximation, and E1+M2 represents values with inclusion of *E1-M2* interference.

(This work was supported by the National Natural Science Foundation of China (grant no. 11274382, 11274254, 11504421, and U1332206) and the Project funded by China Postdoctoral Science Foundation (Grant No. 2016M593019)

References

[1] Z. B. Chen, J. L. Zeng, H. W. Hu , and C. Z. Dong *J. Phys. B* 2015 **48** 144005.

[1] E-mail: chenzb008@qq.com

Radiative Transition Energy and Probability of W^{54+} ions

X.B. Ding*[1], R. Sun*, J.X. Liu*, F. Koike‡, I. Murakami†, D. Kato†, H. A. Sakaue†, N. Nakamura♯, C.Z. Dong*

* Key laboratory of Atomic and Molecular Physics & Functional Materials of Gansu Province, College of Physics and Electronic Engineering, Northwest Normal University, Lanzhou, 730070, China
‡ Department of physics, Sophia University, Tokyo 102-8554, Japan
† National Institute for Fusion Science, Toki, Gifu 509-5292, Japan
♯Institute for Laser Science, The University of Electro-Communications, Chofu, Tokyo 182-8585, Japan

Tungsten(W) has become the focus of attention in fusion research, being considered as a main candidate for the cover of plasma-facing component in the next generation magnetic confined fusion devices like ITER, due to its excellent physical and chemical properties. However, tungsten ions will inevitably be introduced as impurity into the fusion plasma by the plasma-wall interaction and plasma transportation. A thorough knowledge of the atomic energy level structure and transition properties of various tungsten ions would be helpful for monitoring the tungsten impurity flux and to diagnosing the plasma parameters. Meanwhile, the tungsten is a heavy element where the relativistic effects would be very important.

In this paper, the energy levels, E1, M1, E2, M2 transition wavelength and probability as well as the lifetime of the excited states of the ground configuration $3p^6 3d^2$ and low-lying excited state $3p^5 3d^3$ of Ca-like W ion were calculated by using Multi-Configuration Dirac-Fock (MCDF) method and GRASP2K code. The restricted active space method was applied in the present calculation. The most important Valence-Valence, Core-Valence and Core-Core correlation were taken into account. The Breit and QED effects are also included in the present work.

It is found in the preset work that the Core-Core correlation contribution from 3s, 3p orbital is important for the energy structure. The calculated M1 transition wavelength and probability among the levels of ground configuration agreed with previous theoretical and experimental result which implies that the validity of the present correlation model. Based on the convergence of the calculated results, other transition parameters were calculated using the same correlation model. According to the results, some strong E1 transitions in 382-420 eV were identified and predicted. A simple collisional-radiative model analysis was performed to explain the previous experiment observation. Some other strong transitions in the range of 630-670 eV were predicted, which need to be identified in the future experiment.

References

[1] Jönsson et al, 2013, *Comput. Phys. Commun.* **184** 2197.

[2] X.B. Ding et al, 2016, *Phys. Lett. A*. **380** 874.

[3] X. B. Ding et al, 2016, *J. Phys. B: At. Mol. Opt. Phys* (to be submitted).

[1]E-mail: dingxb@nwnu.edu.cn

List of Participants

Name	Affiliation
(Japan)	
Numadate Naoki	Department of Physics, Tokyo Metropolitan University
Tanuma Hajime	Department of Physics, Tokyo Metropolitan University
Sakai Yasuhiro	Dept. of Physics, Toho Univ.
Mita Momoe	Institute for Laser Science, The University of Electro-Communications
Nakamura Nobuyuki	Institute for Laser Science, The University of Electro-Communications
Nishimura Hiroaki	Institute of Laser Engineering, Osaka University
Takahashi Masahiro	Institute of Multidisciplinary Research for Advanced Materials, Tohoku University
Kato Daiji	National Institute for Fusion Science
Morita Shigeru	National Institute for Fusion Science
Murakami Izumi	National Institute for Fusion Science
Oishi Tetsutaro	National Institute for Fusion Science
Sakaue Hiroyuki A.	National Institute for Fusion Science
Koike Fumihiro	Sophia University
(China)	
Gao Xiang	Beijing Computational Science Research Center
Yang Yang	Fudan University
Ma Kun	Huangshan University
He Bin	Institute of Applied Physics and Computational Mathematics
Li Jiguang	Institute of Applied Physics and Computational Mathematics
Long Feiyun	Institute of Applied Physics and Computational Mathematics
Yu Yanmei	Institute of Physics Chinese Academy of Sciences
Gao Wei	Institute of Plasma Physics (ASIPP)
Liu Xiaoju	Institute of Plasma Physics (ASIPP)
Wu Chenrui	Institute of Plasma Physics (ASIPP)
Xu Zong	Institute of Plasma Physics (ASIPP)
Zhang Ling	Institute of Plasma Physics (ASIPP)
Qi Yueyin	Jiaxing University
Li Bowen	Lanzhou University
Qiu Xiyu	Lanzhou University
Hu Zhimin	Laser Fusion Research Center, China Academy of Engineering Physics

Yang Jiaming	Laser Fusion Research Center, China Academy of Engineering Physics
Chen Zhanbin	National University of Defense Technology
Gao Cheng	National University of Defense Technology
Liu Liping	National University of Defense Technology
Liu Pengfei	National University of Defense Technology
Zeng Jiaolong	National University of Defense Technology
Cao Shiquan	Northwest Normal University
Ding Xiaobin	Northwest Normal University
Dong Chenzhong	Northwest Normal University
Dou Lijun	Northwest Normal University
Fu Yanbiao	Northwest Normal University
Man Qianqian	Northwest Normal University
Min Gi	Northwest Normal University
Su Maogen	Northwest Normal University
Sun Duixiong	Northwest Normal University
Sun Rui	Northwest Normal University
Tang Zhiming	Northwest Normal University
Xie Luyon	Northwest Normal University
Yang Jiaoxia	Northwest Normal University
Zhang Denghong	Northwest Normal University
Wang Xiangli	Northwest University for Nationalities
Li Jiaming	Shanghai Jiaotong University
Feng Lei	Sichuan University
Lv Meng	Sichuan University
Cui Zhengying	Southwestern Institute of Physics
Dong Chunfeng	Southwestern Institute of Physics
Yu Deliang	Southwestern Institute of Physics
Liu Xiaobin	Tianshui Normal University
Shi Yinglong	Tianshui Normal University
Tian Shanxi	University of Science and Technology of China
Xu Longquan	University of Science and Technology of China
Zhu Linfan	University of Science and Technology of China

(Korea)

Song Mi-Young	National Fusion Research Institute
Yoon Jung-Sik	National Fusion Research Institute